Southern Federal University
I.I. Vorovich Institute of Mathematics, Mechanics, and Computer Science

---

Proceedings of

Fourth China-Russia Conference

NUMERICAL ALGEBRA WITH APPLICATIONS

Editors: Zhong-Zhi Bai, Lev A. Krukier, Galina V. Muratova

26-29 June 2015
Rostov-on-Don, RUSSIA

UDC 519.6

Editors: Zhong-Zhi Bai, Lev A. Krukier, Galina V. Muratova

NUMERICAL ALGEBRA WITH APPLICATIONS

Proceedings of Fourth China-Russia Conference. – Rostov-on-Don: Southern Federal University Publishing, 2015, 192 p.
ISBN

Fourth China-Russia Conference on Numerical Algebra with Applications (CRC-NAA'15) is organized by I.I. Vorovich Institute of Mathematics, Mechanics, and Computer Science of Southern Federal University. Aims are bringing together researchers, scientists, engineers and graduate students to exchange and stimulate ideas from different disciplines and discussing the practical challenges encountered. The solutions adopted and learning the recent developments on theory and computional methods for numerical simulation of linear algebra and scientific computing will be considered. The topics of CRC-NAA'15 include, but are not limited to: mathematical modeling; applicating of numerical methods and algorithms to solve problems of mathematical modeling, linear and nonlinear equations systems; preconditionining technique; parallel computing.

The China-Russia Conference is supported by RFBR (grant № 15-31-10132)

ISBN

CONTENTS

Plenary Lectures

RIGOROUS CONVERGENCE ANALYSIS OF ALTERNATING VARIABLE MINIMIZATION WITH MULTIPLIER METHODS FOR QUADRATIC PROGRAMMING PROBLEMS WITH EQUALITY CONSTRAINTS[1]

Zhong-Zhi Bai*, Min Tao**

* *State Key Laboratory of Scientific/Engineering Computing, Institute of Computational Mathematics and Scientific/Engineering Computing, Academy of Mathematics and Systems Science, Beijing, P.R. China,*

** *Department of Mathematics, Nanjing University, Nanjing, China*

Let $\mathbb{R}$ be the domain of all real numbers, $\mathbb{R}^n$ be the n-dimensional real linear space equipped with the Euclidean inner product, say, $\langle\cdot,\cdot\rangle$, and $\mathbb{R}^{m\times n}$ be the m-by-n real matrix space. Denote by $(\cdot)^T$ and $\|\cdot\|$ the transpose and the Euclidean norm of either a vector or a matrix of suitable dimension, respectively. We consider numerical solutions of equality-constraint quadratic programming problems of the form

$$\begin{cases} \min & \phi(x)+\psi(y), \\ \text{s.t.} & Ax+By=b, \end{cases} \tag{1}$$

where $A\in\mathbb{R}^{p\times n}$ and $B\in\mathbb{R}^{p\times m}$ are two matrices, $b\in\mathbb{R}^p$ is a known vector, and $\phi:\mathbb{R}^n\to\mathbb{R}$ and $\psi:\mathbb{R}^m\to\mathbb{R}$ are two quadratic functions defined by

$$\begin{cases} \phi(x) &= \frac{1}{2}x^TFx+x^Tf, \\ \psi(y) &= \frac{1}{2}y^TGy+y^Tg, \end{cases} \tag{2}$$

with $F\in\mathbb{R}^{n\times n}$, $G\in\mathbb{R}^{m\times m}$ being symmetric positive semidefinite matrices and $f\in\mathbb{R}^n$, $g\in\mathbb{R}^m$ being given vectors. We assume that some standard assumptions are imposed on the matrices F, G and A, B as well as on the vectors f, g and b such that the solution set of the problem (1)-(2) is nonempty. This class of constraint programming problems occurs in many areas of computational science and engineering applications such as economics [1], electrical circuits and networks [2, 29, 7], electromagnetism [24, 4], finance [21, 22], image reconstruction [17], image registration [23, 15] and optimal control [3]. It also captures a number

[1] * The work of this author is supported by The National Basic Research Program (No. 2011CB309703), The National Natural Science Foundation (No. 91118001) and The National Natural Science Foundation for Creative Research Groups (No. 11321061), P.R. China,

** The work of this author is supported by The National Natural Science Foundation (No. 11301280) and The Fundamental Research Funds for the Central Universities (No. 020314330019), P.R. China

of important applications arising in various areas such as the l_1-norm regularized least-squares problems, the total variation image restoration and the standard quadratic programming problems; see, e.g., [19, 18] for more details.

One of the most popular and effective iterative methods for solving the equality-constraint quadratic programming problem (1) is the so-called *alternating direction* method with *multipliers*, or in short, the **ADM** method. At each iteration step, it first alternatively minimizes the augmented Lagrangian function $\mathcal{L}_a(x, y, z)$ with respect to the variables x, y, and then update the Lagrange multiplier z according to the steepest ascent principle so that violation of the original constraint $Ax + By = b$ is penalized. More precisely, the ADM method for solving the problem (1) can be algorithmically described as follows.

Method 0.1 (ADM Method for the Problem (1))
Given initial guesses $y^{(0)} \in \mathbb{R}^m$ and $z^{(0)} \in \mathbb{R}^p$, for $k = 0, 1, 2, \ldots$ until the iteration sequences $\{x^{(k)}\}_{k=0}^{\infty} \subset \mathbb{R}^n$, $\{y^{(k)}\}_{k=0}^{\infty} \subset \mathbb{R}^m$ and $\{z^{(k)}\}_{k=0}^{\infty} \subset \mathbb{R}^p$ are convergent, compute $x^{(k+1)}$, $y^{(k+1)}$ and $z^{(k+1)}$ according to the following rule:

$$\left\{ \begin{array}{rcl} x^{(k+1)} & = & \mathrm{argmin}_{x\in\mathbb{R}^n} \left\{ \phi(x) - \langle Ax + By^{(k)} - b, z^{(k)} \rangle + \frac{\beta}{2} \|Ax + By^{(k)} - b\|^2 \right\}, \\ y^{(k+1)} & = & \mathrm{argmin}_{y\in\mathbb{R}^m} \left\{ \psi(y) - \langle Ax^{(k+1)} + By - b, z^{(k)} \rangle + \frac{\beta}{2} \|Ax^{(k+1)} + By - b\|^2 \right\}, \\ z^{(k+1)} & = & z^{(k)} - \beta(Ax^{(k+1)} + By^{(k+1)} - b). \end{array} \right. \quad (3)$$

Intuitively, Method 0.1 is an *alternating variable minimization with multiplier* (**AVMM**) method. The AVMM method is intended to blend the decomposability of dual ascent with the superior convergence properties of the method of multipliers [6]. In [12] Gabay illustrated this iteration scheme as an application of the Douglas-Rachford splitting method [20] to the dual of the problem (1), and Eckstein and Bertsekas [9] showed in turn that Douglas-Rachford splitting is a special case of the proximal point method. Hence AVMM is a special case of the proximal point method; see Eckstein and Ferris [10] for more discussions explaining this approach. On the other hand, it is also a natural generalization of the classical Uzawa method for solving the saddle-point problems; see [1, 5, 8].

Many papers have analyzed the AVMM method from the perspective of maximal monotone operators [9, 25, 26, 27, 28]. Its global convergence was proved under some mild conditions such as the solution set of the problem (1) is nonempty; see [13, 11, 12]. Also, it has been known that this method converges linearly, but an accurate estimate about the convergence rate is still in its infancy; see, e.g., [20, 14, 19, 30, 18].

In this paper, based on a weighted inner product and the corresponding weighted norm, by adopting matrix preconditioning strategy and utilizing parameter accelerating technique, we establish a class of *preconditioned alternating variable minimization with multiplier* (**PAVMM**) methods for iteratively solving the equality-constraint quadratic programming problem (1). This method includes the AVMM or the ADM method as special case. By making use of blockwise matrix transformation, from null space relationships of the involved

sub-matrices we discuss solvability of the equality-constraint quadratic programming problem (1)-(2) and give sufficient and necessary conditions for guaranteeing existence and uniqueness of its solution. By exploring an explicit formula about eigenvalues of the iteration matrix, we demonstrate asymptotic convergence property and analyze asymptotic convergence rate of the PAVMM method. By making use of matrix splitting, we also discuss an algebraic derivation of the PAVMM method, which shows that this method is actually a modified block Gauss-Seidel iteration method for solving the augmented linear system resulting from the weighted Lagrangian function with respect to the equality-constraint quadratic programming problem (1)-(2).

Bibliography

1. *K. Arrow, L. Hurwicz and H. Uzawa* Studies in Nonlinear Programming, *Stanford University Press*, Stanford, 1958.

2. *A.R. Bergen* Power Systems Analysis, *Prentice Hall*, Englewood Cliffs, New Jersey, 1986.

3. *J.T. Betts* Practical Methods for Optimal Control Using Nonlinear Programming, *SIAM*, Philadelphia, 2001.

4. *A. Bossavit* "Mixed" systems of algebraic equations in computational electromagnetics, *COMPEL*, 17(1998), 59-63.

5. *F. Brezzi and M. Fortin* Mixed and Hybrid Finite Element Methods, *Springer-Verlag*, New York and London, 1991.

6. *S. Boyd, N. Parikh, E. Chu, B. Peleato and J. Eckstein* Distributed optimization and statistical learning via the alternating direction method of multipliers, *Foundations Trends Machine Learning, 3(2010), 1-122.*

7. *L.O. Chua, C.A. Desoer and E.S. Kuh Linear and Nonlinear Circuits,* McGraw-Hill, *New York, 1987.*

8. *H.C. Elman and G.H. Golub Inexact and preconditioned Uzawa algorithms for saddle point problems,* SIAM J. Numer. Anal., *31(1994), 1645-1661.*

9. *J. Eckstein and D.P. Bertsekas On the Douglas-Rachford splitting method and the proximal point algorithm for maximal monotone operators,* Math. Program., *55(1992), 293-318.*

10. *J. Eckstein and M.C. Ferris Operator-splitting methods for monotone affine variational inequalities, with a parallel application to optimal control,* INFORMS J. Comput., *10(1998), 218-235.*

11. *M. Fortin and R. Glowinski Augmented Lagrangian Methods, Applications to the Numerical Solution of Boundary Value Problems,* North-Holland, *Amsterdam, 1983.*

12. *D. Gabay Applications of the method of multipliers to variational inequalities, in* Augmented Lagrangian Methods: Applications to the Numerical Solution of Boundary-Value Problems, *M. Fortin and R. Glowinski, eds., North-Holland, Amsterdam, 1983, Pages 299-331.*

13. *D. Gabay and B. Mercier A dual algorithm for the solution of nonlinear variational problems via finite element approximations,* Comput. Math. Appl., *2(1976), 17-40.*

14. *R. Glowinski and P. Le Tallec Augmented Lagrangian and Operator-Splitting Methods in Nonlinear Mechanics,* SIAM, *Philadelphia, 1989.*

15. *E. Haber and J. Modersitzki Numerical methods for volume-preserving image registration,* Inverse Problems, *20(2004), 1621-1638.*

16. *A. Hadjidimos and M. Lapidakis Optimal alternating direction implicit preconditioners for conjugate gradient methods,* Appl. Math. Comput., *183(2006), 559-574.*

17. *E.L. Hall Computer Image Processing and Recognition,* Academic Press, *New York, 1979.*

18. *D.-R. Han and X.-M. Yuan Local linear convergence of the alternating direction method of multipliers for quadratic programs,* SIAM J. Numer. Anal., *51(2013), 3446-3457.*

19. *B.-S. He and X.-M. Yuan On the $\mathcal{O}(1/n)$ convergence rate of the Douglas-Rachford alternating direction method,* SIAM J. Numer. Anal., *50(2012), 700-709.*

20. *P.L. Lions and B. Mercier Splitting algorithms for the sum of two nonlinear operators,* SIAM J. Numer. Anal., *16(1979), 964-979.*

21. *H.M. Markowitz Portfolio Selection: Efficient Diversification of Investments,* Wiley, *New York, 1959.*

22. *H.M. Markowitz and A.F. Perold Sparsity and piecewise linearity in large portfolio optimization problems, in* Sparse Matrices and Their Uses, *I.S. Duff, ed., Academic Press, London, 1981, Pages 89-108.*

23. *J. Modersitzki Numerical Methods for Image Registration,* Oxford University Press, *Oxford, 2003.*

24. *I. Perugia A field-based mixed formulation for the two-dimensional magnetostatic problem,* SIAM J. Numer. Anal., *34(1997), 2382-2391.*

25. *R.T. Rockafellar Augmented Lagrangians and applications of the proximal point algorithm in convex programming,* Math. Oper. Res., *1(1976), 97-116.*

26. *R.T. Rockafellar Monotone operators and the proximal point algorithm,* SIAM J. Control Optim., *14(1976), 877-898.*

27. R.T. Rockafellar and R. J.-B. Wets Variational Analysis, Springer-Verlag, *Berlin, 1998.*

28. R. Shefi and M. Teboulle Rate of convergence analysis of decomposition methods based on the proximal method of multipliers for convex minimization, SIAM J. Optim., *24(2014), 269-297.*

29. G. Strang Introduction to Applied Mathematics, Wellesley-Cambridge Press, *Wellesley, 1986.*

30. M. Tao and X.-M. Yuan On the $\mathcal{O}(1/t)$ convergence rate of alternating direction method with logarithmic-quadratic proximal regularization, SIAM J. Optim., *22(2012), 1431-1448.*

PARALLEL IMPLEMENTATION OF MODULUS-BASED MATRIX SPLITTING ITERATION METHOD FOR LINEAR COMPLEMENTARITY PROBLEMS

Zhong-Zhi Bai*, Li-Li Zhang**

* *State Key Laboratory of Scientific/Engineering Computing, Institute of Computational Mathematics and Scientific/Engineering Computing, Academy of Mathematics and Systems Science, Chinese Academy of Sciences, Beijing , P.R.China*

** *School of Mathematics and Information Science, Henan University of Economics and Law, Zhengzhou, P.R.China*

Many problems in scientific computing and engineering applications demand to compute solutions of linear complementarity problems. Such class of problems includes, for example, the convex quadratic programming, the bimatrix game, the free boundary problems of fluid dynamics, the network equilibrium problems, the contact problems, and so on. For given matrix $A \in \mathbb{R}^{n\times n}$ and vector $q \in \mathbb{R}^n$, the linear complementarity problem, abbreviated as LCP$(q,\ A)$, consists of finding a pair of vectors $r, z \in \mathbb{R}^n$ such that

$$r := Az + q \geq 0, \quad z \geq 0 \quad \text{and} \quad z^T(Az + q) = 0,$$

where z^T denotes the transpose of the vector z.

Bai proposed a class of modulus-based splitting iteration methods in [1] for solving the LCP$(q,\ A)$. This class of iteration methods is essentially based on an equivalent transformation of the LCP$(q,\ A)$ into a system of fixed-point equations involving only absolute value of certain vector. It not only includes as special cases the modulus-based relaxation methods such as Jacobi, Gauss-Seidel, SOR and AOR, but also provides a general framework for the existing modulus iteration methods. Theoretical analyses and numerical implementations have shown that the modulus-based relaxation methods are often superior to the projected relaxation methods.

This talk includes two parts. The one is about the synchronous parallel counterpart of the modulus-based splitting iteration method by making use of multiple splittings of the system matrix A. The other is about the two-stage multisplitting iteration method by employing the modulus-based matrix splitting iteration and its relaxed variants as inner iterations.

First, in order to suit computational requirements of the modern high-speed multiprocessor environments, we present the *modulus-based synchronous multisplitting* (**MSM**) iteration method by making use of multiple splittings of the system matrix A. Let (M_k, N_k, E_k) $(k = 1, 2, \ldots, \ell)$ be a multisplitting of the

system matrix A, Ω a positive diagonal matrix and γ a positive constant. Then, the **MSM** iteration method can be described as follows:

1. Choose an initial vector $x^{(0)} \in \mathbb{R}^n$, and set $m := 0$;

2. For $k = 1, 2, \ldots, \ell$, we solve the linear subsystem

$$(\Omega + M_k)x^{(m+1,k)} = N_k x^{(m)} + (\Omega - A)|x^{(m)}| - \gamma q,$$

on the k-th processor, and obtain the solution $x^{(m+1,k)}$;

3. By combining the local updates of ℓ processors together, we get

$$x^{(m+1)} = \sum_{k=1}^{\ell} E_k x^{(m+1,k)} \quad \text{and} \quad z^{(m+1)} = \frac{1}{\gamma}(|x^{(m+1)}| + x^{(m+1)});$$

4. If $z^{(m+1)}$ satisfies a prescribed stopping rule, then terminate. Otherwise, set $m := m + 1$ and return to 2.

This class of modulus-based synchronous multisplitting iteration methods only needs to solve sub-systems of linear equations rather than linear complementarity sub-problems. With special choices of the multiple splittings of the system matrix, we can obtain a sequence of modulus-based synchronous multisplitting relaxation methods, including Jacobi, Gauss-Seidel, SOR and AOR, respectively. When the system matrix A is an H_+-matrix, we prove the convergence of the modulus-based synchronous multisplitting iteration methods as well as their relaxed variants. Numerical results show that the modulus-based synchronous multisplitting Jacobi, Gauss-Seidel and SOR methods can achieve high parallel computing efficiency in actual implementations.

Second, in the matrix multisplitting iteration method discussed by Machida, Fukushima and Ibaraki in [2] and by Bai in [3], we have to spend a vast majority of time in solving the linear complementarity sub-problems exactly at each iteration step. For saving time, inner iteration can be introduced to solve them approximately. Thus, we present the two-stage multisplitting iteration method by employing the modulus-based matrix splitting iteration and its relaxed variants as inner iterations. Let $(M_k\colon F_k, G_k; N_k; E_k)$ $(1 \le k \le \ell)$ be a two-stage multisplitting of the matrix A. Then, the steps of the two-stage multisplitting iteration method are listed as follows:

1. Choose an initial vector $x^{(0)}$ and a positive constant γ. Set $m := 0$ and $z^{(0)} = \frac{1}{\gamma}(x^{(0)} + |x^{(0)}|)$.

2. Given $x^{(m)}$ and $z^{(m)}$. For each k $(1 \le k \le \ell)$, solve the LCP $(q^{(m,k)}, M_k)$, with $q^{(m,k)} := q - N_k z^{(m)}$, by employing the modulus-based matrix splitting

iteration method:

$$(\Omega + F_k)x^{(m,k,j+1)} = G_k x^{(m,k,j)} + (\Omega - M_k)|x^{(m,k,j)}| - \gamma q^{(m,k)}, \quad j = 0, 1, \ldots, l_k^{(m)} - 1, \tag{1}$$

with $x^{(m,k,0)} := x^{(m)}$. Here, Ω is a positive diagonal matrix.

3. Set $x^{(m+1)} = \sum_{k=1}^{\ell} E_k x^{(m,k,l_k^{(m)})}$, and $z^{(m+1)} = \frac{1}{\gamma}(x^{(m+1)} + |x^{(m+1)}|)$.

4. If $z^{(m+1)}$ satisfies a prescribed stopping rule, then terminate. Otherwise, set $m := m + 1$ and return to 2.

In order to solve (1) explicitly, we consider the classic *accelerated overrelaxation* (AOR) splitting $M_k = F_k - G_k$, i.e., the matrices F_k and G_k in (1) are of the forms

$$\begin{cases} F_k = \dfrac{1}{\alpha}\left(D_{M_k} - \beta L_{M_k}\right), \\ G_k = \dfrac{1}{\alpha}\left[(1-\alpha)D_{M_k} + (\alpha - \beta)L_{M_k} + \alpha U_{M_k}\right], \end{cases} \qquad 0 < \beta \leq \alpha,$$

where D_{M_k}, L_{M_k} and U_{M_k} are the diagonal, the strictly lower-triangular and the strictly upper-triangular matrices of the matrix M_k, respectively. In this case, the above two-stage iteration method gives the *two-stage multisplitting MAOR* (**TMMAOR**) iteration method. Specially, if $\alpha = \beta$, the TMMAOR iteration method reduces to the *two-stage multisplitting MSOR* (**TMMSOR**) iteration method, and if $\alpha = \beta = 1$, it further reduces to the *two-stage multisplitting MGS* (**TMMGS**) iteration method. And, if $\alpha = 1$ and $\beta = 0$, it is the *two-stage multisplitting MJ* (**TMMJ**) iteration method.

In the two-stage methods, the modulus-based matrix splitting iteration methods are used as inner iterations to solve the linear complementarity sub-problems inexactly. This makes the two-stage multisplitting iteration methods easier to be programmed and more economical in memory storage. Moreover, these two-stage multisplitting iteration methods are convergent for any number of inner iterations when the system matrix is an H_+-matrix. This makes these methods more flexible and effective than earlier similar methods in actual computation. Numerical experiments show that the two-stage multisplitting relaxation methods are superior to the matrix multisplitting iteration methods in computing time, and can achieve a satisfactory parallel efficiency. Numerical experiments also show that the computing time is the least for only a few inner iterations.

Bibliography

1. *Z.-Z. Bai* Modulus-based matrix splitting iteration methods for linear complementarity problems, Numer. Linear Algebra Appl., 17(2010), 917–933.

2. *N. Machida, M. Fukushima and T. Ibaraki* A multisplitting method for symmetric linear complementarity problems, J. Comput. Appl. Math., 62(1995), 217–227.

3. *Z.-Z. Bai* On the convergence of the multisplitting methods for the linear complementarity problem, SIAM J. Matrix Anal. Appl., 21(1999), 67–78.

CALLS FORECAST FOR THE MOSCOW AMBULANCE SERVICE. THE IMPACT OF WEATHER FORECAST

Bykov F.L.*, Gordin, V.A.**

* *Hydrometeocentre of Russia, Moscow, Russia*

** *Higher School of Economics, Hydrometeocentre of Russia, Moscow, Russia*

The number of calls to the ambulance service in Moscow is equal about 5 million per year. About two thirds of the calls lead to ambulance trips. We analyse here only such kind of the calls (NAT[1]). The function is noted as $Q(t)$. We considered it as a random process. Than we approximate the function by a cubic spline $\Psi_Q(t)$.

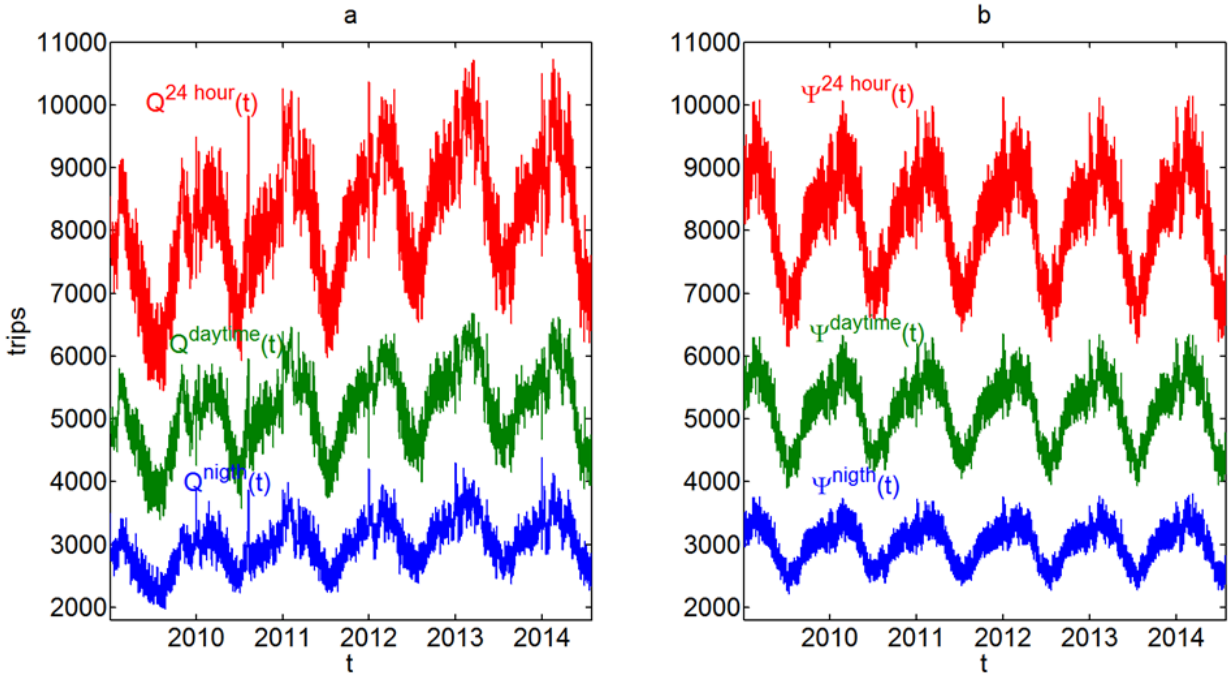

Figure 1. **a**. The long-term trend changes NAT $Q(t)$. **b**. Calculated typical NAT $\Psi_Q(t)$ – the 28 years periodic function, which depends only on the time of year and day of the week. It also shows daytime, night shifts and their sum. On the horizontal axis are marked on January 1.

We can use the function as a forecast of NAT, but the approach is not good; see the curves 1 on the Fig.2. We can realise the approach for various subgroups of diseases, too.

We used in the study the archives of the Ambulance Service in Moscow[2] as well as meteorological archives of the Hydrometeorological Center of Russia. We

[1]The number of the ambulance trips.

[2]The operative data about the calls are available on the site http://www.mos03.ru/about/about.php. We used the depersonalized database of trips during 2009-2013.

used an additional information about the air temperature $T(t)$ to improve the forecast of NAT, see the curves 2.

We use the known statistics of the calls for the current and previous days to predict them for tomorrow and for the following days. We assume that this algorithm will work operatively, will cyclically update the available information and will move the horizon of the forecast.

Sure, the accuracy of such forecasts depends on their lead time, and from a choice of some group of diagnoses. For comparison we used the error of the inertial forecast (tomorrow there will be the same number of calls as today). Our technology has demonstrated accuracy that is approximately two times better compared to the inertial forecast.

We obtained the following result: the number of calls depends on the actual weather in the city as well as on its rate of change. We were interested in the accuracy of the forecast for 12-hour sum of the calls in real situations. We evaluate the impact of the meteorological errors [Bagrov 2014] on the forecast errors of the number of Ambulance calls.

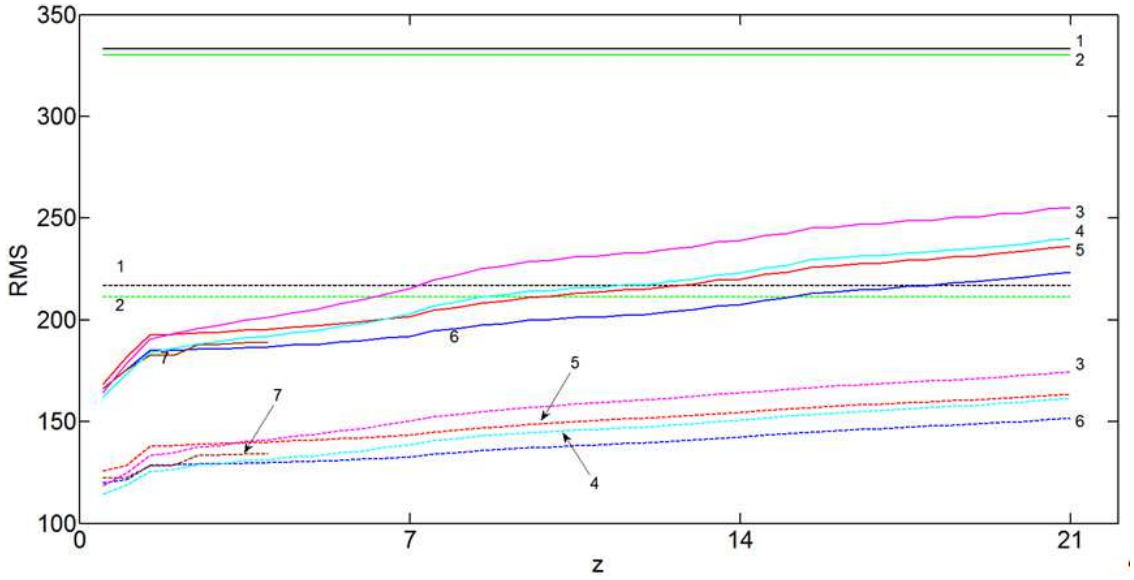

Figure 2. The RMS error of the forecast of the total NAT per 12 hours depending on the lead time z (days). Data is divided into daytime shifts (solid line) and night (dashed line). 1 – the deviation $Q(t)$ from $\Psi_Q(t)$. 2 – the deviation $Q(t)$ from $\Psi_{Q,T_{min},T_{max}}(t)$. 3 – the error of the forecast, which uses information about NAT from several previous days, but without separation into super-groups of diseases; the data about air temperature were ignored. 4 – forecast without separation onto super-groups of diseases, but with impact of the temperature. 5 – we use the separation onto super-groups A, B, C, and do not use air temperature. 6 – we use the separation onto super-groups A, B, C, and take into account the air temperature for our forecasting. Here the temperature was assumed to be known exactly for the curves 2, 4, and 6. Curves 7 describe the forecast which is similar to 6, but it use the forecasted air temperature with corresponding lead time [Bagrov 2014] instead of real air temperature.

The weather and the Ambulance calls number both have seasonal tendencies. Therefore, if we have medical information from one city only, we should separate

the impacts of such predictors as "annual variations in the number of calls" and "weather". We need to consider the seasonal tendencies (associated, e. g. with the seasonal migration of the population and government holidays), week periodicity, and the impact of the air temperature simultaneously, rather than sequentially.

We forecasted separately the number of calls with diagnoses of cardiovascular group, where it was demonstrated the advantage of the forecasting method, when we use the maximum daily air temperature as a predictor. We have a chance to evaluate statistically the influence of meteorological factors on the dynamics of medical problems. In some cases it may be useful for understanding of the physiology of disease and possible treatment options.

In future we are going to assimilate some personal archives of medical parameters for the individuals with concrete diseases and the relative meteorological archive. As a result we hope to evaluate how weather can influence the intensity of the disease. Thus, the knowledge of the weather forecast for several days will help us to predict a state of health. The person will be able to take some proactive actions to avoid the anticipated worsening of his health.

Bibliography

1. *A. N. Bagrov, F. L. Bykov, V. A. Gordin* Complex Forecast of Surface Meteorological Parameters. Meteorology and Hydrology, 2014, N 5, 5-16 (Russian), 283-291 (English).

2. *Bassil KL, Cole DC, Moineddin R, et al (2005)* The relationship between temperature and ambulance response calls for heat-related illness in Toronto, Ontario. J. Epidemiology Community Health 65(9):829-31.

3. *Bykov, Ph.L., Gordin, V.A.* Objective Analysis of the Structure of Three-Dimensional Atmospheric Fronts. Izvestia of Russian Academy of Sciences. Ser. The Physics of Atmosphere and Ocean, 48 (2) (2012), 172-188 (Russian), 152-168 (English), http://dx.doi.org/10.1134/S0001433812020053

4. *Chen Q, Wang J, Tian J, Tang X, Yu C, Marshall RJ, Chen D, Cao W, Zhan S, Lv J, Lee L, Hu Y (2013)* Association between ambient temperature and blood pressure and blood pressure regulators: 1831 hypertensive patients followed up for three years. PLoS One 8(12):e84522. doi: 10.1371/journal.pone.0084522

5. *Dolney TJ, Sheridan SC (2006)* The relationship between extreme heat and ambulance response calls for the city of Toronto, Ontario, Canada. Environ Res 101(1):94-103

6. *Goodwin J, Pearce VR, Taylor RS, Read KL, Powers SJ (2001)* Seasonal cold and circadian changes in blood pressure and physical activity in young and elderly people. Age Ageing 30(4):311-7

7. *V.A.Gordin* Mathematical Problems and Methods in Hydrodynamical Weather Forecasting. Amsterdam etc.: Gordon & Breach Publ. House, 2000, (English).

8. *V.A.Gordin* Mathematics, Computer, Weather Forecasting, and Other Mathematical Physics' Scenarios. Moscow, Fizmatlit, 2010, 2012 (Russian).

9. *Lin S, Luo M, Walker RJ, et al (2009)* Extreme high temperatures and hospital admissions for respiratory and cardiovascular diseases. Epidemiology 20:738-46

10. *Loughnan M, Tapper N, Loughnan T (2014)* The impact of "unseasonably" warm spring temperatures on acute myocardial infarction hospital admissions in Melbourne, Australia: a city with a temperate climate. J Environ Public Health, 483785. doi: 10.1155/2014/483785

11. *Makie T, Harada M, Kinukawa N, Toyoshiba H, Yamanaka T, Nakamura T, Sakamoto M, Nose Y (2002)* Association of meteorological and day-of-the-week factors with emergency hospital admissions in Fukuoka, Japan. Int J Biometeorol 46(1):38-41

12. *Murakami S, Miyatake N, Sakano N (2012)* Changes in air temperature and its relation to ambulance transports due to heat stroke in all 47 prefectures of Japan. J Prev Med Public Health 45(5):309-15. doi: 10.3961/jpmph.2012.45.5.309

13. *Priestley MB (1981)* Spectral Analysis and Time Series. Academic Press Schaffer A, Muscatello D, Broome R, Corbett S, Smith W (2012) Emergency department visits, ambulance calls, and mortality associated with an exceptional heat wave in Sydney, Australia, 2011: a time-series analysis. Environ Health 11(1):3. doi: 10.1186/1476-069X-11-3

14. *Sun X, Sun Q, Yang M, Zhou X, Li X, Yu A, Geng F, Guo Y (2014)* Effects of temperature and heat waves on emergency department visits and emergency ambulance dispatches in Pudong New Area, China: a time series analysis. Environ Health 13(1):76. doi: 10.1186/1476-069X-13-76

15. *Turner LR, Connell D, Tong S (2012)* Exposure to hot and cold temperatures and ambulance attendances in Brisbane, Australia: a time-series study. BMJ Open 2(4) doi: 10.1136/bmjopen-2012-001074

16. *Xie J, He M, Zhu W (2014)* Acute effects of outdoor air pollution on emergency department visits due to five clinical subtypes of coronary heart diseases in Shanghai, China. J Epidemiol 24(6):452-9.

THE SEMI-LAGRANGIAN FEM TO THE NAVIER-STOKES MODEL FOR VISCOUS INCOMPRESSIBLE FLUID[1]

Dementyeva E.V., Karepova E.D., Shaidurov V.V.
Institute of Computational Modeling SB RAS, Krasnoyarsk, Russia

The Navier-Stokes equations are of interest both itself and in combination with additional equations for more complex physical phenomena. At the same time, efficient and robust numerical methods for its solving is extremely challenged up to now.

In present talk the 2D system of the Navier-Stokes equations is considered for a viscous incompressible fluid in a channel Ω with Γ_{in}, Γ_{out} and Γ_{rigid} as inlet, outlet, and rigid sides boundary correspondence. On outlet boundary the modified "do nothing" boundary condition is imposed [1]. Its efficiency is shown by numerical experiments.

To construct a discrete analogue, we use a semi-Lagrangian approach to approximation of the transport derivatives [2]. In our case the set of transport derivatives is considered to be a (Lagrangian) first-order derivative along a given direction $\mathbf{l} = (1, u, v)$:

$$\frac{\partial f}{\partial t} + \underbrace{\frac{\partial}{\partial x}(fu) + \frac{\partial}{\partial y}(fv)}_{+\text{ incompressibility}} = \frac{\partial f}{\partial t} + u\frac{\partial f}{\partial x} + v\frac{\partial f}{\partial y} \equiv \frac{\partial f}{\partial \mathbf{l}},$$

which may be approximated by finite difference or inside the finite element method. Then we consider in a channel the following problem

$$\frac{\partial \mathbf{U}}{\partial \mathbf{l}} - \nu\Delta\mathbf{U} + \frac{1}{\rho_0}\nabla p = \mathbf{f},$$

$$\nabla \cdot \mathbf{U} = 0$$

under the conditions

$$\mathbf{U}(t,\mathbf{x}) = \mathbf{U}_{in} \quad \forall (t,\mathbf{x}) \in (0,T)\times\Gamma_{in}, \qquad \mathbf{U}(t,\mathbf{x}) = (0,0) \quad \forall (t,\mathbf{x}) \in (0,T)\times\Gamma_{rigid},$$

$$-\nu\partial_n\mathbf{U} + \frac{1}{\rho_0}p\mathbf{n} = \frac{1}{\rho_0}p_{ext}\mathbf{n} \quad \forall (t,\mathbf{x}) \in (0,T)\times\Gamma_{out}.$$

Here $\mathbf{U} = (u, v)$ is a velocity vector, p is a pressure, ν is a kinematic viscosity, ρ_0 is a constant density, $\mathbf{f} = (f_1, f_2)$ is a given vector of body forces.

We use combination of semi-Lagrangian approach to approximation of the transport derivatives and a conforming finite element method to approximation

[1]The work was supported by Russian Foundation of Fundamental Researches (grant 14-01-00296-a)

of other terms (namely, Stoks problem). Velocity components are approximated by biquadratic elements and the pressure does by bilinear elements on rectangles.

As a result of this combined approach, the stationary problem with a self-adjoint operator is obtained on each time level. This problem is numerically solved by the multigrid method which allows one to decrease the computational time.

The theoretical results are confirmed by numerical experiments.

Bibliography

1. *Rannacher R.* Incompressible Viscous Flow. In: Encyclopedia of Computational Mechanics, edited by E. Stein et al. New-York: Wiley, 2011.

2. *Pironneau O.* On the Transport-Diffusion Algorithm and Its Applications to the Navier-Stokes Equations // Numerische Mathematik. 1982. Vol. 38. P. 309-332.

FLEXIBLE GLOBAL GENERALIZED HESSENBERG METHODS FOR LINEAR SYSTEMS WITH MULTIPLE RIGHT-HAND SIDES[1]

Chuanqing Gu, Ke Zhang

Department of Mathematics, Shanghai University, Shanghai, P.R.China

A variant of the global generalized Hessenberg method is presented which allows varying preconditioning at each restart. Theoretical results that relate the residual norm of this new method with its original version are developed. As two special variants, the flexible global GMRES method and the flexible global CMRH method are investigated both theoretically and experimentally. Numerical examples are conducted to illustrate the performance of these two flexible global methods in comparison with both the original global methods and weighted global methods.

We consider the solution of large and sparse linear systems with multiple right-hand sides of the form

$$AX = B, \tag{1}$$

where $A \in \mathbb{R}^{n\times n}$ and $X, B \in \mathbb{R}^{n\times s}$ with usually $s \ll n$.

I The matrix Krylov subspace

For $X, Y \in \mathbb{R}^{n\times s}$, we define the Frobenius scalar product $(X, Y)_F = tr(X^T Y)$. Moreover, a system of matrices in $\mathbb{R}^{n\times s}$ is said to be F-orthogonal if it is orthogonal with respect to the product $(\cdot, \cdot)_F$.

The matrix Krylov subspace $\mathcal{K}_m(A, V)$ is spanned by V, AV, $\cdots$, $A^{m-1}V$, or equivalently, for any $W \in \mathcal{K}_m(A, V)$, we have

$$W = \sum_{i=1}^{m} \alpha_i A^{i-1} V, \tag{2}$$

where $V \in \mathbb{R}^{n\times s}$ and $\alpha_i \in \mathbb{R}$ for $i = 1, \cdots, m$. This is different from the block Krylov subspace exploited in the usual block methods. Associate with the matrix Krylov subspace is the product $*$ defined by

$$\mathscr{V}_m * x = \sum_{i=1}^{m} (x)_i V_i, \tag{3}$$

where $\mathscr{V}_m = [V_1, \cdots, V_m] \in \mathbb{R}^{n\times ms}$ and $x = [(x)_1, \cdots, (x)_m]^T \in \mathbb{R}^m$.

[1]The work is supported by Shanghai Natural Science Foundation (10ZR1410900), Key Disciplines of Shanghai Municipality (S30104) and Innovation Program of Shanghai Municipal Education Commission(13ZZ068)

II The global generalized Hessenberg methods with fixed preconditioning

We now consider a right preconditioning for the original linear system (1), namely,

$$AM^{-1}(MX) = B, \tag{4}$$

where M is an appropriate preconditioner. It should be noted that M^{-1} is solved from an equation instead of forming explicitly.

The Gl-GH process generates a matrix basis $\text{span}\{V_1, \cdots, V_m\}$ of the matrix Krylov subspace $\mathcal{K}_m(A, R_0)$ through the relations

$$V_1 = R_0/\beta \ \text{ and } \ (\bar{H}_m)_{i+1,i}V_{i+1} = AV_i - \sum_{j=1}^{i}(\bar{H}_m)_{j,i}V_j, \tag{5}$$

where β and $(\bar{H}_m)_{i+1,i}$ are scaling factors for $i = 1, \cdots, m$. Let $Y_1, \cdots, Y_m$ be linearly independent matrices, where $Y_i \in \mathbb{R}^{n\times s}$ for $i = 1, \cdots, m$. The scalars $(\bar{H}_m)_{j,i}$ in (5) are opted by imposing the orthogonality condition

$$V_{i+1} \perp_F Y_1, \cdots, Y_i, \quad i = 1, \cdots, m. \tag{6}$$

Using (5) and (6), we have

$$(\bar{H}_m)_{j,i} = \frac{(Y_j, U)_F}{(Y_j, V_j)_F} = \frac{tr(Y_j^T U)}{tr(Y_j^T V_j)},$$

where $U = AV_i - \sum_{j=1}^{i}(\bar{H}_m)_{j,i}V_j$. With the above relations, we sketch out the global generalized Hessenberg process with *fixed* preconditioning. Based on Algorithm 1, the global generalized Hessenberg method with fixed preconditioning for solving (4) can be presented as follows.

Algorithm 1. The Gl-GH process with fixed preconditioning.

1: $\beta = \|V\|, V_1 = V/\beta$;
2: **for** $i = 1, \cdots, m$ **do**
3: $\quad Z_i = M^{-1}V_i$; $\quad$ % inner process with a fixed preconditioner M
4: $\quad U = AZ_i$;
5: $\quad$ **for** $j = 1, \cdots, i$ **do**
6: $\quad\quad (\bar{H}_m)_{j,i} = tr(Y_j^T U)/tr(Y_j^T V_j)$; $U = U - (\bar{H}_m)_{j,i}V_j$;
7: $\quad$ **end for**
8: $\quad (\bar{H}_m)_{i+1,i} = \|U\|$; $V_{i+1} = U/(\bar{H}_m)_{i+1,i}$;
9: **end for**

Algorithm 2. Gl-GH: the global generalized Hessenberg method with fixed preconditioning.

1: Choose X_0 and compute $R_0 = B - AX_0$. Set $\beta = \|R_0\|, V_1 = R_0/\beta$;
2: Generate the block matrix $\mathscr{V}_m = [V_1, \cdots, V_m]$ from Algorithm 1. Update $X_m = X_0 + M^{-1}\mathscr{V}_m * y_m$, where $y_m = \arg\min_{y\in\mathbb{R}^m} \|\beta e_1 - \bar{H}_m y\|_2$ and $e_1 = [1, 0, \cdots, 0]^T \in \mathbb{R}^{m+1}$.
3: If converged then stop; otherwise set $X_0 = X_m$ and goto line 2.

III The global generalized Hessenberg methods with flexible preconditioning

In Algorithm 2, recall that the same preconditioner M is used throughout the iterations. On the contrary, if we employ flexible preconditioners M_i, that is, preconditioner changes at each step, then it can be expected the preconditioner will be improved from one step to the next with the newly information. This is the idea behind the main algorithm in this paper, i.e., the flexible global generalized Hessenberg method (FGl-GH) which is shown below. We are ready

Algorithm 3. FGl-GH: the flexible global generalized Hessenberg method.

1: Choose X_0 and the restarting frequency m.
2: Compute $R_0 = B - AX_0$. Set $\beta = \|R_0\|, V_1 = R_0/\beta$;
3: **for** $i = 1, \cdots, m$ **do**
4: $Z_i = M_i^{-1}V_i$; % inner process with a flexible preconditioner M_i
5: $U = AZ_i$;
6: **for** $j = 1, \cdots, i$ **do**
7: $(\bar{H}_m)_{j,i} = tr(Y_j^T U)/tr(Y_j^T V_j)$; $U = U - (\bar{H}_m)_{j,i}V_j$;
8: **end for**
9: $(\bar{H}_m)_{i+1,i} = \|U\|$; $V_{k+1} = U/(\bar{H}_m)_{i+1,i}$;
10: **end for**
11: Form $\mathscr{Z}_m = [Z_1, \cdots, Z_m]$ by solving an inner system at line 4. Update $X_m = X_0 + \mathscr{Z}_m * y_m$, where $y_m = \arg\min_{y\in\mathbb{R}^m} \|\beta e_1 - \bar{H}_m y\|_2$.
12: If converged then stop; otherwise set $X_0 = X_m$ and goto line 2.

to comment on Algorithm 3 in comparison with Algorithm 2. If $M_i \equiv M$, then Algorithm 3 reduces to Algorithm 2. Further, in Algorithm 3, we need to save an additional block matrix $\mathscr{Z}_m$, which presents the major difference between these two algorithms. As a result, a relation of the form holds:

$$A\mathscr{Z}_m = \mathscr{V}_{m+1} * \bar{H}_m, \tag{7}$$

where $\mathscr{V}_{m+1} = [V_1, \cdots, V_{m+1}]$ and $\mathscr{Z}_m = [Z_1, \cdots, Z_m]$.

NUMERICAL METHODS FOR SYSTEMS WITH COMPLEX MATRICES

Xue-Ping Guo

East China Normal University, Shanghai, China

Systems of nonlinear equations with complex symmetric Jacobian matrices can be derived in many practical problems, such as nonlinear waves, chemical oscillations, quantum mechanics, turbulence, and so on. we consider an effective and robust algorithm for solving large sparse systems of nonlinear equations

$$F(x) = 0, \tag{1}$$

where $F : \mathbb{D} \subset \mathbb{C}^n \to \mathbb{C}^n$ is nonlinear and continuously differentiable. The Jacobian matrix of $F(x)$ is large, sparse and complex symmetric, i.e.,

$$F^{'}(x) = W(x) + iT(x)$$

satisfies $W(x)^T = W(x)$, $T(x)^T = T(x)$. Moreover, matrices $W(x)$ and $T(x)$ are real positive definite and real positive semi-definite matrices, respectively.

By making use of the special structure of the coefficient matrix A , Bai et al. in [2] derived a modification of the well-known HSS iteration method [4], i.e., MHSS. In order to further accelerate the convergence rate of MHSS, Bai et al. in [3] preconditioned the complex symmetric linear system by choosing a symmetric positive definite matrix $V \in \mathcal{R}^{n\times n}$. The new splitting iteration method can be described as follows.

The PMHSS iteration method

Let $x_0 \in \mathbb{C}^n$ be an arbitrary initial guess. Compute x_{k+1} for $k = 0, 1, 2, \cdots$ using the following iteration scheme until $\{x_k\}$ converges,

$$\begin{cases} (\alpha I + W)x_{k+\frac{1}{2}} = (\alpha I - iT)x_k + b, \\ (\alpha I + T)x_{k+1} = (\alpha I + iW)x_{k+\frac{1}{2}} - ib, \end{cases} \tag{2}$$

where α is a given positive constant and $V \in \mathcal{R}^{n\times n}$ is a prescribed symmetric positive definite matrix.

By making use of the preconditioned modified Hermitian and skew-Hermitian splitting (PMHSS) iteration as the inner solver to approximately solve the Newton equations, we establish the modified Newton-PMHSS method.

The local convergence properties under the Hölder continuous condition are analyzed and numerical results are given to confirm the effectiveness of our method.

The modified Newton-PMHSS method(MN-PMHSS)

1. Given an initial guess x_0, positive constants α and tol, and two positive integer sequences $\{l_k\}_{k=0}^{\infty}$, $\{m_k\}_{k=0}^{\infty}$;

2. For $k = 0, 1, \cdots$ until $\|F(x_k)\| \leq tol\|F(x_0)\|$ do:

2.1. Set $d_{k,0} = h_{k,0} = 0$;

2.2. For $l = 0, 1, \cdots, l_k - 1$, apply Algorithm PMHSS to the linear system:

$$\begin{cases} (\alpha V(x_k) + W(x_k))d_{k,l+\frac{1}{2}} = (\alpha V(x_k) - iT(x_k))d_{k,l} - F(x_k), \\ (\alpha V(x_k) + T(x_k))d_{k,l+1} = (\alpha V(x_k) + iW(x_k))d_{k,l+\frac{1}{2}} + iF(x_k), \end{cases}$$

and obtain d_{k,l_k} such that

$$\|F(x_k) + F^{'}(x_k)d_{k,l_k}\| \leq \eta_k\|F(x_k)\| \quad for \quad some \quad \eta_k \in [0, 1). \tag{3}$$

2.3. Set $y_k = x_k + d_{k,l_k}$.

2.4. Compute $F(y_k)$.

2.5. For $m = 0, 1, \cdots, m_k - 1$, apply Algorithm PMHSS to the linear system:

$$\begin{cases} (\alpha V(x_k) + W(x_k))h_{k,m+\frac{1}{2}} = (\alpha V(x_k) - iT(x_k))h_{k,m} - F(y_k), \\ (\alpha V(x_k) + T(x_k))h_{k,m+1} = (\alpha V(x_k) + iW(x_k))h_{k,m+\frac{1}{2}} + iF(y_k), \end{cases}$$

and obtain h_{k,m_k} such that

$$\|F(y_k) + F^{'}(x_k)h_{k,m_k}\| \leq \tilde{\eta}_k\|F(y_k)\| \quad for \quad some \quad \tilde{\eta}_k \in [0, 1). \tag{4}$$

2.6. Set $x_{k+1} = y_k + h_{k,m_k}$.

Bibliography

1. *I. S. Aranson and L. Kramer* The world of the complex Ginzburg-Landau equation, Rev. Mod. Phys., 74(2002), pp: 99–143.

2. *Z.-Z. Bai, M. Benzi and F. Chen* Modified HSS iteration methods for a class of complex symmetric linear systems, Computing, 87(2010), pp: 93–111.

3. *Z.-Z. Bai, M. Benzi and F. Chen* On preconditioned MHSS iteration methods for complex symmetric linear systems, Numer. Algor., 56(2011), pp: 297–317.

4. *Z.-Z. Bai, G. H. Golub and M. K. Ng* Hermitian and skew-Hermitian splitting method for non-Hermitian positive-definite linear systems, SIAM J. Matrix Anal. Appl., 24(2003), pp: 603–626.

5. *Z.-Z. Bai, G. H. Golub and J.-Y. Pan* Preconditioned Hermitian and skew-Hermitian splitting method for non-Hermitian positive-definite linear systems, Numer. Math., 98(2004), pp: 1–32.

6. *Z.-Z. Bai, G. H. Golub and C.-K. Li*, Convergence properties of preconditioned Hermitian and skew-Hermitian splitting method for non-Hermitian positive-definite linear systems, Math. Comput., 76(2007), pp: 287–298.

7. *Z.-Z. Bai, G. H. Golub, L.-Z. Lu and J.-F. Yin* Block triangular and skew-Hermitian splitting methods for positive-definite linear systems, SIAM J. Sci. Comput., 26(2005), pp: 844–863.

8. *Z.-Z. Bai, G. H. Golub and C.-K. Li* Optimal parameter in Hermitian and skew-Hermitian splitting method for certain two-by-two block matrices, SIAM J. Sci. Comput., 28(2006), pp: 583–603.

9. *Z.-Z. Bai and G. H. Golub* Accelerated Hermitian and skew-Hermitian splitting iteration methods for saddle-point problems, IMA J. Numer. Anal., 27(2007), pp: 1-23.

10. *Z.-Z. Bai and X.-P. Guo* On Newton-HSS method for systems of nonlinear equations with positive-definite Jacobian matrices, J. Comput. Math., 28(2010), pp: 235–260.

11. *M. Benzi, M. J. Gander and G. H. Golub* Optimization of the Hermitian and skew-Hermitian splitting iteration for saddle-point problems, BIT Numer. Math., 43(2003), pp: 881–900.

12. *T. Bohr, M. H. Hensen, G. Paladin and A. Vulpiani* Dynamical Systems Approach to Turbulence, Cambridge University Press, 1998.

13. *M.-H. Chen, R.-F. Lin and Q.-B. Wu* Convergence analysis of the modified Newton-HSS method under the Hölder continuous condition, J. Comput. Appl. Math., 264(2014), pp: 115-130.

14. *M. T. Darvishi and A. Barati* A third-order Newton-type method to solve systems of nonlinear equations, Appl. Math. Comput., 187(2007), pp: 630–635.

15. *R. S. Dembo, S. C. Eisenstat and T. Steihaug* Inexact Newton methods, SIAM J. Numer. Anal., 19(1982), pp: 400–408.

16. *S. C. Eisenstat and H. F. Walker* Globally convergent inexact Newton methods, SIAM J. Optim. 4(1994), pp: 297–330.

17. *X.-P. Guo* On semilocal convergence of inexact Newton methods, J. Comput. Math., 25(2007), pp: 231–242.

18. *X.-P. Guo and I. S. Duff* Semilocal and global convergence of the Newton-HSS method for systems of nonlinear equations, Numer. Linear Algebra Appl., 18(2011), pp: 299–315.

19. *C. T. Kelley* Iterative Methods for Linear and Nonlinear Equations, SIAM Philadelphia, 1995.

20. *Y. Kuramoto* Chemical Oscillations, Waves, and Turbulence, Dover Publications, Inc., Mineola, New York, 2003.

21. *J. M. Ortega and W. C. Rheinbolt* Iterative Solution of Nonlinear Equations in Several Variables, Academic Press, NewYork, 1970.

22. *Y. Saad* Iterative Methods for Sparse Linear Systems, The 2nd edn., SIAM Philadelphia, 2003.

23. *C. Sulem and P. L. Sulem* The Nonlinear Schrödinger Equation, Self-focusing and Wave Collapse, Springer Verlag, New York, 1999.

24. *Q.-B. Wu and M.-H. Chen* Convergence analysis of modified Newton-HSS method for solving systems of nonlinear equations, Numer. Algor., 64(2013), pp: 659-683.

25. *A.-L. Yang and Y.-J. Wu* Newton-MHSS methods for solving systems of nonlinear equations with complex symmetric Jacobian matrices, Numer. Algebra, Control and Optimization, 2(2012), pp: 839–853.

ON THE COMPUTATION OF THE INVERSE STURM-LIOUVILLE PROBLEM IN IMPEDANCE FORM

Huang Zhengda

School of Mathematical Science, Zhejiang University, China

This is a report of our group's work on the application of numerical algebra methods in the computation of the inverse Sturm-Liouville problem in impedance form.

The inverse Sturm-Liouville problem in impedance form considered here is to recover the unknown impedance function $a(x) > 0$ on $[0, 1]$ in the equation,

$$(a(x)y(x)')' + \lambda a(x)y(x) = 0, \qquad 0 < x < 1, \tag{1}$$

with Dirichlet boundary conditions

$$y(0) = y(1) = 0. \tag{2}$$

Problem 1: Given the first n eigenvalues, $\lambda_1 < \lambda_2 < \cdots < \lambda_n$, of (1) with boundary conditions (2), we seek an approximation to the impedance $a(x)$.

Since the impedance can only be determined up to a multiplicative constant, it will be assumed in what follows that the normalization

$$a(\xi) = 1 \tag{3}$$

for some $\xi \in [0, 1]$.

Over the mesh

$$0 = x_0 < x_1 < x_2 < \cdots < x_K < x_{K+1} = 1, \qquad x_i = ih,\ h = \frac{1}{K+1}, \tag{4}$$

where K is a undetermined positive integer, (1) is approximated by difference equations

$$a_i y_{i-1} - (a_i + a_{i+1})y_i + a_{i+1}y_{i+1} = -\Lambda h^2 y_i(a_i + a_{i+1})/2, \qquad i = 1, 2, \ldots, K \tag{5}$$

with

$$y_0 = 0,\ y_{K+1} = 0, \tag{6}$$

where $y_i \approx y(x_i)$, $\Lambda \approx \lambda$, and $a_i \approx a(x_i - h/2)$ for $i = 1, 2, \ldots, K+1$.

The matrix form of (5) and (6) can be

$$BY = \Lambda DY, \tag{7}$$

where $Y = (y_1, y_2, \ldots, y_K)^T$, D, a diagonal matrix, and B, a tridiagonal matrix, are determined by $a_i, i = 1, 2, \cdots, K$.

Two cases, without and with the symmetric assumption for the impedance, are considered.

For the case without the symmetric assumption, we choose $\xi = 0$ and $K = N$ a suitable positive integer, and seek a least square approximation $a(x) \in 1 + span\{\phi_1(x), \phi_2(x) \cdots, \phi_m(x)\}$, where $\{\phi_i(x)\}_{i=1}^m$ are appropriately chosen basis functions. In other words, $a(x)$ is in the form of

$$a(x) = 1 + \sum_{i=1}^{m} \phi_i(x).$$

Let $\phi_0(x) = 1$ and $c_0 = 1$, then (7) is changed to

$$\big(\sum_{i=1}^{m} c_k B_k\big) Y(\mathbf{c}) = \Lambda(\mathbf{c}) \big(\sum_{i=1}^{m} c_k D_k\big) Y(\mathbf{c}),$$

where $\mathbf{c} = (a_1, c_2, \ldots, c_m)^T$, $\Lambda(\mathbf{c}) \approx \lambda$ and $Y(\mathbf{c}) = (y_1, y_2, \ldots, y_N)^T$, B_i and D_i are diagonal and tridiagonal matrices $i = 1, 2, \cdots, N$.

Now **Problem** 1 for the case without symmetric assumption is transferred to

Problem 2**:** Given the first n eigenvalues, $\lambda_1 < \lambda_2 < \cdots < \lambda_n$, we find $\mathbf{c} \in R^m$ such that the function

$$G(\mathbf{c}) = \sum_{i=1}^{n} (\Lambda_i(\mathbf{c}) + \varepsilon(i, h) - \lambda_i)^2$$

is minimized, where

$$\varepsilon(i, h) = i^2\pi^2 - 4\frac{sin^2(\frac{i\pi h}{2})}{h^2}, \quad i = 1, 2, \cdots, n$$

are corrections (or regular conditions or preconditioners) which will improve accuracies in numerical computations.

Three methods are constructed to solve **Problem** 2. Firstly, by solving the equation

$$\frac{d\mathbf{c}(t)}{dt} = -\nabla G(\mathbf{c})$$

numerically with the fourth order Runge-Kutta method we get the descent flow method, where $\mathbf{c}(t)$ is called the steepest descent flow on R^m for $G(\mathbf{c})$ and t is a certain artificial parameter.

Secondly, let P be a positive matrix. By solving the equation

$$\frac{d\mathbf{c}(t)}{dt} = -P\nabla G(\mathbf{c})$$

numerically with the fourth order Runge-Kutta method combined with BFGS's method we obtain a modified descent flow method.

Thirdly, by solving Problem 2 with ULM-Newton like method combined with the descent flow method above, we construct a ULM-like descent flow method.

For the case of the symmetric impedance, let $K = 2n + 1$. Since the impedance function $a(x)$ is assumed to be symmetric, we have

$$a_i = a_{2n+3-i}, \qquad i = 1, 2, \ldots, n+1,$$

and let $a_{n+1} = 1$ for matching the normalization (3). Then (7) can be substituted with

$$B(\mathbf{a})Y(\mathbf{a}) = \Lambda(\mathbf{a})D(\mathbf{a})Y(\mathbf{a}), \tag{8}$$

where $\mathbf{a} = (a_1, a_2, \ldots, a_n)^T$, and $D(\mathbf{a})$ is a positive definite matrix since $a_i > 0$ for all $i = 1, 2, \ldots, n$.

Now **Problem** 1 is transferred to

Problem 3: Given the first n eigenvalues, $\lambda_1 < \lambda_2 < \cdots < \lambda_n$, we seek based on (8) a n-vector $\mathbf{a}$ whose i-th component, $i = 1, \ldots, n$, is a good approximation to $a((i - 1/2)h)$, where $h = 1/(2n + 2)$.

Define $\mathbf{f}: R^n \to R^n$ by

$$(\mathbf{f}(\mathbf{a}))_i = \Lambda_i(\mathbf{a}) + \varepsilon(i, h) - \lambda_i, \qquad i = 1, 2, \ldots, n, \tag{9}$$

where

$$\varepsilon(i, h) := i^2\pi^2 - 2\frac{1 - \cos(i\pi h)}{h^2}, \ i = 1, 2, \cdots, n$$

are corrections (or regular conditions, preconditioners) too. Then **Problem** 3 may be solved by computing the zeros of the nonlinear equation

$$\mathbf{f}(\mathbf{a}) = 0. \tag{10}$$

We use the simple Newton's method

$$\mathbf{f}'(0)(\mathbf{a_{k+1}} - \mathbf{a_k}) = -\mathbf{f}(\mathbf{a_k}),$$

where the initial approximation $\mathbf{a_0}$ is chosen with all entries equal and $\mathbf{f}'(0) =$ is the nonsingular Jacobian matrix of $\mathbf{f}$ at $\mathbf{a} = \mathbf{a_0}$ with entries

$$[\mathbf{f}'(0)]_{ij} = \frac{2\cos((2j-1)i\pi h)(1 - \cos(2i\pi h))}{h}, \qquad i,\ j = 1, 2, \ldots, n.$$

We have for $n \in N$ if there exists a constant $C(n) > 0$ such that $\|\frac{a'(x)}{a(x)}\|_2 < C(n)$ and $\mathbf{a_k}$ is positive for each k, then the sequence generated by the simple Newton's method with $\mathbf{a_0}$, which is chosen with all entries equal, converges to a solution of (10).

Numerical examples for smooth, non-smooth and discontinuous impedance functions are performed to show the efficiency of these methods.

USING COMPUTER ALGEBRA SYSTEM FOR THE STABILITY ANALYSIS OF NONLINEARLY ELASTIC CYLINDER WITH INTERNAL STRESSES[1]

Karyakin M.I., Shubchinskaya N. Y.
Southern Federal University, Rostov-on-Don, Russia

Introduction. The concept of internal, or residual, stresses existing in solids that are free from external loads was appeared firstly in the works of V.Volterra [1] at the beginning of the XX century. One particular reason of such stresses could be the existence of isolated linear defects, well known due to A.Love [2] terminology as Volterra dislocations. The idea of dislocation as a linear defect of the crystal lattice arose in physics much later – in the thirties of the last century [3]. The concept of disclinations (rotational defects or rotary dislocations) appeared even later though having found practical confirmation not only in lattices but in different various material structures either [4–5].

Simulation of dislocation within the continuum description is quite wide and rapidly developing branch of modern mechanics. A significant contribution to its development was made by the Rostov-on-Don school of mechanics, some results of the work of which had been presented in [6], particularly in matters related to the generalization of the theory of elastic dislocations and disclinations to the nonlinear case.

Isolated screw dislocation was the object rather "convenient" for the study within the framework of the nonlinear continuum mechanics, since the corresponding stress-strain state is described by a function of the radial coordinate, namely the function of radial displacement of the points of the cylinder. Various aspects of this problem, including the elimination of singularities at the axis of dislocation, the existence of discontinuous solutions etc. for incompressible media were considered, for example, in [7]. In this paper we consider the equilibrium and stability of nonlinear elastic cylinder with a screw dislocation in the case of a compressible material. The influence of defect formation on the length of the load-free cylinder was studied. Some questions of the stability of the expansion and contraction processes were discussed.

The main method used for this analysis is so-called "semi-inverse" method when the nonlinear boundary value problem of equilibrium is formulated by means of pre-determined semi-inverse representation of deformation. When applicable this method reduces 3D problem to the BVP of smaller dimension. Despite rather narrow area of usage – simple geometric deformations of canonic-shaped bodies – this method could deliver answers for many fundamental questions of qualitative and quantitative behavior of essentially nonlinear problems' solutions. It is quite effective in analysis of standard experiments – stretching, torsion, bending etc. – which are carried out while studying new materials and developing new

[1]Supported by Russian Ministry of Education and Research, project 9.665.2014/K

models of nonlinear behavior for real-life materials. This method is very algorithmic but for many specific strain energy analytical derivation of boundary value problem is excessively hard and not always reliably.

Within the framework of computer algebra system Maple an interactive program package for analysis of nonlinear elastic problems has been developed [8]. This package is based upon the semi-inverse method and includes set of algorithms of automatic generation of boundary-value problems of equilibrium, in Cartesian as well as in orthogonal curvilinear co-ordinate systems. The goal of the package is full computer automation of semi-inverse method and so releasing the researcher from cumbersome analytic derivation routine. Computer algebra system Maple have been chosen as a shell due to combining powerful and reliable analytic transformation tools, effective algorithms and variety of graphic representation of results.

To analyze the stability the bifurcation approach was used that based on linearization of the equilibrium equations in the neighborhood of the obtained solutions. The bifurcation point was defined as such value of the "loading" parameter (Burgers vector magnitude, stretch ratio or other strain characteristic) for which the linearized problem has a nontrivial solution. Numerical determination of the bifurcation points was based on the analysis of the homogeneous linear boundary value problem of sixth order whose coefficients expressed through the radial displacement function and its derivative. The similar problem of compression was used for verification purposes. Some extensions of the package [8] for stability analysis were used to obtain numerical results presented hereafter.

The equilibrium of the cylinder with a screw dislocation. The appearance of a screw dislocation in the cylinder is described by the following semi-inverse representation:

$$R = P(r),\ \Phi = \varphi + \psi z,\ Z = \gamma z + a\varphi, \tag{1}$$

where $\{R, \Phi, Z\}$, $\{r, \varphi, z\}$ – cylindrical coordinates of the actual and reference configuration, respectively, stretch ratio γ describes changing of the cylinder length, $a = |b|/2\pi$ – dislocation parameter, b – Burgers vector, $P(r)$ – function of radial displacement of points of the cylinder. Since the formation of dislocation may be accompanied by twisting [9, 10], parameter ψ – twist angle per unit length of the cylinder – was introduced in the semi-inverse representation (1).

Given a semi-inverse representation (1) all tensorial characteristics of strain could be determined, namely deformation gradient C, Cauchy-Green strain measure G, and its invariants $I_k, k = 1, 2, 3$ [11]. After setting up the specific potential energy function W, the equilibrium equations for Piola stress tensor D can be written as follows

$$div\, D = 0. \tag{2}$$

We will limit our considerations by the simple boundary conditions on the lateral surface of the cylinder

$$e_r \cdot D = 0, \tag{3}$$

meaning no applied loads there; $\{e_r, e_\varphi, e_z\}$ – orthonormal basis in a cylindrical coordinate system of reference configuration. By using (1) problem (2)–(3) is reduced to a boundary value problem for an ordinary differential equation of second order for the function $P(r)$.

To describe the mechanical properties of the cylinder we will use two models of compressible medium, i.e. two specific energy functions.

$$W = \lambda \frac{1}{2} I_1^2 (U - E) + \mu I_1 \left[(U - E)^2 \right], \tag{4}$$

and

$$W = \mu \frac{1}{2} (1 - \beta) \left[I_2 I_3^{-1} + \frac{1}{\alpha} (I_3^\alpha - 1) - 3 \right] + \mu \frac{1}{2} \beta \left[I_1 + \frac{1}{\alpha} \left(I_3^{-\alpha} - 1 \right) - 3 \right] \tag{5}$$

Model (4) is known as harmonic material, while Eq. (5) presents Blatz and Ko material. In (4)–(5) $U = G^{1/2}$ – distortion tensor, $\lambda, \mu, \beta, \alpha$ - material parameters. In the case of small strains parameter α is associated with Poisson ratio by relation $\alpha = \nu/(1 - 2\nu)$.

Investigation of the stability of the cylinder under tension or compression should obviously begin with an analysis of the "proper" length of the cylinder, due to the formation of dislocations. Following the scheme presented in [12], it is convenient to introduce following representations of axial force Q and twisting moment Min the form:

$$Q = \iint_S D_{zZ} dS \tag{6}$$

$$M = \iint_S D_{z\Phi} R dS. \tag{7}$$

Consider firstly the case of non-twisted cylinder assuming $\psi = 0$ in (1). Then, following the scheme in [12], from the condition $Q = 0$ we obtain the dependence between the stretch factor γ and dislocation parameter a. For the case of harmonic material (4) numerical calculations show that the dislocation formation in the cylinder always leads to its shortening. For the model (5) the situation is more complicated: the cylinder can be shortened or stretched depending on the parameter β. These results are consistent with the asymptotic formulas given in [12].

To analyze the cylinder with free ends both parameters γ and ψ should be considered as varying, wherein to determine these parameters it is necessary to vanish the axial force (6) and twisting moment (7). Calculations show that change of length is not monotonic for values α close to 0.5, which corresponds to a Poisson ratio $\nu = 1/4$; the cylinder is shortened for all other considered values of parameter α. Analysis of the loading diagrams show that for different values of parameter α corresponding curve has the maximum point, followed by a decreasing segment. Such segment may indicate a stability loss of the cylinder at tension.

Stability analysis. Let us give small displacements to all points of the cylinder from the known equilibrium state by changing the semi-inverse representation (1):

$$\begin{cases} R = P(r) + \varepsilon U_1(r, \varphi, z), \\ \Phi = \varphi + \psi z + \varepsilon U_2(r, \varphi, z), \\ Z = \gamma z + a\varphi + \varepsilon U_3(r, \varphi, z), \end{cases} \tag{8}$$

ε – small parameter, $U_k, k = 1, 2, 3$ – new unknown functions. The linearization process is reduced to computation following expressions for all strain characteristics

$$\overset{\circ}{F} = \frac{d}{d\varepsilon} F(R_0 + \varepsilon w)\,|_{\varepsilon=0}. \tag{9}$$

Here R_0 – the radius vector of the known equilibrium position, w – vector of small displacements expressed in terms of the unknown functions. Finally, by linearizing Piola stress tensor we change the original nonlinear problem (2)–(3) by its linearized version:

$$div \overset{\circ}{D} = 0, \tag{10}$$

$$e_r \cdot \overset{\circ}{D} = 0. \tag{11}$$

Equations (10) are linear partial differential equations of second order with respect to the unknown functions U_k. System (10)–(11) admits solution in the form

$$\begin{aligned} U_1(r, \varphi, z) &= u_1(r) \cos(n\varphi + bz), \\ U_2(r, \varphi, z) &= u_2(r) \sin(n\varphi + bz), \\ U_3(r, \varphi, z) &= u_3(r) \sin(n\varphi + bz), \end{aligned} \tag{12}$$

where $b = \pi m/l$; $n, m \in N$; l – initial length of the cylinder.

The substitution (12) turns the system (10)–(11) into a linear boundary value problem for a system of three ordinary differential equations of second order in relation to $u_k(r)$. Detailed scheme of analysis of the existence of non-trivial solutions for such systems was described in [13]. Analysis of typical bifurcation curves was performed for both material models as well as for compression and for tension. Instability of sufficiently long cylinder at compression occurs by the mode $(n, m) = (1, 1)$, at tension – by the mode $(n, m) = (0, 1)$, i.e. by axially symmetric mode. It can be seen in particular that the effect of dislocation on buckling during compression is much more important than in tension. One specific feature of Blatz and Ko model is non-monotonic character of the bifurcation curve at tension that appears to be connected with the inverse Poynting effect [14].

Bibliography

1. *Volterra V.* Sur l'equilibre des corps elastiques multiplement connexes // Annales de l'Ecole Norm. Sup. 1907. Vol. 24, no. 3. P. 401–517

2. *Love A. E. H.* A Treatise on the Mathematical Theory of Elasticity. Cambridge University Press, 2011. 583 p.

3. *Hirth J. P., Lothe J.* Theory of dislocations. Krieger Pub Co; Reprint edition, 1992. 872 p.

4. *Freid E., Todres R. E.* Prediction of disclinations in nematic elastomers // Proc. Natl. Acad. Sci. USA. Dec 18, 2001; 98(26). P. 14773–14777.

5. *Romanov A.E., Vladimirov V. I.* Dislclination in Crystals. Leningrad. Nauka, 1986. 224 p. [in Russian]

6. *Zubov L. M.* Nonlinear theory of dislocations and disclinations in elastic bodies. Berlin, Heidelberg: New-York et al: Springer-Verlag, 1997. 205 p.

7. *Zubov L. M. Volterra dislocations in nonlinear elastic solids* Doklady Akademii Nauk (Proceedings of the Russian Academy of Sciences). 1986. Vol. 287. N 3. P. 579–582.

8. *Gavrilyachenko, T.V., Karyakin, M.I., Sukhov, D.Yu.* Designing of the interface for nonlinear boundary value problem solver using Maple // Proceedings of ICCSA 2008. IEEE Computer Society, Los Alamitos-Washington-Tokyo. P. 284–291.

9. *Eshelby J.* The Continuum Theory of Lattice Defects, *in Frederick Seitz & David Turnbull*, ed., 'Advances in Research and Applications'. Academic Press, 1956. P. 79–144.

10. *Guba, A.V., Zubov, L.M.* Torsion of prismatic elastic bodies containing screw dislocations // Journal of Applied Mathematics and Mechanics. 2002. Vol. 66, Issue 2. P. 307–315.

11. *Lurie A. I.* Nonlinear Theory of Elasticity. North-Holland, Amsterdam. 1990. 617 pp.

12. *Karyakin M. I., Pozdnyakov I. V., Pustovalova O. G., Shubchinskaya N. Y.* On Deformed State of Nonlinearly-Elastic Cylinder with Internal Stresses// Proceedings of the higher educational institutions, North Caucasus region. 2013. Vol 6 (178). P. 46–51. [in Russian]

13. *Karyakin M. I., Sukhov D. Y., Shubchinskaya N. Y.* On an features of a bending of elastic panel with large strains // Ecological Bulletin of Research Centers of the Black Sea Economic Cooperation. 2012. Vol 4. P. 69–75. [in Russian]

14. *Zubov L. M.* Direct and Inverse Poynting Effects in Elastic Cylinders // Doklady Physics, 2001. N 9. P. 675–677.

NUMERICAL SOLUTION OF STEADY CONVECTION-DIFFUSION EQUATION IN COMPRESSIBLE MEDIUM[1]

L. A. Krukier, B. L. Krukier

Southern Federal University, Institute of MM and CS SFU, Rostov-on-Don, Russia

Introduction

The convection-diffusion-reaction (CDR) equation is the base for mathematical modeling in many fields of science and engineering. But up to now the main attention of researchers has been connected with convection-diffusion (CD) problems and their numerical solution [11]. The most difficult problems for numerical solution of CD equation are [23]:

1. diffusion is quite small which means that the dimensionless parameter $Pe > 10^3$,

2. the field of velocity has stagnation points,

Many different approaches have been proposed [15], [19], [23] to resolve the difficulties - exponential fitting, compact differences, upwinding, streamline diffusion [5], artificial viscosity and so on. Approximation of the first order derivatives in CD is the most interesting moment of the solution for problem and very important work. It is well known [22], [15] that using for approximation first order derivatives upwind schemes gives us linear equation systems with M-matrix [21], but matrix which can be obtained by using central FD schemes [6] is positive real. Each of these schemes have their own advantages and deficiencies which have been discussed in [23], [15].

When CRD equations investigate it is necessary to take into account the sign of reaction coefficient. If it is nonnegative than there is no problem with numerical solution, but if it is negative than the difficulties can arise. So if the negative coefficient reaction exists in CDR equation it means that after approximation it moves spectra of arising matrix in the left half part and matrix can lose property of being positive real. So, there is one more difficulty added to CDR equation in this case:

3. the coefficient of reaction is negative.

Consider the convection-diffusion-reaction equation written in symmetric form [10] in bounded domain $\Omega = [0,1] \times [0,1]$ with boundary condition:

$$-\tfrac{1}{Pe}\Delta C + \tfrac{1}{2}\left(u\tfrac{\partial C}{\partial x} + \tfrac{\partial (uC)}{\partial x} + v\tfrac{\partial C}{\partial y} + \tfrac{\partial (vC)}{\partial y}\right) + \alpha C = f(x,y), \qquad (1)$$

[1]This work was supported by RFBR, grants N15-01-00441a, N15-51-53066 and N14-01-31076

$$C|_{\delta\Omega} = C_{gr}, \tag{2}$$

$$\vec{div}\tilde{U} = 0, \tag{3}$$

where Pe is Peclet number, $\tilde{U} = \{u, v\}$ is the field of velocity in Ω, C is unknown function, α is reaction coefficient, $\vec{div}\tilde{U} = 0$ (for incompressible medium), f is the right part of equation, $\delta\Omega$ is the boundary of Ω, C_{gr} is the boundary value.

Finite difference approximation of the equation

The uniform grid Ω_h with step $h_x = h_y = h$ has been introduced in domain Ω. Introduce functions $C(x_i, y_k) = C_{ik}$, $x_i = i * \frac{1}{h}$, $y_k = k * \frac{1}{h}$. All unknowns are calculated in the middle of the cell. The boundary conditions on $\partial\Omega$ are interpolated on the boundary $\partial\Omega_h$ with a second order truncation error. The standard notation originating from [17] is used. The boundary conditions, with appropriate coefficients, are taken into account on the right-hand side of the difference equations. The central difference approximation of the first derivatives has been used. So, we obtain for (1)

$$-\frac{1}{Pe}\Delta_h C + \frac{1}{2}\left(U_{ik}\frac{C_{i+1k} - C_{i-1k}}{2h} + \frac{U_{i+1k}C_{i+1k} - U_{i-1k}C_{i-1k}}{2h} + \right. \tag{4}$$

$$\left. V_{ik}\frac{C_{ik+1} - C_{ik-1}}{2h} + \frac{V_{ik+1}C_{ik+1} - V_{ik-1}C_{ik-1}}{2h}\right) + \alpha C_{ik} = f_{ik}.$$

Here $\Delta_h C$ is the difference analogue of Laplace operator. Transform (4), multiply both parts of equation by Peh^2. Then

$$(4C_{ik} - C_{i+1k} - C_{i-1k} - C_{ik+1} - C_{ik-1}) + \frac{Peh}{2}\left[\frac{U_{ik} + U_{i+1k}}{2}C_{i+1k} - \right.$$

$$\left. -\frac{U_{ik} + U_{i-1k}}{2}C_{i-1k} + \frac{V_{ik} + U_{ik+1}}{2}C_{ik+1} - \frac{V_{ik} + U_{ik-1}}{2}C_{ik-1}\right] +$$

$$+\alpha Peh^2 C_{ik} = Peh^2 f_{ik}$$

or

$$(4 + \alpha Peh^2)C_{ik} + \left[\left(-1 + \frac{Peh}{2}\tilde{U}_{ik}\right)C_{i+1k} + \left(-1 - \frac{Peh}{2}\tilde{U}_{i-1k}\right)C_{i-1k} + \right. \tag{5}$$

$$\left.\left(-1 + \frac{Peh}{2}\tilde{V}_{ik}\right)C_{ik+1} + \left(-1 - \frac{Peh}{2}\tilde{V}_{ik-1}\right)C_{ik-1}\right] = \tilde{f}_{ik},$$

where

$$\tilde{U}_{ik} = \frac{U_{ik} + U_{i+1k}}{2}, \tilde{U}_{i-1k} = \frac{U_{ik} + U_{i-1k}}{2},$$
$$\tilde{V}_{ik} = \frac{V_{ik} + V_{ik+1}}{2}, \tilde{V}_{ik-1} = \frac{V_{ik} + V_{ik-1}}{2},$$
$$\tilde{f}_{ik} = Peh^2 f_{ik}.$$

The coefficients in (5) include the quantity

$$Re_h = Peh/2 \tag{6}$$

which was called cell Reynolds number or the skew-symmetry coefficient of the problem.

System of linear algebraic equation

Using natural ordering of the unknowns, we transform (5) to the nonsymmetric linear system of equations

$$\begin{gathered} Au = f, \\ A = A_\Delta + A_1 + D,\ A_0 = \tfrac{1}{2}\left(A + A^T\right) = A_\Delta + D = A_0^T, \\ A_1 = \tfrac{1}{2}\left(A - A^T\right) = -A_1^T, \end{gathered} \tag{7}$$

where A is $(N-1)\times(N-1)$ matrix, $N = \frac{1}{h}$, $u = \{u_{11}, u_{12}, ..., u_{N-1N-1}\}^T$ is the vector of solution, $f = \{f_{11}, f_{12}, ..., f_{N-1N-1}\}^T$ is the vector of the right part. Matrix A can be naturally expressed [6] in the case of central difference approximation of the convective terms in (5) as a sum of symmetric positive definite matrix A_Δ, skew-symmetric matrix A_1 and diagonal matrix D. A_Δ is a difference analogue Δ_h of operator Δ, describing a diffusion process, D is discrete analogue of the reaction term in the equation (1). A_1 is a difference analogue of the convective terms. Thus, linear system (7) with non-symmetric matrix A is constructed.

If in (7)

$$A_0 = A_0^T > 0,$$

then matrix A is called positive real.

The linear system (7) is called strongly non-symmetric if

$$\|A_0\| \,/\, \|A_1\| \sim O(1),$$

where $\|*\|$ is one of matrix norms.

It can be easily verified that system (7) becomes strongly nonsymmetric for large values of Pe and $\alpha = 0$. As a result we have

$$\|A_0\|_\infty = 4,$$

$$\|A_1\|_\infty = Re_h \max_i(|v_{1i,j} + v_{1i,j-1}| + |v_{1i,j} + v_{1i,j+1}| + \\ + |v_{2i,j} + v_{2i+1,j}| + |v_{2i,j} + v_{2i-1,j}|)/2,$$

Theorem 1. *Let equation (1) be approximated by finite difference scheme (5). Then the system (7) is positive real if* $\alpha \geq 0$.

Proof.

The symmetric part A_0 of matrix A has the form $A_0 = A_\Delta + D$ and doesn't have a definite sign in general case, but it is well known [17] that matrix A_Δ is positive definite. So, if diagonal matrix D has nonnegative elements than A_0 will be positive definite as the sum of positive definite and nonnegative definite matrices. The last means that $A_0 > 0$ if $\alpha \geq 0$ and system (7) is positive real.

It is well-known [15], [19] that using upwind scheme for equation (1) leads us to the system (7) with A being M-matrix [20], but in this case the obtained system won't be essentially nonsymmetric because matrix A has diagonal dominant. It is necessary to pay our attention [10] that the form in which we will approximate convection-diffusion equation plays a great role in successful numerical solution.

Consider case when coefficient $\alpha < 0$. If $\Omega = [0,1] \times [0,1]$, boundary conditions are (2) and regular mesh is used, then eigenvalues and eigenvectors of $L_h = -\frac{1}{Pe}\Delta_h + \alpha$ are well-known [18], [12]:

$$\lambda_{mp}(L_h) = \frac{4}{Peh^2}\left(\sin^2\frac{m\pi h}{2} + \sin^2\frac{p\pi h}{2}\right) + \alpha,$$

$$m = 1, 2, \ldots n-1; \quad p = 1, 2, \ldots n-1,$$

$$\frac{2\pi^2}{Pe} + \alpha \leq \lambda_i \leq \frac{8}{Peh^2} + \alpha,$$

$$i = 1, 2, \ldots N, \quad N = (n-1) * (n-1).$$

So, for $\alpha \leq -\frac{2\pi^2}{Pe}$, difference operator for diffusion and reaction terms can lose the property of being positive real then from Hirsh theorem [13], its spectrum can move to the left half plane.

Theorem 2. *Matrix (7), obtained from (5) is positive real, if*

$$\alpha_{conv} \geq -\frac{2\pi^2}{Pe}.$$

Two-parameters skew-symmetric iterative solvers

Besides important role in the mathematical modeling convection-diffusion-reaction equation is a good test for iterative methods. A lot of papers [1], [4],

[23] have already described numerical experiments with CD or CDR equations for different parameters.

Different basic iterative methods such as ILU [1], [3], [16], SOR [21], [22] have been used directly for solution of arising after approximation of CD or CDR equations by linear equation systems as well as preconditioners for CG or BiCG type's methods [14]. As it was shown in [1], ILU as a preconditioner for GMRES(20) and BiCGStab has been broken for large Re_h, $\alpha = 0$ from (6) and natural ordering of the unknowns.

We present a two parameters triangular [7] and product triangular iterative [2] methods that use the skew-symmetric part of the matrix as an input and only require the matrix (7) to be positive real. Some ideas for using the splitting of skew-symmetric part of the matrix to solve linear equation systems arising after central difference approximation of first order terms in (5) have been firstly proposed in [6].

Let us approach (7) by considering the iterative method of the following form:

$$B(\omega)\frac{y^{n+1}-y^n}{\tau} + Ay^n = f\,, \quad n \geq 0\,, \tag{8}$$

where $f, y_0 \in H, H$ is an n-dimensional real Hilbert space, f is the right part of (7), A, $B(\omega)$ are matrices)in H, A is given by equation (7), $B(\omega)$ is invertible, y_0 is an initial guess, y_k is the k-th approach, $\tau, \omega > 0$ are iterative parameters, u is the solution that we obtain, $e^k = y^k - u$ and $r^k = Ae^k$ denote the error and the residual in the k-th iteration, respectively.

Here it is important to note that $B(\omega)$ is in a certain sense a preconditioned matrix. In general, $B(\omega)$ is supposed to be nonsymmetric.

Method (8) may be also represented as

$$y^{n+1} = Gy^n + \tau f,$$

$$G = B^{-1}(\omega)(B(\omega) - \tau A)\,. \tag{9}$$

Consider the two ways of choosing matrix B. The first is

$$B(\omega) = B_C + \omega((1+j)K_L + (1-j)K_U), \quad j = \pm 1,\ B_c = B_c^T \tag{10}$$

and the second is

$$B(\omega) = (B_C + \omega K_U)B_C^{-1}(B_C + \omega K_L), B_c = B_c^T \tag{11}$$

where $K_L + K_U = A_1, K_L = -K_U^T$, $B_C = B_C^T$. The matrices K_L and K_U represent strictly upper and lower triangular parts of a skew-symmetric matrix A_1 from (7) and matrix B_C can be chosen arbitrarily, but has to be symmetric. These methods are called two-parameters triangular (TM) and product triangular (PTM) methods respectively.

Matrix B is non-symmetric and can be represented as

$$B = B_0 + B_1, B_0 = \frac{1}{2}\left(B + B^T\right) = B_0^T, B_1 = \frac{1}{2}\left(B - B^T\right) = -B_1^T.$$

We find the symmetric and the skew-symmetric parts of matrix B for TM

$$B_0 = B_C + \frac{1}{2}\omega j\left(K_U - K_L\right), j = \pm 1,\ B_1 = \frac{1}{2}\omega A_1 \tag{12}$$

and PTM

$$B_0 = B_C + \omega^2 K_U B_C^{-1} K_L, B_1 = \omega A_1. \tag{13}$$

The iteration matrix G from (9) for these methods is

$$G = B^{-1}\left(B - \tau A\right) = \left(B_0 + B_1\right)^{-1}\left(B_0 + B_1 - \tau A_0 - \tau A_1\right). \tag{14}$$

We consider the norm of iteration matrix G in (14). Let us require that matrices (10) and (11) are positive real and define matrices

$$L_{0T} = B_0 - \frac{1}{2}\omega A_0, \tag{15}$$

and

$$L_{0PT} = B_0 - \omega A_0. \tag{16}$$

Using (12), (14) and (15) iterative matrix G_T for TM can be represented as

$$\begin{aligned} &G_T = \left(B_0 + \tfrac{1}{2}\omega A_1\right)^{-1}\left(B_0 + \tfrac{1}{2}\omega A_1 - \tau A_0 - \tau A_1\right) = \\ &= \left(B_0 - \tfrac{1}{2}\omega A_0 + \tfrac{1}{2}\omega A_0 + \tfrac{1}{2}\omega A_1\right)^{-1}\left(B_0 - \tfrac{1}{2}\omega A_0 + \tfrac{1}{2}\omega A_0 + \tfrac{1}{2}\omega A_1 - \tau A_0 - \tau A_1\right) = \\ &= \left(L_{0T} + \tfrac{1}{2}\omega A\right)^{-1}\left(L_{0T} - (\tau - \tfrac{1}{2}\omega)A\right) \end{aligned}$$

Introduce matrices

$$P_{0T} = L_{0T}^{-\frac{1}{2}} A L_{0T}^{-\frac{1}{2}}, \tag{17}$$

and

$$P_{0PT} = L_{0PT}^{-\frac{1}{2}} A L_{0PT}^{-\frac{1}{2}}. \tag{18}$$

and require for TM that

$$L_{0T} = B_0 - \frac{1}{2}\omega A_0 = L_{0T}^T > 0 \tag{19}$$

and for PTM

$$L_{0PT} = B_0 - \omega A_0 = L_{0PT}^T > 0 \tag{20}$$

Then

$$\begin{aligned} &G_T = L_{oT}^{-1/2}(I + \tfrac{1}{2}\omega P_{0T})^{-1}(I - (\tau - \tfrac{1}{2}\omega)P_{0T})L_{oT}^{-1/2} = L_{0T}^{-\frac{1}{2}} G_P L_{0T}^{\frac{1}{2}}, \\ &G_P = (I + \tfrac{1}{2}\omega P_{0T})^{-1}(I - (\tau - \tfrac{1}{2}\omega)P_{0T}). \end{aligned}$$

The last equality means that matrix L_0 generates energy norm $\|G_T\|_{L_{0T}}$ and

$$\|G_T\|_{L_{0T}} = \left\|(I + \frac{1}{2}\omega P_{0T})^{-1}(I - (\tau - \frac{1}{2}\omega)P_{0T})\right\| \tag{21}$$

Lemma 1. *Let C be positive real, α, β are positive numbers. Then inequality*

$$-\alpha < \beta \leq \alpha, \alpha > 0 \tag{22}$$

$$\left\|(I + \alpha C)^{-1}(I - \beta C)\right\| < 1 \tag{23}$$

Proof.

First of all we point out that matrices $(I + \alpha C)^{-1}$ and $(I - \beta C)$ are commutative. Later we consider matrix

$$T = (I + \alpha C)^{-1}(I - \beta C)$$

and estimate its norm

$$\|T\|^2 = \sup_{v\neq 0} \frac{\|Tv\|^2}{\|v\|^2} = \sup_{v\neq 0} \frac{((I+\alpha C)^{-1}(I-\beta C)v,(I+\alpha C)^{-1}(I-\beta C)v)}{(v,v)} =$$
$$= \sup_{v\neq 0} \frac{((I-\beta C)(I+\alpha C)^{-1}v,(I-\beta C)(I+\alpha C)^{-1}v)}{(v,v)}.$$

Let

$$u = (I + \alpha C)^{-1}v$$

then

$$\|T\|^2 = \sup_{u\neq 0} \frac{((I-\beta C)u,(I-\beta C)u)}{((I+\alpha C)u,(I+\alpha C)u)} = \sup_{u\neq 0} \frac{(u,u)-2\beta(Cu,u)+\beta^2(Cu,Cu)}{(u,u)+2\alpha(Cu,u)+\alpha^2(Cu,Cu)} =$$
$$= 1 - (\alpha + \beta)\inf_{u\neq 0} \frac{2(Cu,u)+(\alpha-\beta)(Cu,Cu)}{(u,u)+2\alpha(Cu,u)+\alpha^2(Cu,Cu)}.$$

So, if

$$\left\{ \begin{array}{c} \alpha + \beta > 0 \\ \alpha - \beta \geq 0 \\ \alpha > 0 \end{array} \right\} \tag{24}$$

and

$$(Cu, u) \geq 0$$

then

$$\|T\| < 1.$$

and (23) fulfills. Inequalities (24) transform to (22).

□

Lemma 2. [8] *Let $D = D^T > 0$ and A be positive real. Then*

$$\left\|(D + \sigma A)^{-1}(D - \sigma A)\right\|_D < 1\,,$$

where $\sigma > 0$ *is parameter.*

Proof Let

$$T = (D + \sigma A)^{-1}(D - \sigma A).$$

First we note that

$$T = D^{-1/2}(I + \sigma D^{-1/2} A D^{-1/2})^{-1} \times \\ \times (I - \sigma D^{-1/2} A D^{-1/2}) D^{1/2}$$

and

$$\|T\|_D = \left\|\widetilde{T}\right\| \tag{25}$$

where

$$\widetilde{T} = (I + \sigma M)^{-1}(I - \sigma M), \\ M = C^{-1/2} A C^{-1/2}$$

Then we obtain from (25) and Lemma 1 with $\alpha = \beta = \omega$ result of Lemma 2.

□

We applied Lemma 1 to matrix G_T in (21) and get following Theorem.

Theorem 3. *Let* A *in (7) be positive real. Then iterative method (8), (10) converges in* $H_{L_{0T}}$ *if (19) fulfills and*

$$0 < \tau \leq \omega \tag{26}$$

Proof of this theorem consists of two step:

-show that P_{0T} is positive real (Its the property of positive real matrix [18], if A is positive real, then $C = QAQ^T$ is positive real, too). So, from (17) P_{0T} is positive real.

- insert in (22) $\alpha = \frac{1}{2}\omega, \beta = (\tau - \frac{1}{2}\omega)$ then we've got (26).

Similar laying out we can repeat for PTM just replace (21) on

$$\|G_T\|_{L_{0PT}} = \left\|(I + \omega P_{0PT})^{-1}(I - (\tau - \omega)P_{0PT})\right\|$$

using (13), (14), (16), (18) and (20).

□

Theorem 4. *Let* A *in (7) be positive real. Then iterative method (8), (11) converges in* $H_{L_{0PT}}$ *if (20) fulfills and*

$$0 < \tau \leq 2\omega$$

The proof of this theorem is the same of the previous one.

□

Problem No.	v_1	v_2
1	1	-1
2	$1-2x$	$2y-1$
3	$x+y$	$x-y$
4	$\sin 2\pi x$	$-2\pi y \cos 2\pi x$

Table 1. Velocity coefficients for test problems.

Numerical experiments

In this section we present the results of numerical experiments in which the technique described above is used to solve nonsymmetric linear systems with $\alpha < 0$ and $\alpha = 0$. We compare the performance of SSOR [14] and PTM [2] iterative methods to solve linear systems arising from the standard 5-point FD approximation of the steady convection–diffusion-reaction problem (1) - (3) where F is chosen so that the solution of (1) is defined as

$$\tilde{u}(x,y) = \mathrm{e}^{xy} \sin \pi x \sin \pi y \,.$$

Equation (1) has been discretized by centered differences on a uniform grid with 33×33. In the table 1 the used velocity coefficients of (1) are presented. Note that, for each model problem they are chosen to satisfy the constraint $\mathrm{div}\,\vec{v} = v_{1x} + v_{2y} = 0$ (which follows from the medium incompressibility for the problem (2)). On the whole, in order to the test results to be comparable with those obtained in the other adjacent papers we take the analytical solution and the velocity coefficients similar to those in [3].

The initial guess in all runs was a zero vector and iterations were performed until

$$\|r^m\| \Big/ \|r^0\| \leq 10^{-6}\,, \tag{27}$$

where r^m is the residual vector, and $\|\star\|$ represents the Euclidean norm. Checking and comparing iterative methods SSOR and PTM for different negative α (Table 2) we show that methods are very good for $|\alpha| > 100$. It means that matrix (7) is strongly diagonal dominant. This is connected with existence on main diagonal of elements $a_1 = (4 + \alpha Peh^2)$, which we obtain after approximation of coefficient of reaction. It includes numbers α and Re_h, grows by module α and Re_h. As we can see from the Table 2 the number of iteration for $\alpha = 0$ grows with the increasing Peclet number. In contrast of this behavior of both iterative methods, the number of iteration decreases with grow of Peclet number and modula coefficient of reaction.

Pe	Problem 1		Problem 2		Problem 3		Problem 4	
	PTM	SSOR	PTM	SSOR	PTM	SSOR	PTM	SSOR
$\alpha = 0$								
10^3	77	113	50	106	66	107	68	157
10^4	565	863	297	565	279	632	369	1054
10^5	5196	6725	1990	3531	1694	4980	2538	7416
$\alpha = -10$								
10^3	51	72	31	37	45	54	59	108
10^4	32	41	22	23	33	34	33	65
10^5	30	41	23	23	32	33	32	65
$\alpha = -100$								
10^3	7	5	9	6	9	7	12	13
10^4	7	5	9	6	9	7	12	13
10^5	7	5	9	6	9	7	12	13
$\alpha = -1000$								
10^3	5	3	6	3	5	3	7	4
10^4	5	3	6	3	5	3	7	4
10^5	5	3	6	3	5	3	7	4
$\alpha = -5000$								
10^3	5	2	4	3	4	3	6	3
10^4	5	2	4	3	4	3	6	3
10^5	5	2	4	3	4	3	6	3
$\alpha = -10000$								
10^3	4	2	4	3	4	3	5	3
10^4	4	2	4	3	4	3	5	3
10^5	4	2	4	3	4	3	5	3

Table 2. Number of iterations for different α

Conclusions

The behavior of iterative methods to solve (7) which was obtained after approximation of CD ($\alpha = 0$) and CDR ($\alpha < 0$) equations is quite different (Table 2). The case with $\alpha = 0$ shows that matrix loses the property of diagonal dominance and the methods require more iterations as Re_h increasing. Case with $\alpha \leq 0$ for big numbers α shows a very quick convergence of both methods for big numbers of Re_h.

Bibliography

1. *M.Benzi, D.B.Szyld and A.van Duin* Orderings for incomplete factorizations preconditioning of nonsymmetric problems, Temple University, Department of Mathematics, Report 97-91, 1997.

2. *M.A. Botchev and L.A. Krukier* Iterative solution of strongly nonsymmetric systems of linear algebraic equations, J.Comp. Math.& Math.Physics, v.37, N. 11, 1997, 1241-1251

3. *H.C.Elman* Relaxed and stabilized incomplete factorizations for nonself-adjoint linear systems, BIT(Dan.), 29(4), 1989, 890–915.

4. *H.C. Elman and G.H.Golub* Line iterative methods for cyclically reduced discrete convection-diffusion problems, SIAM J.Sci.Stat.Comput., 13(1), 1992, 339–363

5. *B. Fischer, A. Ramage, D. Silvester, A.Wathen* Towards parameter - free streamline upwinding for advection - diffusion problems. - Strathclyde Mathematics Research Report, No 37, 1996, 18 p.

6. *Krukier L.A.* Implicit Difference Schemes and an Iterative Method for Their Solution for One Class of Quasilinear Systems of Equations, Izvestija Vuzov, Mathematics, **7** (1979), 41–52. (*In Russian.*)

7. *Krukier L.A.* Convergence acceleration of triangular iterative methods based on the skew-symmetric part of the matrix, Appl. Numer. Math, 30, (1999), 281-290

8. *L.A. Krukier, L.G. Chikina* Skew-symmetric iterative method for solution of steady convection-diffusion equation, Izvestija vuzov., Mathematics, 11, 2000, 62 - 75. *(In Russian)*

9. *Krukier L.A., L.G.Chikina, T.V.Belokon* Triangular skew-symmetric iterative solvers for strongly nonsymmetric positive real linear system of equations, Appl. Numer. Math., 41(2002), 89—105.

10. *L.A. Krukier, T.S.Martynova* Influence of the form of convection-diffusion equation on the convergence of the SOR, J.of Comp. Math.J.&Math. Physics, 1999, v. 39, N. 11, pp.1821-1827

11. *Krukier L.A., Pichugina O.A., Krukier B.L.* Numerical solution of the steady convection-diffusion equation with dominant convection // Procedia Computer Science - 2013. - V. 18. - P.2095-2100.

12. *G.I.Marchuk* Methods of Computational Mathematica, Moscow, Nauka, 1989 (*in Russian)*

13. *Marcus M., Minc H.* A Survey of Matrix Theory and Matrix Inequalities, Allyn&Bacon, Boston,1964

14. *Meurant G.* Computer Solutions of Large Linear Systems. - Amsterdam: Elsevier Science, 1999.

15. *K.W.Morton* Numerical solution of Convection-Diffusion Problems, Appl. Math. &Mathematical Computation, Chapman and Hall, London, 1996.

16. *Y.Saad* Iterative methods for sparse linear systems - PWS Pub. Co, Boston, M.A., 1996

17. *A.A. Samarskii* Theory of difference schemes, Moscow, Nauka, 1977.

18. *A.A. Samarskii and E.S. Nikolaev* Numerical methods for grid equations, (Vol. 2,Iterative methods), Birkhäuser, Basel, 1989

19. *A.A. Samarskii, P.N.Vabizevich* Numerical solution of convection-diffusion equation, Moscow, Nauka, 1999 (*in Russian*)

20. *H.A. van der Vorst* Iterative solution methods for certain sparse linear systems with a non-symmetric matrix arising from PDE-problems, J. Comput. Physics, 44(1981), 1–19.

21. *Varga R.S.* Matrix Iterative Analysis, Prentice-Hall, Englewood Cliffs, 1962.

22. *Young D.M.* Iterative Solutions of Large Linear Systems. Academic Press, New York, 1971

23. *J.Zhang* Preconditioned iterative methods and finite difference schemes for convection-diffusion, Appl. Math.& Comp., 109, 2000, p.11-30

ITERATIVE SOLUTION OF THE CONSTRAINED NONLINEAR LEAST-SQUARES PROBLEMS[1]

Martynova T.S.
Southern Federal University, Rostov-on-Don, Russia

Solving the nonlinear least squares problems arising in nonlinear data fitting is considered. This problem holds, for example, in the simulating of the environment pollutants by X-ray analysis.

Let x_* a local minimizer, $R : \mathbb{R}^n \to \mathbb{R}^m$ continuously differentiable. Nonlinear least squares problem (NLLS) can be written in the following form:

$$\min_{x\in\mathbb{R}^n} F(x) = \frac{1}{2}R(x)^T R(x) = \frac{1}{2}\sum_{i=1}^{m} r_i(x)^2,$$

where $m > n$ (usually, $m \gg n$), $r_i(x)$ are nonlinear functions. Parameter estimation and curve fitting are typical applications for NLLS, where data sets (t_i, y_i), $i = 1, ..., m$ should be approximate by nonlinear model $M(x, t)$. The vector $x \in \mathbb{R}^n$ contains the n parameters to be estimated. The residual functions $r_i(x) = M(x, t_i) - y_i$ are the differences between the model and the observations. Most specialized algorithms for NLLS exploit the special structure of the nonlinear least-squares objective function. Let $J(x) \in \mathbb{R}^{m\times n}$ is the Jacobian of the $R(x)$, i.e. $J(x)_{ij} = \partial r_i(x)/\partial x_j$, $H(x)$ is the Hessian and $g(x)$ is the gradient of the $F(x)$ respectively. Then [1] $H(x) = J(x)^T J(x) + Q(x)$, $g(x) = J(x)^T R(x)$, where $Q(x) = \sum_{i=1}^{m} r_i(x)H_i(x)$. For NLLS problems we approximate the Hessian as $H \approx J^T J$, so far as $Q(x) \to 0$ if $x \to x_*$.

For solving unconstrained NLLS we have used trust-region algorithm. The quadratic model function m_k at each iterate x_k is

$$m_k(d) = \frac{1}{2}\|R_k\|_2^2 + d^T J_k^T R_k + \frac{1}{2}d^T J_k^T J_k d. \qquad (1)$$

Thus at each iteration, we seek a solution $d_k \in \mathbb{R}^n$ of the subproblem based on the (1) subject to some trusted region:

$$\min_d \frac{1}{2}\|J_k d + R_k\|_2^2, \quad \|D_k d\|_2 \le \Delta_k, \qquad (2)$$

where $\Delta_k > 0$ is the trust-region radius, $D_k \in \mathbb{R}^{n\times n}$ is a diagonal matrix with positive diagonal entries. The solution of the (2) satisfies an equation of the form $(J_k^T J_k + \lambda D_k^2)d = -J_k^T R_k$, $\lambda \ge 0$ [1]. It is the Levenberg-Marquardt method.

Many approaches exist for the solution of nonlinear least-squares problems, however, most research has focused on the NLLS without constraints.

[1]Supported by Ministry of Education and Science of the Russian Federation (basic part, project N1420) and RFBR, grant N15-01-00441-a, grant N15-51-53066 GFEN-a.

Let the constraint function $h(x)$ is a vector-valued linear function describing any constraints on the parameters. The method of Lagrange multipliers can be used to solving this problem. Optimality conditions for the problems with equality constraints are as follows [2]:

$$\begin{cases} \nabla_x \mathcal{L}(x,\lambda) = \nabla F(x) + \nabla h(x)\lambda = 0, \\ \nabla_\lambda \mathcal{L}(x,\lambda) = h(x) = 0, \end{cases} \tag{3}$$

where $\mathcal{L}(x,\lambda)$ is the Lagrange function, i.e. $\mathcal{L}(x,\lambda) = F(x) + \lambda^T h(x)$, $\lambda \in \mathbb{R}^p$ is a vector of Lagrange multipliers, $p \leq n$ is a number of the constraints. Then $(x_*, \lambda_*) \in \mathbb{R}^{n+p}$ is a saddle point of the Lagrange function.

The Gauss-Newton (GN) method for solving (3) is [2]:

$$x_{k+1} = x_k + \Delta x_k, \quad \lambda_{k+1} = \lambda_k + \Delta\lambda_k,$$

were $(\Delta x_k, \Delta\lambda_k) \in \mathbb{R}^{n+p}$ can be obtained from the following system:

$$\nabla^2 \mathcal{L}(x_k,\lambda_k) \begin{bmatrix} \Delta x_k \\ \Delta\lambda_k \end{bmatrix} = -\nabla \mathcal{L}(x_k,\lambda_k)$$

or

$$\begin{bmatrix} J_k^T J_k & \nabla h(x_k) \\ \nabla h(x_k)^T & 0 \end{bmatrix} \begin{bmatrix} \Delta x_k \\ \Delta\lambda_k \end{bmatrix} = - \begin{bmatrix} \nabla_x \mathcal{L}(x_k,\lambda_k) \\ h(x_k) \end{bmatrix}.$$

Let $h(x) = Ex - f = 0$, the matrix $E \in \mathbb{R}^{p\times n}$ has full rank and $f \in \mathbb{R}^p$. Then

$$\begin{bmatrix} M_k & E^T \\ E & 0 \end{bmatrix} \begin{bmatrix} \Delta x_k \\ \Delta\lambda_k \end{bmatrix} = - \begin{bmatrix} u_k \\ v_k \end{bmatrix}, \tag{4}$$

where $M_k = J_k^T J_k \in \mathbb{R}^{n\times n}$ are positive semidefinite, $(u_k^T, v_k^T)^T \in \mathbb{R}^{n+p}$, and $u_k = J_k^T R_k + E^T\lambda_k$, $v_k = Ex_k - f$, $u_k \in \mathbb{R}^n$, $v_k \in \mathbb{R}^p$, $k = 0, 1, \ldots.$

We employ the augmented Lagrangian method [3], the matrix M will be replaced by a positive definite matrix $\widetilde{M}_k \equiv M_k + \gamma_k E^T E$, $\gamma_k > 0$ and iteration methods can be applied to solve the augmented linear system.

$$\begin{bmatrix} \widetilde{M}_k & E^T \\ E & 0 \end{bmatrix} \begin{bmatrix} \Delta x_k \\ \Delta\lambda_k \end{bmatrix} = - \begin{bmatrix} u_k + \gamma_k E^T v_k \\ v_k \end{bmatrix}. \tag{5}$$

Many computational difficulties can be overcome by using preconditioning (4)-(5). We can rewrite the saddle-point linear system into non-symmetric form [4]

$$\mathcal{A}\mathbf{w} = \mathbf{b},$$

$$\mathcal{A} = \begin{bmatrix} \widetilde{M} & E^T \\ -E & 0 \end{bmatrix}, \quad \mathbf{w} = \begin{bmatrix} \Delta x \\ \Delta\lambda \end{bmatrix}, \quad \mathbf{b} = \begin{bmatrix} -\widetilde{u} \\ v \end{bmatrix},$$

where $\widetilde{u} = u + \gamma E^T v$ (hereinafter subscript of the Gauss-Newton iterations omitted for convenience).

Analogous to [5] the matrix $\mathcal{A}$ can be split into its symmetric and skew-symmetric parts as

$$\mathcal{A} = \mathcal{A}_0 + \mathcal{A}_1,$$

where

$$\mathcal{A}_0 = \frac{1}{2}(\mathcal{A} + \mathcal{A}^T), \quad \mathcal{A}_1 = \frac{1}{2}(\mathcal{A} - \mathcal{A}^T)$$

are the symmetric and the skew-symmetric parts of the matrix $\mathcal{A}$:

$$\mathcal{A}_0 = \begin{bmatrix} \widetilde{M} & 0 \\ 0 & 0 \end{bmatrix}, \quad \mathcal{A}_1 = \begin{bmatrix} 0 & E^T \\ -E & 0 \end{bmatrix}.$$

The skew-symmetric part $\mathcal{A}_1$ can be split into

$$\mathcal{A}_1 = \mathcal{K}_L + \mathcal{K}_U = \begin{bmatrix} 0 & 0 \\ -E & 0 \end{bmatrix} + \begin{bmatrix} 0 & E^T \\ 0 & 0 \end{bmatrix},$$

where 0 is a zero matrix with suitable dimension, $\mathcal{K}_L$ and $\mathcal{K}_U$ are the strictly lower- and the strictly upper- triangular parts of $\mathcal{A}_1$. Note that $\mathcal{K}_L = -\mathcal{K}_U^T$.

Based on these splittings in [6] the authors established generalized skew-Hermitian triangular splitting iteration method (GSTS) for solving non-Hermitian saddle-point linear systems. Let the matrix $\mathcal{B}_C$ be defined as

$$\mathcal{B}_C = \begin{bmatrix} B_1 & 0 \\ 0 & B_2 \end{bmatrix},$$

where B_1 and B_2 are symmetric and nonsingular matrices. Then GSTS - preconditioner is defined as [6]:

$$\mathcal{B}(\omega_1, \omega_2) = (\mathcal{B}_C + \omega_1 \mathcal{K}_L)\mathcal{B}_C^{-1}(\mathcal{B}_C + \omega_2 \mathcal{K}_U),$$

or in block form

$$\mathcal{B}(\omega_1, \omega_2) = \begin{bmatrix} B_1 & 0 \\ -\omega_1 E & B_2 \end{bmatrix} \begin{bmatrix} B_1^{-1} & 0 \\ 0 & B_2^{-1} \end{bmatrix} \begin{bmatrix} B_1 & \omega_2 E^T \\ 0 & B_2 \end{bmatrix},$$

where ω_1 and ω_2 are nonnegative acceleration parameters and, at least, one of them is nonzero. In actual implementations we choose $B_1 = \widetilde{M}$. Then

$$\mathcal{B}(\omega_1, \omega_2) = \begin{bmatrix} \widetilde{M} & \omega_2 E^T \\ -\omega_1 E & B_2 - \omega_1 \omega_2 E \widetilde{M}^{-1} E^T \end{bmatrix},$$

and preconditioned block-structured linear system is:

$$\mathcal{B}^{-1}(\omega_1, \omega_2)\mathcal{A}\mathbf{w} = \mathcal{B}^{-1}(\omega_1, \omega_2)\mathbf{b}.$$

We consider three cases for the GSTS according to the different choices of the matrix B_2, and obtain the GSTS-preconditioned GMRES iteration method.

We construct a model of the scattering group of chemical elements that may be contained in water. In the description of the profile of experimental scattering pattern we select the profile function for the peak shape. Clarification of the line profile based on the introduction of the function F which must be minimized with respect to all parameters:

$$F = \frac{\sum_{i=1}^{m} |y_i^{obs} - y_i^{calc}|^2}{\sum_{i=1}^{m} |y_i^{obs}|^2},$$

where y_i^{obs} are experimental data set, y_i^{calc} are calculation data set and

$$y_i^{calc} = \sum_{j=1}^{k} I_j PV(t_i, x_0^{(j)}, \Delta x^{(j)}, \eta^{(j)}) + \varphi(t_i, x_1, ..., x_s).$$

Here k is the number of peaks, I_j is the integrated intensity, $\varphi(t_i, x_1, ..., x_s)$ is the background. The parameter sets specifies by the nonlinear least squares are peak shape $\{I_j, x_0^{(j)}, \Delta x^{(j)}\}$, weight coefficients $\{\eta^{(j)}\}$, $j = 1, ..., k$ and the parameters belonging to the φ: $\{x_l\}, l = 1, ..., s$. We approximate φ by a cubic spline with natural boundary conditions. Equality constraints in the constrained NLLS problem are $I_1/I_j = \mathfrak{I}_1/\mathfrak{I}_j, j = 2, ..., k, \eta^{(j)} = \eta^{(i)}, \Delta x^{(j)} = \Delta x^{(i)}, i, j = 1, ..., k$, the values $\{\mathfrak{I}_j\}$, $j = 1, ..., k$ are taken from the [7].

At first we solve unconstrained NLLS problem by the Levenberg-Marquardt method. Our implementation of this algorithm uses QR-decomposition of the Jacobian matrix and does not require any matrix factorization for determination of the parameter λ. Figure 1 shows experimental and model scattering pattern for the problem with 112 parameters. Then the equality-constrained large-scale NLLS problem is solved by the GN method. Iterations of the Levenberg-Marquardt algorithm and outer iterations of the GN method are terminated if the current iterations satisfy $\|R\|_1 \leq \varepsilon_1$, $\|x_{k+1} - x_k\|_1 \leq \varepsilon_2$, $\varepsilon_1 = 10^{-6}, \varepsilon_2 = 10^{-7}$.

When the saddle-point linear system is solved by preconditioned GMRES at each step of the GN method then inner iterations terminated if

$$\|\mathcal{B}^{-1}\mathbf{b} - \mathcal{B}^{-1}\mathcal{A}\mathbf{w}^k\|_2 \leq 10^{-6}\|\mathcal{B}^{-1}\mathbf{b} - \mathcal{B}^{-1}\mathcal{A}\mathbf{w}^0\|_2.$$

The iteration methods GSTS(1), GSTS(2) and GSTS(3) with different choices of the matrix B_2 (Table 1) are employed as preconditioners to full GMRES. In actual calculations $B_1 = \widetilde{M}$. The optimal values of the parameters are numerical optimal values, $\omega_1 = \omega_2 = \omega_{exp}$. The choice $\gamma_k = \|M_k\|_2/\|E\|_2^2$ [3] has been found to perform well in practice.

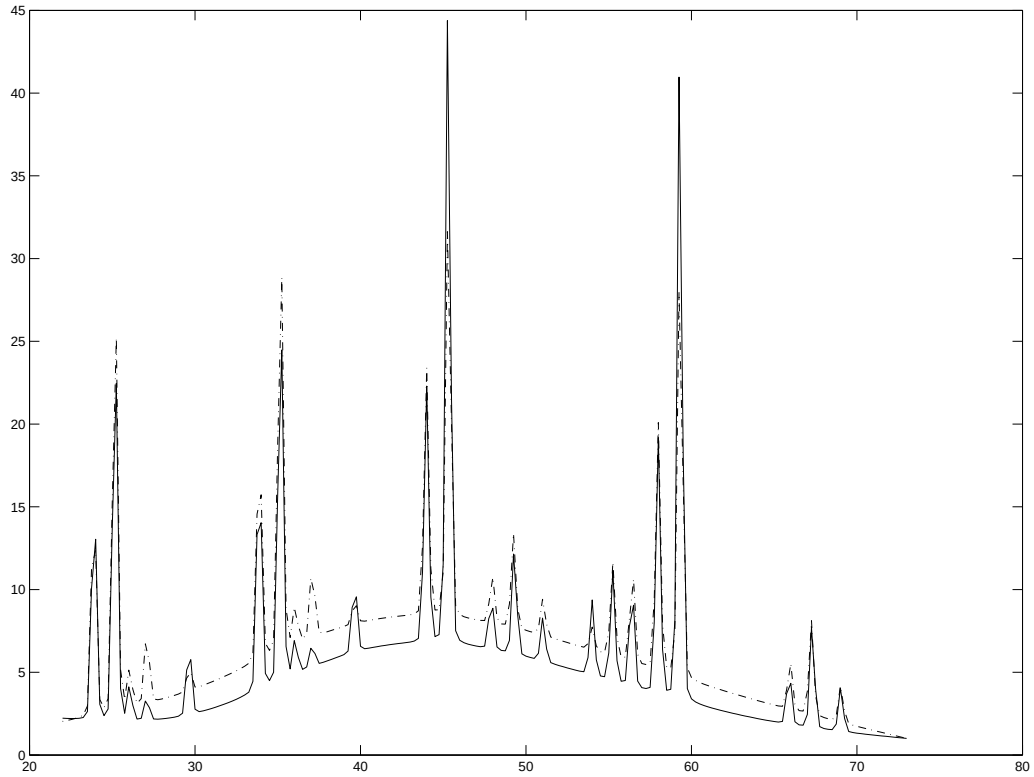

Figure 1. Experimental (dash-dot line) and model (continuous line) of the scattering pattern for the problem with 112 parameters

Bibliography

1. *J. Nocedal and S.J. Wright* Numerical optimization. Springer Series in Operations Research, Springer-Verlag, 1999. 634 p.

2. *D.P. Bertsekas* Constrained Optimization and Lagrange Multiplier Methods. Academic Press, 1982. 395 p.

3. *G.H. Golub and C. Greif* On solving block-structured indefinite linear systems // SIAM Journal on Scientific Computing. 2003. Vol. 24. P. 2076–2092.

Preconditioner	Matrix B_2	Description
GSTS(1)	$E\widehat{M}^{-1}E^T$	$\widehat{M} = tridiag(\widetilde{M})$
GSTS(2)	$E\widehat{M}^{-1}E^T$	$\widehat{M} = tridiag(M) + \gamma diag(E^TE)$
GSTS(3)	$tridiag(E\widetilde{M}^{-1}E^T)$	

Table 1. Choices of the matrix B_2

4. *M. Benzi, G.H. Golub and J. Liesen* Numerical solution of saddle point problems // Acta Numerica. 2005. Vol. 14. P. 1–137.

5. *Z.-Z. Bai, G.H. Golub and M.K. Ng* Hermitian and skew-Hermitian splitting methods for non-Hermitian positive definite linear systems // SIAM Journal on Matrix Analysis and Applications. 2003. Vol. 24. P. 603–626.

6. *Krukier L.A., Krukier B.L., Ren Z.-R.* Generalized skew-Hermitian triangular splitting iteration methods for saddle-point linear systems // Numer. Linear Algebra Appl. 2014. Vol. 21. P. 152–170.

7. *Plechaty E.F., Cullen D.E., Howerton R.J* Tables and Graphs of Photon Interaction Cross Sections from 0.1 keV to 100 MeV Derived from the LLL Evaluated Nuclear Data Library // Report UCRL-50400, NTIS DE82-004819, Lawrence Livermore National Laboratory. Livermore, CA. 1981. Vol. 6.

MATHEMATICAL MODELING OF NEURAL ACTIVITY[1]

Muratova G.V., Andreeva E.M., Bavin V.V., Belous M.A.
Southern Federal University, Rostov-on-Don, Russia

An important development in present science is the increased use of methods from mathematics, computer science and theoretical physics in the exploration of biological systems. This is due to great advances in the understanding of living systems, establishment of new experimental techniques, methodological advances in mathematical modeling, and the continuing growth in available computer power for numerical calculations and simulations.

Neuroscience is among the biological sub-disciplines where the use of mathematical techniques are most established and recognized. An important reason for this is the success of Hodgkin and Huxley [1] more than 50 years ago of describing signal transport in a single neuron (nerve cell) as a modified electrical circuit where the charge carriers are Na^+, K^+, Ca^{++}, Cl^- and other ions flowing through the neuron cell membrane. This mathematical formulation, known as Hodgkin-Huxley theory, could not only account for the results from experiments used to construct the model and fit the model parameters. From their model they could also predict the shape and velocity of the so called *action potential* which is a pulse-like electrical disturbance travelling down thin outgrowths, called *axons*, of neurons [2].

Due to its obvious success in describing action potentials, the Hodgkin-Huxley approach has later been generalized to include modeling of the signal processing properties of entire neurons [3]-[4]. Thus modelers now have a relatively firm starting point for mathematical explorations of neural activity.

Mathematical models in neuroscience can be distinguished by their purpose [5].

Mechanistic models aim to account for the properties of neurons or neural circuits on the basis of the underlying biophysical properties of neurons and neural networks. This corresponds to the traditional physics approach to modeling nature.

Descriptive (or statistical) models try to account mathematically for experimental data without the aim to explain what aspects of the neurons or neuronal circuitry gives rise to the mathematical structure. *Interpretive* models aims to elucidate the functional roles of neural systems, i.e., relating neural responses to the task of processing useful information for the animal. Information theory is typically used in such modeling [5]. Interpretive modeling is unique to biological systems which have developed under evolutionary pressure.

So there exist the various approaches for modeling neural activity.

On the basis of dynamic mechanisms of neuron various mathematical models are constructed. Among them there are relatively simple ones, such as “Inregrate

[1]This work was supported by RFBR, N15-51-53066

and Fire", in which a neuron is represented as a capacitor connected in parallel, corresponding to the capacitive current for the membrane, and a resistor simulating the leakage of ions through ion channels [6]. More complex, biologically plausible model were created, for example, Hodgkin-Huxley model [1], which is much more difficult computationally and in terms of the analysis of its dynamics, but it is much more accurate to describe the dynamics of the membrane potential of the neuron. This model belongs to the class of point models. Point models do not share a neuron into segments, not isolated parts of the dendrite and soma.

The spatial geometry of the nerve cells is complex and diverse. Therefore, modeling of neurons using the point model is big enough simplification. More complex multisegment models were constructed for example cable equation.

I Izhikevich model

We investigate Izhikevich model [7], which is a certain compromise between computational complexity and biophysical verisimilitude. Despite the computational simplicity of the model, depending on the parameters it can operate in different dynamic modes, relevant neurons present. Izhikevich model described as a fast-slow system of two differential equations describing the dynamics of the membrane potential of the neuron. Depending on the initial conditions and the applied current model can be in two dynamic modes, the movement to the rest potential $P1$, or the generation of an electrical pulse $P2$ [8].

Izhikevich model belongs to the class of phenomenological models. In these models the dynamics of the membrane potential is reproduced as a phenomenon.

The full Izhikevich model is the following:

$$\begin{cases} C_m \dfrac{dV}{dt} = k(v - v_r)(v - v_t) - u + I_{syn} + I_{ext} \\ \dfrac{dU}{dt} = a\,(b(v - v_r) - u) \\ if \quad v > V_p, B > \begin{cases} V \leftarrow c \\ U \leftarrow U + d \end{cases} \end{cases},$$

where b – sensitivity U to subliminal volatility of V, C_m – membrane capacitance, c – potential after spike, d – growth U after spike, v_r – rest potential, v_t – minimum potential of generating action potential, k – coefficient inverse membrane resistance.

As a result of research the model of the neural electrical activity based on the Izhikevich model is constructed. The algorithm of its implementation using technologies GPGPU is suggested. GPGPU technology enabled the maximum use of the processing power of the computer by dividing the original data stream of neural network model into a plurality of parallel processing threads in a GPU.

Some numerical results are presented. The vector field and nerve impulse form obtained by Izhikevich model are shown on the figure 1.

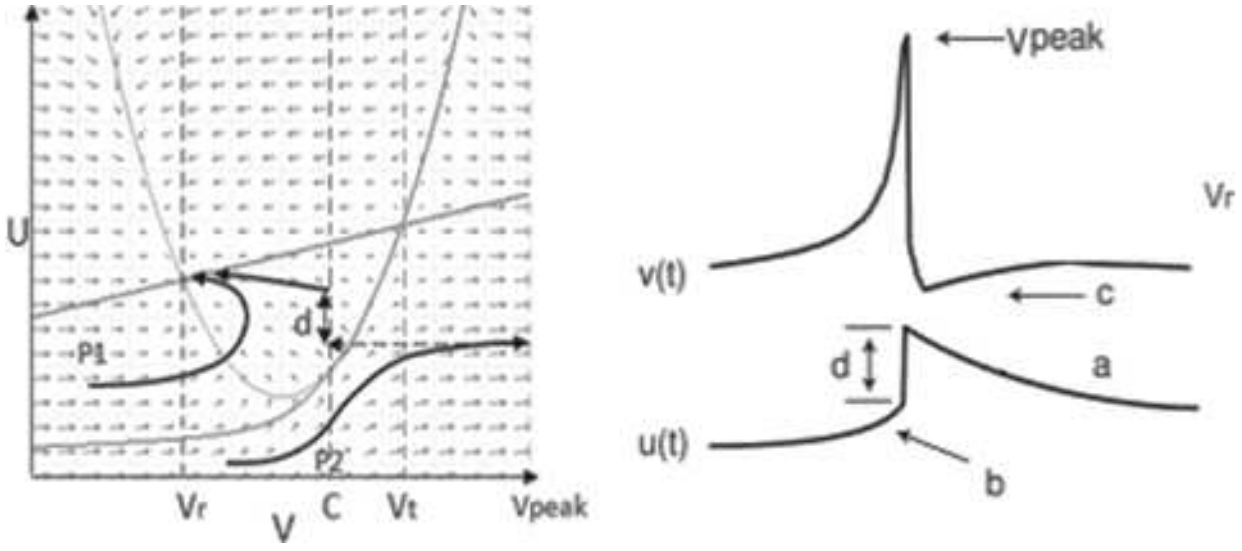

Figure 1. The Izhikevich model

Bibliography

1. *Hodgkin A.L., Huxley A.F.* A quantitative description of ion currents and its applications to conduction and excitation in nerve membranes //Journal of Neurophysiology. 1952. Vol. 117. N. 4. P. 500-544.

2. *Einevoll G.T.* Mathematical modeling of neural activity //Department of Mathematical Sciences and Technology Norwegian University of Life Sciences, 1432 As, Norway. http://arken.umb.no/∼gautei/forskning/einevoll_NATO_2006.pdf

3. *Koch C., Segev I. (eds.)* Methods in Neuronal Modeling (2 ed.). Cambridge, MA: MIT Press, 1998.

4. *Bower J.M., Beeman D. (eds.)* The Book of Genesis: Exploring Realistic Neural Models with the General Neural Simulation System (2.ed.). New York: Springer, 1998.

5. *Dayan P., Abbott L.F.* Theoretical Neuroscience. Cambridge, MA: MIT Press, 2001.

6. *Jolivet R., Lewis T.J., Gerstner W.* Generalized integrate-and-fire models of neuronal activity approximate spike trains of a detailed model to a high degree of accuracy //Journal of Neurophysiology. 2004. Vol. 92. N. 2. P. 959-976.

7. *Izhikevich E.M.* Dynamical systems in neuroscience: the geometry of excitability and bursting. Cambridge, MA: MIT Press, 2007. 464 p.

8. *Hale J., Kocak H.* Dynamics and Bifurcations. New York: Springer, 1991. 567 p.

DISCRETE ANALOG OF CONJUGATE-OPERATOR MODEL OF A PROBLEM OF HEAT CONDUCTIVITY ON NON-MATCHING GRIDS[1]

Sorokin S.B.

Institute of Computational Mathematics and Mathematical Geophysics SB RAS, Novosibirsk State University, Novosibirsk, Russia

Using a nonuniform non-matching grid for variable parameters of the medium (in particular, a discontinuous parameter), we construct and numerically investigated a new difference scheme for the conjugate-operator model of the heat conductivity problem [1]: in the domain Ω equations hold

$$R^*\mathbf{w} = div\ \mathbf{w} = \left[\ \frac{\partial}{\partial x_1}\ ,\ \ \frac{\partial}{\partial x_2}\ \right] \left[\begin{array}{c} w_1 \\ w_2 \end{array}\right] = f,$$

$$\mathbf{w} = \mathbf{K}\mathbf{q} = \left[\begin{array}{cc} k_{11} & k_{12} \\ k_{21} & k_{22} \end{array}\right] \mathbf{q},$$

$$\mathbf{q} = Ru = -grad\ u = -\left[\begin{array}{c} \frac{\partial}{\partial x_1} \\ \frac{\partial}{\partial x_2} \end{array}\right] u,$$

boundary conditions $u|_{\partial\Omega} = 0$.

The difference scheme has second order accuracy.

Computational domain and grids used are shown in Figure 1.

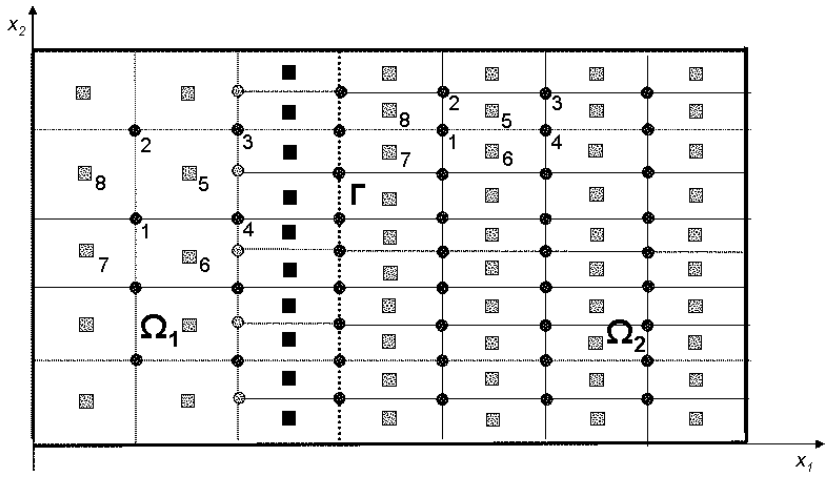

Figure 1. The calculation domain and grids.

[1]Supported by program 1.3 Basic research Division of the RAS "Modern computer and information technologies for solving large problems", program of the Presidium of RAS 15 "Information, control and intelligent technologies and systems"

Vertical line Γ (dashed) divides the domain into two parts

$$\Omega = \Omega_1 \cup \Omega_2.$$

In domain Ω was set grids: grid ω for u^h – dark circles, grid $\omega_{\frac{1}{2}}$ for $\mathbf{w^h}, \mathbf{q^h}$ – dark and gray squares. Gray circles auxiliary and do not participate in the calculation.

H_h – space of grid functions u^h defined in points ω and becomes zero at the boundary $\partial\Omega$. H_h^* – space of grid functions $\mathbf{w^h}$ defined in the points $\omega_{\frac{1}{2}}$.

The operator R in the defining relations is taken as the support operator. His approximation $R_h : H_h \to H_h^*$ is determined in each rectangular cell of grid area as follows [2, 3] (numbering points see Figure 1)

$$[\mathbf{q}^h]_5 = (R_h u^h)_5 = -\left[\begin{array}{c} \frac{1}{2}(\frac{u_4^h - u_1^h}{\tilde{h}_1} + \frac{u_3^h - u_2^h}{\tilde{h}_1}) \\ \frac{1}{2}(\frac{u_2^h - u_1^h}{\tilde{h}_2} + \frac{u_3^h - u_4^h}{\tilde{h}_2}) \end{array}\right]_5 = (\left[\begin{array}{c} R_{1h} \\ R_{2h} \end{array}\right] u^h)_5.$$

Here $\tilde{h}_1, \tilde{h}_2$ grid steps in the first and second directions, respectively. They shall take appropriate value for each subregion. For points (x_1, x_2) of the Ω_1 : $\tilde{h}_1 = h_{11}, \tilde{h}_2 = h_{21}$, for points (x_1, x_2) of the Ω_2 : $\tilde{h}_1 = h_{12}, \tilde{h}_2 = h_{22} = h_{21}/2$. The first index indicates the number of coordinate direction, the second – the number of the subregion.

For nodes $\omega_{\frac{1}{2}}$ black squares marked the action of R_h is determined by the same rule. The differences is that $\tilde{h}_2 = h_{22}$ and in this case involved the fictitious nodes marked gray circles are replaced by interpolation from the closest vertical neighboring nodes ω :

near $\partial\Omega$ from three nodes interpolation type

$$u(x_2 + \frac{h}{2}) = \frac{3}{8}\,u(x_2) + \frac{6}{8}\,u(x_2 + h) + \frac{-1}{8}\,u(x_2 + 2h) + O(h^3),$$

otherwise from four nodes interpolation type

$$u(x_2 + \frac{h}{2}) = -\frac{1}{16}\,u(x_2 - h) + \frac{9}{16}\,u(x_2) + \frac{9}{16}\,u(x_2 + h) - \frac{1}{16}\,u(x_2 + 2h) + O(h^4).$$

We define a scalar product in the H_h and H_h^* :

$$(u^h, v^h)_{H_h} = \sum_{(x_1,x_2)\in\omega} u^h(x_1, x_2) v^h(x_1, x_2) \tilde{h}_1 \tilde{h}_2 \quad \forall\, u^h \in H_h,\ v^h \in H_h,$$

$$(\mathbf{w}^h, \sigma^h)_{H_h^*} = \sum_{(x_1,x_2)\in\omega_{\frac{1}{2}}} \sum_{k=1}^{2} w_k^h(x_1, x_2) \sigma_k^h(x_1, x_2) \tilde{h}_1 \tilde{h}_2, \quad \forall\, \mathbf{w}^h \in H_h^*,\ \sigma^h \in H_h^*.$$

For the points $(x_1, x_2) \in \Gamma$ the first step $\tilde{h}_1 = \frac{h_{11}}{2} + \frac{h_{12}}{2}$, the second $\tilde{h}_2 = h_{22}$. For nodes $(x_1, x_2) \in \omega_{\frac{1}{2}}$ black squares marked: $\tilde{h}_1 = h_{11}$, the second $\tilde{h}_2 = h_{22}$.

In the approximation $R_h^* : H_h^* \to H_h$ of the operator R^* choose adjoint to R_h [4, 3]:

$$(R_h u^h, \mathbf{w}^h)_{H_h^*} = (u^h, R_h^* \mathbf{w}^h)_{H_h}.$$

If you enter e_i – orthogonal basis in H_h (in the scalar product $(\cdot,\cdot)_{H_h}$) the $R_h^* \mathbf{w}^h$ – element of H_h can be represented as an expansion

$$R_h^* \mathbf{w}^h = \sum_{j=1}^{N} \frac{(R_h^* \mathbf{w}^h, e_j)_{H_h}}{(e_j, e_j)_{H_h}} e_j = \sum_{j=1}^{N} \frac{(\mathbf{w}^h, R_h e_j)_{H_h^*}}{(e_j, e_j)_{H_h}} e_j.$$

As a basis in H_h take the system of network functions $e_{(x_1,x_2)}$, each of which is equal to one in one of the grid points ω and at all other points is equal to zero:

$$e_{(x_1,x_2)}(\tilde{x}_1, \tilde{x}_2) = \begin{cases} 0, & (x_1, x_2) \neq (\tilde{x}_1, \tilde{x}_2), \\ 1, & (x_1, x_2) = (\tilde{x}_1, \tilde{x}_2), \end{cases} \qquad \forall (x_1, x_2), (\tilde{x}_1, \tilde{x}_2) \in \omega.$$

Then the value $R_h^* \mathbf{w}^h$ at the point $(x_1, x_2) \in \omega$ is represented as

$$R_h^* \mathbf{w}^h(x_1, x_2) = \sum_{(\tilde{x}_1,\tilde{x}_2)\in\omega} \frac{(\mathbf{w}^h, R_h e_{(\tilde{x}_1,\tilde{x}_2)})_{H_h^*}}{(e_{(\tilde{x}_1,\tilde{x}_2)}, e_{(\tilde{x}_1,\tilde{x}_2)})_{H_h}} e_{(\tilde{x}_1,\tilde{x}_2)}(x_1, x_2) = \frac{(\mathbf{w}^h, R_h e_{(x_1,x_2)})_{H_h^*}}{(e_{(x_1,x_2)}, e_{(x_1,x_2)})_{H_h}} e_{(x_1,x_2)}(x_1, x_2) \ .$$

For all grid points ω, except for the points located on the vertical nearest Γ, latter formula gives (numbering points see Figure 1).

$$R_h^* \mathbf{w}^h{}_1 = \tfrac{1}{2}\left[\frac{(w_1^h)_6 - (w_1^h)_7}{\tilde{h}_1} + \frac{(w_1^h)_5 - (w_1^h)_8}{\tilde{h}_1}\right] + \tfrac{1}{2}\left[\frac{(w_2^h)_8 - (w_2^h)_7}{\tilde{h}_2} + \frac{(w_2^h)_5 - (w_2^h)_6}{\tilde{h}_2}\right].$$

For the grid points located in the vertical nearest Γ expression for $R_h^* \mathbf{w}^h$ more complicated.

Approximation of tensor $\mathbf{K} : H_h^* \to H_h^*$:

$$[\mathbf{w}^h]_5 = [\mathbf{K}_h \mathbf{q}^h]_5 = \begin{bmatrix} k_{11} & k_{12} \\ k_{21} & k_{22} \end{bmatrix}_5 [\mathbf{q}^h]_5.$$

Finally, discrete conjugate-operator model has the form of

$$\begin{gathered} R_h^* \mathbf{w}^h = f^h, \\ \mathbf{w}^h = \mathbf{K}_h \mathbf{q}^h, \\ \mathbf{q}^h = R_h u^h, \\ u^h \in H_h, \ \ \mathbf{w}^h \in H_h^*. \end{gathered}$$

The tables contains the results of test calculations, confirming the second order convergence of difference scheme.

The calculations were made in the domain $\Omega = (0,2) \times (0,1)$. The area was divided into two equal parts

$$\Omega = \Omega_1 \cup \Omega_2 = (0,1) \times (0,1) \cup (1,2) \times (0,1).$$

In each sub-region was set uniform grid: in Ω_1 with the steps $h_{11} = h_{21}$, in $\Omega_1 - h_{12} = h_{22} = h_{21}/2$. Use the steps shown in the first two columns.

The remaining columns indicate different characteristics of error

$$\mathbf{Z}^h = \left[\mathbf{w}^h, \ u^h \right]^T - \left[\mathbf{w}, \ u \right]^T.$$

Here $\left[\mathbf{w}, \ u \right]^T$ – a solution of the differential problem, $\left[\mathbf{w}^h, \ u^h \right]^T$ – the solution of the difference problem.

In the third column the error rate of the second component

$$\max_{(x_1,x_2)\in\omega} \left| u(x_1,x_2) - u^h(x_1,x_2) \right| = max_u.$$

The fourth – the rate of the second component of the error

$$\max[\max_{(x_1,x_2)\in\omega_{\frac{1}{2}}} |w_1(x_1,x_2) - w_1^h(x_1,x_2)|, \max_{(x_1,x_2)\in\omega_{\frac{1}{2}}} |w_2(x_1,x_2) - w_2^h(x_1,x_2)|] = max_{\mathbf{w}}.$$

In the fifth column of the norm of the projection of the second component error on interface of subdomains Γ

$$\max_{(x_1,x_2)\in\Gamma} \left| u(x_1,x_2) - u^h(x_1,x_2) \right| = max_\Gamma.$$

Finally, in the last – error rate

$$\left\| \mathbf{Z}^h \right\|_{\mathbf{H}} = \sqrt{\begin{array}{l} \displaystyle\sum_{(x_1,x_2)\in\omega} \left(u(x_1,x_2) - u^h(x_1,x_2) \right)^2 \tilde{h}_1 \tilde{h}_2 + \\ \displaystyle + \sum_{(x_1,x_2)\in\omega_{\frac{1}{2}}} \sum_{k=1}^{2} \left(w_k(x_1,x_2) - w_k^h(x_1,x_2) \right)^2 \tilde{h}_1 \tilde{h}_2 \end{array}}.$$

Table 1 corresponds to the calculations with the thermal conductivity tensor

$$\mathbf{K}(x_1,x_2) = \begin{bmatrix} 1 & 0 \\ 0 & 1 \end{bmatrix}, \ (x_1,x_2) \in \Omega_1 \cup \Omega_2,$$

and the exact solution $u(x_1,x_2) = \sin^3(\pi x_1)\sin^3(\pi x_2), \ (x_1,x_2) \in \Omega_1 \cup \Omega_2$.

Table 2 corresponds to the calculations with the thermal conductivity tensor (mixed derivatives and discontinuous coefficients)

$$\mathbf{K}(x_1,x_2) = \begin{bmatrix} 0.002 & 0.01 \\ 0.01 & 0.002 \end{bmatrix}, (x_1,x_2) \in \Omega_1, \quad \mathbf{K}(x_1,x_2) = \begin{bmatrix} 2 & 1 \\ 1 & 2 \end{bmatrix}, (x_1,x_2) \in \Omega_2$$

$h_{11} = h_{21}$	$h_{12} = h_{22}$	max_u	$max_{\mathbf{w}}$	max_Γ	$\left\|\mathbf{Z}^h\right\|_{\mathbf{H}}$
1/10	1/20	0.8802E-01	0.2137E+00	0.1043E-01	0.1158E+00
1/20	1/40	0.2069E-01	0.5404E-01	0.2492E-02	0.2765E-01
1/40	1/80	0.5096E-02	0.1348E-01	0.6164E-03	0.6837E-02
1/80	1/160	0.1266E-02	0.3371E-02	0.1534E-03	0.1705E-02

Table 1.

and the exact solution

$$u(x_1, x_2) = \sin^3(\pi x_1)\sin^3(\pi x_2),\ (x_1, x_2) \in \Omega_1,$$
$$u(x_1, x_2) = \sin^3(\mathbf{10}\pi x_1)\sin^3(\mathbf{10}\pi x_2),\ (x_1, x_2) \in \Omega_2.$$

$h_{11} = h_{21}$	$h_{12} = h_{22}$	max_u	$max_{\mathbf{w}}$	max_Γ	$\left\|\mathbf{Z}^h\right\|_{\mathbf{H}}$
1/40	1/80	0.1514E+00	0.8146E+01	0.6161E-01	0.4028E+01
1/80	1/160	0.3462E-01	0.1944E+01	0.1453E-01	0.9287E+00
1/160	1/320	0.8446E-02	0.4831E+00	0.3501E-02	0.2281E+00
1/320	1/640	0.2065E-02	0.1199E+00	0.8270E-03	0.5677E-01

Table 2.

This study differs from those above by the following:

1. All components of the discrete analogs of vectors are given at the same grid nodes. This enables us to correctly define the action of the discrete analog of the thermal conductivity tensor on the discrete analog of the temperature gradient and, in conjunction with the approximation method for the gradient, have the second order of convergence.

2. The second order of convergence holds not only for scalar grid function (approximations to temperature) but also for the grid vector functions (approximations to the heat flow).

3. A scheme of the second order of accuracy (on nonuniform non-matching grids for the variable medium parameters) is constructed only by the approaches of the theory of difference schemes. From a methodological point of view, the method for scheme designing presented in this is much clearer and easier than constructing a second-order scheme with the use of projectional statements.

Bibliography

1. *Konovalov A. N.* Conjugate-factorized models in mathematical physics problems //Sibirskii Zhurnal Vychislitel'noi Matematiki. - 1998. - Vol. 1. - No. 1. - pp. 25-58.

2. *Olshanskii M. A.* Analysis of semi-staggered finite-difference method with application to Bingham flows// Comput. Methods Appl. Mech. Engrg., - 2009. - 198. - pp. 975-985

3. *Sorokin S. B.* Justification of a Discrete Analog of the Conjugate-Operator Model of the Heat Conduction Problem// Journal of Applied and Industrial Mathematics, - 2015, - Vol. 9, - No. 1, - pp. 1-15.

4. *Lebedev V.I.* Difference analogues of orthogonal decompositions, basic differential operators and some boundary problems of mathematical physics. I // USSR Computational Mathematics and Mathematical Physics, Vol 4, No. 3, 1964, pp. 69-92.

DYNAMIC BEHAVIOUR OF HETEROGENEOUS POROELASTIC STRUCTURES

Vatulyan A.O., Gusakov D.V.

Southern Federal University, Rostov-on-Don, Russia

We consider the steady oscillations of heterogeneous poroelastic transversely isotropic layer under the action of harmonic load applied to the upper face in the framework of the plane deformation. All mechanical characteristics considered to be the functions of transverse coordinate. We follow the Biot [1] theory for modeling poroelastic media.

The dimensionless equations of motion, constitutive equations and the equation of pressure in the pores are:

$$\begin{aligned}
&\bar{\sigma}_{11,1} + \bar{\sigma}_{13,3} + \kappa^2 \bar{u}_1 = 0, \\
&\bar{\sigma}_{13,1} + \bar{\sigma}_{33,3} + \kappa^2 \bar{u}_3 = 0, \\
&\bar{\sigma}_{11} = \gamma_1 \bar{u}_{1,1} + \gamma_7 \bar{u}_{3,3} - \beta_1 \bar{p}, \\
&\bar{\sigma}_{33} = \gamma_7 \bar{u}_{1,1} + \gamma_4 \bar{u}_{3,3} - \beta_3 \bar{p}, \\
&\bar{\sigma}_{13} = \gamma_5 \left(\bar{u}_{1,3} + \bar{u}_{3,1} \right), \\
&\mu_1 \bar{p}_{,11} + \left(\mu_3 \bar{p}_{,3} \right)_{,3} + i\kappa \left(\eta_1 \bar{u}_{1,1} + \eta_3 \bar{u}_{3,3} \right) + i\kappa\delta\bar{p} = 0.
\end{aligned} \tag{1}$$

where the following dimensionless parameters and functions are introduced: $\bar{u}_i$ – displacement vector elements, $\bar{p}$ – pore pressure, $\bar{\sigma}_{ij}$ – stress tensor elements, $\bar{\gamma}_j$ – elastic tensor elements, $\bar{\beta}_j$ – Biot effective stress coefficients, $\bar{\mu}_j$ – intrinsic permeability coefficients, κ – frequency.

It is important to note that order of the material constants and the values of the functions in original equations several orders of magnitude different from each other. In this case dimensionless equations (1) are employed. The symbol $\bar{e}$ is dropped below.

The Fourier transform along the longitudinal coordinate is applied to the equations (1). The transformed equations are second order differential equations on functions u_k and p with variable coefficients. For solving this equations shooting method [2] is employed. Main idea of this method is representing solutions as the linear combinations of the solutions for several Cauchy problems. Note that with the growth of the transformation parameter $|\alpha|$ system takes the form of "stiff" system of differential equations, which is equivalent to the presence of a small parameter at the highest derivative. To solve such a system we use Gear method [3], with the boundary conditions replaced by:

$$\begin{aligned}
I : \xi_3 = 0 : &\quad u_1 = 0, \quad u_3 = 0, \quad p' = 0 \quad \sigma_{33} = e^{-|S\alpha|}, \quad \sigma_{13} = 0, \qquad p = 0 \\
II : \xi_3 = 0 : &\quad u_1 = 0, \quad u_3 = 0, \quad p' = 0 \quad \sigma_{33} = 0, \qquad \sigma_{13} = e^{-|S\alpha|}, \quad p = 0 \\
III : \xi_3 = 0 : &\quad u_1 = 0, \quad u_3 = 0, \quad p' = 0 \quad \sigma_{33} = 0, \qquad \sigma_{13} = 0, \qquad p = e^{-|S\alpha|}
\end{aligned}$$

where S is the normalization parameter [4].

To obtain values for the parameter S all variable coefficients in (1) replaced by their top estimates $\hat{\gamma}_i \geq |\gamma_i|$. The characteristic equation takes the form:

$$\begin{vmatrix} \hat{\gamma}_5\lambda^2 + (\kappa^2 - \alpha^2\hat{\gamma}_1) & -i\alpha(\hat{\gamma}_7 + \hat{\gamma}_5)\lambda & i\alpha\hat{\beta}_3 \\ -i\alpha(\hat{\gamma}_7 + \hat{\gamma}_5)\lambda & \hat{\gamma}_4\lambda^2 + (\kappa^2 - \alpha^2\hat{\gamma}_5) & -\hat{\beta}_3\lambda \\ \kappa\alpha\hat{\eta}_1 & i\kappa\hat{\eta}_3\lambda & \hat{\mu}_3\lambda^2 + (i\kappa\hat{\delta} - \alpha^2\hat{\mu}_1) \end{vmatrix} = 0 \quad (2)$$

We introduce replacement $\lambda = S|\alpha|$, and $\alpha \to \infty$. In this case equation (2) splits into two equations:

$$\hat{\mu}_3 S^2 - \hat{\mu}_1 = 0$$

$$\hat{\gamma}_5\hat{\gamma}_4 S^4 - ((\hat{\gamma}_7 + \hat{\gamma}_5)^2 + \hat{\gamma}_5^2 + \hat{\gamma}_1\hat{\gamma}_4)S^2 + \hat{\gamma}_1\hat{\gamma}_5 = 0$$

Obtained S values for cancellous bone [5] are: $S_1 = -S_4 = 1$, $S_2 = -S_5 = 0.497$, $S_3 = -S_6 = 1.463$.

Solution of the original problem in general has the form:

$$u_j(\xi_1, \xi_3) = \frac{1}{2\pi}\int_{-\infty}^{\infty} \frac{D_j(\alpha, \kappa, \xi_3)}{D_0(\alpha, \kappa)} e^{-i\alpha\xi_1} d\alpha, \quad (3)$$

where D_j, D_0 – is analytical functions of their arguments.

It can be shown that for the $\alpha \in R_1, D_0 \neq 0$ this representation of the solution is correct. At the same time, due to decreasing integrands when $|\alpha| \to \infty$, it is possible to calculate the integral (3) within finite limits, the choice the parameter R allows controling accuracy.

$$u_j(\xi_1, \xi_3) \approx \frac{1}{2\pi}\int_{-R}^{R} \frac{D_j(\alpha, \kappa, \xi_3)}{D_0(\alpha, \kappa)} e^{-i\alpha\xi_1} d\alpha$$

It should be noted that with the increase of parameter α solutions in transformants tend to 0 according to the law $1/|\alpha|$. Consequently, it seems reasonable to replace trasformants for large α values with approximation of the form $G/|\alpha|$, where G is complex constant determined separately for each of the transformants at $|\alpha| > R$. Experimentally found that in most cases values of $R = 20$ is enough to build solutions with an accuracy more than 10^{-3}. This fact allows reducing the number of the α parameter values, which are necessary to build a solution in transformants, and significantly reduces the running time.

To find the original solutions we use "Filon" quadrature formulas from [6].

We have obtained numerical data for displacement field for different laws of variation of the elastic moduli. Figure 1 represents results of calculating displacement fields on the upper layer face for the load concentrated at $\xi_1 = 0$ in the case of various inhomogeneities $\hat{\gamma}_j = \gamma_j * f(\xi_3)$. As shown in Figure 1 displacements have a logarithmic singularity at $\xi_1 = 0$. And with the growth of the coordinates have the form of attenuating wave.

Finally, we note that numerical solutions were obtained of the problem for various characteristics of the layer irregularities laws. Based on the analysis of the solutions we have revealed the influence of these characteristics on the displacement field at the upper layer face.

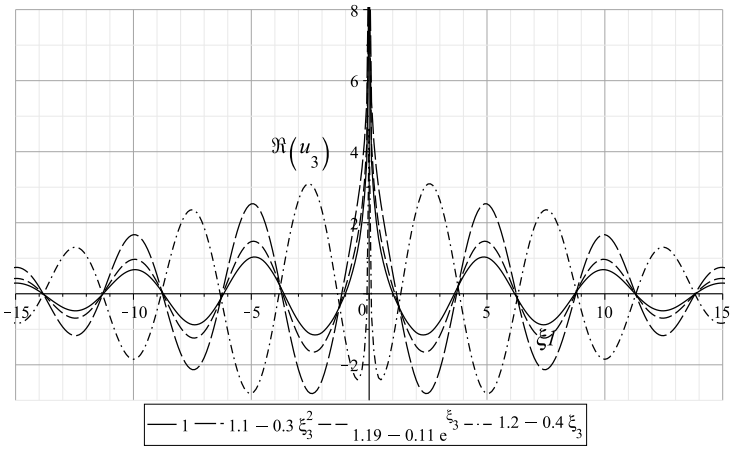

Figure 1. Displacements $Re(u_3)$ for various inhomogeneities of γ_j, concentrated load at $\xi_1 = 0$

Bibliography

1. *Biot M. A.* Theory of propogation of elastic waves in a fluid-saturated porous solid // J. Acoustic. Soc. Am. 1956. V. 28. - 2. -P.179-191.

2. *Kalitkin N. N.* Computational methods. M. Nauka, 1978. 512 p.

3. *Hairer E., Norsett S. P., Wanner G.* Solving Ordinary Differential Equations. Berlin etc., Springer-Verlag 1987. 480 p.

4. *Vorovich I. I., Babeshko V. A.* Dynamic mixed problem of elasticity theory for nonclassical areas. M. Nauka, 1979. 320 p.

5. *Coussy O.* Poromechanics. — London: Wiley, 2004. — 312 p.

6. *Filon L. N. G.* On a quadrature formula for trigonometric integrals. // Proc. R. Soc. Edinb. 1928. V. 49. -P.38-47.

TWO NEW SPLITTINGS AND PRECONDITIONER FOR ITERATIVELY SOLVING NON-HERMITIAN POSITIVE DEFINITE SYSTEMS

Rui-Ping Wen

Higher Education Key Laboratory of Engineering and Scientific Computing in Shanxi Province, Taiyuan Normal University, Taiyuan, China

Consider a large sparse system of linear equations

$$Ax = b, \tag{1}$$

where the coefficient matrix $A = (a_{ij}) \in \mathbb{R}^{n\times n}$ is a non-Hermitian positive definite matrix and $b \in \mathbb{R}^n$.

Based on the *Hermitian/skew-Hermitian* (HS) splitting

$$A = H + S, \tag{2}$$

where

$$H = \frac{1}{2}(A + A^*), \qquad S = \frac{1}{2}(A - A^*)$$

with A^* being the conjugate transpose of A, of the coefficient matrix A. In articles [1-3] Bai et al. derived some alternative methods named HSS and PSS iteration methods. It is proven that for a non-Hermitian positive definite linear systems, the HSS and PSS iteration methods both converge unconditionally to the unique solution of the system (1). However, both HSS and PSS iteration schemes are variants of an alterative iteration method. The Hermitian or the skew-Hermitian system needs to be solved at each iteration step. The research into a skew-Hermitian system of linear equations is also conducted in [4-6].

In this talk, a new iteration method for solving a linear system with coefficient matrix being non-Hermitian positive definite is presented as follows; An accelerated method is proposed, which will find the optimal solution in hyperplane generated by $\{x_k, \cdots, x_{k+m}\}$.

Our new method is just presented in view of the splitting (2). Let

$$H = M - N,$$

$$P = M + \alpha S,$$

$$Q = N + (\alpha - 1)S,$$

where α is a parameter. Then

$$A = P - Q,$$

and the iteration matrix is given by

$$T = P^{-1}Q.$$

Method 1.

Step 0. Give an initial point x_0 and a tolerance $\epsilon > 0$, for $k = 0, 1, 2, \ldots$ until the iteration converges.

Step 1. Solve the system of linear equations for x_k

$$Px_k = Qx_{k-1} + b$$

Step 2. If $\|Ax_k - b\| < \epsilon$, stop; Otherwise, $k \Leftarrow k + 1$ and go back to Step 1.

Method 2.

Step 0. Given an initial point $x^{(0,0)}$, the precision $\varepsilon > 0$, for $k = 0, 1, 2, \cdots$ until the process converges.

Step 1. For $l = 0, 1, 2, \cdots, m$, computing

$$Px^{(k,l+1)} = Qx^{(k,l)} + b.$$

Step 2. Let

$$r^{(k,l)} = Ax^{(k,l)} - b,$$

$$r = \sum_{l=1}^{m} \alpha_l^{(k)} r^{(k,l)},$$

$$\min_{\alpha} r^* H_1^{-1} r$$

$$\text{s.t.} \sum_{l=1}^{m} \alpha_l^{(k)} = 1.$$

Step 3.

$$x^{(k+1,0)} = \sum_{l=1}^{m} \alpha_l^{(k)} x^{(k,l)}.$$

Step 4. If $\|r\|_2 < \varepsilon$, stop; Otherwise, goto Step 1.

Remark In fact, the method 2 is the acceleration of method 1. If $m = 2$, it can be straightly shown in the following:

$$x^{(k+1,0)} = \alpha^{(k)} x^{(k,1)} + (1 - \alpha^{(k)}) x^{(k,2)}.$$

We study the spectral radius and contraction properties of the iteration matrices and then analyze the best possible choice of the parameters. With the results obtained, we show that the new methods are convergent for a non-Hermitian positive definite linear system. Furthermore, a preconditioner generated by the splitting is proposed, the condition number of preconditioned matrix is discussed. The numerical examples show these methods are effective.

Bibliography

1. *Z.-Z. Bai, G.H. Golub, M.K. Ng* Hermitian and skew-Hermitian splitting methods for non-Hermitian positive definite linear systems, SIAM J. Matrix Anal. Appl. 24(2003)603-626.

2. *Z.-Z. Bai, G.H. Golub, M.K. Ng* On successive-overrelaxation acceleration of the Hermitian and skew-Hermitian splitting iterations, Numer. Linear Algebra Appl. 14(2007)319-335.

3. *Z.-Z. Bai, G.H. Golub, L.-Z. Lu, J.-F. Yin* Block triangular and skew-Hermitian splitting methods for positive definite linear systems, SIAM J. Sci. Comput. 26(2005)844-863.

4. *E.-X. Jiang* Algorithm for solving a shifted skew-symmetric linear system, Front. Math. China 2(2007)1-16.

5. *L.A. Krukier, T.S. Martynova, Z.-Z. Bai* Product-type skew-Hermitian triangular splitting iteration methods for strongly non-Hermitian positive definite linear systems, J. Comput. Appl. Math. 232(2009)3-16.

6. *L. Wang, Z.-Z. Bai* Skew-Hermitian triangular splitting iteration methods for non-Hermitian positive definite linear systems of strong skew-Hermitian parts, BIT Numer. Math. 44(2004)363-386.

TWO-STAGE ITERATION METHODS FOR SADDLE POINT PROBLEMS

Guo-Feng Zhang, Mu-Zheng Zhu, Jing-Yu Zhao
School of Mathematics and Statistics, Lanzhou University, Lanzhou, P.R.China

In this talk, we will focus on the solution of large sparse saddle point problems

$$\mathscr{A}u \equiv \begin{bmatrix} A & B^* \\ B & 0 \end{bmatrix} \begin{bmatrix} x \\ y \end{bmatrix} = \begin{bmatrix} f \\ g \end{bmatrix} \equiv b \tag{1}$$

with Case 1 or Case 2.
Case 1: $A \in \mathbb{R}^{n\times n}$ is a symmetric positive definite (SPD) matrix, $B \in \mathbb{R}^{m\times n}$ is of full rank, $x, f \in \mathbb{R}^n, y, g \in \mathbb{R}^m$ and $m \leq n$.
Case 2: $A \in \mathbb{C}^{n\times n}$ is a non-Hermitian matrix and its Hermitian part $H = \frac{1}{2}(A + A^*)$ is positive definite (Non-HPD), $B \in \mathbb{C}^{m\times n}$ is of full rank, $x, f \in \mathbb{C}^n, y, g \in \mathbb{C}^m$ and $m \leq n$.

Linear systems of the form (0.1) arises in a variety of scientific computing and engineering applications, including computational fluid dynamics[8, 11], constrained and weighted least squares optimization[8, 13], image reconstruction and registration[14, 15], mixed finite element approximations of elliptic PDEs and Navier-Stokes problems[7, 12, 10] and so on; see [2, 7, 8] and reference therein.

In recent years, there has been a surge of interest in linear systems of the form (1) and a large numerical solution methods for (0.1) have been proposed. For examples, direct solves, stationary iteration methods [9, 4, 1, 3, 6], null space methods and preconditioned Krylov subspace methods[8, 10, 5] and so on on. Iteration methods and preconditioned Krylov methods are interested because of their preservation of sparsity and lower requirement for storage. We refer to some comprehensive surveys [8, 7, 13] and the references therein for algebraic properties and solving methods for saddle point problems.

We define a matrix $P(\alpha)$ as

$$P(\alpha) := \begin{bmatrix} I_n & -B^*(BB^*)^{-1} \\ 0 & I_m \end{bmatrix} \begin{bmatrix} I_n & 0 \\ B & -\alpha BB^* \end{bmatrix} = \begin{bmatrix} I_n - B^*(BB^*)^{-1}B & \alpha B^* \\ B & -\alpha BB^* \end{bmatrix},$$

where α is a positive constant. By preconditioning the saddle point problem (1) from the left with $P(\alpha)$, we can get the following preconditioned linear system:

$$P(\alpha)\mathscr{A} = P(\alpha) \begin{bmatrix} f \\ g \end{bmatrix} \Longleftrightarrow$$

$$\begin{bmatrix} (I - B^*(BB^*)^{-1}B)A + \alpha B^*B & 0 \\ BA - \alpha(BB^*)B & BB^* \end{bmatrix} \begin{bmatrix} x \\ y \end{bmatrix} = \begin{bmatrix} f - B^*(BB^*)^{-1}Bf + \alpha B^*g \\ Bf - \alpha BB^*g \end{bmatrix}$$

$$\Longleftrightarrow \begin{bmatrix} A_1 & 0 \\ A_3 & A_2 \end{bmatrix} \begin{bmatrix} x \\ y \end{bmatrix} = \begin{bmatrix} b1 \\ b2 \end{bmatrix}$$

with

$$A_1 := (I - B^*(BB^*)^{-1}B)A + \alpha B^*B, \quad A_2 := BB^*, A_3 := BA - \alpha(BB^*)B, \quad (2)$$

$$b_1 = f - B^*(BB^*)^{-1}Bf + \alpha B^*g, \quad b_2 = Bf - \alpha BB^*g.$$

We can get the solution of the system (0.1) by solving the coupled linear systems of the form

$$A_1x \equiv \big((I - B^*(BB^*)^{-1}B)A + \alpha B^*B\big)x = b_1,$$
$$A_2y \equiv (BB^*)y = b_2 - A_3x.$$

Thus it can be solved by first computing x from

$$A_1x = b_1 \quad (3)$$

and then computing y from

$$A_2y = b_2 - A_3x. \quad (4)$$

Theorem 1 *Let A defined in (0.1) be nonsingular and B be of full rank. Then the matrix A_1 defined in (0.2) is nonsingular for any iteration parameter $\alpha \neq 0$.*

Since the system (0.4) is SPD, any solver for SPD systems can be applied. This could be a Cholesky factorization, or a preconditioned conjugate gradient (PCG) method, or some specialized solvers.

Generally, the coefficient matrix A_1 in (0.3) is large and dense, so direct computations are very costly and impractical in actual implementations. Then we will solve the linear system (0.3) iteratively by splitting technology.

Algorithm 1: ($A \in \mathbb{R}^{n\times n}$ being a SPD matrix)
Stage 1: solve the linear system (0.3) iteratively by PCG or Cholesky factorization:

$$M_1(\alpha)x^{(k+1)} = N_1x^{(k)} + b_1 \quad (5)$$

with $M_1(\alpha) := A + \alpha B^*B$ and $N_1 := B^*(BB^*)^{-1}BA$.
Stage 2: solve the system (0.4) by using Cholesky factorization, or PCG method.
Theorem 2 *Let $A \in \mathbb{R}^{m\times m}$ be SPD, and $B \in \mathbb{R}^{m\times n}$ be of full column rank. Then, the iteration (0.5) is convergent when $\alpha > \alpha^*$, where $\alpha^* = \frac{\lambda_{\max}^2}{\mu_{\min}\lambda_{\min}}$. Furthermore, we have $\lim_{\alpha\to\infty}\rho(T(\alpha)) = 0$. Here, $T(\alpha) = M^{-1}(\alpha)N$ is the iteration matrix. $\lambda_{\max}^2$ and $\lambda_{\min}$ are the maximum and minimum eigenvalues of $T(\alpha)$, $\mu_{\min}$ is the minimum eigenvalue of B^TB.*
Algorithm 2: (A being large and non-Hermitian matrix)
Stage 1: solve the linear system (0.3) iteratively by PCG or Cholesky factorization:

$$M_2(\alpha)x^{(k+1)} = N_2x^{(k)} + b_1 \quad (6)$$

with $M_2 := H + \alpha B^*B$ and $N_2 := B^*(BB^*)^{-1}BA - S$, where $H = \frac{1}{2}(A + A^*)$ and $S = \frac{1}{2}(A - A^*)$.

Stage 2: solve the system (0.4) by using Cholesky factorization, or PCG method[5, **?**].

Theorem 3 *Let $A \in \mathbb{C}^{n\times n}$ be a non-Hermitian matrix and its Hermitian part $H = \frac{1}{2}(A + A^*)$ is positive definite (Non-HPD) and $B \in \mathbb{C}^{m\times n}$ be of full rank. Then the iterative method (0.6) is convergent if the following condition is satisfied:*

$$\alpha > \max\left\{\frac{\sqrt{\eta_1^2 + (\beta - \eta_2)^2} - \gamma}{\tau},\ 0\right\}.$$

Here,

$$\eta_1 + \mathrm{i}\eta_2 = \frac{x^*B^*(BB^*)^{-1}BAx}{x^*x}, \quad \mathrm{i}\beta = \frac{x^*Sx}{x^*x}, \quad \gamma = \frac{x^*Hx}{x^*x}, \quad \tau = \frac{x^*B^*Bx}{x^*x},$$

and x is an eigenvector of the iterative matrix $M^{-1}N$ in stage I. Furthermore, we have $\rho(M_2^{-1}N_2)$ monotonically decreases and tends to 0 as $\alpha \to +\infty$.

Bibliography

1. *Z.-Z. Bai, M. K. Ng* On inexact preconditioners for nonsymmetric matrices, SIAM J. Sci. Comput. 26 (5) (2005) 1710–1724.

2. *Z.-Z. Bai* Structured preconditioners for nonsingular matrices of block two-by-two structures, Math. Comput. 75 (254) (2006) 791–815.

3. *Z.-Z. Bai* Several splittings for non-Hermitian linear systems, Sci. China Ser. A: Math. 51 (8) (2008) 1339–1348.

4. *Z.-Z. Bai, G. H. Golub, M. K. Ng* Hermitian and skew-Hermitian splitting methods for non-Hermitian positive definite linear systems, SIAM J. Matrix Anal. Appl. 24 (3) (2003) 603–626.

5. *Z.-Z. Bai, G.-Q. Li* Restrictively preconditioned conjugate gradient methods for systems of linear equations, IMA J. Numer. Anal. 23 (4) (2003) 561–580.

6. *Z.-Z. Bai, B. N. Parlett, Z.-Q. Wang* On generalized successive overrelaxation methods for augmented linear systems, Numer. Math. 102 (1) (2005) 1–38.

7. *F. Brezzi, M. Fortin* Mixed and Hybrid Finite Element Methods, Springer-Verlag, New York and London, 1991.

8. *M. Benzi, G. H. Golub, J. Liesen* Numerical solution of saddle point problems, Acta Numer. 14 (2005) 1–137.

9. *J. H. Bramble, J. E. Pasciak, A. T. Vassilev* Uzawa type algorithms for nonsymmetric saddle point problems, Math. Comput. 69 (230) (2000) 667–690.

10. *H. C. Elman* Preconditioning for the steady-state Navier-Stokes equations with low viscosity, SIAM J. Sci. Comput. 20 (4) (1999) 1299–1316.

11. *H. C. Elman, G. H. Golub* Inexact and preconditioned Uzawa algorithms for saddle point problems, SIAM J. Numer. Anal. 31 (6) (1994) 1645–1661.

12. *H. C. Elman, D. J. Silvester* Fast nonsymmetric iterations and preconditioning for Navier-Stokes equations, SIAM J. Sci. Comput. 17 (1) (1996) 33–46.

13. *C. Greif, E. Moulding, D. Orban* Bounds on eigenvalues of matrices arising from interior-point methods, SIAM J. Optim. 24 (1) (2014) 49–83.

14. *E. L. Hall* Computer Image Processing and Recognition, Academic Press, New York, 1979.

15. *E. Haber, J. Modersitzki* Numerical methods for volume-preserving image registration, Inverse Probl. 20 (5) (2004) 1261–1638.

GROUP ANALYSIS OF INTEGRO-DIFFERENTIAL EQUATIONS DESCRIBING STRESS RELAXATION BEHAVIOR OF ONE-DIMENSIONAL VISCOELASTIC MATERIALS

Longqiao Zhou[1,2], **Sergey V. Meleshko**[1]

[1] *School of Mathematics, Institute of Science, Suranaree University of Technology, Nakhon Ratchasima, Thailand*

[2] *School of Mathematics and Statistics, Guizhou University of Finance and Economics, Guiyang, China*

Many important physical processes in nature are governed by differential equations. Nonlinearity and the presence of a large number of variables in the initial equations are sources of significant mathematical difficulties in the analysis of the solutions of these equations. Frequently, it is virtually impossible to give explicit solutions, and while a multitude of numerical methods has been developed to obtain approximate solutions, there remains intense interest in finding exact solutions. Each solution has value, first, as the exact description of the real process in the framework of a given model; secondly, as a model to compare various numerical methods; thirdly, as a basis to improve the models used. One of methods for constructing exact solutions is group analysis.

The group analysis method, besides constructing exact solutions, provides a regular procedure for mathematical modeling by classifying differential equations with respect to arbitrary elements. We mention here that modeling a given system of differential equations with the use of difference equations and meshes can also be based on symmetries [1].

The classical Lie group theory provides a universal tool for calculating admitted Lie group for a system of differential equations. However, applications of the group analysis method to integro-differential equations presents some difficulties. The main difficulty comes from their nonlocal terms (integral terms). Since the definition of an admitted Lie group given of partial differential equations cannot be applied to integro-differential equations, this concept requires further investigation. A regular method for calculating an admitted Lie group of integro-differential equations was recently introduced in [2, 3, 4]. A Lie group admitted by integro-differential equations is also defined as a Lie group satisfying determining equations. The way of obtaining determining equations for integro- differential equations is similar (and not more difficult) to the way used for differential equations. The main difficulty in obtaining an admitted Lie group of integro-differential equations consists of solving the determining equations. Notice that the determining equations of integro-differential equations are integro-differential.

In the present work we focus on the application of the group analysis method to the one-dimensional equations describing behaviour of viscoelastic materials

$$v_t = \sigma_x, \quad e_t = v_x, \quad \varphi(\sigma) = e + \int_0^t H(t,\tau)e(\tau)d\tau, \quad \varphi'(\sigma) \neq 0. \qquad (1)$$

Here time t and distance x are independent variables, the stress σ, the velocity v, and the strain e are dependent variables, $H(t,\tau)$ is the kernel of relaxation, $\varphi(\sigma)$ is a smooth function of the stress. If $\varphi(\sigma)$ is a linear function, then system (1) describes linear behavior of a viscoelastic material. Notice that system (1) is a system of integro-differential equations. The admitted Lie group of (1) is found. Invariant solutions of this system of equations are also discussed in this study.

Bibliography

1. *V. A. Dorodnitsyn* Applications of Lie Groups to Difference Equations. CRC Press, Boca Raton, 2011.

2. *Yu. N. Grigoriev and S. V. Meleshko* Group analysis of the integro-differential Boltzman equation. Dokl. AS USSR, 297(2):323-327, 1987.

3. *S. V. Meleshko* Methods for Constructing Exact Solutions of Partial Differential Equations: Mathematical and Analytical Techniques with Applications to Engineering. Springer Science and Business Media, Inc., New York, 2005.

4. *Yu. N. Grigoriev, N. H. Ibragimov, V. F. Kovalev, and S. V. Meleshko* Symmetries of integro-differential equations and their applications in mechanics and plasma physics. Lecture Notes in Physics, Vol. 806. Springer, Berlin / Heidelberg, 2010.

Invited talks

MULTIGRID METHOD WITH SPECIAL APPROXIMATION FOR THE NAVIER-STOKES EQUATIONS IN A VISCOUS INCOMPRESSIBLE FLUID[1]

Andreeva E.M., Muratova G.V.
Southern Federal University, Rostov-on-Don, Russia

I Introduction

We propose some approach for solving the two-dimensional Navier-Stokes equations for a viscous incompressible fluid. In this paper we construct special FEM basis functions for these equations. They are of the usual form at the time level where an approximate solution is sought, and they have useful properties for the approximation of transport derivatives between time levels. As a result, at each time level a stationary problem of a simpler form with a self-adjoint operator is obtained. To solve this problem, we apply the conforming finite element method with the bilinear elements for velocities and piecewise-constant elements for the pressure on rectangles [1], [2].

II Problem formulation

Consider classical formulation of the Navier-Stokes equations in domain $\Omega = (0,1) \times (0,1)$ with boundary $\partial\Omega$

$$\frac{\partial \mathbf{V}}{\partial t} + (\nabla \cdot \mathbf{V})\,\mathbf{V} - \frac{1}{Re}\Delta \mathbf{V} + \nabla p = \mathbf{F}, \tag{1}$$

$$div\mathbf{V} = 0, \tag{2}$$

where Re is Reynolds's number, and $\mathbf{V} = (u(x,y,t), v(x,y,t))$ is the velocity, p is the pressure.

To provide uniqueness of the pressure, we use the condition

$$\int_\Omega p, d\Omega = 0, \quad \forall t \in [0,T]. \tag{3}$$

The initial conditions are as follows:

$$\begin{gathered} u(0,x,y) = u_0(x,y), \\ v(0,x,y) = v_0(x,y), \quad (x,y) \in \Omega. \end{gathered} \tag{4}$$

[1]This work was supported by RFBR, N15-51-53066

The boundaries conditions are as follows:

$$\begin{array}{c} u(t,x,y) = u_g(t,x,y), \\ v(t,x,y) = v_g(t,x,y), \quad (t,x,y) \in (0,T) \times \partial\Omega. \end{array} \tag{5}$$

To approximate the time derivative and inertial first space derivatives a method of characteristics is used. The method of characteristics was suggested by the he French and American scientists for approximating the equations of viscous incompressible liquid with the first order of approximation. It has special theoretical and practical development in Pirrono's work for mass transfer equation [4].

Space discretization is carried out by finite element method. It's used a mixed formulation in the finite element method, when a combination of simple finite elements – bilinear for velocities and constant elements for pressure is applied. This combination provides stability of pressure calculation with additional application of a numerical filtration.

Consider the following basis functions for the velocity components ($i = 0, ..., n_1, j = 0, ..., n_2$):

$$\varphi_{i,j}(x,y) = \begin{cases} \left(\frac{1-|x-x_i|}{h_1}\right)\left(\frac{1-|y-y_j|}{h_2}\right), & if (x,y) \in [x_{i-1}, x_{i+1}] \times [y_{j-1}, y_{j+1}], \\ 0, & otherwise. \end{cases} \tag{6}$$

The basis functions for the pressure are of a more simple form ($i = 0, ..., n_1 - 1, j = 0, ..., n_2 - 1$):

$$\psi_{i+\frac{1}{2}}(x,y) = \begin{cases} 1, & if (x,y) \in [x_i, x_{i+1}) \times [y_j, y_{j+1}), \\ 0, & otherwise. \end{cases} \tag{7}$$

An approximate solution at level $t = t_k$ has the following form:

$$u^h(x,y) = \sum_{0 \le i \le n_1, 1 \le j \le n_2 - 1} \alpha_{i,j} \varphi_{i,j}(x,y), \tag{8}$$

$$v^h(x,y) = \sum_{0 \le i \le n_1, 1 \le j \le n_2 - 1} \beta_{i,j} \varphi_{i,j}(x,y), \tag{9}$$

$$p^h(x,y) = \sum_{0 \le i \le n_1 - 1, 0 \le j \le n_2 - 1} \gamma_{i,j} \psi_{i+\frac{1}{2}, j+\frac{1}{2}}(x,y). \tag{10}$$

As a result of the approximation we get the block system of algebraic equations at level t_k:

$$\mathbf{Au} \equiv \begin{bmatrix} A_{11} & O & A_{13} \\ O & A_{22} & A_{23} \\ A_{13}^T & A_{23}^T & O \end{bmatrix} \begin{bmatrix} u \\ v \\ p \end{bmatrix} = \begin{bmatrix} f_1 \\ f_2 \\ f_3 \end{bmatrix} \equiv \mathbf{f}. \tag{11}$$

which is solved by multigrid method. Here, O denotes a zero matrix of the corresponding dimension. Note that matrices A_{11} and A_{22} are self-adjoint and positive definite.

III Multigrid method

The multigrid method (MGM) is one of the effective and enough universal iterative methods for solving the systems of the linear algebraic equations. The multigrid method belongs to a class of quickly converging iterative methods [3], [5].

The multigrid idea is based on two principles: error smoothing and coarse grid correction. Some iterative methods have a smoothing effect on the error of approximation. This property is fundamental for the multigrid idea and is connected with fast damping high-frequency Fourier components of an initial error in decomposition on the basis from eigenvectors.

The multigrid algorithm allows to increase considerably efficiency of the main iterative method, combining usual iterative process with the coarse-grid correction. One of the MGM components is basic iterative method or smoothing procedure. This is the most sensitive part of the method of the problem under consideration.

There are some classical iterative methods for saddle point problems which can be used as the smoothers in MGM:

- The generalized minimal residual (GMRES) method, which, in exact arithmetic, converges within m iterations for any non-singular matrix $K \in \mathbb{R}^{m\times m}$.

- The Uzawa method. The rate of convergence of iterative methods depends on the type Uzawa resampling on time and with a decrease in the value of this step falls. Therefore, iterative methods such as preconditioners Uzawa are used for multigrid methods.

- The semi-implicit method for pressure-linked equations (SIMPLE) method. SIMPLE is based on finite-volume discretization of the Navier-Stokes equations. One of the important properties of finite volume method is the exact preservation of the integral quantities such as mass, momentum and energy for any group of control volumes and, consequently, the entire computational domain.

- Braess-Sarazin smoother. In contrast to the exact Uzawa and the SIMPLE methods, the Braess-Sarazin smoother computes the iterates u^{t+1} and p^{t+1} from the old velocity iterate u^t.

- Vanka Smoothers were first introduced within the context of a multigrid method for staggered mesh discretizations of the Navier-Stokes equations.

This smoother can be constructed without knowledge of the geometry or the discretization of the underlying PDE. The additive version of this smoother can be interpreted as an inexact Uzawa relaxation scheme.

On the first stage of our investigation we use simple iteration method as the smoother because after discretization we obtain a linear algebraic equation system with a symmetric matrix which has a spectrum with alternating signs.

$$u_h^{n+1} = u_h^n - \tau A_h^T (A_h u_h^n - f_h).$$

The second component of a multigrid method is the coarse grid correction determined by restriction operator R_h^{2h} and prolongation operator P_{2h}^h, which are realized for velocity components by templates:

$$R_h^{2h} = \frac{1}{16} \begin{bmatrix} 1 & 2 & 1 \\ 2 & 4 & 2 \\ 1 & 2 & 1 \end{bmatrix}_h^{2h} \quad \text{and} \quad P_{2h}^h = \frac{1}{4} \begin{bmatrix} 1 & 2 & 1 \\ 2 & 4 & 2 \\ 1 & 2 & 1 \end{bmatrix}_{2h}^{h}.$$

The operators of restriction R_h^{2h} and prolongation P_{2h}^h are realized for pressure components by other templates:

$$R_h^{2h} = \frac{1}{4} \begin{bmatrix} 1 & 1 \\ 1 & 1 \end{bmatrix}_h^{2h} \quad \text{and} \quad P_{2h}^h = \begin{bmatrix} 1 & 1 \\ 1 & 1 \end{bmatrix}_{2h}^{h}.$$

The results of some numerical experiments allow to conclude the efficiency of the suggested approach for solving the Navier-Stokes equations.

IV Numerical results

We consider the equation (1)-(2) with initial and boundary conditions (3)-(5) and the exact solution:

$$\begin{aligned} u(x,y,t) &= x * (1-x) * y * (1-y) * (t+2) \\ v(x,y,t) &= sin(x) * (1-x) * y * (1-y) * (t+1) \\ p(x,y,t) &= (x-1/2) * (y-1/2) * t \end{aligned} \tag{12}$$

Table 1 presents a comparison of the numbers iterations and times calculation of the multigrid method with a different numbers of levels MGM and simple iteration method. Peclet numbers is 1000, number of smoothing iteration is 5.

Table 2 presents a comparison of the multigrid method for solving the problem with a different number of smoothing iterations. Peclet numbers is 1000, mesh size is 65×65.

V Conclusion

For the the Navier-Stokes equations it has been shown that by mixing the method of characteristics and the finite element method we are able to derive first and second order accurate conservative schemes of the upwinding type.

Mesh grid	Sample iteration	MGM l=2	MGM l=3	MGM l=4	MGM l=5	MGM l=6
33×33	76306	4362	5452	4884		
	12sec	11sec	11sec	11sec		
65×65	787942	98376	72425	55989	43307	
	5min	8min	4min	4min	3min	
129×129	5857643	868407	639641	464102	325721	226555
	87min	108min	105min	78min	58min	30min

Table 1. Multigrid method with a different number of levels

Smoothing iterations	MGM l=5	MGM l=4	MGM l=3
5	43307	55989	72425
	3min	4min	4min
10	31131	37341	44069
	3min	3min	3min
15	24347	28054	31715
	2min	3min	3min

Table 2. Multigrid method with a different number of smoothing iterations

Application of a combination of the method of characteristics and the finite element method allows building the effective numerical algorithm. These schemes are numerically better than the usual upwinding schemes because they require numerical solution of symmetric systems only. After discretization we obtain a linear algebraic equation system with a symmetric matrix which has a spectrum with alternating signs. We use multigrid method with simple iteration method as the smoother for solving this system.

The results of some numerical experiments allow to conclude the efficiency of the suggested approach for solving the Navier-Stokes equations.

Bibliography

1. Andreeva E., Vyatkin A., Shaidurov V., The semi-Lagrangian approximation in the finite element method for Navier-Stokes equations for a viscous incompressible fluid, AIP Conference Proceedings, 1611, 3 (2014)

2. Chen H., Lin Q., Shaidurov V.V., Zhou J., Error estimates for triangular and tetrahedral finite elements in combination with a trajectory approximation of the first derivatives for advection-diffusion equations, Numerical Analysis and Applications, 4, 4. 345-362 (2011)

3. Muratova G.V., Andreeva E.M., Multigrid method for fluid dynamic problems, Journal of Computational Mathematics, 32, 3, 233-247 (2014)

4. Pironneau, O., On the Transport-Diffusion Algorithm and Its Applications to the NavierStokes Equations, Numerische Mathematik, 38, 309-332 (1982)

5. Trottenberg U., Oosterlee C.W., Schuller A., Multigrid. Academic Press, New York, (2001)

SIMULATIONS OF RADIOACTIVE CONTAMINATION WITHIN AN INDUSTRIAL SITE

Blagodatskykh D.V.*, Dzama D.V.*, Sorokovikova O.S.**

* *The Nuclear Safety Institute of the Russian Academy of Sciences, Moscow, Russia*

** *National Research Nuclear University MEPhI, Moscow, Russia*

This paper concerns some practical aspects of the application of a 3D hydrodynamic code [1] to modelling of radioactive contamination within an industrial site. The 3D code is intended to simulate the propagation of contamination taking into account the actual geometry of obstacles and to calculate doses from various external sources and via different paths of exposure (clouds of arbitrary shape, inhomogeneous surface deposition, inhalation). The CFD model allows for calculating doses received by the personnel for the whole territory of a facility in the case of a non-uniform wind field and non-isotropic turbulence.

An essential feature of Gaussian models still widely used in safety assessment analysis is their poor adaptation to real urban conditions. A comparison of concentrations calculated via a Gaussian model and obtained by experiment for the same weather conditions demonstrates that Gaussian models fail even in quantitative estimation of the distribution of concentrations. They are not able to reproduce the complexity of flows around an obstacle of realistic geometry. This gives a reason for using a CFD code which could in principle to predict the actual distribution of velocities.

The main goal of our research is to make estimations of doses in a more realistic and accurate fashion. Known analytical solutions such as the point or linear source approximation are not sufficiently accurate for our purposes. To attain this objective we take into account the radiation emitted by all points of a radioactive cloud

$$\dot{d}_{vol}\left(\vec{r}_0, n\right) = \iiint_{\Omega} I\left(\vec{r}, \vec{r}_0\right) \cdot \rho_{vol}\left(\vec{r}\right) \cdot \sigma\left(\vec{r}, n\right) \cdot \, dV$$

or a contaminated surface

$$\dot{d}_{surf}\left(\vec{r}_0, n\right) = \iint_{\partial S} I\left(\vec{r}, \vec{r}_0\right) \cdot \rho_{surf}\left(\vec{r}\right) \cdot \sigma\left(\vec{r}, n\right) \cdot \, dS$$

where $\sigma\left(\vec{r}, n\right)$ is the dose rate $[Sv/\left(s \cdot Bq\right)]$ from the point source of radiation of the nuclide n on the distance r, $I\left(\vec{r}, \vec{r}_0\right)$ is the visibility (can be only 0 or 1) of the point with radius-vector $\vec{r}$ from the point with radius-vector $\vec{r}_0$, $\rho_{vol}\left(\vec{r}\right), \rho_{surf}\left(\vec{r}\right)$ - volume and surface concentration, $\dot{d}_{vol}\left(\vec{r}_0, n\right), \dot{d}_{surf}\left(\vec{r}_0, n\right)$ - volume and surface dose rate at the point with radius-vector $\vec{r}_0$. Thus, the whole source is divided into a set of point sources. The dose of radiation received by the exposed object from a point source is determined by whether or not there

is any obstacle in the straight line connecting the source and the recipient. If there is, we leave out the amount of radiation delivered by the source. Such an integral method calls for a huge amount of calculations to be performed. A way to accelerate calculations is the application of a parallel algorithm.

In this paper we present a description of a 3D CFD code capable of making estimations of doses in a more realistic and accurate fashion for the needs of emergency analysis. As a result, a robust CFD model is implemented on the base of the Navie-Stokes equations. The conversation laws of mass

$$\frac{\partial \rho}{\partial t} + div(\rho \vec{u}) = 0$$

impulse

$$\rho \frac{\partial \vec{u}}{\partial t} + \rho\left(\vec{u}\vec{\nabla}\right)\vec{u} = -\vec{\nabla}\delta P + \vec{\nabla}\left(\rho\nu_T\vec{\nabla}\right)\vec{u} + \rho\vec{g}\,\frac{\delta\theta}{\theta} + \vec{f}$$

an equation for potential temperature to better account for pressure drop with height due to a significant vertical scale

$$\frac{d\theta}{dt} = \frac{\partial\theta}{\partial t} + \vec{u}\vec{\nabla}\theta = \vec{\nabla}\left(\chi\vec{\nabla}\theta\right)$$

and equations for dispersion of around 20 radionuclides taking into account their decay rates

$$\frac{\partial C_n}{\partial t} + (u + w_n)\vec{\nabla}C_n = \vec{\nabla}\left(D_T\vec{\nabla}C_n\right) + Q_{C_n}$$

are applied. Due to the fact that an essentially subsonic flow is considered, the surrounding medium approximates to an incompressible one. Since the little difference between actual and dry-adiabatic temperature is assumed, perturbations of potential temperature are supposed to be small.Moreover, for the given range of hydrodynamic parameters the Boussinesque approximation is justifiable, hence

$$\rho\left(\theta\right) = \rho\left(\theta_0\right) + \left.\frac{\partial\rho}{\partial\theta}\right|_{\theta=\theta_0}(\theta - \theta_0)$$

The effect of turbulence is modelled via a RANS approach. A modified version of $k-\epsilon$ model is applied to avoid mesh refinement near solid surfaces, thereby significantly decreasing computational costs. To avoid small dimensions of boundary cells, adapted boundary conditions on solid surfaces for k and ϵ are utilized on the base of Monin-Obukhov theory. An assumption is made that a velocity profile in a boundary cell is given by the formula

$$u\left(\triangle\right) = \frac{u_*}{\kappa}\left[\ln\left(\frac{\triangle}{r}\right) + \phi(p)\right]$$

derived in Monin-Obukhov theory. Then we substitute the friction velocity in formulas

$$k = \frac{u_*^2}{C_\mu^{1/2}} \quad \varepsilon = \frac{u_*^3}{\kappa\triangle}$$

thereby achieving for the turbulent coefficient a formula identical to that in Prandtl theory for the case of neutral stratification, as far as other types of stratifications are concerned the modified coefficient is used. A positive feature is that we do not have to refine mesh significantly near solid surfaces, but the size of the boundary cells should be from 10 to 15 times larger than the roughness length.

There is a conventional practice [2] to reproduce the conditions of a field experiment in a wind-tunnel to augment the amount of data obtained in the field test. We tested our code with a field data of the experiment carried out in Oklahoma-city [3]. A comparison of measured and calculated concentrations are shown in fig. 1 only for surface points, where squares represent calculated values and triangles denote measured values.

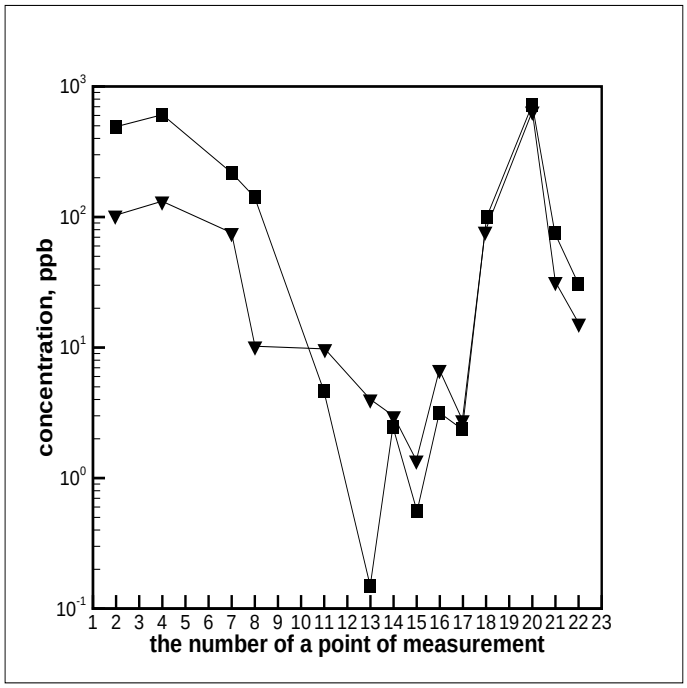

Figure 1. A comparison of measured and calculated concentrations

As can be seen, our prediction of the maximum value of surface concentration is close to the measured value with an accuracy of 5%.Taking into account that it is a crucial point for our code to predict maximum concentrations fairly well due to the fact that it concerns safety analysis issue, we can consider the result as a good one.Nevertheless, our code sufficiently underestimates the value of concentration measured at the point 13. It can be explained by an existence of steep gradients of concentration in the vicinity of the point.

Actually, a thorough examination of the site of station 13 disposition distinctly reveals a presence of several trees down the street, which could be a significant obstacle for the flow and may dramatically change the character of concentration iso-lines. Since it is difficult to embed in geometry such complex objects as trees, the simulated and experimentally measured flow may differ considerably. Therefore, to make reasonable judgements about simulated results one should carry

out a sensitivity analysis of the results obtained. As can be seen from fig. 2, which demonstrates a sharp growth of concentration along the street, the results strongly depends on the selection of the measurement point.

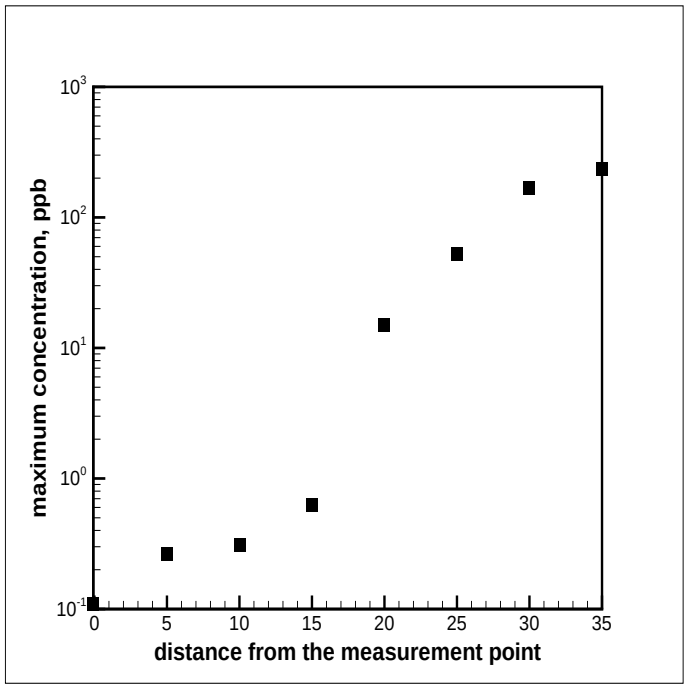

Figure 2. A sensitivity analysis of concentration distribution

Despite of the, so-called engineering problems, the issues considered in our report can not be solved rigorously. It is required,in a sense, a simplistic approach to be applied to all the aspects of such a problem, including the geometry of objects, initial and boundary conditions. All in all, our approach provides a sufficient degree of accuracy in comparison with more sophisticated models such as FEM3MP (USA,LLNL) [4].

Bibliography

1. *Sorokovikova O.S.,Semenov V.N. and Dzama D.V.* A RANS model of atmospheric dispersion for estimation of radiation situation in complex geometries of an object.Some other models and software packages applied to the tasks of radioecology. // Proc. Modern issues of mathematical modelling. 2013. Abrau-Durso, Russia, P. 233–240.

2. *Schatzmann M.,Olesen H. and Franke J.* COST 732 model evaluation case studies: approach and results. University of Hamburg, 2010.

3. *Allwine J., Leach M.* Special Issue Joint Urban 2003. Journal of applied meteorology and climatology, Vol. 46, Issue 12

4. *Chan S. and Leach M.* A validation of FEM3MP with joint urban 2003 data.Lawrence Livermore National Laboratory, 2006, UCRL-JRNL-220878-REV-1

ABOUT REGULARIZATION METHOD FOR THE INTENSITY IDENTIFICATION PROBLEM OF ATMOSPHERIC POLLUTION SOURCE

Chubatov A.A.*, Karmazin V.N.**

* *Armavir State Pedagogical Academy, Armavir, Russia*

** *Kuban State University, Krasnodar, Russia*

Introduction

For the description of processes of impurity distribution in the atmosphere (domain) it is used three-dimensional linear turbulent diffusion equation [1]

$$\frac{\partial q}{\partial t} + \vec{v} \cdot grad\, q = div(\vec{K} \cdot grad\, q) + f(M) \cdot g(t), \qquad (1)$$

at following conditions $q\Big|_{t=0} = q_0$, $q\Big|_{\partial D \times [0,H]} = 0$, $\frac{\partial q}{\partial z}\Big|_{z=0} = 0$, $q\Big|_{z=H} = 0$, where $q = q(M,t)$ — concentration of an pollution impurity, $M = (x,y,z)$ — spatial coordinates of a point, $\vec{v} = (v_x, v_y, v_z)$ — vector of speeds of a wind, $\vec{K} = (K_x, K_y, K_z)$ — vector of coefficients of turbulent diffusion, $f(M)$ — function describing spatial arrangement of a pollution source, $g(t)$ — action intensity of source.

In present study a special case of the identification problem for intensity of the source is studied in application to the modelling of the transport of air pollution [2]. The considered approach uses as input parameters the set of known sensitivity coefficients and corresponding pollution measured in given locations $M_j = (x_j, y_j, z_j)$:

$$c_{ji}, \quad j = 1, \ldots, J, \quad i = 1, \ldots, N,$$

where c_{ji} — concentration measured by j^{th} sensor at the moment of time t_i, J is the number of sensors, N is the number of time steps.
Measurements are taken in time intervals Δt.

Let's consider, that an error of concentration measurements is additive

$$c_{ji} = q(M_j, t_i) + \delta \cdot \gamma,$$

where δ — root-mean-square error of sensor measurements, γ — standardized Gaussian random variable ($Average(\gamma) = 0$, $Variance(\gamma) = 1$).

The identification problem for a source is characterized by solution instability to errors of concentration measurements also demands special methods of the solution [3, 4, 5]. To solve the problem were used methods step-by-step regularization and sequential function specification.

Sequential function specification method

Linearity of the problem (1) allows to use the superposition principle and numerical analogue of Duhamel's theorem

$$q_{ji} = q_0 + \sum_{n=1}^{i} g_n \cdot \Delta\phi_{j(i-n)}, \tag{2}$$

where $q_{ji} = q(M_j, t_i)$, $\Delta\phi_{j(i-n)} = \phi_{j(i-n+1)} - \phi_{j(i-n)}$, $\phi_{ji} = \mathcal{Q}(M_j, t_i)$, $\mathcal{Q}(M,t)$ — solution of the direct problem (1) at $g(t) = 1$ and $q\Big|_{t=0} = 0$.
The value ϕ_{ji} is called step sensitivity coefficient, and the value $\Delta\phi_{ji}$ — pulse sensitivity coefficient.

We shall estimate g_i, considering $g_1, g_2, \ldots, g_{i-1}$ are known values, calculated on the previous steps. For giving stability to the solution of the inverse problem we shall consider $g(t)$ on several (r) time intervals at once. At $r = 1$ the method step-by-step regularization turns out. r is discrete parameter of regularization. Let's consider, that $g_i, g_{i+1}, \ldots, g_{i+r-1}$ are connected by some functional dependence.

Using (2) for the moments of time $t_i, t_{i+1}, \ldots, t_{i+r-1}$ let's write down the matrix equation

$$\mathbf{\Phi} \cdot \mathbf{g} = \mathbf{Q} - q_0 - \mathbf{Q}|_{\mathbf{g}=0}, \tag{3}$$

where $\mathbf{\Phi} \in R^{r\cdot J \times r}$, $\mathbf{g} \in R^r$, $\mathbf{Q}, \mathbf{Q}\big|_{\mathbf{g}=0} \in R^{r\cdot J}$, $\Phi_k, Q_k, Q_k|_{\mathbf{g}=0} \in R^J$,

$$\mathbf{\Phi} = \begin{pmatrix} \Phi_0 & 0 & \cdots & 0 \\ \Phi_1 & \Phi_0 & \cdots & 0 \\ \vdots & \vdots & \ddots & \vdots \\ \Phi_{r-1} & \Phi_{r-2} & \cdots & \Phi_0 \end{pmatrix}, \ \mathbf{Q} = \begin{pmatrix} Q_0 \\ Q_1 \\ \vdots \\ Q_{r-1} \end{pmatrix}, \ \mathbf{Q}|_{\mathbf{g}=0} = \begin{pmatrix} Q_0|_{\mathbf{g}=0} \\ Q_1|_{\mathbf{g}=0} \\ \vdots \\ Q_{r-1}|_{\mathbf{g}=0} \end{pmatrix},$$

$$\mathbf{g} = \begin{pmatrix} g_i \\ g_{i+1} \\ \vdots \\ g_{i+r-1} \end{pmatrix}, \ \Phi_k = \begin{pmatrix} \Delta\phi_{1(i+k)} \\ \Delta\phi_{2(i+k)} \\ \vdots \\ \Delta\phi_{J(i+k)} \end{pmatrix}, \ Q_k = \begin{pmatrix} q_{1(i+k)} \\ q_{2(i+k)} \\ \vdots \\ q_{J(i+k)} \end{pmatrix}, \ Q_k|_{\mathbf{g}=0} = \begin{pmatrix} q_{1(i+k)}|_{\mathbf{g}=0} \\ q_{2(i+k)}|_{\mathbf{g}=0} \\ \vdots \\ q_{J(i+k)}|_{\mathbf{g}=0} \end{pmatrix},$$

$q_{j(i+k)}|_{\mathbf{g}=0} = \sum\limits_{n=1}^{i-1} g_n \cdot \Delta\phi_{j(i+k-n)}$. The $\mathbf{\Phi}$ is the low triangular block matrix of Toeplitz type.

The equation (3) can be solved exactly only for the case $r = 1$ and $J = 1$ (Stolz solution) [5]. In this case the solution of the inverse problem frequently instably. In case using of several time steps $(r > 1)$ or several sensors $(J > 1)$ the equation can be solved only approximately by means of the least-squares method.

We minimize the sum of squares of differences between measured $\mathbf{C}$ and calculated $\mathbf{Q}$ values of concentration

$$S = (\mathbf{C} - \mathbf{Q})^T \cdot (\mathbf{C} - \mathbf{Q}) \to min, \tag{4}$$

where $\mathbf{C} = \begin{pmatrix} C_0 \\ C_1 \\ \cdots \\ C_{r-1} \end{pmatrix}$, $C_k = \begin{pmatrix} c_{1(i+k)} \\ c_{2(i+k)} \\ \cdots \\ c_{J(i+k)} \end{pmatrix}$.

It is possible to approach the solution of the equation (**??**) in two ways:

- to solve equations set with r unknown values $g_i, g_{i+1}, \ldots, g_{i+r-1}$;
- to reduce number of unknown values considering, that $g_{i+1}, g_{i+2}, \ldots, g_{i+r-1}$ is expressed by mean of some functional dependence from g_i and from the previous values $g_{i-1}, g_{i-2}, \ldots, g_{i-p}$.

In the first case values $g_i, g_{i+1}, \ldots, g_{i+r-1}$ can turn out unrelated values themselves, though in practice of values of intensity $g(t)$ cannot vary at arbitrarily. In the second case the chosen functional dependence provides improvement of smoothness and stability of solution. The functional dependence is a regularization factor.

Then the sequential estimation algorithm will look like

1. for the chosen functional dependence $g_{i+1}, g_{i+2}, \ldots, g_{i+r-1}$ from g_i and g_{i-1} we shall estimate the unique unknown value g_i;
2. we shall pass to a following step, temporarily assuming dependence $g_{(i+1)+1}, g_{(i+1)+2}, \ldots, g_{(i+1)+r-1}$ from $g_{(i+1)}$ and $g_{(i+1)-1}$.

Let this functional dependence looks like

$$\mathbf{g} = A \cdot g_i + B \cdot g_{i-1},$$

where $A, B \in R^r$.

We consider the elementary case of functional dependence — the assumption of a constancy $g(t)$ during r the sequential intervals of time

$$g_i = g_{i+1} = \cdots = g_{i+r-1},$$

and also a case of linear dependence between $g_i, g_{i+1}, \ldots, g_{i+r-1}$

$$g_{i+k} = g_i + k \cdot (g_i - g_{i-1}) = (k+1) \cdot g_i - k \cdot g_{i-1}, \quad k = 0, 1, \ldots, r-1.$$

We shall find the estimation of intensity g_i

$$\hat{g}_i = \left((\mathbf{\Phi} \cdot A)^T \cdot (\mathbf{\Phi} \cdot A)^{-1} \cdot (\mathbf{\Phi} \cdot A)^T \cdot (\mathbf{C} - q_0 - \mathbf{Q}|_{g=0} - \mathbf{\Phi} \cdot B \cdot g_{i-1} \right. \qquad (5)$$

Results of computing experiments

Using number of methodical problems numerous calculation experiments are lead. Stability numerical approximation to desired value intensity are constructed, including at presence of measurement errors in measurements ($\delta = 0 \div 0,03 \cdot q_{max}$). Sensors are settled down outside of an operative range of a source ($f(M) = 0$) and in an operative range of a source ($f(M) \neq 0$). The root-mean-square error was used for the account of accuracy of intensity estimation $g(t)$

$$\sigma_g = \sqrt{\frac{1}{N}\sum_{n=1}^{N}\left(g((n-1/2)\cdot\Delta t) - g_n\right)^2}.$$

For each sensor there is the critical step $\Delta t_{st[1]}$, such, that as each step of the solution of the inverse problem $\Delta t > \Delta t_{st[1]}$ the solution is stability, i.e. the step-by-step regularization effect takes place.

The desire to increase the accuracy of intensity estimation, reducing a step on time, leads to instability of the solution of inverse problem. Using several sensors ($J > 1$) the sensor with smaller $\Delta t_{st[1]}$ has prevailing influence. In this case it is possible to use function specification method with several ($r > 1$) sequential steps on time.

The analysis of results of numerical experiments allows to draw a conclusion, that for pair numbers $(\Delta t/\Delta t_{st[1]}, \delta)$, $\Delta t/\Delta t_{st[1]} \in [0,1;1]$, $\delta \in [0;0,03\cdot q_{max}]$ it is possible to pick up r and in this case errors of estimation $g(t)$ will be minimal.

The information of concentration measurements from sensors is understanding sequentially in the considered method, that allows to organize the on-line monitoring over emissions of pollution in the atmosphere.

Bibliography

1. *G. I. Marchuk* Mathematical modeling in the problem of environment, Nauka, Moscow, 1982, 320 p.
2. *Chubatov A.A., Karmazin V.N.* The operative control of the atmospheric pollution source on the base of function specification method //Vestn. Sam. state. tech. univ-ty. 2008, Vol. 2, pp. 210–214.
3. *Morozov V.A.* Algorithmic bases of methods of the solution of ill-posed problems //Vychisl. methods and programming. 2003, Vol. 45, pp. 130–141.
4. *A. N. Tikhonov, V. Ya. Arsenin* Methods of the solution of ill-posed problems, Nauka, Moscow, 1986, 286 p.
5. *J. Beck, B. Blackwell, Ch. Chent-Clair, Jr.* Ill-posed inverse problems of heat conductivity, Mir, Moscow, 1989, 312 p.

A VERIFICATION OF THE BLOCKS FOR 3D AEROTHERMODYNAMICS MODELLING AND DOSES CALCULATION FROM A CLOUD OF ARBITRARY GEOMETRY AS PARTS OF A SOFTWARE PACKAGE FOR ESTIMATION OF THE RADIATION SITUATION WITHIN AN INDUSTRIAL SITE AT RADIATION RISK[1]

Dzama D.V.*, Sorokovikova O.S., Blagodatskykh D.V.***

* *The Nuclear Safety Institute of the Russian Academy of Sciences, Moscow, Russia*

** *National Research Nuclear University MEPhI, Moscow, Russia*

Due to the drastic growth of computer performance in the last decades, urban emission simulations can provide a sufficient resolution of flows around buildings and other obstacles. Despite of the promising prospects a cross-verification of different numerical models applied to the same problem clearly demonstrated a substantial discrepancy of the results. Taking into account that such models are intended for dealing with many crucial problems (e.g. a safety analysis of nuclear objects, the estimation of terroristic threats, urban planning), a thorough experimental validation of obtained results is needed.

To fill the gap between calculated results and experimental data an initiative [1], called COST 732, in the frame of COST (European Cooperation in Science and Technology) activity was proposed. The main goals of the initiative were to establish a commonly accepted quality assurance procedure for the models in question and provide researchers with data sets that are quality checked and commonly accepted as a standard for model validation purposes .

To attain these objectives the researchers from 22 European countries carried out a set of numerical simulations using 12 CFD models and compared the calculated results with two field experiments selected as sufficiently complex test cases: the Mock Urban Setting Test (MUST) and the Joint Urban 2003 Oklahoma City (OKC) Atmospheric Dispersion Study.This work is dedicated to cross-verification of a programm block for aerothermodynamics modelling in case of a real 3D object comprising numerous obstacles(the MUST experiment) and a block for calculation of the radiation situation in the vicinity of an object of complex geometry.

MUST presents a regular array of 120 containers situated in a flat desert in the state of Utah. The field data was supplemented with data measured in a wind-tunnel experiment [2]. The data are collected in form of Excel sheets free-available from Internet.

[1]The work of this author is supported by GK №H.4x.44.9Б.14.1037

The CFD models involved in verification include general purpose codes (e.g. CFX, FLUENT, STAR_CD) as well as specially developed codes for urban emission simulations (M2UE, MISKAM, VADIS). Table 1 presents the some results of the statistics processing of the measured and calculated values of two wind components based on conventional criteria for a quantitative analysis of aerothermodynamics modelling in case of industrial and urban buildings.The total amount of the measurement points is 566.

MISCAM	Length (Number of grid points per obstacle)	Width (Number of grid points per obstacle)	Height (Number of grid points per obstacle)	U, hit rate %	W, hit rate %	U, FAC2 %	W, FAC2 %
Standard $k-\epsilon$	24	6	5	73	16	93	14
Standard $k-\epsilon$	12	3	5	77	21	92	27
Standard $k-\epsilon$	12	3	5	75	21	90	29
Modified $k-\epsilon$	12	3	5	81	15	89	12
Modified $k-\epsilon$	15	3	5	79	14	91	12
Modified $k-\epsilon$	24	5	5	75	20	90	31
CFX							
Standard $k-\epsilon$	≈ 13	≈ 5	≈ 4	82	18	94	23
Standard $k-\epsilon$	13	5	4	76	15	86	16
Shear Stress Transport (SST) $k-\omega$	13	5	4	1	11	1	11
SSG Reynold Stress turbulence model	13	5	4	60	20	73	27
Our model	24	5	5	71	20	86	27

Table 1. Models cross-verification

The first criterion, called hit rate q, specifies the fraction of model results that differ within an allowed range D or W from the comparison data. D accounts for the relative uncertainty of the comparison data. W describes the repeatability of the comparison data.

$$q = \frac{N}{n} = \frac{1}{n}\sum_{i=1}^{n} N_i \;\; with \;\; N_i = \begin{cases} 1 & \text{for } \left|\frac{P_i - O_i}{O_i}\right| \leq D \text{ or } |P_i - O_i| \leq W \\ 0 & \end{cases}$$

where P_i and O_i are modelled and experimental results respectively.The second criterion is the factor of two observations (FAC2) defined in a similar fashion.

$$FAC2 = \frac{N}{n} = \frac{1}{n}\sum_{i=1}^{n} N_i \;\; with \;\; N_i = \begin{cases} 1 & \text{for } 0.5 \le \frac{P_i}{O_i} \le 2 \\ 1 & \text{for } |P_i| \le W \text{ or } |O_i| \le W \\ 0 & \end{cases}$$

The results of our model is compared against the results obtained by two models(specialized MISCAM and general purpose CFX) on grids of approximately the same resolution as ours.The researchers conducted series of calculations varying the type of wall functions and grid resolution of the obstacles. Parameters W and D are taken to be equal to 0.034 and 0.25 respectively.

Our model achieves comparable results without using wall-functions and for practically the same grid resolution

To calculate doses in case of complex geometry of the object and an arbitrary shape of the cloud one should define the visibility function for all the points of the air space and then integrate exposure incomes from all visible elementary volumes. Due to a large amount of calculations to be performed a parallel algorithm is proposed.

To verify the proposed algorithm a program is written for calculation of dose rates from the cloud in the vicinity of a cube or hemisphere, as well as dose rates from the surface in the vicinity of a hemisphere taking into account the surface of the hemisphere itself.The visibility function of arbitrary points is derived from the analytical equation of the surface of the object. The scattering and absorbtion effects are also taken into account.

The tests were carried out in a domain with dimensions : $x = [-500; 500], y = [-500; 500], z = [0; 500]$, and the size of cells equal to 10 m. This size is confirmed as a relevant one on the base of calculations on finer meshes. As test objects a hemisphere and a cube were taken with radius and edge equal to 200 m. Volume and surface concentration was considered to be 1 Bq/m^3 in all the space and 1 Bq/m^2 on all surfaces respectively. The figures below demonstrate the dependency of dose rate relative error along a straight line on the distance from an arbitrary point of this line. Fig.1 presents the relative error change along a straight line lying at a height of 245 m and parallel to the horizontal plane. The configuration of the segment of the line is shown in fig. 2.

In fig. 3 and 4 the case with a cube is presented

An example of more realistic distribution of concentration is shown in fig. 5 and 6. The dimensions of the domain were 100 m in each direction.The computational grid was homogeneous and the mesh size was equal to 1 m.There were two pairs of parallelepipeds with dimensions $16 \times 16 \times 70$ and $21 \times 21 \times 50$. The geometric centers of the first pair were in the points with coordinates (37,5; 37.5; 35) and (62,5; 62,5; 35), of the second - in (70; 30; 25) and (30; 70; 25). A source with intensity 0.2 GBq/s and duration of 500 c was situated in point(39; 20; 7). The velocity of dry deposition no horizontal and vertical surfaces was taken as

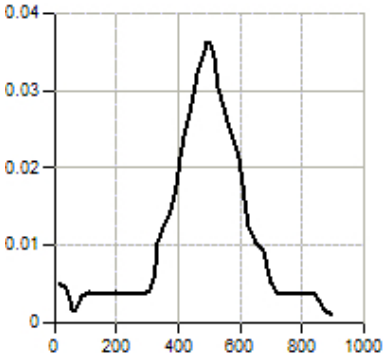

Figure 1. Relative error

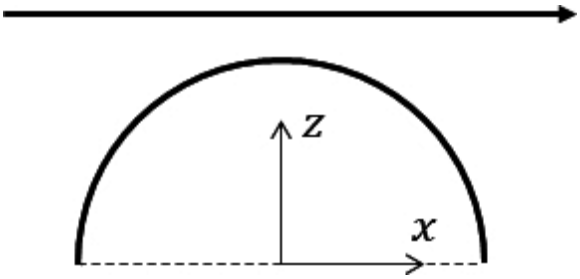

Figure 2. The configuration of the segment

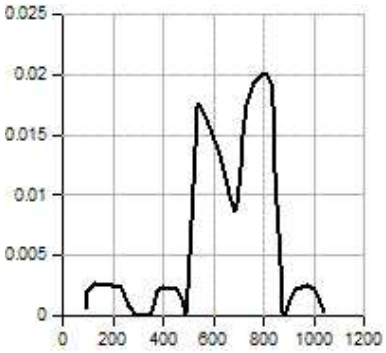

Figure 3. Relative error

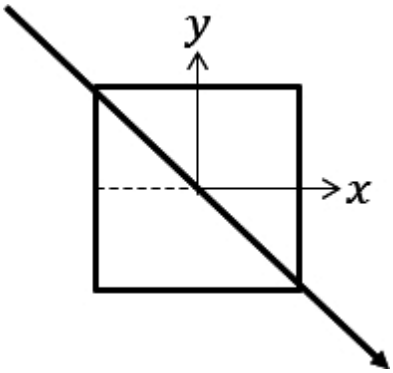

Figure 4. The configuration of the segment

0.02 m/s. it is worth mentioning that in fig. 5 and 6 the distributions of dose rates from the cloud and the surface are demonstrated on the moment the release is finished.Moreover all values are normalized in reference to the maximum value

of dose rates from the cloud and the surface respectively.

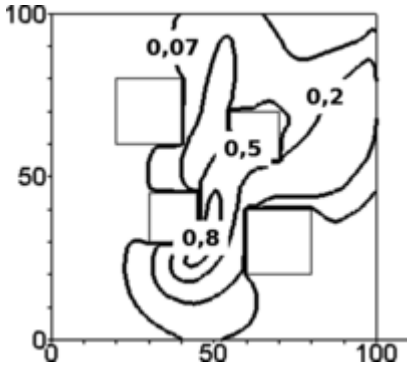

Figure 5. Isolines of dose rate from the cloud

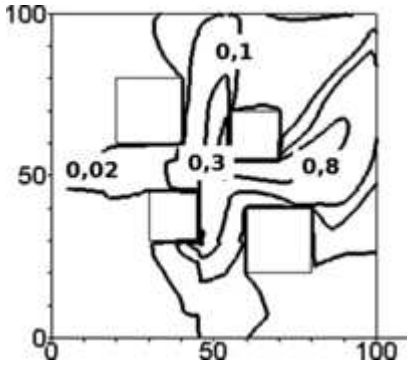

Figure 6. Isolines of dose rate from the contaminated surfaces (buildings and ground)

Bibliography

1. *Schatzmann M.,Olesen H. and Franke J.* COST 732 model evaluation case studies: approach and results. University of Hamburg, 2010.

2. *Leitl B., Bezpalcova C. and Harms F.* Wind tunnel modelling of the MUST experiment // COST 732 ,2007

COMPARISON ANALYSIS AND PARALLEL IMPLEMENTATIONS OF TWO SEMI-LAGRANGIAN TECHNOLOGIES FOR AN ADVECTION PROBLEM[1]

Efremov A.A., Karepova E.D., Vyatkin A.V.

Institute of Computational Modeling SB RAS, Krasnoyarsk, Russia

Nowadays there is a lot of algorithms of the family of semi-Lagrangian methods. This approach provides unconditional stability and allows one to use large time steps.

The method presented in [1] is based on a square grid only, it takes into account the boundary conditions, and it has theoretical justification of convergence with the first order of accuracy. Moreover, a discrete analogue of the balance equation holds when going from an actual time layer to the next one. However, this algorithm is both compute-intensive and resource-intensive, therefore its parallel implementation is an urgent and preferable task. Notwithstanding the algorithm is well-parallelizable (it is explicit with respect to time and data independence in the general space loop) our first attempts to use CUDA technology [1] faced severe restrictions of general-purpose GPU architecture.

We have scrutinized the bottleneck of our sequential algorithm and its parallel versions and the primary causes of poor CUDA performance have been detected. In our algorithm the biggest part of computation is occupied by integration stage. The procedure of determining the mutual arrangement of a curvilinear quadrangle and a grid on a previous time level is especially resource-intensive. This code has many flow control instructions ("if" statements, mainly) and a deep nesting level of functions.

We have revised the integration stage at the previous time level in order to improve an efficiency of the parallel implementation of our algorithm. In this regard, in [2] another algorithm of integration over a curvilinear quadrangle at the previous temporal level was proposed. The algorithm is based on an integral transformation and its Jacobian approximation. We have developed this approach in such a way that now it allows to escape deep nesting level of functions and to solve effectively the problem under the fine grids. However, we sacrificed a conservatism of the discrete analogue and a theoretical justification of convergence.

Numerical experiments corroborate a good CUDA performance of the new version of the algorithm.

[1]The work was supported by Russian Foundation of Fundamental Researches (grant 14-01-00296-a)

Bibliography

1. *Efremov A., Karepova E., Shaydurov V., Vyatkin A.* A Computational Realization of a Semi-Lagrangian Method for Solving the Advection Equation // Journal of Applied Mathematics. 2014. Vol. 2014. Article ID 610398.

2. *Shaydurov V., Vyatkin A.* The semi-lagrangian algorithm based on an integral transformation // AIP Conference Proceedings. 2015. Vol 1648. Article ID 850041.

ON NUMERICAL CALCULATION OF SHAPES OF CYLINDRICAL INCLUSIONS MIGRATING THROUGH A CRYSTAL FOR PARTICULAR CASE OF INTERFACIAL ENERGY ANISOTROPY

Garmashov S.I., Prikhodko Y.V.

Southern Federal University, Rostov-on-Don, Russia

The migration of liquid inclusions through a non-uniformly heated crystal [1-3] occurs because of the thermodynamic disequilibrium originating along the solid-liquid interface under the action of temperature gradient. The tendency of the system to restore the equilibrium state leads to the dissolution of the crystal substance at the hotter parts of the solid-liquid interface, the crystallization at the colder parts of the interface, and mass transfer in the liquid inclusion. As a result of this mass transfer, the liquid inclusion moves through the crystal. Experimental data on the inclusion migration in crystals under different conditions and, in particular, on the non-equilibrium inclusion shape, contain information on kinetics of the crystallization and dissolution processes, the interfacial energy and its anisotropy, and other parameters. In order to extract this information from the experimental data it is necessary to have a mathematical model of the inclusion shape.

One of such models (for the case of cylindrical inclusions) has been proposed in [4]. The advantage of this model is in opportunity of calculating the inclusion shape and velocity for arbitrary anisotropy of both the interfacial energy and the interface kinetics, and for arbitrary orientation of the temperature gradient. It is possible due to an approximation (proposed in [2]) of the solid-liquid interface by a set of flat facets, each of which is characterized by both the prescribed mechanism of growth (dissolution) and the value of specific interfacial energy γ_i in accordance with a fixed dependence $\gamma(\varphi_i)$, where φ_i is the angle determining the orientation of the ith facet. The calculation of the inclusion shape and velocity in accordance with model [4] is based on numerical solving a system nonlinear algebraic equations for the facet sizes. But because the computational time increases considerably with increasing the number of facets, it makes sense to use the model [4] in the case if the anisotropies of interface kinetics and interfacial energy are described by rather complicated functions.

In the present paper we consider a particular case of the interfacial energy anisotropy described by the function $\gamma(\varphi)$ in the form:

$$\gamma(\varphi) = \gamma_{min} + (\gamma_{max} - \gamma_{min})|\sin(\varphi)|, \qquad (1)$$

where γ_{min}, γ_{max} are the minimal and maximal values of the interfacial energy. The dependence (1) (see Fig. 1(a)) corresponds to the case when the inclusion is confined by two atomically-flat (singular) parts of the solid-liquid interface with the interfacial energy γ_{min} (at $\varphi = 0, \pi$) and by two atomically-rough

curvilinear (non-singular) parts with the interfacial energy $\gamma_{min} < \gamma \leq \gamma_{max}$. The equilibrium cross-sectional shape of a cylindrical inclusion for $\gamma(\varphi)$ in the form [1] is plotted in Fig. 1(b).

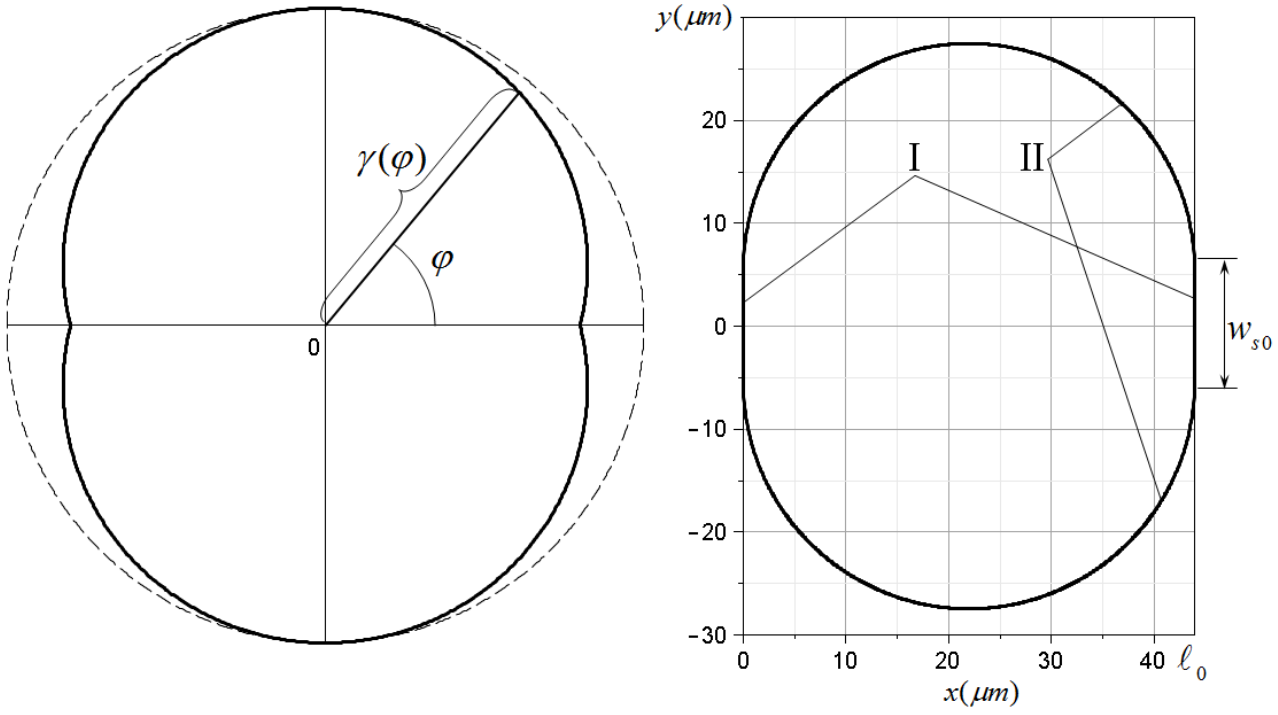

(a) (b)

Figure 1. The dependence $\gamma(\varphi)$ in the form (1) (a) and the corresponding cross-sectional shape of cylindrical inclusion in equilibrium (b) (the inclusion boundary parts I are the singular interfaces with the width of w_{s0} and the inclusion boundary parts II are the non-singular interfaces)

A similar problem have been considered in [3] with an assumption that the interfacial energy anisotropy is described by the function

$$\gamma(\varphi) = \begin{cases} \gamma_{min}, \varphi = 0, \pi \\ \gamma_{max}, \varphi \neq 0, \varphi \neq \pi. \end{cases} \tag{2}$$

However, the function $\gamma(\varphi)$ in the form (1) is more adequate to the real situation and, therefore, the construction of the inclusion shape model is of interest for this case. In the present work, similar to the model [3], we consider the case when the temperature gradient is directed normally to the singular parts of the inclusion boundary.

The complexity of calculating the inclusion cross-sectional shape for $\gamma(\varphi)$ in the form (1) (in contrast to the problem considered in [3]) is caused by that the function $y(x)$ describing the inclusion shape is the improper integral as follows:

$$y(x) = \frac{w_c}{2} + \int_0^x \frac{-a\xi^2/2 - b\xi + 1}{\sqrt{1 - (-a\xi^2/2 - b\xi + 1)^2}} d\xi, \tag{3}$$

where a, b are the coefficients calculated from the migration process parameters; w_c is the width of the colder singular part of the interface (at $x = 0$). The x-values change from 0 to ℓ, where ℓ is the thickness of the cylindrical inclusion; the value $2y(\ell)$ corresponds to the width (w_d) of the hotter singular part of the interface (at $x = \ell$).

The integrand from (3) and the numerically calculated function $y(x)$ are plotted in Fig. 2. As follows from Fig. 2(a), the integrand is an unbounded function at $x = 0$ and $x = \ell$. These singularities of the integrand restrict the application of Simpson's rule [5] for calculating the function $y(x)$ because the calculation error of this method for the considered case becomes rather high near the bounds of integration.

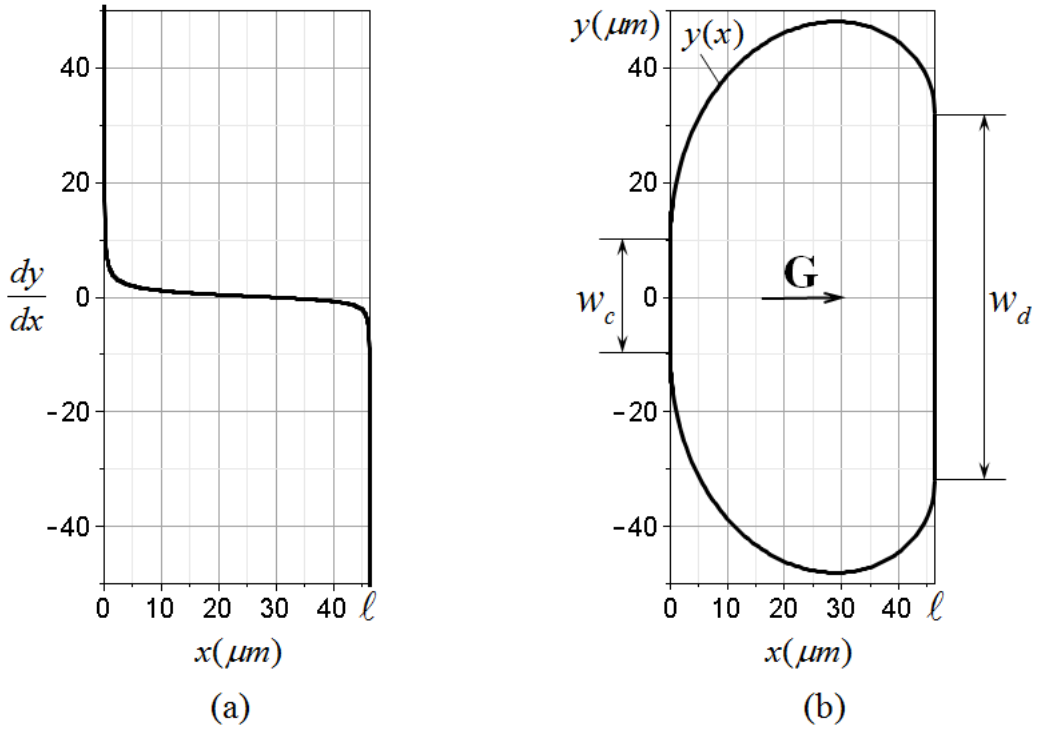

Figure 2. A plot of the integrand (a) and the corresponding calculated cross-sectional shape of the cylindrical inclusion (b), migrating in the direction of the temperature gradient **G**

Fig. 3 shows the rather slow convergence of Simpson's rule (the dush-dotted curve). Aitken's process [5] allows to decrease the calculation error of Simpson's rule, but the convergence remains slow (see the dushed curve in Fig. 3).

To solve the problem we used a technique described in [5], the essence of that is in separating out the singularities and using special quadrature formulas taking into account the character of these singularities. Besides, Aitken's process [5] was used to rise the accuracy of the numerical integration with using the deduced quadrature formulas. As follows from both Fig. 3 and the inset in it (see the solid curve), the proposed technique for calculating the inclusion shapes possesses the high convergence and, therefore, provides the small computational time.

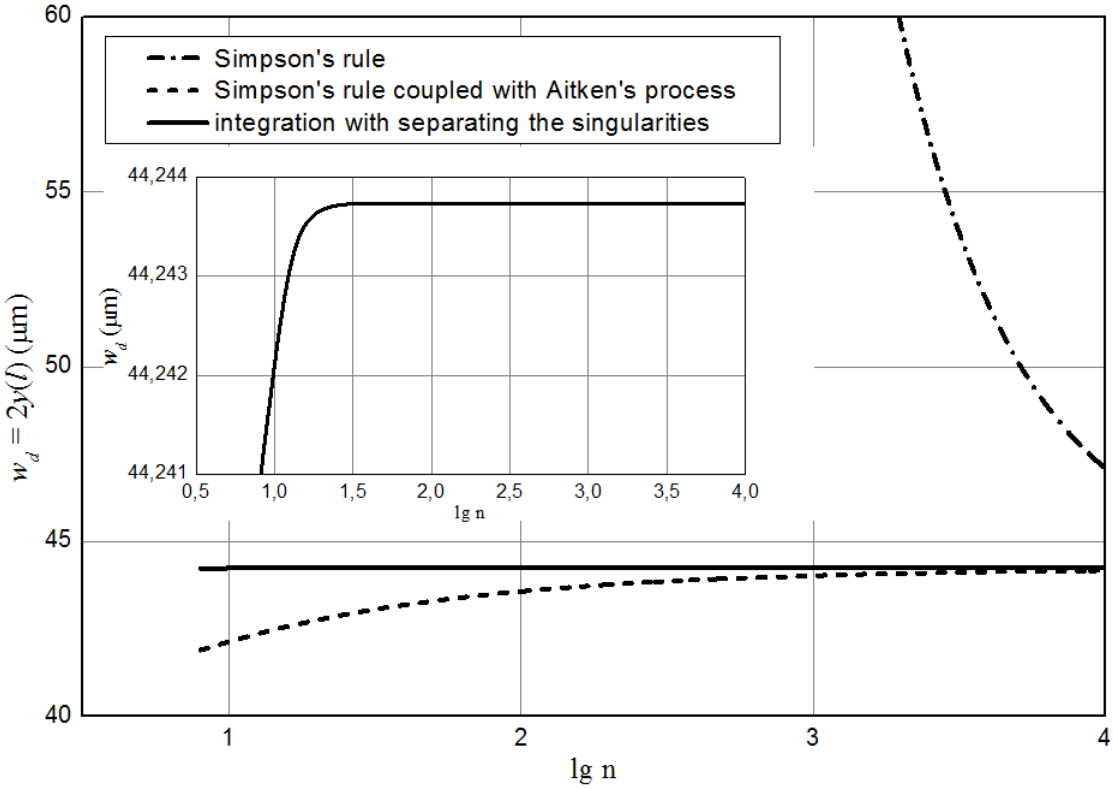

Figure 3. The convergence of numerical integration in the case of using Simpson's rule (dush-dotted curve), Aitken's process for Simpson's rule (dushed curve), and the method of separating singularities (with Aitken's process) (solid curve) (n is the number of nodes)

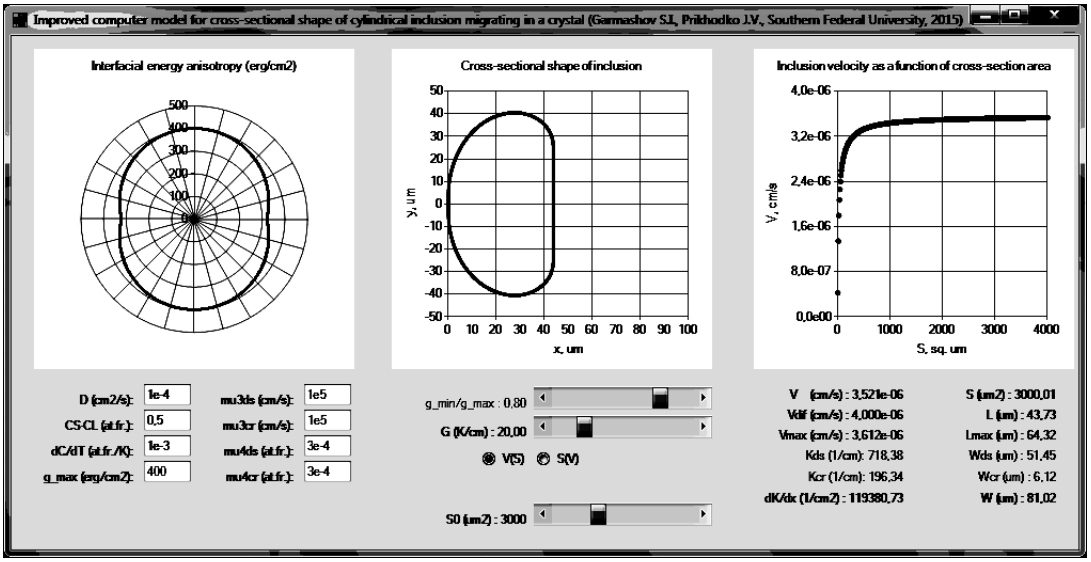

Figure 4. The computer program developed for calculating the velocity and cross-sectional shape of the migrating inclusion in the case of the interfacial energy anisotropy described by the function (1)

On the base of this technique, the computer program for calculating the cross-section shape and velocity of cylindrical inclusions migrating through a crystal has been developed. The program interface is presented in Fig.4.

The inclusion shape and velocity are calculated with assumptions that: (i) the interfacial energy anisotropy is described by the function (1); (ii) the temperature gradient is normal to the singular (flat) parts of the solid-liquid interface with the orientation angles $\varphi = 0, \varphi = \pi$. The program allows calculating and plotting the dependences of the inclusion velocity and geometric parameters of the inclusion shapes on various parameters of the migration process, such as the cross-sectional area, the temperature gradient, the ratio $\gamma_{max}/\gamma_{min}$, and so on.

Bibliography

1. *Tiller, W.A.* Migration of a liquid zone through a solid: Part I. /W.A. Tiller // J. Appl. Phys. - 1963, V. 34. - P. 2757-2762.

2. *Cline, H.E.* Nonequilibrium Morphology Of Liquid Inclusions Migrating In Solids / H.E. Cline, T.R. Anthony // J. Appl. Phys. - 1977, V. 48. - P. 5096-5104.

3. *Garmashov, S.I.* Velocity and Cross-Section Shape of Liquid Cylindrical Inclusions Migrating Normally to Close-Packed Planes of a Non-Uniformly Heated Crystal under Stationary Thermal Conditions / S.I. Garmashov , V.Yu. Gershanov // J. Cryst. Growth. - 2009. - V. 311, N. 2. - P. 413-419.

4. *Garmashov, S.I.* A computer model of steady-state cross-sectional shape of liquid cylindrical inclusion migrating through a crystal with account of thermal gradient direction and anisotropy of interfacial energy and interface kinetics /S.I. Garmashov, V.I. Surnin // Abstracts of Lecturers and Young Scientists of Second China-Russia Conference on Numerical Algebra with Applications (CRC-NAA'13), June 25-29 , 2013, Rostov-on-Don, Russia. - Rostov-on-Don: Southern Federal University Publishing, 2013. - PP. 74-76. (ISBN 978-5-9275-1107-5)

5. *Kalitkin, N.N.* Numerical methods / N.N. Kalitkin // Nauka, Moscow, 1978 (in Russian).

IMPULSION IN MODELS OF CONCORDANCE OF PUBLIC AND PRIVATE INTERESTS

Gorbaneva O.I.
Southern Federal University, Rostov-on-Don, Russia

The present work is devoted to the system compatibility with feedback (impulsion mechanism) in models of concordance of public and private interests (CPPI-models) and, in particular, to investigation of economic and administrative corruption if the corruption functions are given. These functions describe the influence of bribe on economic and administrative control.
A two-level system consisting of the supervisor and several agents subordinated to him is considered [1]-[2]. The models of concordance of public and private interests have the form

$$g_i(u) = p_i(r_i - u_i) + s_i c(u) \to \max, 0 \le u_i \le r_i, i \in N; \tag{1}$$

$$g_0(u) = \sum_{j \in I} g_j(u) \to \max, 0 \le s_i \le 1, \sum_{j \in I} s_j = \begin{cases} 1, & \exists i : s_i > 0, \\ 0, & otherwise, \end{cases} \tag{2}$$

where r_i is a resource of the i-th agent; u_i is a share of the resource assigned by him for the public purposes; $c(u)$ is the public payoff function; s_i is the i-th agent's share of public payoff; $p_i(r_i - u_i)$ is a private payoff function of the i-th agent, $g_i(u)$ is the agent's total payoff, $g_0(u)$ is the supervisor's payoff, N is the set of agents. Functions are continuously differentiable and concave on all variables.
In the case of economic impulsion, $s_i = s_i(u_i)$ or $s_i = s_i(u)$. Using the first order condition we obtain that the system compatibility inside the area of admissible controls is possible only if

$$\frac{\partial s_i(u)}{\partial u_i} c(u) = [1 - s_i(u)] \frac{\partial c(u)}{\partial u_i}, i \in N; \tag{3}$$

For farther analysis it is possible to use two approaches: empirical and theoretical ones [3]. Within empirical approach the widespread practical methods of public payoff allocation are investigated. For example, proportional allocation mechanism

$$s_i(u) = \begin{cases} \frac{u_i}{\sum_{j \in N} u_j}, & \exists m : u_m > 0, \\ 0, & otherwise, \end{cases}$$

In this case (3) has the form

$$\sum_{j \ne i} u_j [\frac{\partial c(u)}{\partial u_i} \sum_{j \in N} u_j - c(u)] = 0, i \in N.$$

The expression in square brackets is equal to zero only if $c(u)$ is linear, hence the proportional allocation mechanism is system compatible in CPPI-models in which the public payoff function is linear.
Theoretical approach is based on the Germeyer theorem.
In the case of administrative impulsion, the most natural interpretation of feedback is corruption, and an additional control level level is appeared.
As far as corruption in CPPI-models is concerned it is reasonable to distinguish administrative and economic corruption according to the authors' approach. The principal effects on the set of admissible strategies or on purpose functions of the agents and performs administrative and/or economic control of agents' activity respectively. The principal is assumed to be non-corruptive, but real control functions on behalf of him are performed by a supervisor who can weak administrative or economic demands in exchange for a bribe. Respectively, administrative and/or economic corruption, i.e. feedback on bribes of these controls occurs.
We assume that if there is no corruption the public payoff in model (1) - (2) is allocated among principal, supervisor and agents in ratio p^0, r^0, $\sum_{j=1}^{n} s_j^0$, where $p^0 + r^0 + \sum_{j=1}^{n} s_j^0 = 1$.
This scheme can be described by the relation

$$p = p^0 - \sum_{j=1}^{n} \delta_j, r = r^0 + \sum_{j=1}^{n} b_j \delta_j, s_i = s_i^0 + (1 - b_i)\delta_i, i \in N. \qquad (4)$$

where the new shares (4) also satisfy $p + r + \sum_{j=1}^{n} s_j = 1$. Here δ_i is increase of the i-th agent's share of public payoff in exchange for a "kickback", b_i is a share of the i-th agent "kickback" to the supervisor. Taking into account economic corruption the CPPI-model (1) - (2) takes the form

$$g_S(b, \delta, u) = [r^0 + \sum_{j=1}^{n} b_j \delta_j] c(u) \to \max, 0 \le \delta_i \le 1, \qquad (5)$$

$$g_i(b_i, \delta_i, u) = p_i(r_i - u_i) + [s_i^0 + (1 - b_i)\delta_i] c(u) \to \max, 0 \le b_i \le 1, 0 \le u_i \le r_i, i \in N, \qquad (6)$$

where g_S, g_i are payoff functions of supervisor and the i-th agent correspondingly. The summand $r^0 c(u)$ in function (5) describes official supervisor payoff, and the summand $c(u) \sum_{j=1}^{n} b_j \delta_j$ describes his corruption payoff.
The model (5) - (6) can be investigated by two methods: descriptive and normative ones. In the case of descriptive approach the corruption function $\delta_i(b_i)$ is assumed to be known. Then for agents the game in normal form occurs in which agent strategies are the pair (b_i, u_i). In the case of normative approach function $\delta_i(b_i)$ is defined as an optimal guaranteeing supervisor strategy (control mechanism).
So, in this work the impulsion mechanism in models of concordance of public and private interests is investigated, in particular, mechanisms of administrative

and economic corruption. To investigate impulsion mechanism theoretical and empirical methods are applied. Within empirical methods proportional and uniform allocations are considered. To describe corruption two methods: descriptive and normative, are applied.

Bibliography

1. *Gorbaneva O., Ougolnitsky G.A.* Purpose and non-purpose resource use models in two-level control systems// Advances in Systems Science and Applications. 2013. 13, Is. 14. P. 379-391.

2. *Gorbaneva O.I., Ougolnitsky G.A.* A problem of purpose resource use in two-level control systems // Contributions to game theory and management. 2014. P. 81-92.

3. *Novikov D.A.* Mechanism Design and Management: Mathematical Methods for Smart Organizations Couple–stresses in the theory of elasticity // N.Y.: Nova Science Publishers, 2013.

MESHLESS ALGORITHM FOR VORTICES DYNAMICS ANALYSIS[1]

Govorukhin V.N.
Southern Federal University, Rostov-on-Don, Russia

In this talk the algorithm based on variant of vortex-in-cells method is developed. The governing equations are the geophysical models of the atmosphere formulated in terms of stream function and potential vorticity. It is a system of two PDE equations:

$$\frac{D\omega}{Dt} \equiv \omega_t + \psi_y \omega_x - \psi_x \omega_y = 0, \tag{1}$$

$$\omega = -\Delta\psi + \Lambda^2\psi - \frac{1}{2}\gamma r^2. \tag{2}$$

where ω is a vorticity, ψ is a stream function and D/Dt denotes the material derivative. Here $\psi_x = \partial\psi/\partial x$, $\psi_y = \partial\psi/\partial y$, $\psi_{xx} = \partial^2\psi/\partial x^2$, etc. $\gamma = const$, $r = \sqrt{x^2 + y^2}$ is the polar radius, $\Lambda^2 = f_0^2/gh = const$, g is the acceleration due to gravity, and h is the thickness of the fluid layer. The velocity of the fluid $v = (v_1, v_2)$ is expressed via the stream function ψ as

$$v_1 = \psi_y, \quad v_2 = -\psi_x, \tag{3}$$

The developed algorithm includes calculating the dynamics of vortex configuration using a variant of the vortices-in-cells method, the calculation heuristic characteristics of vortex structure and construction of the field of local Lyapunov exponents in each moment.

The variant of the vortices-in-cells method was presented in [1, 2, 3]. The method is based on vorticity field approximation by its values at a set of N fluid particles and the stream function computation using the Galerkin method. The flow domain is divided into rectangular cells. Vorticity in every cell is interpolated by a third order polynomial. The resultant piecewise continuous polynomial approximation of vorticity is employed to derive analytically Galerkin's coefficients of stream function expansion. Computed velocity field is used for fluid particles trajectories calculation as a solution of ODE system of hight dimension

$$\dot{x}_i = \psi_y(x_i, y_i), \qquad \dot{y}_i = -\psi_x(x_i, y_i) = v_2, \; i = 1..N \tag{4}$$

Analysis of heuristic characteristics of structures is based on calculation of coordinates of centers of vorticity of patches

$$x^{(k)} = \frac{1}{\Omega^{(k)}} \int_{S^{(k)}} x\, \omega^{(k)}(x, y) dS, \quad y^{(k)} = \frac{1}{\Omega^{(k)}} \int_{S^{(k)}} y\, \omega^{(k)}(x, y) dS. \tag{5}$$

[1]Supported by RFBR Grant N 14-01-00470

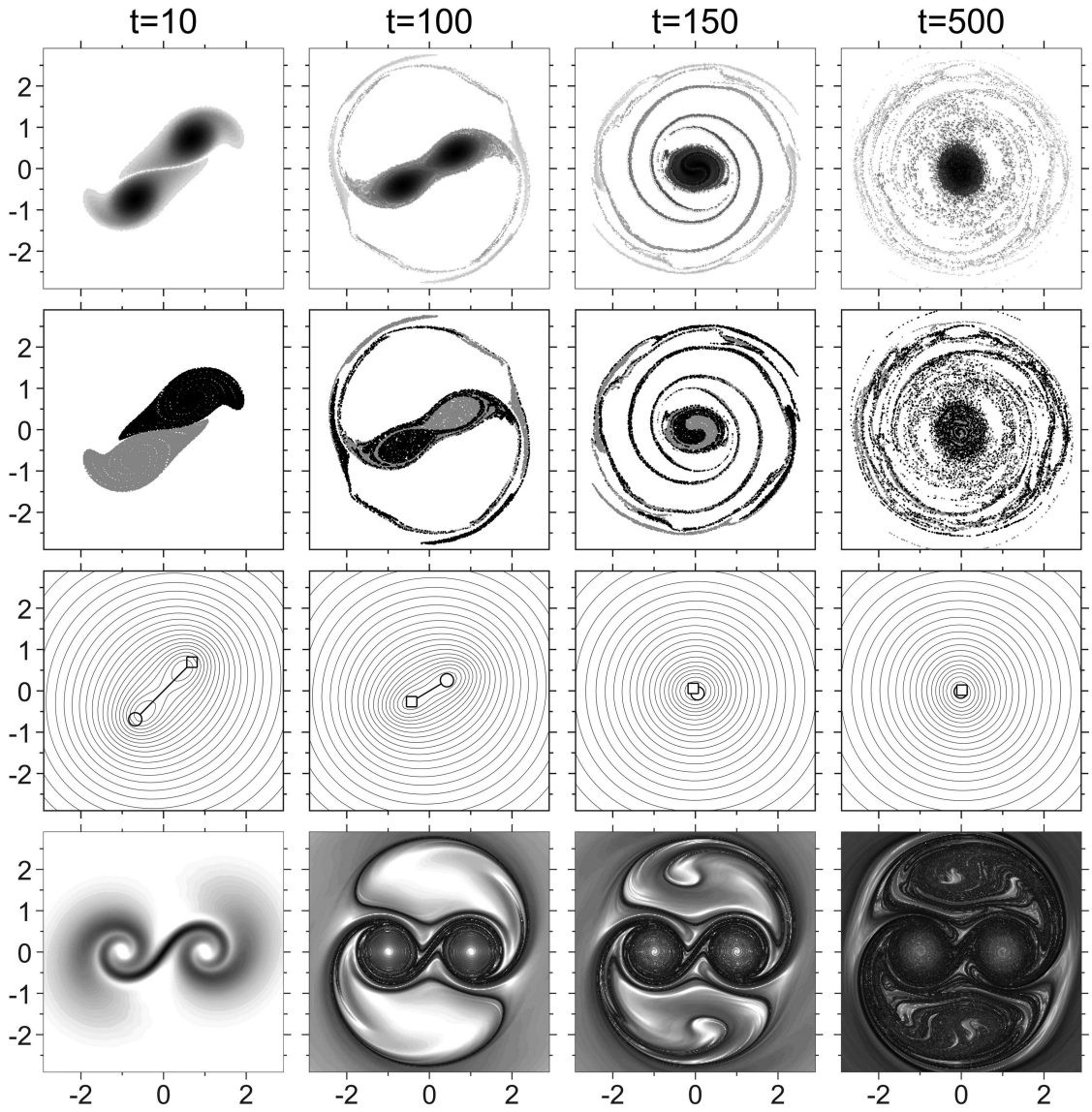

Figure 1. Vorticity field (top line), mixing map (second line), streamline and centers of vorticity (third line) and FTLE field (bottom line) for different time moments.

were in summation uses particles wich was included in vortice with number k in initial state. The topology of vortex structures can be studied using (5) and two heuristic characteristics: the distances $d_{i,j}$ between patches and orientation of triangles

$$\theta_{i,j,k} = \begin{vmatrix} x^{(i)} & y^{(i)} & 1 \\ x^{(j)} & y^{(j)} & 1 \\ x^{(k)} & y^{(k)} & 1 \end{vmatrix} \tag{6}$$

The evolution of particles through the flow is tracked using a flow map, whose spatial gradients are subsequently used to setup a Cauchy Green deformation tensor for quantifying the amount by which the neighboring particles have diverged over the length of the integration. The maximum eigenvalue of the tensor is used to construct a Finite Time Lyapunov Exponent (FTLE) field. The FTLE struc-

tures divide flow into regions of qualitatively different dynamics and are used to locate boundaries of the flow segments. Any change in the number of flow segments over time is regarded as an instability, which is detected by establishing correspondences between flow segments over time.

The effectiveness of the algorithm was studied in a number of test cases the interaction known vortex configurations. We considered the vortex configuration at the initial time of two or three vortex patches with the following distribution of vorticity

$$\omega_I(x_c, y_c) = \begin{cases} K\, e^{-5\left((x-x_c)^2+(y-y_c)^2\right)}, \sqrt{(x-x_c)^2+(y-y_c)^2} \le \frac{9}{10} \\ 0, \sqrt{(x-x_c)^2+(y-y_c)^2} > \frac{9}{10} \end{cases} \tag{7}$$

were $K \approx 1.6195\ldots$

The figure shows the calculation results for the initial configuration

$$\omega_0(x, y) = \omega_I\left(-1 - \frac{d}{2}, 0\right) + \omega_I\left(1 + \frac{d}{2}, 0\right) \tag{8}$$

Calculations fully reproduce the results of physical experiments presented in citeGov5.

Bibliography

1. *Govorukhin, V. N.; Il'in, K.I.* Numerical study of an inviscid incompressible flow through a channel of finite length // Int. J. Numer. Methods Fluids 60, 2009, N. 12, 1315-1333.

2. *Govorukhin, V.N.* A vortex method for computing two-dimensional inviscid incompressible flows // Computational Mathematics and Mathematical Physics, 51 (6), 2011, pp. 1061-1073.

3. *Govorukhin, V.N.* A meshfree method for the analysis of planar flows of inviscid fluids // Lecture Notes in Computational Science and Engineering, 89 LNCSE, 2013, pp. 171-180.

4. *P Meunier, P.; Le Dizes, S; Leweke, T.* Physics of vortex merging // Comptes Rendus Physique, V.6, N4, 2005, pp. 431-450.

COMPACT DIFFERENCE SCHEMES FOR ROD LATERAL VIBRATIONS EQUATION

Vladimir A.Gordin *, Evgeniy A.Tsymbalov**

* *Higher School of Economics, Hydrometeorological Center of Russia, Moscow, Russia*

** *Higher School of Economics, Moscow, Russia*

Introduction

We consider finite-difference approximations for the rod lateral vibrations equation

$$\rho\frac{\partial^2 u}{\partial t^2} - \frac{\partial}{\partial x}\left[R^2\rho\frac{\partial^3 u}{\partial x \partial t^2}\right] + \frac{\partial^2}{\partial x^2}\left[ER^2\frac{\partial^2 u}{\partial x^2}\right] = f, \tag{1}$$

where ρ is rod's density, R – radius, – Young module; $x \in [0, L], f = f(t, x)$ – forcing. The equation in partial derivatives is not resolved with respect to higher temporal derivative, i. e. it has not Cauchy-Kovalevsky type, but Poincare-Sobolev one. However, it is not an obstacle for its high-order approximation.

We have investigated here the both cases: $R = const$, and $R = R(x)$. We compare high-order difference compact and Crank-Nicolson-type schemes. We compare the following properties: order of approximation, stability, energy conservation law (for homogeneous case $f = 0$). The case of the variable coefficients of the differential equation is much more difficult for a good approximation. High-order compact approximation for a set of boundary conditions is also discussed.

Compact difference scheme

We use the following 3-5-3-point stencil, see Fig.1, for a compact difference scheme, which can be expressed as a linear algebraic equations for the values of the grid functions u and f in stencil's knots:

$$\begin{gathered}
a^*(u_0^{n+1} + u_0^{n-1}) + a_{left}(u_{-h}^{n+1} + u_{-h}^{n-1}) + a_{right}(u_h^{n+1} + u_h^{n-1}) + bu_0^n + \\
+c_{left}u_{-h}^n + c_{right}u_h^n + d_{left}u_{-2h}^n + d_{right}u_{2h}^n = \\
= p_{0,left}(f_{-2h,j}^{n+1} + f_{-2h,j}^{n-1}) + p_{0,right}(f_{2h,j}^{n+1} + f_{2h,j}^{n-1}) + \\
+q_{0,left}(f_{-h,j}^{n+1} + f_{-h,j}^{n-1}) + q_{0,right}(f_{h,j}^{n+1} + f_{h,j}^{n-1}) + r_0(f_{0,j}^{n+1} + f_{0,j}^{n-1}) + \\
+p_{1,left}f_{-2h,j}^n + p_{1,right}f_{2h,j}^n + q_{1,left}f_{-h,j}^n + q_{1,right}f_{h,j}^n + r_1 f_{0,j}^n
\end{gathered} \tag{2}$$

Here n is a temporal step number, and the lower index shows spatial position of stencil points over the stencil's center. These seventeen constants are calculated

for every spatial grid point x_j by substituting the following test monomials $u_k(t,x)$ (see Fig. 1) and the corresponding right-hand sides, were calculated according to (1), see for details (Gordin, Tsymbalov, 2014):

$$f_{kj}(t,x) = \frac{\partial^2 u_k}{\partial t^2} - R_j^2 \frac{\partial^4 u_k}{\partial x^2 \partial t^2} - 2R_j(R_j^{'}) \frac{\partial^3 u_k}{\partial x \partial t^2} + 2E\rho^{-1}(R_j^{'})^2 \frac{\partial^2 u_k}{\partial t^2} + \\ + E\, R_j^2 \rho^{-1} \frac{\partial^4 u_k}{\partial x^4} + 4E\, R_j(R_j^{'})\rho^{-1} \frac{\partial^3 u_k}{\partial x^3} + 2ER_j\rho^{-1} \frac{\partial^2 u_k}{\partial x^2}(R_j^{''}).$$

Here $R_j, R_j^{'}, R_j^{''}$ are values of $R(x), \frac{\partial R(x)}{\partial x}, \frac{\partial^2 R(x)}{\partial x^2}$ at x_j. The derivatives may be evaluated either analytically or numerically (the high-order compact relations for the first and second derivatives, see (Patterson, 1983)).

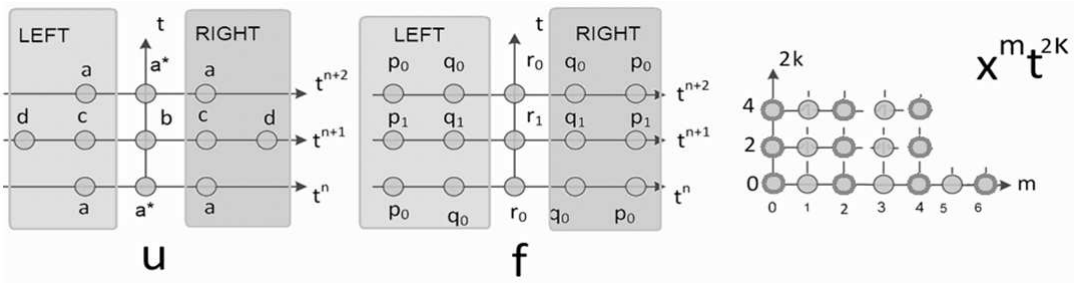

Figure 1. Stencil and Newton's diagram of test monomials $u_k(t,x)$ for compact difference scheme (2).

Crank-Nicolson-type scheme

The Crank-Nicolson-type scheme can be written as:

$$a^*(u_0^{n+1} + u_0^{n-1}) + a_{left}(u_{-h}^{n+1} + u_{-h}^{n-1}) + a_{right}(u_h^{n+1} + u_h^{n-1}) + \\ + e_{left}(u_{-2h}^{n+1} + u_{-2h}^{n-1}) + e_{right}(u_{2h}^{n+1} + u_{2h}^{n-1}) + bu_0^n + c_{left}u_{-h}^n + c_{right}u_h^n = \\ = p_{0,left}(f_{-2h,j}^{n+1} + f_{-2h,j}^{n-1}) + p_{0,right}(f_{2h,j}^{n+1} + f_{2h,j}^{n-1}) + \\ + q_{0,left}(f_{-h,j}^{n+1} + f_{-h,j}^{n-1}) + q_{0,right}(f_{h,j}^{n+1} + f_{h,j}^{n-1}) + r_0(f_{0,j}^{n+1} + f_{0,j}^{n-1}) + \\ + p_{1,left}f_{-2h,j}^n + p_{1,right}f_{2h,j}^n + q_{1,left}f_{-h,j}^n + q_{1,right}f_{h,j}^n + r_1 f_{0,j}^n \qquad (3)$$

We need to inverse on every temporal step of CN-scheme a five-diagonal matrix (see Fig.2) against three-diagonal one for the compact scheme (2).

Stability

Our numerical experiments demonstrated:

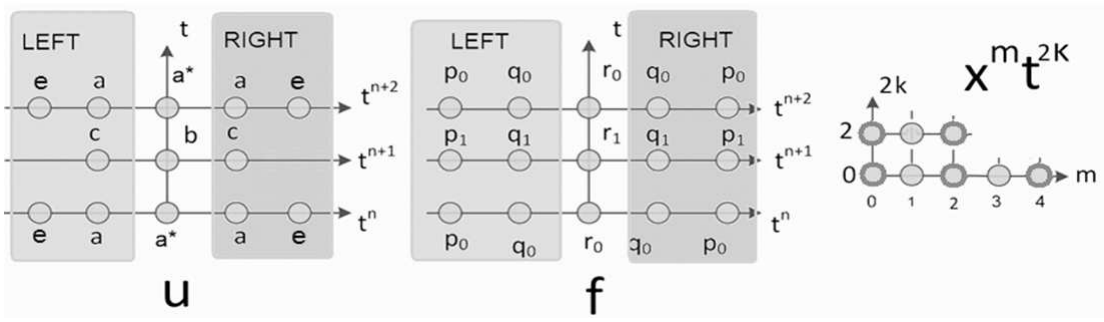

Figure 2. Stencil and Newton's diagram of test monomials $u_k(t,x)$ for Crank-Nicolson-type scheme (3).

- The conditional stability of the compact difference scheme (2) if $\nu^* < \mu^* + 1/12$; here and after $\mu^* = (R^*)^2 h^{-2}, \nu^* = (R^*\tau)^2 E\rho^{-1}h^{-4}, R^* = max_j R(x_j)$.

- The absolute stability of Crank-Nicolson scheme (3).

We have also discovered stability issues for a small number of spatial grid points N in case of low smoothness order of rod's radius function $R(x)$.

Numerical experiments

For schemes' errors evaluation, we use mesh norms C and L_2 as well as the mesh energy norm

$$\sqrt{\frac{R(x)^2 \left\|(\partial_t u_{anal} - \delta_t u_{diff})^2 + E\, R(x)^2 \rho^{-1} (\partial_x u_{anal} - \delta_x u_{diff})^2\right\|_{L_2}}{\left\|R(x)^2 (\partial_t u_{anal})^2 + E\, R(x)^2 \rho^{-1} (\partial_x u_{anal})^2\right\|_{L_2}}} \qquad (4)$$

Here u_{anal} is analytical solution, u_{diff} is a difference one. Usage of norm (3) allows us to account the kinetic part of solution, while standard C and L_2 mesh norms ignore it.

Table 1. Errors and orders of accuracy of the solution of (1) with compact difference scheme (2) (left) and Crank-Niconsol-type scheme (3) (right). Orders of accuracy exceed fourth for both schemes in energy norm, second order for norms C and L_2. Scheme (2) is more accurate than (3). $L = 4\pi, \rho = 7000, E = 2.1{*}10^8, u_{test} = sin(x)sin(t){+}2, R(x) = 0.4{+}0.01cos^2(x), T = 0.2, \nu^* = 0.05$

Norm	N = 12	N = 24	N = 48	N = 96	RMS
C	1.99-3	6.72-4	1.75-4	4.42-5	1.84
L_2	1.62-3	4.75-4	1.24-4	3.13-5	1.90
(4)	3.59-5	9.67-7	4.41-8	2.52-9	4.62

	N = 12	N = 24	N = 48	N = 96	RMS
C	3.70-2	9.30-3	2.24-3	5.56-4	2.02
L2	3.02-2	6.57-3	1.59-3	3.93-4	2.09
(4)	3.91-2	1.80-3	1.04-4	6.38-6	4.20

Conclusion

We confirmed high accuracy order for the compact scheme (2) and for the Crank-Nicolson-type scheme (3). The CS is more exact and economical. CN is absolutely stable and more effective when the right-hand side or coefficients of the equation (1) are not sufficiently smooth.

Bibliography

1. *Gordin V.A.* Mathematics Computer, Weather Forecasting and Other Scenarios of Mathematical Physics (in Russian), Fizmatlit, M., 2010, 2012.

2. *Gordin V.A., Tsymbalov E.A.* Compact differential schemes for the diffusion and Schr?dinger equations. Approximation, stability, convergence, effectiveness, monotony Journal of Computational Mathematics. - 2014. - T. 32 (3). 348-370.

3. *Lele S.K.* Compact finite difference schemes with spectral-like resolution Journal of Computational Physics. - 1992. - 103. - 16-42.

4. *Patterson J.C.* General derivative approximations for finite difference schemes International Journal for Numerical Methods in Engineering. – 1983. – 19. – 1235-1241.

5. *Spotz W.F.* High-Order Compact Finite Difference Schemes for Computational Mechanics [Report] : PhD Thesis University of Texas at Austin. – Austin, TX, 1995.

NUMERICAL AND ASYMPTOTICAL ANALYSIS OF RAYLEIGH REACTION-DIFFUSION SYSTEM

Kazarnikov A.V.[*,**], **Revina S.V.**[*], **Haario H.**[**]

[*] *Southern Federal University, Rostov-on-Don, Russia*

[**] *Lappeenranta University of Technology, Lappeenranta, Finland*

At the present time, a significant attention is given to the analysis of nonlinear parabolic systems, called reaction-diffusion systems. These partial differential equations have found a wide range of of practical applications in theoretical biology, chemistry, physiology, etc. In this paper we consider well-known FitzhHugh-Nagumo model, a two-component reaction-diffusion system with cubic nonlinear reaction term, which was initially developed as nerve impulse propagation model and has become a classical example of exitable media:

$$\begin{aligned} v_t &= \nu_1 \Delta v + \varepsilon(w - \alpha v - \beta) \\ w_t &= \nu_2 \Delta w - v + \mu w - w^3 \end{aligned} \tag{1}$$

Here $v = v(x,t)$, $w = w(x,t)$, $x \in D$, $t > 0$, $D = [0,1]$ or $D = [0,1] \times [0,1]$, $\mu \in \mathbb{R}$ is a varying control parameter, $\alpha > 0$, $\beta > 0$, $\varepsilon > 0$, $\nu_1 > 0$, $\nu_2 > 0$ are fixed model parameters. By setting $\alpha = 0$, $\beta = 0$, $\varepsilon = 1$ in (1) and assuming diffusion coefficient equal to each other ($\nu_1 = \nu_2 = \nu$), we arrive at Rayleigh reaction-diffusion system:

$$\begin{aligned} v_t &= \nu \Delta v + w \\ w_t &= \nu \Delta w - v + \mu w - w^3 \end{aligned} \tag{2}$$

When no spatial dependence is assumed, i.e. by setting $y_1(t) = v(t)$, $y_2(t) = w(t)$, we arrive at classical Rayleigh ODE system:

$$\dot{y_1} = y_2; \quad \dot{y_2} = -y_1 + \mu y_2 - y_2^3 \tag{3}$$

This system could be transformed to Van-der-Pol system by variable change. Both are well-known models, describing nonlinear relaxation oscillations.

The main purpose of the present work is to construct an asymptotic approximation of secondary time-periodic solutions of system (2), which branch from zero stationary solution as control parameter μ varies. It is a well-known fact that diffusion does not affect the behaviour of auto-oscillations when zero-flux (Neumann) boundary conditions are set on the boundary of domain D, so here we consider homogeneous Dirichlet and Neumann boundary conditions, taking into account the mixed case. For more details, see [5]. Coefficients of asymptotic series are computed by using standard numerical algebra packages. We also study numerically the bifurcations, taking place in the system, and the destruction of periodic regime, which occurs as control parameter μ varies.

We employ Lyapunov-Schmidt method in the form, developed by V.I. Yudovich [1] for constructing asymptotic expansions. The method is applicable to ODEs and PDEs, including Navier-Stokes equation [2, 3, 4].

We could rewrite system (2) as ODE in functional space $\boldsymbol{H}$:

$$\dot{\boldsymbol{u}} = \mathrm{A}(\mu)\boldsymbol{u} - K(\boldsymbol{u},\boldsymbol{u},\boldsymbol{u}); \quad \boldsymbol{u} \in \boldsymbol{H}. \tag{4}$$

Here $\boldsymbol{H} = L_2(D) \times L_2(D)$, $\boldsymbol{u} = (v, w)$. Linear operator $A(\mu) : \boldsymbol{H} \to \boldsymbol{H}$ acts on vector function $\boldsymbol{u} = (v, w)$, $v, w \in W_2^2(D)$ by the following rule:

$$\mathrm{A}(\mu)\mathbf{u} = \nu\Delta\boldsymbol{u} + \mathrm{B}\boldsymbol{u} + \mu\mathrm{C}\boldsymbol{u}.$$

where Δ is Laplace operator, $\mathrm{B} = \begin{pmatrix} 0 & 1 \\ -1 & 0 \end{pmatrix}$, $\mathrm{C} = \begin{pmatrix} 0 & 0 \\ 0 & 1 \end{pmatrix}$. Boundary conditions of the system are taken into account by choosing the domain of operator A. Hereinafter we assume that homogeneous Dirichlet boundary conditions ($\boldsymbol{u}|_{\partial D} = 0$) or mixed boundary conditions ($\boldsymbol{u}|_{S_1} = 0$; $\frac{\partial \boldsymbol{u}}{\partial n}|_{S_1} = 0$; $S_1 \cup S_2 = \partial D$) are set on the boundary of D. Trilinear operator $K(\boldsymbol{a},\boldsymbol{b},\boldsymbol{c}) : H^3 \to H^3$ is defined by:

$$K(\boldsymbol{a},\boldsymbol{b},\boldsymbol{c}) = (0, a_2 b_2 c_2)\,.$$

Let us find critical value of control parameter μ (i.e. such value μ_{cr} that some eigenvalues of linear operator $A(\mu_{cr})$ are located on the imaginary axis and other eigenvalues are located on the left-hand half plane).

$$\mu_{\mathrm{cr}} = \frac{1}{\nu\lambda_1} + \nu\lambda_1 \quad \text{if} \quad \nu \geq \frac{1}{\lambda_1}; \quad \mu_{\mathrm{cr}} = 2\nu\lambda_1 \quad \text{if} \quad \nu < \frac{1}{\lambda_1}.$$

If $\nu \geq \dfrac{1}{\lambda_1}$ then monotonous instability takes place in the system, otherwise oscillatory instability is observed. Hereinafter we assume that $\nu < \dfrac{1}{\lambda_1}$, restricting our attention to the case of oscillatory instability.

To find $\dfrac{2\pi}{\omega}$-periodic in time solution of (2), where ω-unknown cyclic frequency of oscillations, we set $\tau = \omega t$ and $\varepsilon^2 = \mu - \mu_{cr}$ in (4) and arrive at:

$$\omega\dot{\boldsymbol{u}} - A(\mu_{cr})\boldsymbol{u} = \varepsilon^2\mathrm{C}\boldsymbol{u} - K(\boldsymbol{u},\boldsymbol{u},\boldsymbol{u}), \tag{5}$$

where differentiation by τ is denoted by dot symbol. We seek nontrivial 2π-periodic by τ solution of (5) and unknown cyclic frequency ω in the form of series:

$$\boldsymbol{u} = \sum_{i=1}^{\infty} \varepsilon^i \boldsymbol{u}_i, \qquad \omega = \sum_{i=0}^{\infty} \varepsilon^i \omega_i \tag{6}$$

Inserting these series into (5) and equating the coefficients of like powers of ε in both parts of the equation, we arrive at the sequence of equations for the

unknown 2π-periodic functions $\boldsymbol{u}_i$ and numbers ω_i. By solving these equations one after the other, we find first terms of the series (6). We showed that soft loss of stability occurs in Rayleigh reaction-diffusion system (2). When $\varepsilon << 1$ a stable limit cycle exists in the system. First three terms of the series for cyclic frequency ω are equal to zero: $\omega_1 = \omega_2 = \omega_3 = 0$, $\omega_4 \neq 0$. The expressions for first terms of the series for 2π-periodic by τ solution of (2) are given by:

$$\begin{cases} \boldsymbol{u} = \varepsilon\alpha_1(e^{i\omega t}\boldsymbol{\varphi} + e^{-i\omega t}\boldsymbol{\varphi}^*) + \varepsilon^3(\alpha_3(e^{i\omega t}\boldsymbol{\varphi} + e^{-i\omega t}\boldsymbol{\varphi}^*) + \boldsymbol{u}_3^p(\omega t)) + O(\varepsilon^4) \\ \omega = \sqrt{1-\nu^2\lambda_1^2} + \varepsilon^4\omega_4 + O(\varepsilon^5) \end{cases} \tag{7}$$

Expressions for α_1, $\boldsymbol{u}_3^p$, α_3, ω_4 are found explicitly.

We found out that in case where $x \in [0,1]$ derived formulas have a much simpler form. It was shown that for Dirichlet boundary conditions or Neumann boundary conditions with additional requirement of zero average, expressions for n-th term of series for 2π-periodic solution contains only finite linear combinations of basis functions ψ_k, where $k = 2*n+1$, $n \in \mathbb{N}$, $k \leq n$. For mixed boundary conditions, expressions for n-th term of series also contains linear combinations of basis functions ψ_k, but $k = 2*n+1$, $n \in \mathbb{N}$, $k \leq \dfrac{n+1}{2}$.

For Dirichlet boundary conditions we have:

$$\mu_{cr} = 2\nu\pi^2, \qquad \omega_0 = \sqrt{1-\nu^2\pi^4} \qquad \boldsymbol{\varphi} = \frac{i}{2\omega_0}\begin{pmatrix} 1 \\ \nu\pi^2 + i\omega_0 \end{pmatrix}\sin(\pi x)$$

$$\boldsymbol{u}_3^p = \boldsymbol{w}_{13}(x)e^{i\tau} + \boldsymbol{w}_{33}(x)e^{3i\tau} + \text{c.c.}$$

$$\boldsymbol{w}_{13}(x) = \frac{i\sqrt{2}}{9}(\nu\pi^2 + i\omega_0)\boldsymbol{P}_1^3\sin(3\pi x)$$

$$\boldsymbol{w}_{33}(x) = -\frac{i\sqrt{2}}{9}(\nu\pi^2 + i\omega_0)^3[\boldsymbol{P}_3^1\sin(\pi x) - \frac{1}{3}\boldsymbol{P}_3^3\sin(3\pi x)]$$

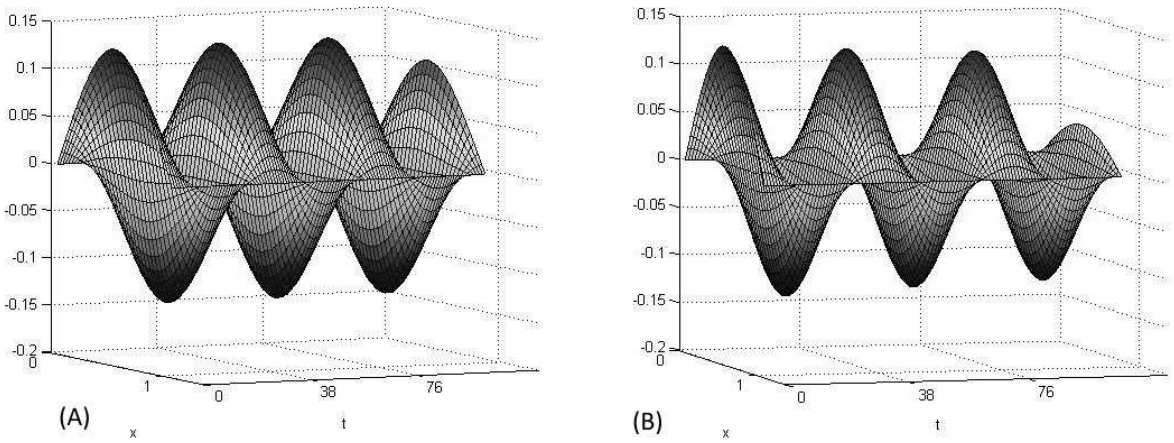

Figure 1. Asymptotical (A) and numerical (B) solution of system (2) in the case of Dirichlet boundary conditions (first component). System parameters are set to: $\nu = 0.1$, $\mu = \mu_{cr} + 0.01$

System (2) was also studied numerically in cases where $x \in [0,1]$. Diffusion coefficient ν was set to $\nu = 0.1$ and values for control parameter μ were taken such that $\mu >> \mu_{cr}$. Several numerical methods were used for numerical integration of the system: grid method, method of lines, Galerkin method. The results of all numerical experiments were fully consistent with each other.

For the case of Dirichlet boundary conditions, the destruction of self-oscillating mode was studied numerically. Critical value μ_{cr}, corresponding to diffusion coefficent $\nu = 0.1$ was equal to $\mu_{cr} = 1.9739$ in this case. For values of control parameter, less than $\mu_{cr} + 0.01$, self-oscillating mode was observed in the system. Self-oscillations were replaced by dual-frequency quasi-periodic oscillations as values of control parameter were increasing. When $\mu > \mu_{cr} + 0.05$, an inhomogeneous stationary solution was observed in the simulations.

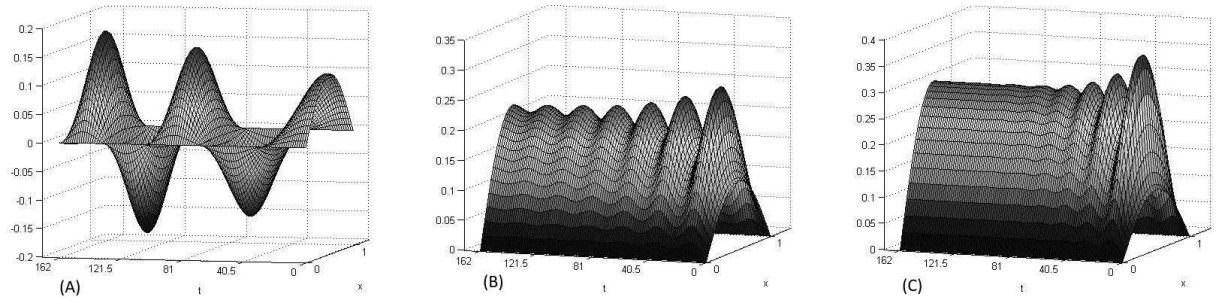

Figure 2. Numerical solution of system (2) (first component) for three values of control parameter μ: $\mu = \mu_{cr} + 0.03$ (A), $\mu = \mu_{cr} + 0.06$ (B), $\mu = \mu_{cr} + 0.1$ (C). Diffusion coefficient ν is set to: $\nu = 0.1$

For the case of Neumann boundary conditions, numerical simulations revealed a set of spatially inhomogeneous stationary solutions. Simulations for functions $u_0(x) = v_0(x) = \cos(\pi n x), n \in \mathbb{N}$ as initial conditions converged to stationary solutions, while simulations for all other initial conditions converged to spatially homogeneous periodic oscillations.

We also studied numerically a generalized version of Rayleigh reaction-diffusion system:

$$\begin{aligned} v_t &= \nu_1 \Delta v + \varepsilon(w - \alpha u) \\ w_t &= \nu_2 \Delta w - v + \mu w - w^3 \end{aligned} \tag{8}$$

where $x \in [0,1] \times [0,1]$. We used Odeint C++ library together with NVidia CUDA v. 7.0 to improve performance of the simulations. Numerical integration of the system was carried out by the method of lines. We considered the case of mixed boundary conditions and set the following values of system parameters: $\nu_1 = 0.05, \nu_2 = 0.00028, \mu = 1, \varepsilon = 10$. Parameter α was varied. Noisy initial conditions were considered. We observed for $\alpha < 0.01$ a stable periodic mode in the system. Starting from $\alpha = 0.04$, periodic oscillations are replaced by spot patterns during the evolution of the system. When $\alpha > 0.4$, oscillations are no longer observed in the system and it demonstrates the fast convergence to

spot patterns. We noted that the final configuration of spots strongly depends on initial conditions of the system.

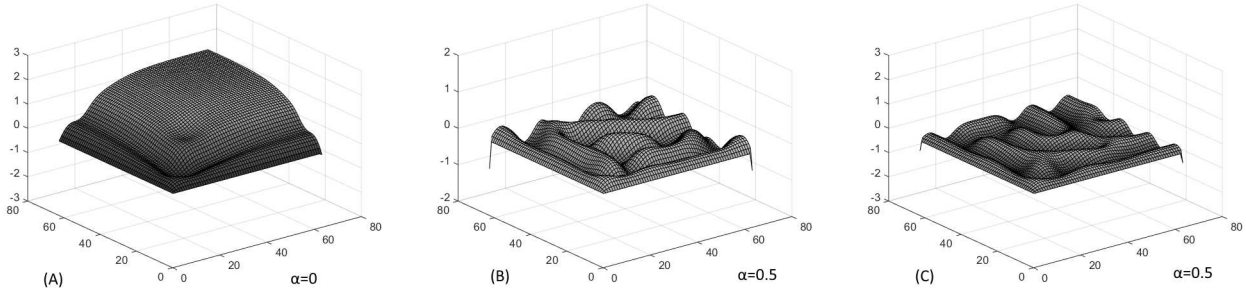

Figure 3. Numerical solution of system (8) for different values of parameter α

Bibliography

1. *Yudovich V.I.* Investigation of auto-oscillations of a continuous medium, occurring at loss of stability of a stationary mode // Journal of Applied Mathematics and Mechanics, 1972, vol. 36, No 3, pp. 424–432.

2. *Revina S.V., Yudovich V.I.* Initiation of Self-Oscillations at Loss of Stability of Spatially-Periodic, Three-Dimensional Viscous Flows with Respect to Long-Wave Perturbations // Fluid Dynamics, 2001, vol. 36, No 2, pp. 29–41.

3. *Melekhov A.P., Revina S.V.* Onset of self-oscillations upon the loss of stability of spatially periodic two-dimensional viscous fluid flows relative to long-wave perturbations // Fluid Dynamics, 2008, vol. 43, No 2., pp. 41–56.

4. *Revina S.V.* Recurrence formulas for long wavelength asymptotics in the problem of shear flow stability // Computational Mathematics and Mathematical Physics, 2013, vol. 53, No 8, pp. 1387–1401.

5. *Kazarnikov A.V., Revina S.V.* The bifurcational behaviour of Rayleigh system with diffusion in the case of one spatial variable (in Russian) // Proceedings of XVII International Conference "Modern problems of Continuum Mechanics". Rostov-on-Don: Southern Federal University. 2014. Vol. 2, Pp. 6-10.

NUMERICAL MODELING OF THE SHALLOW AND LONGITUDIAL TURBULENT STREAM BASED ON THE 3D REDUCED MODEL

Nadolin K.A.[1], **Zhilyaev I.V.**[1,2]

[1] *Southern Federal University, Rostov-on-Don, Russia*

[2] *Southern Scientific Center of Russian Academy of Sciences, Rostov-on-Don, Russia*

Summary: The results of analytical and numerical study of the reduced 3D mathematical models of free water flows in non-deformable beds are presented. Full hydrodynamic models were simulated in finite-element software package *Comsol Multiphysics* to verify the reduced model. These results suggest that the proposed 3D reduced model of the longitudial slightly sinuous channel flow adequately describes its hydrodynamics.

Keywords: shallow stream, viscous fluid, free surface, mathematical modelling, numerical study.

Introduction. Different types of mathematical models are used to simulate hydrological characteristics of the water streams. The most accurate of them are based on the full 3D hydrodynamic equations of turbulent flows. However, the data of the real hydrological measurements don't have the required precision of the values of the hydrophysical parameters to obtain accurate solution in practice, as well as exact formulation of the initial and boundary conditions for the three-dimensional partial differential equations. This work is devoted to analytical and numerical study of one of the proposed in [1] reduced mathematical models of an longitudial shallow stream. The model is verified by comparing the data of direct numerical simulation based on the original equations for a viscous fluid and the results obtained on the basis of the reduced model.

Reduced model equations. Let's consider slow water flow in a non-deformable channel. We introduce rectangular Cartesian coordinates, where the plane xy lies on the flow surface and the axis z points to riverbed. Assume that the axis x denote the direction of the flow and the axis y goes from the left bank to the right one. The origin of the coordinate system is located at the middle of the inlet section (see Fig. 1). Let's assume that free surface of the stream is weakly deformable and is defined as $z = \xi(x, y, t)$, where $\xi(x, y, t)$ – unknown function. The form of channel is known and described as $z = h(x, y)$. Riverbanks can be identified by functions $y = l(x, t)$ and $y = r(x, t)$ implicitly through the equation

$$h(x, y) - \xi(x, y, t) = 0 \tag{1}$$

The technique of deriving the reduced 3D mathematical models of the flow is based on small parameter technique, which has been applied to Reynolds equations (coupled with the Boussinesq turbulence hypothesis [2]) written in the special dimensionless form. This technique was presented in details in [1].

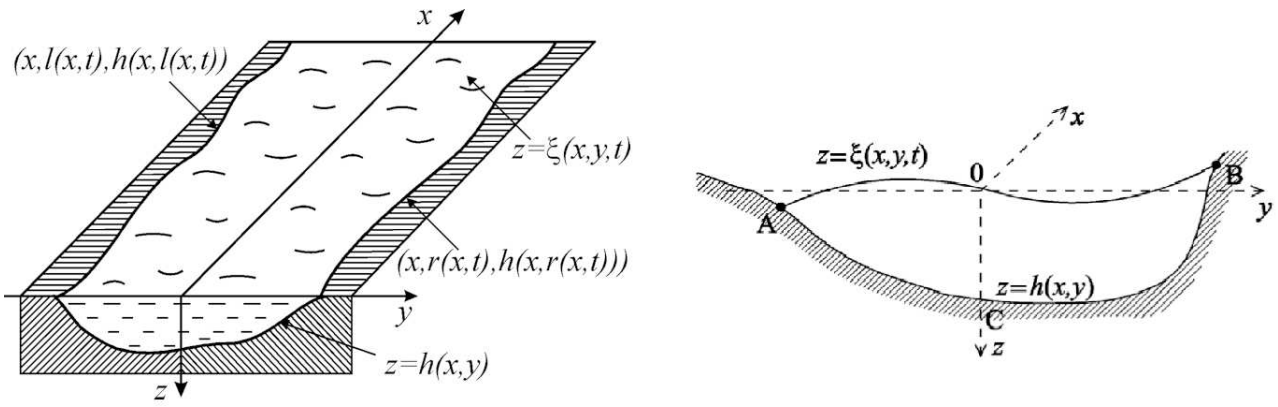

Figure 1. Flow layout and coordinate system and flow cross-section

Reduced equations in dimensionless form for shallow and longitudial stream are

$$p = G(z - \xi)$$

$$u = ReGI(J_2 - \xi J_1) + F_x(h - z)$$

$$v = ReG\frac{\partial \xi}{\partial y}(J_2 - \xi J_1) + F_y(h - z)$$

$$w = ReG\left(I\frac{\partial}{\partial x}(J_4 - \xi J_3) + \frac{\partial}{\partial y}\left((J_4 - \xi J_3)\frac{\partial \xi}{\partial y}\right)\right) +$$

$$+(h - z)\left(F_x\frac{\partial h}{\partial x} + F_y\frac{\partial h}{\partial y}\right)$$

$$\frac{\partial \xi}{\partial t} = ReG\left(I\left(\frac{\partial}{\partial x}(J_4 - \xi J_3) - (J_2 - \xi J_1)\frac{\partial \xi}{\partial x}\right) + (J_4 - \xi J_3)\frac{\partial^2 \xi}{\partial y^2} +\right.$$

$$\left. +\frac{\partial \xi}{\partial y}\frac{\partial}{\partial y}(J_4 - \xi J_3) - (J_2 - \xi J_1)\left(\frac{\partial \xi}{\partial y}\right)^2\right) +$$

$$+(h - \xi)\left(F_x\left(\frac{\partial h}{\partial x} - \frac{\partial \xi}{\partial x}\right) + F_y\left(\frac{\partial h}{\partial y} - \frac{\partial \xi}{\partial y}\right)\right)$$

where

$$J_1 = \int_z^h \frac{d\tau}{\nu}, \qquad J_2 = \int_z^h \frac{\tau d\tau}{\nu},$$

$$J_3 = \int_z^h J_1(x, y, \tau)d\tau, \qquad J_4 = \int_z^h J_2(x, y, \tau)d\tau$$

Here u, v, w – longitudinal, transverse and vertical components of the flow velocity, respectively; p – pressure; h – riverbed function; ξ – free surface function; Re – Reynolds number; G – gravity parameter; I – slope parameter; F_x and F_y – parameters, that denote values and direction of the external forces; ν – dimensionless function parameter, that determines viscosity of the stream turbulence.

Reduced model analysys. The hypothesis of Boussinesq can be successfully used to take into account the turbulence in longitudial channel flow with the reduced hydrodynamic models. In this case, it is assuming that the viscosity of the liquid at a given point of the flow does not depend on the flow velocity, but it depends of the coordinates that determine the distance to the bottom of the rigid bed.

To select correctly the functional dependence of $\nu(x, y, z)$, it should be identified as $O(1)$ at the stream's free surface ($z = \xi$) because of the choice of the Reynolds number [1]. On the other hand, in the boundary layer ($z = h$) viscosity is defined by the molecular properties of the liquid, so values of the viscosity function parameter should be very small.

Let's consider the simplest case of describing the viscosity function $\nu(x, y, z)$ as the linear dependence of z-axis

$$\nu = h^2 - \left(h - \frac{\nu_h}{h}\right) z \qquad (*)$$

where parameter ν_h is defined as

$$\nu_h = \mu \left(\frac{S_x}{S_0}\right)^a$$

Here μ is determined by molecular viscosity of the liquid; S_0 and S_x – areas of the stream cross-sections at $x = 0$ and at the current point x; a – adjustment parameter that defines the sensitivity of the model to the riverbed deformations.

Formula $(*)$ has been tested numerically and provides good correlation with the solutions of the full equations of hydrodynamics.

Computational experiments. To verify the reduced model we compare results of the simulation with the data, obtained by solution of the full Navier-Stokes equations in laminar flow and the Reynolds equations for the turbulent stream ($k-\epsilon$ turbulence model). For that numerical simulation the CFD module of the finite-element package *Comsol Multiphysics* was used [3].

For the comparison of the models the form of riverbed was taken as $h(y) = \sqrt{1-(0.2y)^2}$, $I = 0.0001$ and aspect ratio of the flow is 1:10:100 (depth:width:lenght). The longitudinal velocity of the flow is depicted on the Fig.2.

The form of the channel $h(x, y) = (1 + 0.1 \sin 0.1x)(1 - (0.2y)^2)$ was chosen to compare models in the case of curvilinear riverbed (see Fig.3).

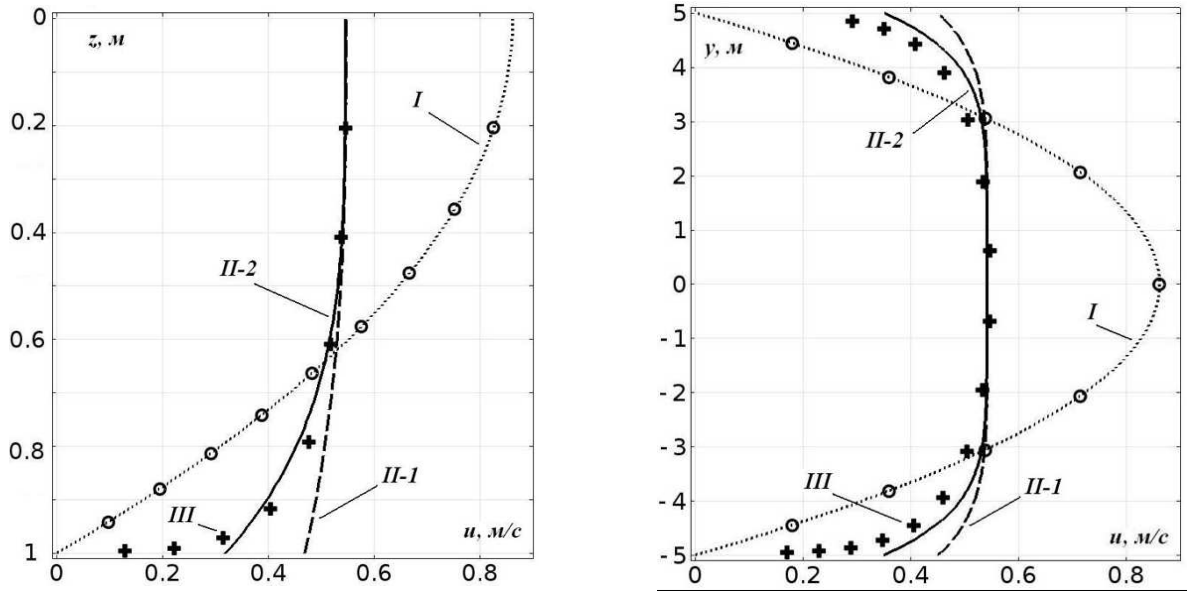

a) b)

Figure 2. The longitudinal velocity of the flow: (a) – due to the depth on the fairway's line; (b) – due to the width on the surface;*I* – laminar flow; *II* – the $k-\epsilon$ model turbulent flow (*1* – coarse mesh, *2* – fine mesh); *III* – the 3D reduced model

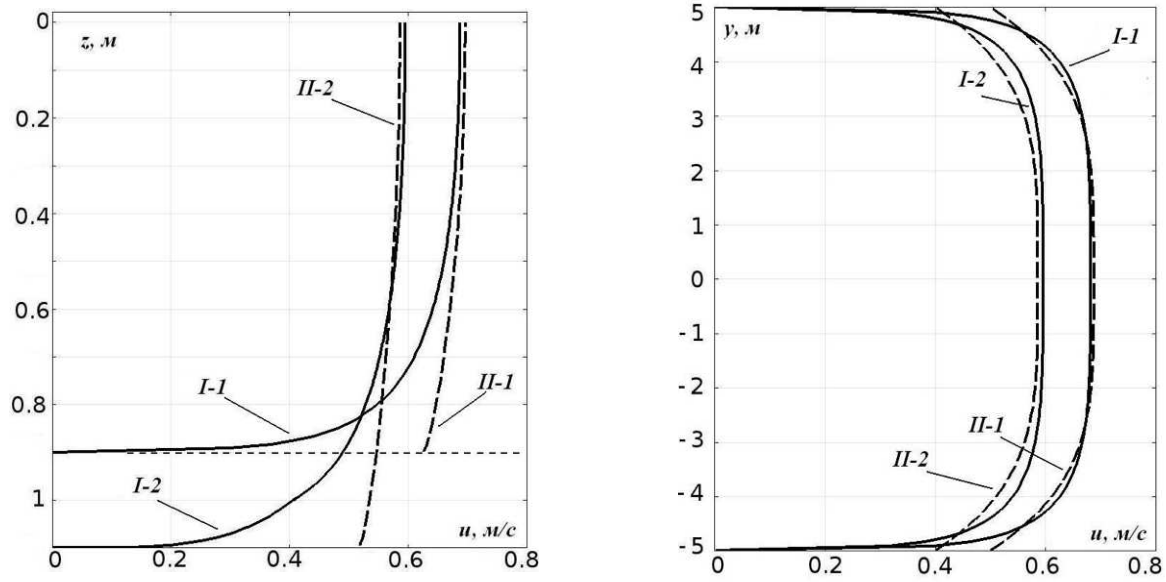

a) b)

Figure 3. The longitudinal velocity of turbulent flow in the curvilinear channel: (a) – due to the depth on the fairway's line; (b) – due to the width on the free surface; *I* – 3D reduced model; *II* – $k-\epsilon$ turbulence model; *1* – at the cross-section of minimum depth; *2* – at the cross-section of maximum depth

On Fig.4 the results of the simulation of permanent tail and adverse wind are presented.

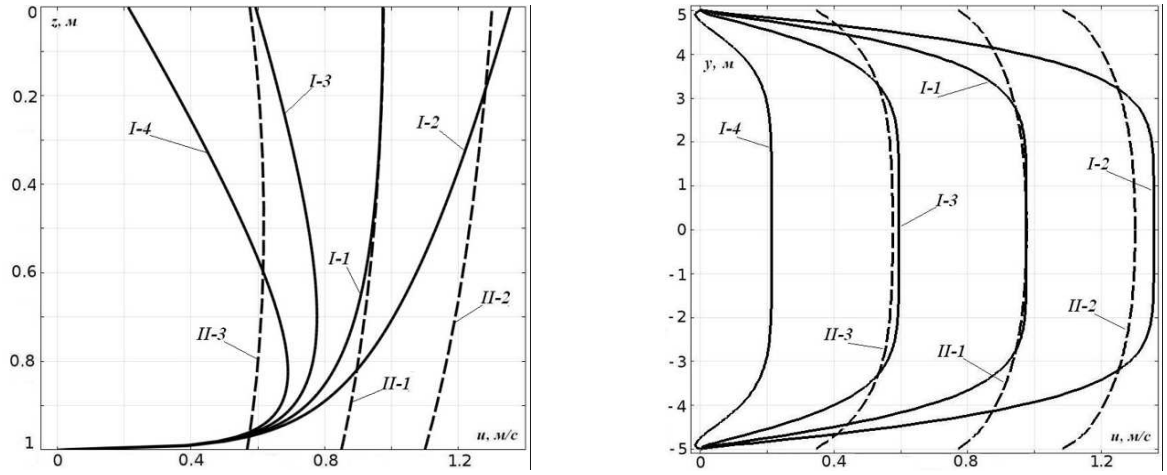

a) b)

Figure 4. The longitudinal velocity of the turbulent flow under external force F_x: (a) – due to the depth on the fairway; (b) – due to the width on the free surface; I – 3D reduced model; II – $k-\epsilon$ turbulence model; *1* – $F_x = 0$; *2* – $F_x = 0.5$; *3* – $F_x = -0.5$; *4* – $F_x = -1.5$

Conclusion. To test proposed mathematical models numerical simulations were made. The results show that reduced 3D models adequately describe the hydrodynamics of the natural shallow and longitudial streams. The proposed model are quite simple and allows us to analyse the influence of the shape of the channel bed and the effect of some external forces (e.g. wind) to the characteristics of the flow.

Bibliography

1. *Nadolin K.A.* On the approach to modelling the mass transfer in river-bed stream // Matematicheskoe Modelirovanie N 2. 2009. P. 14-28 (in Russian)

2. *Loitsyanskii L.G.* Mechanics of liquids and gases. Oxford Pergamon Press, 1966. 481 p.

3. *Zhilyaev I.V.* Numerical Simulation of the Model of the Hydrodynamics of the Shallow Longitudial Flow // Vestnik Yuzhnogo Nauchnogo Tsentra, N 1. 2013. P. 3-7 (in Russian)

MODIFICATION OF FINITE-VOLUME METHOD FOR APPROXIMATION DIFFERENTIAL EQUATIONS IN COMPLEX DOMAIN ON RECTANGULAR GRIDS[1]

Shishenya A.V., Chistyakov A.E.
Southern Federal University, Taganrog, Russia

Motivation

When solving modern problems for partial differential equations with numerical methods, typically there is a number of requirements for the solution algorithm, such as the following:

1. Sufficient accuracy of the solution of the problems including those in complex domains must be provided;

2. The algorithm of the numerical solution must allow efficient implementation for multiprocessor systems;

One of the most popular methods of numerical solution of differential equations is the method of grids. The solving of the differential equations on unstructured grids allows describing the geometry of the domain more accurately, however, these grids have a number of disadvantages:

1. Derivation of a grid equation from the differential one requires more effort on unstructured grids compared with structured;

2. A grid generator is required for creating unstructured grid each time the computational domain changes;

3. The working with unstructured grids requires more operations with RAM;

4. Parallel implementation of numerical algorithms on unstructured grids with domain decomposition method requires splitting the nodes of the computational grids by processors.

The algorithms of solving differential equations on structured grids don't have the former drawbacks, but they have another significant disadvantage – low precision of the approximation of the computational domain boundary. Besides, the discrete boundary of the domain doesn't converge to the continuous one as the spatial step tends to zero; moreover, the limit of the discrete boundary is nowhere smooth function. Therefore, the discrete problem doesn't converge to the continuous one and instead it tends to an ill-posed problem.

Modification of the finite-volume method with partial "fullness"

The proposed finite volume method with partial "fullness" allows creating grid equation on uniform rectangular grid such that the obtained discrete problem

[1]Supported by RFBR 15-07-08408

converges to the continuous one with first order on the boundary and with second order in the inner nodes. We assume that the computational domain Ω is defined with the indicator function q that we also call continuous fullness function. The grid fullness function is defined according to the following formula:

$$q_{i+\frac{1}{2},j+\frac{1}{2},k+\frac{1}{2}} = \frac{1}{h_x h_y h_z} \iiint\limits_{\Omega^{1,1,1}_{i,j,k}} \mathrm{d}\omega = \frac{1}{h_x h_y h_z} \iiint\limits_{D^{1,1,1}_{i,j,k}} q\mathrm{d}\omega,$$

where $D^{1,1,1}_{i,j,k}$ is a cell of the computational grid and $\Omega^{1,1,1}_{i,j,k} = D^{1,1,1}_{i,j,k} \cap \Omega$ is a control volume. We assume that the grid fullness function is set in the centers of the cells and the rest grid functions are set in the nodes. Formulas for approximation the first and the second derivatives with the proposed method are derived in [1, 2]. Here we give only final formulas:

$$\begin{aligned} \iiint\limits_{\Omega^{1,1,1}_{i,j,k}} a\varphi'_x \mathrm{d}\omega \simeq q_{i+1,j+\frac{1}{2},k+\frac{1}{2}} a_{i+\frac{1}{2},j,k} \tfrac{\varphi_{i+1,j,k}-\varphi_{i,j,k}}{2} h_y h_z + \\ + q_{i,j+\frac{1}{2},k+\frac{1}{2}} a_{i-\frac{1}{2},j,k} \tfrac{\varphi_{i+1,j,k}-\varphi_{i,j,k}}{2} h_y h_z, \end{aligned} \tag{1}$$

$$\begin{aligned} \iiint\limits_{\Omega^{1,1,1}_{i,j,k}} (\eta\phi'_x)'_x \mathrm{d}\omega \simeq q_{i+1,j+\frac{1}{2},k+\frac{1}{2}} \eta_{i+\frac{1}{2},j,k} \tfrac{\varphi_{i+1,j,k}-\varphi_{i,j,k}}{h_x} h_y h_z - \\ - q_{i,j+\frac{1}{2},k+\frac{1}{2}} \eta_{i-\frac{1}{2},j,k} \tfrac{\varphi_{i,j,k}-\varphi_{i-1,j,k}}{h_x} h_y h_z + \\ + (q_{i,j+\frac{1}{2},k+\frac{1}{2}} - q_{i+1,j+\frac{1}{2},k+\frac{1}{2}}) \eta_{i,j,k} \varphi'_{xi,j,k} h_y h_z. \end{aligned} \tag{2}$$

The formulas (1) and (2) coincide with the classical ones if the grid fullness function take only values zero and one.

Comparison of the approximation order of the classical and proposed method

When estimating order of the grid equation approximation the errors of the boundary approximation are usually not taken into account. The finite volume method is based on approximation of integrals of differential operators, so estimating the errors of approximation of integrals will take into account errors of the domain approximation. The finite volume method utilizes two formulas for approximating integrals: Newton-Leibniz formula and mean value theorem. The former is precise formula and the latter is approximate, so error that it introduces is an error of approximation. The error of averaging is defined as follows:

$$\psi = \tfrac{1}{h_x h_y h_z} \Big(\iiint\limits_{\Omega^{1,1,1}_{i,j,k}} \varphi(\mathbf{x}) \mathrm{d}\omega - q_{i+\frac{1}{2},j+\frac{1}{2},k+\frac{1}{2}} \iiint\limits_{D^{1,1,1}_{i,j,k}} \varphi(\mathbf{x}) \mathrm{d}\omega \Big) \tag{3}$$

In the work we have showed that error (3) has the second order by spatial steps in the inner nodes and the first order in the boundary nodes for propose modified finite-volume method with partial "fullness". In case of using classical finite-volume method, the error of approximation in inner nodes is the second as well, but in boundary nodes the approximation error is constant and the discrete

problem doesn't approximate the continuous one. Comparison of the proposed modification of the finite-volume method with partial fullness and the classical method is performed for the model of viscid flow in the sloped reservoir. In case of using classical finite-volume method, the flow near the sloped boundary is significantly reduced due to the stair-stepping of the boundary compared to the proposed method. Besides, pressure field values are different even in the inner nodes.

Conclusion

Modification of the finite volume method with partial "fullness" for approximation differential equations on structured rectangular grids is proposed. Investigation of the order approximation with respect to the errors of the boundary approximation has shown that the proposed method has the first order of approximation in the boundary nodes while the classical one introduce constant error. Although both methods have second order of approximation in the inner nodes, in case of the usage of the classical finite-volume method, the errors in boundary nodes noticeably change the entire solution that is confirmed by numerical experiments.

Bibliography

1. *Sukhinov A.V., Chistyakov A.E., Timofeeva E.F., Shishenya A.V.* Mathematical model for modelling coastal wave processes. Mathematical Models and Computer Simulations, 2013, 5:2, p. 122–129.

2. *Sukhinov A.V., Chistyakov A.E., Timofeeva E.F., Shishenya A.V.* Parallel implementation of a three-dimensional model of hydrodynamics of shallow reservoirs on supercomputer system. Almanac of modern science and education, 1(68), 2013, p. 139–141.

SIMULATION OF OIL POLLUTION IN THE KERCH STRAIT[1]

Shabas I.N.*, Chikina L.G.*, Muratova G.V.*, Chikin A.L.**

* *Southern Federal University, Rostov-on-Don, Russia*

** *Southern Scientific Center of Russian Academy of Sciences (SSC RAS), Rostov-on-Don, Russia*

Oil pollution is the imminent danger arising during the oil transport by water from the place of its extraction to places of processing. That's one example. On the 11-th of November in 2007 during a severe storm in the Kerch Strait four ships sank, six ships stranded, two tankers were damaged. About 2 million tons of fuel oil spilled into the sea because of tanker "Volgoneft-139" faults.

Oil entering the water basin has a negative influence on all physical, chemical and biological processes. Therefore, it is necessary to predict the behavior of the oil trapped in the water area for rapid decision-making in case of liquidation of negative consequences. Mathematical modeling the oil pollution spread on the water surface, as well as its thickness and on its borders, is one of the important ways of this prediction.

The object of the research is the behavior of oil spills in the Kerch Strait. The spread of oil in the water basin is a complex process. It's necessary to consider a wide variety of factors in the simulation. Physical and chemical properties of oil (boiling point fractions, density, viscosity) have an impact on the behavior of pollutionis and external environmental conditions (wind field, the air temperature, the water temperature, the presence of oil-oxidizing bacteria in the water, salinity, solar radiation etc). Processes of spreading oil spill dominate on the first stage of the oil spread.

The inevitable degradation of the oil comes under the influence of external environmental factors in parallel with these processes. Besides that, the movement of the oil slick occurs under the influence of winds and currents in the water. Three modes of [1, 2]: inertial, gravitational, and viscous regime of surface tension exist at the stage of oil spreading on the the water basin surface.

For spills of less than 2000 m^3 the most important phase of proliferation is the phase under the action of surface tension forces. In the works of [2]-[4] semi-empirical formula simulation ellipse describing asymmetric shape oil slick stretched along the direction of the wind is proposed. According to these formula, the spot diameter in a direction perpendicular to the direction of the wind is calculated as follows:

$$l_{min} = 53.76(\frac{\Delta\rho}{\rho_{oil}})^{1/3} V_{oil}^{1/3} t^{1/4},$$

[1]Supported by The Ministry of Education and Science of Russia (grant 1420)

and the spot diameter in the direction of the wind:

$$l_{max} = l_{min} + 0.95U_{wind}^{4/3}t^{3/4},$$

уфх $\Delta\rho = \rho_w - \rho_{oil}$, ρ_w ш ρ_{oil} – density of water and oil, respectively, V_{oil} – the amount of the original oil spill, U_{wind} – wind speed, t – after the spill.

It is obvious that the area of the ellipse will be $A_s = \ frac\ pi4 l_{max} l_{min}(m^2)$.

Drift spots under the influence of currents and wind is described by the convection-diffusion equation [4]:

$$\begin{gathered}\frac{\partial h}{\partial t} + \overline{\nabla}(h\overline{v}) - \overline{\nabla}(D\overline{\nabla}h) = R_h,\\ \overline{v} = \left(u_x + \frac{\tau_x^w}{C_f}, u_y + \frac{\tau_y^w}{C_f}\right),\\ D = \frac{g \cdot h^2(\rho_w - \rho_O il)}{\rho_w C_f},\end{gathered} \tag{1}$$

where h – the thickness of the oil, ∂v – drift velocity of the film, $\frac{\tau_x^w}{C_f}$ – shear stress due to wind, D – function of the diffusion spread Spot crude oil, C_f – coefficient of friction between the oil film and surface water (0.02kg / m^2c), R_h – the sources (Stock) function, g – acceleration of gravity, $\overline{\nabla} = (\partial/\partial x, \partial/\partial y)$. Initial thickness of spots is calculated as follows: $h = \frac{V_{oil}}{A_s}$.

The boundary and initial conditions [5] are added to the equation (1) . It is assumed that the velocity field is known at every time step. The resulting system of equations is solved by finite difference method using implicit schemes. The computational domain is constructed as rectangular uniform in all directions of the grid. To approximate equations upwind scheme for the convective terms is used. As a result of the finite-difference approximation we obtain a system of linear algebraic equations with five-diagonal matrix.

The mathematical model was implemented as a set of programs. The solution is carried out on high-performance computing systems with distributed memory parallel programming environment MPI. The Parallel Library program Aztec is used for solving the linear algebraic equation system with sparse matrix. Aztec includes procedures that realizing iterative methods from Krylov's subspace – conjugate gradient method (CG), generalized method of minimal residual (GMRES), quadratic conjugate gradient method (CGS), a method quasiminimal residuals (TFQMR), biconjugate gradient method (BiCGSTAB) with stabilization. All methods are used with various preconditioners (polynomial method and domain decomposition using both the direct method LU, and incomplete LU decomposition in subdomains). According to research results [6] biconjugate gradient (BiCGSTAB) method was chosen for solving this system.

The numerical experiments to simulate an emergency situation in the Kerch Strait in November 2007 were made using constructed computer system [7].

Bibliography

1. *J.A.Fay* "The spread of oil slicks on a calm sea" // Oil on the sea, Plenum Press. – New-York, 1969, p.53-63.

2. *J.A.Fay* "Physical processes in the spread of oil on a water surface" // Proceeding of the Joint Conference on Prevention and Control of Oil Spills. Washington, DC. American Petroleum Institute. 1971. P. 117-125.

3. *W. J. Lehr, H. M. Cekirge, R. J. Fraga, and M. S. Belen* // "Empirical studies of the spreading of oil spills," Oil and Petrochemical Pollution, vol. 2, no. 1, pp. 7-11, 1984.

4. *Ehsan Sarhadi Zadeh1 and Kourosh Hejazi* "Eulerian Oil Spills Model Using Finite-Volume Method with Moving Boundary and Wet-Dry Fronts" //. Modelling and Simulation in Engineering Volume 2012 (2012), Article ID 398387, 7 pages, http://dx.doi.org/10.1155/2012/398387

5. *Shabas I.N.* Modelling of processes of spreading and drift of oil pollution of water bodies // Coll. works XV Russian conference school of young researchers "Modern problems of mathematical modeling", Rostov-on-Don, Publ TSVVR, 2013., ss.274-278 (in Russia)

6. *Shabas I.N.* Simulation on High Performance Computing Systems processes of multicomponent mixture in the reservoir. // Bulletin of the South Ural State University, a series of "Computational Mathematics and Informatics", Chelyabinsk: South Ural State University Publishing Center, 2014, s.89-96 (in Russia)

7. *Chikin A.L., Shabas I.N., Chikina L.G.* Calculation of hydrodynamic parameters in the Azov Sea on multiprocessor system using Web-based interface. Certificate of official registration of the computer program № 2005612497, 26.09.2005

GROUP-LATTICE APPROACH TO COMPUTATION OF SOCIAL CONSTANTS IN THE MODELLING OF EVOLUTION PATHS OF THE ARCHAIC SOCIETY[1]

Shvedovsky Vyacheslav, Standrik Anton

Lomonosov Moscow State University, Faculty of Sociology, Faculty of Computational Mathematics and Cybernetics, Moscow, Russia

Since ancient times cultural codes of different countries, ethnic groups and nation were formed during the evolution depending on the evolution paths that were traversed and the problem of find- ing formation paths and laws of these codes is posed. It is hypothesized that the macrodescription of evolution routes is effective if a set of the most highly aggregated categories to describe way of life of various communities of the society is used: the assignment, work, exchange, distribution and consumption. As a subject of consideration of the author chose the primitive clan community epoch of mesolite, located in the neighbors ' relations we-they with the same community. As models of these relations, he applies the group of permutations, reflecting possible the reproductive cycles of the graphs with 4, 6 and 8 vertices.

Each graph puts the macro-level system of social reproduction, in which a set of n – vertices is the set of reproduction kernels, covered by the range of reproductive cycles – RC. In this case the evolution of an archaic society is modeled sequence of nested subgroups – H_n for which removed law of changes, which defines the complexity of the society at the mastering of the mass of its representatives of discoveries and inventions:

$$... \subset H_n \subset H_m \subset H_p \subset ..., n < m < p$$

First members of this sequence are guaranteed by select of subgroups with necessary devisors for group S_4. Next members of this sequence are subgroups of octahedrons symmetries S_6, and group of tetrahedron S_4 is subgroup of S_6 group.

Discoveries and inventions are displayed on graphs by addition of new oriented edges, permitting a new reproduction cycles, or new vertices (reproduction kernels) – evidence of the emergence of new social institutions that are ordered by the complexity level.

At formation of the criterion for the selection of the evolutionary trajectories of society on the group lattices there arises need to clarify the calculated entropy estimates of the complexity of each trajectory. It is obtained an initial macroestimate of compound $\mathcal{H}(n)$ for compounding spectrum RC:

$$(n-1)*lnn - lnln(n-1) - n < \mathcal{H}(n) < lnL + (n-1)*lnn - lnln(n-1) - n,$$

[1]This work was supported by RFH(Russian Foundation for Humanities) 15-03-00435

where n degree of group S_n for system of social reproduction, and L – *const*. [2]

Based on the evaluation of the complexity of the spectrum of reproductive cycles of the collective economy of the archaic society, the autor calculated the number of social constants L for the phase transition from the Mesolithic to Neolithic age. The author used the idea that fundamental changes in society occur throught new inventions and discoveries that end up in the development of new effective technologies (Behterev's Law of Changes) that significantly change the lifestyle of society and complicate relations in it.

Received constants will allow us to specify a road map of the evolution of the most ancient slav society and some other societies in order to justify the formation of a social heredity of its different groups, manifesting the cultural code of conduct on different subsequent historical periods.

The problem of finding all subgroups in a group was proved to be NP-complete problem by mapping groups on the Cayley graph therefore there is no efficient algorith of solving it. Computation algoritm is based on Lagrange's theorem and shows satisfactory computational time in theory and in practice in relation to finding subgroups in permutation group of order eight which is equivalent to 8-vertex ordered graph. Estimated time of the algorithm is:

$$T(k) = \mathcal{O}(k!^2) * S_n \sim \mathcal{O}(2\pi k(\frac{k}{e})^{2k}) * S_n$$

$$Sn = \sum_{i=1}^{n-1} C_n^i S_{n-i}.$$

Subgroups complexity was evaluated with Uemov criterium of oriented graph complexity which is based on the number of hierarchical relationships of different types.[1]

$$U(m,r) = -\sum_{j=1}^{n}\sum_{i=1}^{k} \frac{l_{j,i}}{n-1} ln(\frac{l_{j,i}}{n-1})$$

m – set of vertices and r is a set of all possible types of relationships between these vertices. This approach allows us to use median probability criterium:

$$0.5 - \epsilon \leq P(\xi_{i,j}) \leq 0.5 + \epsilon$$

$\xi_{i,j}$ – discontinuous variate on the set of complexities of transitions from level i to level j and to make suggestions about preferable(optimal) evolution routes. Due to constant overall complexity for each route, too complex or too simple routes were dropped from evolution tree. Finally the evolution lattice or evolution tree was introduced. Example of counted nested groups:
$T_0 = \{1,2,3,4,5,6,7,8\}$
$T_1 = \{2,1,3,4,5,6,7,8\}$
$T_2 = \{1,3,2,4,5,6,7,8\}$
... ...

$H_2 = \{T_0, T_1\}$
$H_{18} = \{T_0, T_1, T_{14}, T_{15}, T_{20}, T_{21}, T_{174}, T_{175}, T_{180}, T_{181}, T_{186}, T_{187}, T_{366}, T_{367}, T_{372}, T_{373}, T_{378}, T_{379}\}$
$H_{36} = \{T_0, T_1, T_{14}, T_{15}, T_{20}, T_{21}, T_{54}, T_{55}, T_{60}, T_{61}, T_{66}, T_{67}, T_{120}, T_{121}, T_{134}, T_{135}, T_{140}, T_{141}, T_{174}, T_{175}, T_{180}, T_{181}, T_{186}, T_{187}, T_{366}, T_{367}, T_{372}, T_{373}, T_{378}, T_{379}, T_{390}, T_{391}, T_{396}, T_{397}, T_{402}, T_{403}\}$

$|H_{144}| = 144$
$|H_{576}| = 576$
$|H_{1152}| = 1152$
$|H_{40320}| = 40320$

$H_2 \subset H_{18} \subset H_{36} \subset H_{144} \subset H_{576} \subset H_{1152} \subset H_{40320}$
Complexities:
$U_{2\to 18} = 4.591761, U_{18\to 36} = 2.983394, U_{36\to 144} = 37.935890, U_{144\to 576} = 195.189507, U_{576\to 1152} = 627.671115, U_{1152\to 40320} = 37863.326155$

Every nation in the beginning of it's evolution in this can be specified with a set of restrictions that affects it's development and formation of it's cultural code. For example poor soil fertility in China forced ancient tribes to cooperate in order to survive. Agriculture strategy in China was based on manpower surplus and was aimed on increasing the fertility by chemical fertilizers while the European strategy was based on high soil fertility and lack of manpower therefore aimed on the invention of effective agricultural tools. These conditions can be reflected in two kernel graphs that initiate the evolution process.

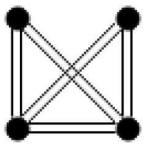

(a) $\mathcal{W}$: West

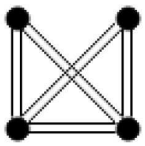

(b) $\mathcal{E}$:East

In the terms of computation technology we can say that there are two types of initial graphs: the Eastern and the Western graph. Relationships between upper and lower kernels can be considered ad hierarchical. Relationships between kernels on the same level can be considered as exchange or cooperate relations. Considering full groups on these graphs that appear in the end of evolution routes and counting the relative values of hierarchy and exchange relations in both groups we can see that there are 1.8 times more hierarchical and 2 time more cooperation relations in the Eastern groups. This explains the emergence and the development of traditionalist cultural values in the East and indivisualistic values in the West.[3]

As a result:

1. Social constants that describe complexity level of society at each stage of it's development level were recieved.

2. The process of cultural values priority formation in East and West societes was described by means of group-lattice approach.

Bibliography

1. *A.Uemov* Veshchi, svojstva i otnosheniya. Nauka, Moskva, 1963 (Things, features, and relations, Moscow, 1963)

2. *V.Shvedovsky* "On the computation of the social constants in the modelling of the evolution of the archaic society". Space and Time 4(14)/2013, p.72-80

3. *I.Derugina* "To the issue of predicting agricultural production in East and West". Eastern Analytics p.144-152 4 / 2014

SPECTRAL DECOMPOSITION AND GEOMETRICAL ANALYSIS OF SPATIAL DATA AND IMAGES

Simonov K.V., Kurako M.A., Cadena L.

* *Siberian Federal University, Krasnoyarsk, Russia*

Abstract

Computer technologies allow the production, transfer and storage of huge amounts of different types of data. We need effective methods for processing and analyzing these data for extracting new information and new knowledge. It is important not only to ensure the adequacy of methods for processing different types of data, but also the opportunity to analyze the accuracy of methods to better understanding the internal structure of the data.

Thus, the first task is to decompose the source data (images) into chunks, process each chunk separately and then analyze the results. Let's introduce class $l \subset L^2(\mathbb{R}^d), d \geq 1$ and appropriately chosen set of functions $(\varphi_i)_{i \in I} \subseteq L^2(\mathbb{R}^d)$, called "analyzing functions", that each $f \in l$ satisfies the equation:

$$f = \sum_{i \in I} c_i(f)\varphi_i.$$

A countable set of coefficients $c_i(f), i \in I$ represents a signal decomposition based on analyzing functions $(\varphi_i)_{i \in I}$. On the other hand, this equation describes the process of restoring the source signal using coefficients $c_i(f)$.

A separate issue is the finding fragments of images with anisotropic characteristics or breaks (lines or curves, object's edges), because traditional image processing techniques are not sensitive to this kind of characteristics.

There are various image-processing methods for finding anisotropic objects in the image, such as directional wavelets, complex wavelets, contourlets, curvelets, etc. offered over the past 20 years. A new approach to the analysis of anisotropic characteristics of images, called shearlet transform, proposed in 2006. Unlike wavelets or curvelets, shearlets built in the class of affine systems and have the ability to determine the direction through additional shear parameter [1-7].

Shearlets have a number of properties, which distinguish them from other image processing methods: a finite number of generating functions; optimal representation of anisotropic characteristics of analyzed data; fast algorithmic implementation; a unified approach to processing continuous and discrete data.

The main usages of the discrete shearlet transform (DST) are image denoising, edge detection, morphological analysis (splitting images to objects of different types, such as points, lines and curves), and improving the quality of images [1-10]. Existing approaches to the analysis of the images allow extension

into a space of more than two dimensions (video) and applicable to problems in medicine and geomonitoring [14].

The goals of the work are comparison of DST algorithms and development a DST-based computer technology for image processing of catastrophic natural events. The main problems are image separation (morphological analysis), denoising and edge detection.

I Computing technology

Based on the theoretical and methodological review, let us consider a modification of the method of geometrical analysis of visual data, which allows solving a wide class of problems in image processing of complex images of environmental monitoring. We outline three types of problems: image separation (to points and curves), edge detection and data visualization using 4 distinct DST algorithms [8-13]. Algorithms defined as follows: A – FFST (Fast Finite Transform Algorithm) algorithm [12, 13]; B – Shearlet Toolbox algorithm [1-8]; C – ShearLab algorithm [3-10]; D – TGVSHCS algorithm [10, 11].

We propose the computing technology and computing system for solving specified problems. In a preliminary phase, the original image is broken down to the computational chunks and computing system planning the sequence of procedures for the optimal solution of the problem. In a configuration phase, computing system chooses concrete algorithms depending on the problem and the brightness and contrast of images. In the next phase the system loading and processing images depending on the set of conditions. The final phase is an analysis and contrasting of the processed images.

For comparison, computations made on the images of different sizes. The quantitative indicator of the effectiveness of algorithms is algorithm's mean working time. The results of comparison are the following: algorithm C is faster than algorithm A on images of large sizes, while algorithm A has a slight advantage on small images. Algorithm D is the slowest. Images larger than 512 on 512 pixels analyzed by chunks.

Analyzed images belong to a number of related areas: wildfire propagation snapshots, medical imaging, geoecology and geodynamics. All images processed with various brightness and contrast values. Gaussian noise used for solving denoising problem and for comparison of denoising algorithms [14].

II Solution of geomonitoring problems

Geometric separataion of visual data. In accordance with the study of DST algorithms proposed to use algorithm C for solving the first task for geometric separation of visual data of geoenvironmental monitoring. Estimation of the image separation improving is 5-12% compared to curvelets.

Edge detection. The second task is detection of edges in the image. Study of algorithm A shows that the edges of objects can be obtained as the sum of the shearlet transform coefficients at the last (maximum) scale. It's proposed to use this approach for edge detection:

$$f_{cont} = \sum_{k=0}^{k_1} \sum_{m=0}^{m_1} sh_\psi(f(j^*, k, m)),$$

where sh_ψ is a mapping from $L^2(\mathbb{R}^2)$ to space of shearlet transform coefficients, j^* – the last scale, k_1 – number of directions and m_1 – number of translations.

Modified FFST algorithm (algorithm A) tested on various types of geomonitoring images and compared with classical Sobel and Prewitt filters. Modified algorithm is comparable in accuracy to the Sobel and Prewitt algorithms.

III Comparison of denoising algorithms

The comparative analysis of DST-based image denoising algorithms and algorithms for filtering (enhancing) visual data performed. Also we studied algorithm A as method of extracting information about linear singularities of visual data of ecological monitoring.

Research of algorithms for solving image denoising problem performed for algorithms B, C and D for images from various subject areas (wildfire propagation snapshots, medical imaging, geoecology and geodynamics). Algorithms tested for images with various brightness and contrast, with and without gaussian noise.

Algorithms B and C analyzed with PSNR metrics and estimation of visual quality perception for different images. Estimation of visual quality perception performed by three expert groups, five experts in each group. Grading scale has 10 grades. Algorithms B and C analyzed with PSNR metrics in the image denoising problem.

Conclusion

The results of this study show that:

- Image separation problem can be solved using algorithm C (ShearLab). Estimation of the image separation improving is 5-12% compared to curvelets;
- Edge detection problem can be solved with modified algorithm A (FFST). Modified algorithm is comparable in accuracy to the Sobel and Prewitt algorithms;
- Image denoising problem can be solved using algorithms B, C, D. Algorithm D is the slowest (compared to algorithms B and C). Algorithm B (Shearlet

Toolbox) is more effective than algorithm C for all types of tested images (with different brightness and contrast) by quantitative indicator (22-26%) and by visual quality perception. But algorithm C is 1.7-2.6 times faster than algorithm B depending on the image size. We recommend to use algorithm B for solving image denoising problem.

Bibliography

1. *Guo K., Labate D.* Optimally Sparse Multidimensional Representation using Shearlets // SIAM J Math. Anal. 39 (2007), 298-318.

2. *Guo K., Labate D., W.-Q Lim* Edge analysis and identification using the Continuous Shearlet Transform // Appl. Comput. Harmon. Anal. 27 (2009), 24-46.

3. *Kutyniok G., Labate D.* Construction of regular and irregular shearlet frames // J. Wavelet Theory and Appl. 1 (2007), 1-10.

4. *Kutyniok G., Sauer T.* From wavelets to shearlets and back again // In Approximation theory XII. Proceedings of the 12th international conference, San Antonio, TX, USA, March 4-8, 2007, p. 201-209. - Brentwood, TN: Nashboro Press, 2008.

5. *Kutyniok G., Lemvig J., Lim W.-Q.* Compactly Supported Shearlets // Approximation Theory XIII (San Antonio, TX, 2010). - Springer, 2010.

6. *Kutyniok G., Labate D.* Introduction to shearlets. In Shearlets. Multiscale analysis for multivariate data. - Boston, MA: Birkhauser, 2012, p. 1-38.

7. *Labate D., Lim W.-Q., Kutyniok G., Weiss G.* Sparse multidimensional representation using shearlets // Wavelets XI (San Diego, CA, 2005), 254-262, SPIE Proc. 5914, SPIE. - Bellingham, WA, 2005.

8. *Labate D., Easley G., Lim W.* Sparse directional image representations using the discrete shearlet transform // Applied Computational Harmonic Analysis, 25 (2008), 25-46.

9. *Lim W.-Q.* The discrete shearlet transform: a new directional transform and compactly supported shearlet frames // IEEE Trans. Imag. Proc 19 (2010), 1166-1180.

10. *Lim W., Kutyniok G., Zhuang X.* Digital shearlet transforms. Shearlets: Multiscale Analysis for Multivariate Data, preprint, 2010.

11. *Zhuang X.* University of Osnabrueck. ShearLab A rationally designed digital shearlet transform. - URL: http://shearlab.org.

12. *Hauser S.* Fast finite shearlet transform: a tutorial, preprint University of Kaiserslautern, 2011.

13. *Hauser S.* Fast Finite Shearlet Transform. - URL: http://www.mathematik.uni-kl.de/imagepro/software/ffst/.

14. *Simonov K.V. Kirillova S.V., Cadena L.* Fast shearlet transform algorithms // Abstracts of Lecturers and Young Scientists Second China-Russia Conference "Numerical Algebra with Applications". - Rostov-on-Don: Southern Federal University Publishing, 2013. - P. 122-123.

RESEARCH OF INITIAL BOUNDARY VALUE PROBLEMS WITH MOVING BOUNDARIES

Stolyar A.M.

Southern Federal University, Rostov-on-Don, Russia

Studies of initial boundary value problems with moving and variable boundary have been carried out in different fields. The corresponding models describe the phenomena of melting and solidification, oscillating and diffusion, etc. A brief overview of those problems and methods of their solution is given in monograph [1]. Methods of asymptotic and numerical integration of hyperbolic, parabolic and elliptical equations for Dirichlet, Poisson and Roben problems are developed in [1] as well. The mentioned methods are applied to the problems of longitudinal and transverse oscillations of the rope of variable length [1, 2]. In this paper the methods of numerical and asymptotic integration are applied to the problems which describe the oscillations of visco-elastic rope with a rigid body (see Fig. 1). The modified finite-difference, Runge-Kutta and small parameter methods are used here. The corresponding problem may be written as follows

$$\rho F\left(\frac{\partial^2 u}{\partial t^2}-\frac{d^2\xi}{dt^2}\right)=EF\frac{\partial^2 u}{\partial x^2}+\mu EF\frac{\partial^3 u}{\partial x^2\partial t}-\rho Fg, \tag{1}$$

$$m\frac{d^2\xi}{dt^2}=-EF\frac{\partial u}{\partial x}\bigg|_{x=0}+mg,$$

$$\xi(t)=\ell(t)+u(\ell(t),t),\quad u(x,t)\big|_{x=0}=0,\quad u(x,t)\big|_{x=0}=0,$$

$$u(x,t)\big|_{t=0}=\varphi_1(x),\quad \frac{\partial u(x,t)}{\partial t}\bigg|_{t=0}=\varphi_2(x),$$

$$\ell(t)\big|_{t=0}=\ell_0,\quad \frac{d\ell}{dt}\left[1+\frac{\partial u(\ell,t)}{\partial \ell}\right]=\varepsilon\psi(t).$$

Here $u(x,t)$ is a rope section x displacement at time moment t; ρ, F, E are the parameters of density, sectional area and a Young's modulus for the rope respectively; g is acceleration of gravity; m is mass of a rigid body; $\ell(t)$ is a length of rope at time moment t in the undeformed state; $\xi(t)$ is an actual distance between the run-off point of a rope from the reel and a rigid body. We assume that the rate of unwinding (or winding) of the rope is small relatively to the speed of propagation of the wave in the rope (the actual speed of propagation of the wave can be 4000–5000 m/s). Parameter ε is equal to this relation. The given problem (1) may be reduced to the following one

$$\frac{\partial^2 w}{\partial t^2}+F_1(t)\varepsilon_{\pm}+F_2(t)\varepsilon_{\pm}^2=a^2\left(1+\mu_1\frac{\partial}{\partial t}\right)\frac{\partial^2 w}{\partial x^2}, \tag{2}$$

$$\left.\frac{\partial^2 w}{\partial t^2}\right|_{x=0} + F_1(t)\varepsilon_{\pm} + F_2(t)\varepsilon_{\pm}^2 = \mu_2 \left.\frac{\partial w}{\partial x}\right|_{x=0},$$

$$w\big|_{t=0} = \Phi_1(x), \quad \left.\frac{\partial w}{\partial t}\right|_{t=0} = \Phi_2(x), \quad w\big|_{x=\ell(t)} = 0.$$

Here $w(x,t)$ is a new unknown function F_1, F_2, Φ_1, Φ_2 — are the known functions. Asymptotic solution of the problem (2) has been built as the series

$$w(x,t) = \sum_{k=0}^{\infty} w_k(x,t)\varepsilon_{\pm}^k.$$

The solution of the given problem on the changeable domain $[0, \ell(t)]$ has been reduced to the solution of initial boundary value problems on the constant domain $[0, \ell_0]$.

For the sake of numerical integration we need to use the moving grid in order to apply the finite-difference and Runge-Kutta methods (See Fig. 2). This grid was firstly proposed by Dr. I. M. Bermous in [3].

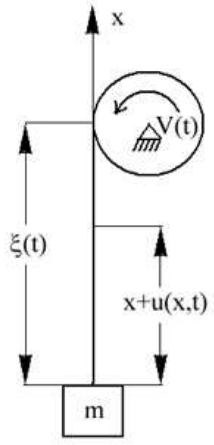

Figure 1. The model of a rope with rigid body

One may see the comparison of results of numerical and asymptotic integration on the Fig. 3 in the case of elastic rope's winding. The given curves describe the deformation of the highest section of the rope in dependence of time.

The problem of finite-difference algorithm convergence has been considered in the paper in the case of the constant boundary.

Acknowledgements: 1. The author is very much obliged to Pinchuck N. A. who made all the computations used here. 2. This work was substantially funded by grant No. 14.A18.21.0356 of Russian federal scientific program.

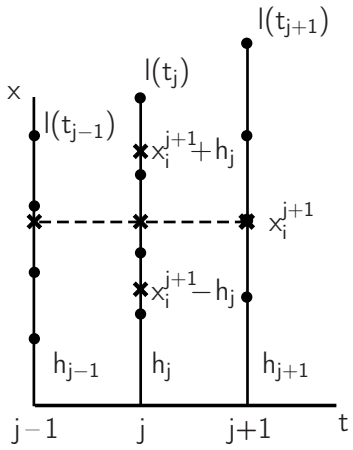

Figure 2. The moving grid of finite-difference method

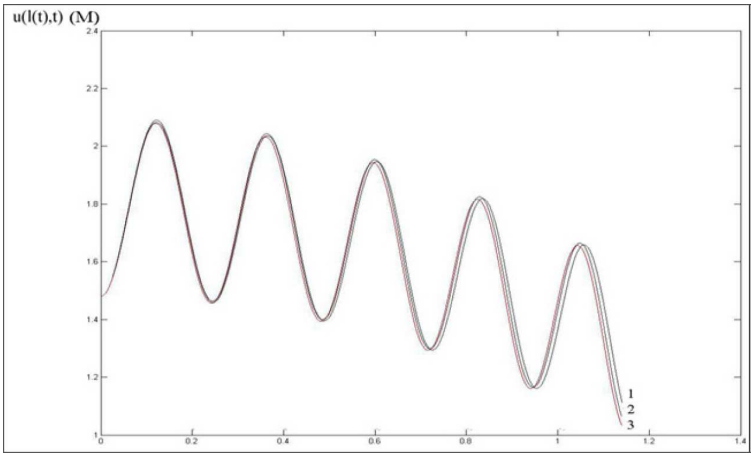

Figure 3. Comparison of numerical and asymptotic integration

Bibliography

1. *Stolyar A.* Mathematical physics problems with moving and variable boundaries. — Saarbrücken: LAP Lambert Academic Publishing, 2013. 60 p. (Russian).

2. *Stolyar A.M.* Integration of initial boundary value problems with free and moving boundaries // Science and world. 2014. No. 8 (12). P. 26–29.

3. *Bermous I.M.* Longitudinal oscillations of cargo on a rope of variable length // Reports of extended sessions of a seminar on Applied Mathematics. Tbilisi, 1989. Vol. 4, No. 3. P. 29–32 (Russian).

Posters

GPGPU TECHNOLOGIES FOR GENETIC ALGORITHMS

Agibalov O.I.

Southern Federal University, Rostov-on-Don, Russia

Genetic algorithms today is the perspective type of methods for mathematical optimization. Based on the Darwin's theory of evolution, they perform operations on dozens of so-called "chromosomes", each encoding appropriate solution of the problem as a set of "genes" – parameters of the purpose function [1]. Convenient genetic algorithm may operate hundreds and thousands of chromosomes, that are indepenedent from each other and thus may be computed concurently. The most efficient way for accelerating programs is using parallel technologies, such as GPGPU (General-Purpose graphics processing units). It means that the hardware which traditionally were applied for rendering computer graphics, today are suitable for non-graphical computations. Apparent advantage of GPUs is their massive parallel architecture. GPUs contain up to several thousand cores that work independently concurently. This is why GPGPU is the perfect technology for computing independent chromosomes [2].

The first model of parallel GA was proposed many years ago and was called "Island Model". All the chromosomes were splitted into several "islands" that evolved and exchanged their best individuals with other islands. Another parallel model of GA is suggested in this research. Using GPGPU we are able to operate each chromosome in independent thread. But before doing this, we have decided to redevelop our previous GA and make it faster. First af all we have changed coding system - decimal values were used instead of binaries. In couple with other cosmetic changes we have reached eleven times speeding up even without parallelization. Furthermore, alterings in coding system have allowed us to reduce the ammount of data transferred between CPU and GPU [3].

Working with GAs on GPGPU our goal was to study possibilities and restraints of new hardware. Acceleration of GPU-algorithm in comparrison with CPU-algorithm is about 30 percents – 165 ms against 211.

Figure 1 shows us comparison of total performing time for CPU ang GPU algorithms and the time of initialization. Thus we can see that GPU-environment requires 96 ms of 165 to be initialized. For CPU-algorithm this time will only be 5 ms of 211. Considering that 96 ms we have discovered that 93 percent of them is behind the initialization of GPU libraries. It means that we cannot optimize this time interval.

Using these and other results we may show when the use of GPU for accelerating GA is reasonable.

Thus it is possible to say that for little sets of chromosomes the use of GPGPU is unefficient. But as the chromosome number increases as GPU becomes more and more preferable. Only the huge number of individuals allows GPU-algorithm to overcome initialization delay and and ahead fast, but serial CPU.

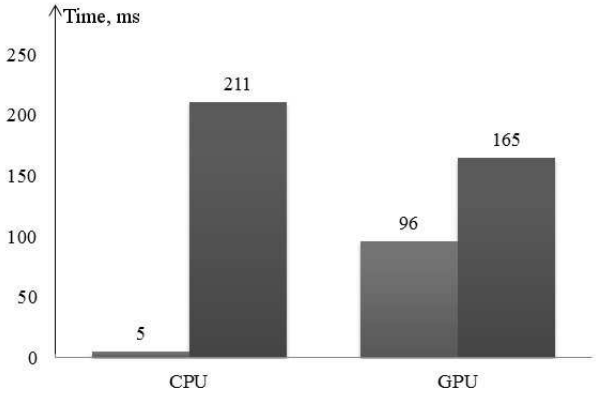

Figure 1. Total performing time and initialization time for CPU and GPU algorithms

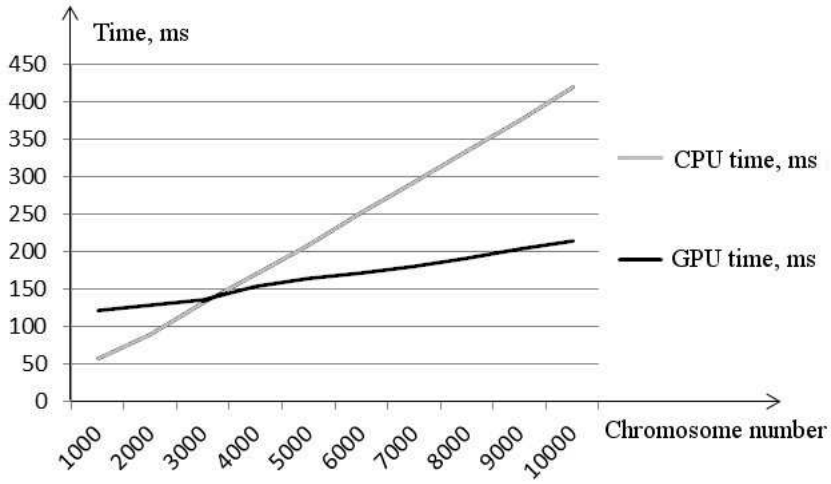

Figure 2. The performance of GPU-algorithm and CPU-algorithm in solving the test problem

Bibliography

1. *Panchenko T.* Genetic algorithms. University of Astrakhan, 2007. 87 p.

2. *Agibalov O., Zolotarev A.* Decimal way of coding values in genetic algorithm // In the proceeding of the 2014 scientific-practical conference "Modern information technologies: trends and perspectives of development", P. 31-33.

3. *Boreskov A.* Parallel computations on CUDA. Architecture and programming model of CUDA. Moscow State University, 2012. 336 p.

PROPAGATION OF LONG PULSE WAVES IN AORTA

Batishchev V.A., Getman V.A., Safronenko O.I.
Southern Federal University, Rostov-on-Don, Russia

Long waves in a fluid which fills a cylindrical tube with elastic border have been studied by many authors since the end of the nineteenth century [1, 2]. An important contribution to the study of the theoretical aspect was made by the Russian physicist I.S. Gromeka [2]. Literature review on this subject is provided in a well - known monograph by T. Pedley "Hydrodynamics of large blood vessels" (1983) [1]. The calculated phase velocity of the waves in a liquid in an elastic tube is well proved experimentally. Prof. Ustinov Yu.A. was the first to investigate long helical waves in a blood vessel with the anisotropy of walls [3, 4]. Great difficulties arise when calculating short spiral waves in elastic tubes [5]. When doing the asymptotic research of these short waves, one needs to calculate the oscillating boundary layers which are formed on the vessels walls. Note that the researchers named above did not use the method of a boundary layer. The results of asymptotic and numerical calculations of long longitudinal and spiral waves with the use of boundary layer are provided. Compared to the prominent investigations, the experimental case is considered when the pressure in an input cross-section of a vessel is given, taking into account the time parameter in a non-symmetrical way.

Long longitudinal and spiral waves were calculated on the basis of the Navier-Stokes's system and the dynamic equations of a thin elastic isotropic membrane, taking into consideration infinitesimality of a viscosity coefficient. The aorta is modelled as a cylinder that is limited by a thin membrane. Some small parameters arise upon transition to dimensionless variables. The parameter connected with viscosity is proportional to the thickness of the boundary layer arising by the wall. The second small parameter is inversely proportional to the phase speed of the Mouensa-Kortevega wave. A well-known method to calculate long waves with the use of a slow axial coordinate is applied. Asymptotic expansions are presented in the form of a series based on the degrees of the second-order small parameter. In the main approach there is a linear problem which serves the basis to calculate the long waves propagating in the steady flow. The velocity vector of this flow has only one nonzero component (Poiseuille's parabola), directed along the cylinder axis. The solution of the problem consists of the sum of functions of two types. The first type of the functions in the main approach describes an ideal flow. The second type of the functions describes boundary layers on vessel walls. Note that boundary layers in large blood vessels are observed by surgeons when performing operations on heart and vessels.

It is shown that in a flow core (out of the boundary layer) longitudinal component of velocity of long waves is constant in its cross-section. This phenomenon is experimentally observed. In the case of ideal fluid the phase velocity of waves is determined. Two waves - the wave of pressure and the quasilongitudinal wave are obtained. It is shown that only the pressure wave is of paramount significance in

the out of the boundary layer case. The amplitudes of both waves, however, have an identical order inside the boundary layer. Damping decrement is obtained while calculating the functions of a boundary layer. To define the amplitude of long waves the pressure at the entrance of a vessel taken as a time function is determined. This function doesn't possess the property of symmetry on time. Numerical calculations of a wave form and pressure depending on time, both in a systole and axial coordinate, have been carried out.

It is shown that amplitude longitudinal velocity component at the beginning of a systole grows in time, reaches a maximum, and further on, in the second half of a systole, decreases to zero. At the end of a systole there is a inverse flow zone, this zone being localized in a boundary layer. The speed of a countercurrent tends to zero when it leaves the boundary layer, and approaches a vascular wall.

Bibliography

1. *Pedley T.* Hydrodynamics of large blood vessels. - Academic Press, 1983. 400 p.

2. *Gromeka I.S.* The velocity of spread of the wave-like movement of fluids in elastic tubes - Collected Works. Izd. USSR Academy of Sciences, 1952. p.172-183

3. *Ustinov Y.A.* Model of helical pulse motion of blood in the arterial vessels // DAN. 2004. T. 398. № 3. Pp. 71-76

4. *Bogachenko S.E., Ustinov Y.A.* Model of blood flow in the arteries during systole and analysis of the stress state of the wall with the helical anisotropy // Russian Journal of Biomechanics. 2009. T. 13. № 1. Pp. 29-42

5. *5. Orlovsky P.I., Gritsenko V.V, Uglov F.G., etc.* Whether to take account of the swirling flow of blood in the left ventricle and aorta in the design of artificial valves? // Journal of Surgery. 1998. T.157. № 1. P.10-16 71-76

NUMERICAL METHODS OF MULTI-CRITERIA REGULATION ALTERNATIVES TO SELECT FINANCIAL INSTRUMENTS

Bodrova Y.S., Mermelshtein G.G.

Institute for Mathematics, Mechanics, and Computer Science in the name of I.I. Vorovich, SFEDU, Rostov-on-Don.

The problem under consideration: The goal is to select the bank for deposit. The problem has three criteria f_1, f_2 and f_3. Where, f_1 – criterion that determines the increase of equity capital of the bank for the year. The second criterion is f_2 – criterion that determines interest rates on deposits. The last criterion is f_3 – criterion determining the rating of the bank. There are three choices: SberBank, Center-Invest Bank, Stella Bank respectively x_1, x_2 and x_3.

	$\mathbf{f}_1$	$\mathbf{f}_2$	$\mathbf{f}_3$
$\mathbf{x}^1$	13,200	6,400	67 006,000
$\mathbf{x}^2$	12,200	8,250	92 060,000
$\mathbf{x}^3$	10,400	8,500	84 311,000

The method assumes the following steps:

1. the creation of a hierarchical structure of the original problem with multiple levels;

2. setting priorities (coefficients of the importance or the weight) criteria for the choice of the set goal;

3. evaluation (based on these estimates) values priority for the lower level criteria regarding the purpose of the upper level;

4. evaluation of priorities of alternatives for each of the lower level criteria with the help of quantitative paired comparisons;

5. aggregation of all of the estimates obtained in the integral priorities – evaluate alternatives regarding the purpose;

6. selecting the alternative having the highest priority, as the best, or the ranking the alternatives by the preference according to the calculated priorities;

7. analysis sustainability of the solution obtained.

The method used to select the financial instruments: to the determination of the bank for the deposit, to the forming of a package of shares, to the buying a package of bonds.

The first step is the construction of the hierarchical structure of the original problem with a few levels. The using of the hierarchical structure is very productive because it allows presenting the original problem with a large number of criteria, which as a single whole is too complex to analyze, as a system of interconnected significantly simpler "subtasks" with a small number of criteria [3]. The most often used structure has the next form: the upper level – the purpose, the intermediate levels – the criteria, the lower level – the options [1].

The next step is to determine the weights for criteria and alternatives. The matrix of pairwise comparisons is compiled for to determine of the weights of criteria and alternatives by using numerical methods. Two criteria or two alternatives are compared and the degree of excellence in the "power" (importance or preference) of one of the criteria or alternatives over the other is evaluated for each paired comparison [4]. The filled matrices are inversely symmetrical with positive elements. Various numerical comparison methods are used, and the results obtained are analyzed.

The next step is the calculation of the vector s of the local priorities by using method of principal characteristic vector from equation $As = \lambda_{max} * s$, and $\|s\| = 1$, where λ_{max} – greatest characteristic value [1]. The values of the characteristic vector are evaluated by using numerical method. This method is allows to determine the approximate assessments by using the geometric mean of the matrix elements of the rows. Then, the values obtained are normalized for the convenience of further calculations. The eigenvalue λ_{max} is calculated by the same numerical method.

To find the approximate value λ_{max} necessary:

1. Find the sum of each of the columns of the matrix of pairwise comparisons $\sum_{i=1}^{n} a_{ij}$.

2. Multiply the values obtained $\sum_{i=1}^{n} a_{ij}$ on the values of the normalized characteristic vector: the first sum is multiplied by the first value, the second – the second, etc.

3. Sum the results obtained. The result of the calculation will be the approximate maximum eigenvalue λ_{max} of the matrix of pairwise comparisons.

An indicator of the consistency of the estimates is a super-transitive matrix of the pairwise comparisons A. An indicator of the consistency of obtained estimates is a highly-transitive of the matrix of the pairwise comparisons A. Therefore, if the matrix of the pairwise comparisons is not super-transitive, then is required to assess the degree of the consistency of the matrix elements, or the consistency of the matrix A. The method for the evaluating the degree of consistency is given in [3] [5]. If the consistency is high, then you can proceed to the calculation of the priorities. Otherwise, you must to correct the results of pairwise comparisons.

Integral priorities (regarding the purpose) $v(x)$ of alternatives x are calculated by using an additive function of the value: $v\,(x) = \sum_{i=1}^{m} w_i * v_i(x)$, where m – number of criteria, w_i – priorities (weight) of these criteria, $v_i\ (x)$ – priorities of the alternative to these criteria [2]. The best alternative is the alternative with the highest integral priority.

Checked the execution of the axioms of regularizing by the addition and removal of wittingly worst alternative. Is carried out numerically experiments and sensitivity analysis, with the help of minor changes to the values of criteria weights to trace the impact of these changes on the result of regularizing. If the ranking of the alternatives is saved, the results can be considered stable.

We apply the described method on the our task.

- the creation of a hierarchical structure of the original problem with multiple levels;

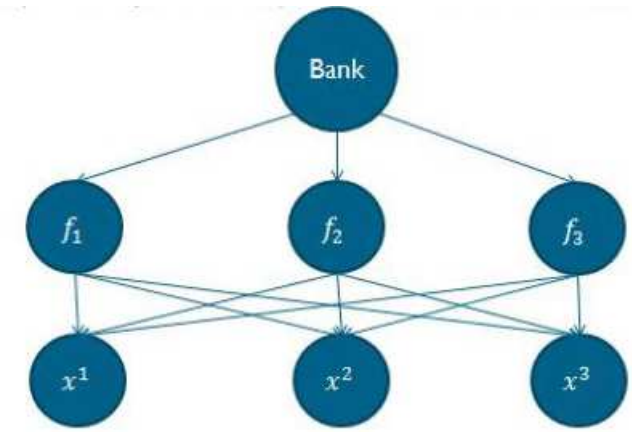

- setting priorities (coefficients of the importance or the weight) criteria for the choice of the set goal;

Bank	$\mathbf{f}_1$	$\mathbf{f}_2$	$\mathbf{f}_3$	
f^1	1,000	1,000	1,000	**0,333**
f^2	1,000	1,000	1,000	**0,333**
f^3	1,000	1,000	1,000	**0,333**

- evaluation of priorities of alternatives for each of the lower level criteria with the help of quantitative paired comparisons;

$\mathbf{f}_1$	x^1	x^2	x^3
x^1	1,000	4,000	9,000
x^2	0,250	1,000	6,000
x^3	0,111	0,167	1,000

$\mathbf{f}_2$	x^1	x^2	x^3
x^1	1,000	0,125	0,111
x^2	8,000	1,000	0,500
x^3	9,000	2,000	1,000

$\mathbf{f}_3$	x^1	x^2	x^3
x^1	1,000	0,11	0,143
x^2	9,000	1,000	3,000
x^3	7,000	0,333	1,000

- aggregation of all of the estimates obtained in the integral priorities - evaluate alternatives regarding the purpose;

V	$\mathbf{f}_1$	$\mathbf{f}_2$	$\mathbf{f}_3$	
Criteria	0,333	0,333	0,333	
$\mathbf{x}^1$	0,540	0,143	0,143	**0,275**
$\mathbf{x}^2$	0,297	0,429	0,429	**0,385**
$\mathbf{x}^3$	0,163	0,429	0,429	**0,340**

- selecting the alternative having the highest priority, as the best, or the ranking the alternatives by the preference according to the calculated priorities;

1.	x^2 - Center-Invest Bank	0.385
2.	x^3 - Stella Bank	0.340
3.	x^1 - SberBank	0.275

- sustainability analysis of the solution obtained.

Adding knowingly worst alternative x^4:

	$\mathbf{f_1}$	$\mathbf{f_2}$	$\mathbf{f_3}$
$\mathbf{x^4}$	10%	6%	60 000

T	f_1	f_2	f_3	
Criteria	0,333	0,333	0,333	
$\mathbf{x}^1$	0,588	0,067	0,073	**0,243**
$\mathbf{x}^2$	0,297	0,437	0,594	**0,443**
$\boldsymbol{x}^3$	0,069	0,452	0,286	**0,269**
$\boldsymbol{x}^4$	0,046	0,043	0,046	**0,045**

1.	x^2 - Center-Invest Bank	0.443
2.	x^3 - Stella Bank	0.269
3.	x^1 - SberBank	0.243
4.	x^4	0.045

Adding the worst alternative x^4 on two criteria:

	$\mathbf{f_1}$	$\mathbf{f_2}$	$\mathbf{f_3}$
$\mathbf{x^4}$	11%	6%	60 000

T	$\mathbf{f}_1$	$\mathbf{f}_2$	$\mathbf{f}_3$	
Criteria	0,333	0,333	0,333	
$\mathbf{x}^1$	0,634	0,067	0,073	**0,258**
$\mathbf{x}^2$	0,241	0,437	0,594	**0,424**
$\boldsymbol{x}^3$	0,048	0,452	0,286	**0,262**
$\boldsymbol{x}^4$	0,077	0,043	0,046	**0,056**

1.	x^2 - Center-Invest Bank	0.424
2.	x^3 - Stella Bank	0.262
3.	x^1 - SberBank	0.258
4.	x^4	0.056

Adding the worst alternative x^4 on one criterion:

	$\mathbf{f_1}$	$\mathbf{f_2}$	$\mathbf{f_3}$
$\mathbf{x^4}$	11%	7%	60 000

T	$\mathbf{f_1}$	$\mathbf{f_2}$	$\mathbf{f_3}$	
Criteria	0,333	0,333	0,333	
$\mathbf{x^1}$	0,634	0,041	0,073	**0,25**
$\mathbf{x^2}$	0,241	0,349	0,594	**0,395**
$\boldsymbol{x^3}$	0,048	0,528	0,286	**0,287**
$\boldsymbol{x^4}$	0,077	0,082	0,046	**0,068**

1.	x^2 - Center-Invest Bank	0.395
2.	x^3 - Stella Bank	0.287
3.	x^1 - SberBank	0.25
4.	x^4	0.068

The numerical experiment shows the opportunity to use this method to select financial instruments. It satisfies the axiom of the choice and streamlining of the objects under consideration. The values of the criteria that characterize the objects selected from the developed databases that are updated with the help of Internet resources.

Bibliography

1. *Saaty T.L.* The analytic hierarchy process. - N.-Y .: McGraw Hill, 1980.
2. *Saaty R.W.* The analytic hierarchy process: what is it and how it is used // Mathematical modeling. - 1987. - Vol. 9. - P. 161-176.
3. *Podinovskaya O.V.* Analytic hierarchy as a method of multi-criteria decision support solutions // IT modeling and management. - 2010. – 1. – P. 71-80.
4. *Podinovskii V.V.* Multicriteria problem with homogeneous criteria equivalent // Computational Mathematics and Mathematical Physics. - 1975. – 2. – P. 330-344.
5. Development and adopt decisions in the management of innovation tutorial. / Tukkel I.L., Yashin S.N., Koshelev E.V., etc. - BHV-Petersburg, 2011 – 352 p.

OSCILLATORY CONVECTION IN A HORIZONTAL LAYER OF A BINARY MIXTURE

Denisenko V.V., Morshneva I.V.
Southern Federal University, Rostov-on-Don, Russia

The present work investigates the onset of convection in an infinite horizontal layer of a binary fluid mixture consisting of two non-reacting components. We suppose that the boundaries are rigid, isothermal and impermeable, with slip allowed. A constant temperature and concentration distribution is specified on the boundaries. In the model under consideration the effects of thermal diffusion and diffusive heat conductivity are neglected. Let in addition assume that the layer, as a whole, undergoes no displacement in the horizontal plane. The convective flow of the binary mixture is governed by the Navier-Stokes equations under Oberbeck-Boussinesq approximation ([1]):

$$\begin{aligned}
&\frac{\partial \boldsymbol{v}}{\partial t} + \boldsymbol{v}\cdot\nabla\boldsymbol{v} = -\nabla p + \Delta\boldsymbol{v} + (\widetilde{\mathrm{Gr}}T - \widetilde{\mathrm{Gr}_\mathrm{s}}S)\boldsymbol{k},\\
&\frac{\partial T}{\partial t} + \boldsymbol{v}\cdot\nabla T = \mathrm{Pr}^{-1}\Delta T,\\
&\frac{\partial S}{\partial t} + \boldsymbol{v}\cdot\nabla S = {\mathrm{Pr}_\mathrm{d}}^{-1}\Delta S,\\
&\mathrm{div}\boldsymbol{v} = 0.
\end{aligned} \tag{1}$$

The corresponding boundary conditions are:

$$\begin{aligned}
&\left.\frac{\partial v_1}{\partial x_3}\right|_{\substack{x_3=1\\x_3=0}} = \left.\frac{\partial v_2}{\partial x_3}\right|_{\substack{x_3=1\\x_3=0}} = \left. v_3\right|_{\substack{x_3=1\\x_3=0}} = 0,\\
&T\big|_{x_3=1} = \tau_1, \quad T\big|_{x_3=0} = \tau_0,\\
&S\big|_{x_3=1} = \sigma_1, \quad S\big|_{x_3=0} = \sigma_0,
\end{aligned} \tag{2}$$

where $\boldsymbol{v} = \boldsymbol{v}(x_1, x_2, x_3, t)$ is the velocity field, $T = T(x_1, x_2, x_3, t)$ is the temperature field, $S = S(x_1, x_2, x_3, t)$ is the concentration field of the heavier component of the mixture, $p = p(x_1, x_2, x_3, t)$ is the pressure field, $\boldsymbol{k} = (0, 0, -1)^T$ is the down-directed vertical vector.

The problem (1) contains four dimensionless parameters: $\mathrm{Pr} = \dfrac{\nu}{\chi}$ is the Prandtl number, $\mathrm{Pr_d} = \dfrac{\nu}{D}$ is the diffusion Prandtl number (the Schmidt number), $\widetilde{\mathrm{Gr}} = \dfrac{g\beta h^4 Q}{\varkappa\nu^2}$ is the Grashof number, $\widetilde{\mathrm{Gr_s}} = \dfrac{g\beta_s h^3 \bar{S}}{\nu^2}$ is the Grashof number for mass transfer, where ν is the kinematic viscosity coefficient, χ is the thermal diffusivity, D is the mass diffusivity, g is acceleration due to gravity, β is

the thermal expansion coefficient, β_s is the concentration expansion coefficient, $\varkappa$ is the thermal conductivity coefficient, Q is the heat flux, $\bar{S}$ is the mean concentration of the heavier component of the mixture.

The problem (1) with boundary conditions (2) has the following stationary solution corresponding to the state of rest, which we would call in the following the basic solution

$$\begin{aligned} &\boldsymbol{v}_0 = 0, \\ &T_0(x_3) = a_1 x_3 + a_0, \\ &S_0(x_3) = b_1 x_3 + b_0, \\ &p_0(x_3) = \frac{1}{2}(\widetilde{\mathrm{Gr}} a_1 - \widetilde{\mathrm{Gr_s}} b_1) x_3^2 + (\widetilde{\mathrm{Gr}} a_0 - \widetilde{\mathrm{Gr_s}} b_0) x_3 + \mathrm{const}, \end{aligned} \tag{3}$$

where $a_1 = \tau_1 - \tau_0, \quad a_0 = \tau_0, \quad b_1 = \sigma_1 - \sigma_0, \quad b_0 = \sigma_0$.

This research is devoted to the study of branching and stability of time-periodic flow modes arising from oscillatory stability loss of the basic regime relatively to spatial perturbations. These perturbations are assumed to be $2\pi/\alpha_1$–periodic in x_1 and $2\pi/\alpha_2$–periodic in x_2. We seek another solution of the problem (1) with boundary conditions (2) in the form

$$\check{\boldsymbol{v}} = \boldsymbol{v}_0 + \boldsymbol{v}, \quad \check{T} = T_0 - a_1 T, \quad \check{S} = S_0 - b_1 T, \quad \check{p} = p_0 + p, \tag{4}$$

Inserting (4) into (1)–(2), we obtain the following system for the perturbations $\boldsymbol{v}$, T, S, p:

$$\begin{aligned} &\frac{\partial \boldsymbol{v}}{\partial t} + \boldsymbol{v} \cdot \nabla \boldsymbol{v} = -\nabla p + \Delta \boldsymbol{v} + (\mathrm{Gr}\, T - \mathrm{Gr_s}\, S)\boldsymbol{k}, \\ &\frac{\partial T}{\partial t} - v_3 + \boldsymbol{v} \cdot \nabla T = \mathrm{Pr}^{-1} \Delta T, \\ &\frac{\partial S}{\partial t} - v_3 + \boldsymbol{v} \cdot \nabla S = {\mathrm{Pr_d}}^{-1} \Delta S, \\ &\mathrm{div}\boldsymbol{v} = 0, \end{aligned} \tag{5}$$

where $\mathrm{Gr} = -a_1 \widetilde{\mathrm{Gr}}$, $\mathrm{Gr_s} = -b_1 \widetilde{\mathrm{Gr_s}}$, with corresponding boundary conditions

$$\left.\frac{\partial v_1}{\partial x_3}\right|_{\substack{x_3=1 \\ x_3=0}} = \left.\frac{\partial v_2}{\partial x_3}\right|_{\substack{x_3=1 \\ x_3=0}} = \left. v_3 \right|_{\substack{x_3=1 \\ x_3=0}} = \left. T \right|_{\substack{x_3=1 \\ x_3=0}} = \left. S \right|_{\substack{x_3=1 \\ x_3=0}} = 0. \tag{6}$$

The parameter Gr can be written in the form $\mathrm{Gr} = \mathrm{Gr}_* + \delta$, where Gr_* denotes the critical value of the Grashof number, when for $\mathrm{Gr} = \mathrm{Gr}_*$ the stability spectrum contains a pair of purely imaginary eigenvalues $\pm i\omega_0$ $(\omega_0 \neq 0)$. Thus the problem (5) with boundary conditions (6) may be rewritten in the following equivalent form

$$\frac{d}{dt}\mathrm{M}\boldsymbol{u} + \mathrm{A}\boldsymbol{u} = \delta \mathrm{B}\boldsymbol{u} + \mathrm{K}(\boldsymbol{u}, \boldsymbol{u}), \tag{7}$$

where

$$\boldsymbol{u} = (\boldsymbol{v},\, T,\, S)^T \in \mathrm{H}, \tag{8}$$

H is the closure of a set of smooth solenoidal vectors, vanishing at the layer boundary, in the metric

$$\big(\boldsymbol{u_1} \cdot \boldsymbol{u_2}\big)_{\mathrm{H}} = \int\limits_{\Omega} \boldsymbol{u_1} \cdot \boldsymbol{u_2^*}\, d\Omega, \tag{9}$$

$$\Omega = \Big\{(x_1,\, x_2,\, x_3) \in \mathbb{R} :\ 0 \leqslant x_1 \leqslant \frac{2\pi}{\alpha_1},\ 0 \leqslant x_2 \leqslant \frac{2\pi}{\alpha_2},\ 0 \leqslant x_3 \leqslant 1 \Big\}, \tag{10}$$

A, B, M — linear operators, K — bilinear operator.

The onset of auto-oscillations at transition of the Grashof number through its critical value is investigated. The auto-oscillations is analyzed by the use of the Liapunov-Schmidt method suggested by V. I. Yudovich [2], [3].

Substituting $\tau = \omega t$ in (5), where ω is unknown cyclic frequency, we obtain

$$\omega \frac{d}{d\tau} \mathrm{M}\boldsymbol{u} + \mathrm{A}\boldsymbol{u} = \delta \mathrm{B}\boldsymbol{u} + \mathrm{K}(\boldsymbol{u}, \boldsymbol{u}), \tag{11}$$

We seek a solution of (11) in the form of series in powers of the parameter $\varepsilon = s\sqrt{|\mathrm{Gr} - \mathrm{Gr}_*|}$, $(s = \mathrm{sign}\delta)$

$$\boldsymbol{u} = \varepsilon \boldsymbol{u}_1 + \varepsilon^2 \boldsymbol{u}_2 + \varepsilon^3 \boldsymbol{u}_3 + \ldots, \quad \omega = \omega_0 + \varepsilon\omega_1 + \varepsilon^2\omega_2 + \ldots \tag{12}$$

Inserting these series into (11) and equating the coefficients of like powers of ε in both parts of the equation, we arrive at the sequence of equations for the unknown 2π–periodic functions $\boldsymbol{u}_k$, and numbers ω_k. Solving these equations one after other, we will obtain

$$\boldsymbol{u}_1 = \gamma_1(\boldsymbol{\varphi} e^{i\tau} + \boldsymbol{\varphi}^* e^{-i\tau}),\ \ \omega_1 = 0, \tag{13}$$

where φ is the eigenfunction of the following problem

$$(\mathrm{A} + i\omega_0 \mathrm{M})\boldsymbol{\varphi} = 0; \tag{14}$$

$$\boldsymbol{u}_2 = \gamma_2(\boldsymbol{\varphi} e^{i\tau} + \boldsymbol{\varphi}^* e^{-i\tau}) + \gamma_1^2(\boldsymbol{\psi} e^{2i\tau} + \boldsymbol{\psi}^* e^{-2i\tau} + \boldsymbol{\theta}), \tag{15}$$

where $\boldsymbol{\psi}$ and $\boldsymbol{\theta}$ are the solutions of the following problems

$$(\mathrm{A} + 2i\omega_0 \mathrm{M})\boldsymbol{\psi} = \mathrm{K}(\boldsymbol{\varphi}, \boldsymbol{\varphi}), \tag{16}$$

$$\mathrm{A}\boldsymbol{\theta} = \mathrm{K}^{\circ}(\boldsymbol{\varphi}, \boldsymbol{\varphi}^*). \tag{17}$$

The condition of solvability of the equation, which can be found by equating the coefficients of ε^3 in both parts of the equation (11), yields γ_1^2 and ω_2

$$\gamma_1^2 = s\Gamma_1 = -s\frac{\mathrm{Re}(\mathrm{B}\boldsymbol{\varphi}\cdot\boldsymbol{\Phi})}{\mathrm{Re}\Big(\Big(\mathrm{K}^\circ(\boldsymbol{\varphi},\boldsymbol{\theta})+\mathrm{K}^\circ(\boldsymbol{\varphi}^*,\boldsymbol{\psi})\Big)\cdot\boldsymbol{\Phi}\Big)}, \tag{18}$$

$$\omega_2 = \frac{s\,\mathrm{Im}(\mathrm{B}\boldsymbol{\varphi}\cdot\boldsymbol{\Phi})+\gamma_1^2\mathrm{Im}\Big(\Big(\mathrm{K}^\circ(\boldsymbol{\varphi},\boldsymbol{\theta})+\mathrm{K}^\circ(\boldsymbol{\varphi}^*,\boldsymbol{\psi})\Big)\cdot\boldsymbol{\Phi}\Big)}{\mathrm{M}\boldsymbol{\varphi}\cdot\boldsymbol{\Phi}}, \tag{19}$$

where $\mathrm{K}^\circ(\boldsymbol{u}_1,\boldsymbol{u}_2)=\mathrm{K}(\boldsymbol{u}_1,\boldsymbol{u}_2)+\mathrm{K}(\boldsymbol{u}_2,\boldsymbol{u}_1)$, and $\boldsymbol{\Phi}$ is the eigenfunction of the conjugate problem

$$(\mathrm{A}^*-i\omega_0\mathrm{M})\boldsymbol{\Phi}=0. \tag{20}$$

The type of bifurcation is depends on the sign of Γ_1: in the case for $\Gamma_1>0$ there is a supercritical bifurcation, in the case for $\Gamma_1<0$ there is a subcritical bifurcation. The results, obtained numerically at differen values of parameters, show that both types of bifurcation are realized.

The condition of solvability of the equation, which can be found by equating the coefficients of ε^4 in both parts of the equation (11), yields $\gamma_2=\omega_3=0$.

Hereby, first two terms of series (12) are found, and the solution can be written in following form

$$\boldsymbol{u}=\gamma_1(\boldsymbol{\varphi}e^{i\tau}+\boldsymbol{\varphi}^*e^{-i\tau})\varepsilon+\gamma_1^2(\boldsymbol{\psi}e^{2i\tau}+\boldsymbol{\psi}^*e^{-2i\tau}+\boldsymbol{\theta})\varepsilon^2+O(\varepsilon^3), \tag{21}$$

$$\omega=\omega_0+\omega_2\varepsilon^2+O(\varepsilon^4),\quad \varepsilon\to 0. \tag{22}$$

Bibliography

1. *Gershuni G. Z., Zhukhovitskii E. M.* Convective Stability of Incompressible Fluid. Moscow, Nauka, 1972.

2. *Yudovich V.I.* The onset of self-oscillations in a fluid // PMM 1971. Vol. 35. N 4. P. 638–655.

3. *Yudovich V.I.* Investigation of auto-oscillations of a continuous medium, occurring at loss of stability of a stationary mode // PMM 1972. Vol. 36. N 3. P. 450–459.

EVALUATION PROBLEM FOR GENERAL HIDDEN SEMI-MARKOV ERROR SOURCE MODEL

Deundyak V.M.*, Zhdanova M.A.**

* *Southern Federal University, Rostov-on-Don, Russia*

** *Southern Federal University, FSSO "SRI "Spetsvuzavtomatika", Rostov-on-Don, Russia*

1. Introduction. Mathematical modeling of error sources is one of the main problems appearing when simulating digital communication channels. Channel simulation provides a way to analyze error-correcting capability of codes against different types of errors. The main aim of such an analysis is to select the appropriate error-correcting codec for particular channel. To carry out the simulation experiments one needs to find an adequate representation of jamming environment in the channel by means of mathematical error source model, i.e. to solve the inverse problem. The class of hidden semi-Markov models (HSMMs) seems convenient for describing error sources [1]. These models are able to simulate different types of jamming environment and inverse problems can be solved for them.

Let us consider a nonbinary digital data transmission channel C that is supposed to be symmetric, stationary and perfectly synchronized. Channel C can stay in one of N physical states during some period of time and then changes the state. The probability distribution of possible durations is specified a'priori for each state particularly and is never changed. Each channel state emits additive error sequences according to its own probability distribution.

In the paper we consider a general hidden semi-Markov error source model for the channel described above. For this model we provide a solution of classical evaluation problem in case of error sequences long enough. The problem we refer to as "evaluation problem" is to calculate the probability of the fact that the observed error sequence is generated by the given general semi-Markov error source model. The suggested solution is based on forward algorithm proposed by Yu [2].

2. General hidden semi-Markov model. According to [2] general hidden semi-Markov model (GHSMM) is the set

$$\lambda = \{\mathcal{S}, \mathcal{D}, A, \Pi, V, B\},$$

where $\mathcal{S} = \{1, .., N\}$ – the set of states; $\mathcal{D} = \{1, .., D\}$ – the set of possible durations; $A = \{a_{(i,d)(i',d')}\}_{(i,d),(i',d')\in\mathcal{S}\times\mathcal{D}}$ – the transition matrix for generalized states from $\mathcal{S}\times\mathcal{D}$ and $a_{(i,d)(i',d')} = 0$; $\Pi = \{\pi_{i,d}\}_{(i,d)\in\mathcal{S}\times\mathcal{D}}$ – the set of initial probabilities of generalized states; $V = \{v_1, .., v_M\}$ – the output alphabet; $B = \{b_{i,d}(\hat{o}_1, .., \hat{o}_d)\}_{(i,d)\in\mathcal{S}\times\mathcal{D},(\hat{o}_1,..,\hat{o}_d)\in V^d}$ – the set of emission probabilities.

Note that the model from [2] assumes zero self-transition probabilities $a_{(i,d)(i',d')} = 0$. However, this requirement is not important for solving evaluation problem. Thus, we consider the extended model allowing self-transitions. Moreover, we suppose that $\pi_{i,d}$ are marginal probabilities of transition matrix.

GSMM generalizes such well-known models as explicit duration hidden Markov model [1], variable duration hidden Markov model [3], segment hidden Markov models [4].

3. Evaluation problem. Let λ be a GSMM and $O_{1:T}$ be a sequence over the alphabet V. In this section we consider evaluation problem for GSMM, i.e. the problem to calculate the probability if the fact that $O_{1:T}$ is generated by λ.

In [2] Yu proposes the solution of this problem under the following assumptions:

1) the first observed state starts at $t = 1$ or before it,

2) the last observed state ends exactly at $t = T$.

Notice that 1) means that we observe only the part of symbols emitted by the first state. In this case Yu suggests replacing the probability $b_{i,d}(O_{t-d+1:t})$ $(t - d + 1 \leq 1, t \geq 1)$ by the marginal probability $b_{i,d}(O_{1:t})$.

We denote by $P_{Yu}[O_{1:T}]$ the probability of $O_{1:T}$ being generated by λ under assumptions 1)-2).

However, for some applications the evaluation problem should be considered without any additional assumptions, i.e. the first state can start before or at $t = 1$ and the last state can end at or after $t = T$. In this case we obtain the following solution of the evaluation problem.

Theorem. The probability that the observed sequence $O_{1:T}$ is generated by general hidden semi-Markov model λ can be calculated as follows:

$$P[O_{1:T}] = \sum_{(j,d)\in\mathcal{S}\times\mathcal{D}} \frac{\pi_{j,d}}{d} \sum_{d_1=1}^{d} P_{Yu}[O_{1:T-d_1}] b_{j,d}(O_{T-d_1+1:T}),$$

where $P_{Yu}[O_{1:T-d_1}]$ is calculated as in [2], p. 225.

Using this theorem the evaluation problems for hidden semi-Markov Ferguson model and hidden semi-Markov QP-model can be solved [5], [6], [7]. The obtained theoretical results can be used to choose the appropriate error source model for the given digital transmission channel.

Bibliography

1. *Rabiner L.R.* A tutorial on Hidden Markov Models and selected applications in speech recognition // Proceedings of the IEEE 77 (2). 1989. P. 257 –286.

2. *Yu Shun-Zheg.* Hidden semi-Markov models // Artificial Intelligence. 2010. V. 174. n. 2. P. 215 -243.

3. *Levinson S.E.* Continuously variable duration hidden Markov models for automatic speech recognition // Computer Speech and Language. 1986. 1 (1). P. 29 –45.

4. *Ostendorf M., Digalakis V. V., Kimball O.A.* From HMM's to segment models: A unified view of stochastic modeling for speech recognition // IEEE Transactions on Speech and Audio Processing. 1996. 4 (5). P. 360 –378.

5. *Deundyak V. M., Zhdanova M. A.* Polynomial representation for hidden semi-Markov model of Ferguson's type // Vestnik Voronezhskogo gosudarstvennogo universiteta, Ser.: Sistemnyj analiz i informacionnye tehnologii. 2013. n. 2. P. 71 –78. (in Russian)

6. *Deundyak V. M., Zhdanova M. A.* On the solution of the evaluation problem for Hidden Semi-Markov QP-models// Vestnik DGTU. 2014. V.14, n. 4. P. 22 –39. (in Russian)

7. *Zhdanova M. A.* Inverse problems of HSMM-based mathematical modeling of jamming environment// Proceedings of the Modern methods, problems and applications of operator theory and harmonic analysis - V, 2015. P. 185

COMPUTER MODEL OF PLANE WITH FORWARD-SWEPT WING IN UNUSUAL CONDITIONS

Kazakov E.A.

Faculty of Physics, Southern Federal University, Rostov-on-Don, Russia

The report presents some specific ways of development of aircraft. At the dawn of aviation all types of airplanes had simple linear form of wing. With the development of the jet engine flight speed increased significantly and planes became like arrows. This constructive scheme was actual till birth the 5th generation jet fighter (nowadays). But there is another concept of aircraft's design: when wings situated backwards. The absurd scheme proved a very perspective one. Especially in combination with other nonstandard solution – "canard" a configuration in which a small horizontal surface, also named the canard or foreplane, is positioned forward of the main wing in contrast to the conventional position at the tail (because of this it is sometimes described as "tail-first").

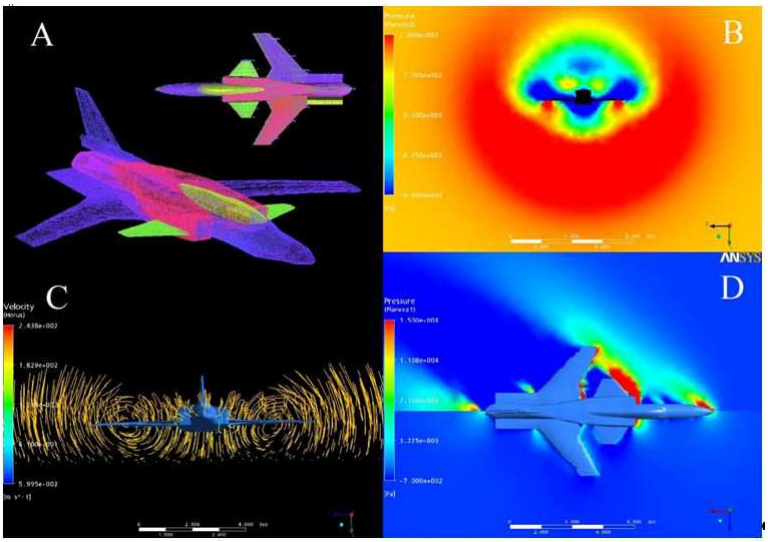

Figure 1. The panel (A) shows a realistic model of Northrop Grumman X-29A aircraft. The panel (B) shows the distribution of pressures in a plane perpendicular to the direction of flow. The panel (C) shows streamlines of velosity of the flow and demonstrates advantages of FSW flow's slipping. The panel (D) shows differences in pressure at subsonic and supersonic flight and demonstrates the Mach cone

Swept wing has an impressive number of advantages and imposes higher requirements for the development of the profile than the classical design of wing. Using present in the database NASA drawings I create in ANSYS a full model of the aircraft Grumman X-29A, which is the first prototype with the swept wing, officially broke the sound barrier. Provided simulation of airplane moving through

airflow as a whole allowed me to estimate the dependence of flight characteristics on the configuration elements, stability and construction balance.

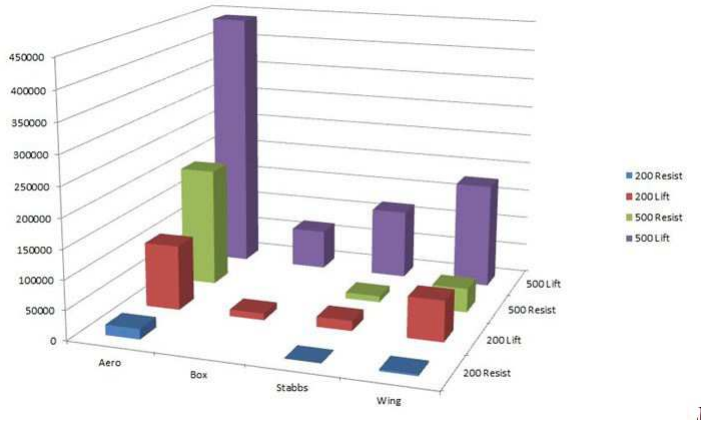

Figure 2. Comparative analysis of the emerging forces (lift and drag), depending on the mode of flight and involved airplane's parts

The report discusses the features of the wing swept behavior at extreme temperatures, in a dust storm and the threat of dry ice at subsonic and supersonic flight conditions.

LONG-WAVE INSTABILITY NEAR SEMI-SELECTIVE ION-EXCHANGE MEMBRANE[1]

Khasmatulina N.Yu., Ganchenko G.S.
Kuban State University, Krasnodar, Russia

Introduction

Rapid developments in micro-, nano-, and bio-technology originate a lot of interesting and comlicated problems of electrokinetics. Numerous modern applications of electrokinetics include micro-pumps, desalination devices, biological cells, electro-polishing of mono- and poly-crystalline aluminium, and the growth of aluminium oxide layers for creating micro- and nano-scale regular structures such as quantum dots and wires.

There is not only practical interest in the problem, but also a fundamental one. The study of the space charge in an electric double-ion layer in an electrolyte solution between semi-selective ion-exchange membranes under a potential drop is a fundamental problem of modern physics, first addressed by Helmholtz. Hydrodynamics was not involved in either of the underlimiting or limiting regimes, and both regimes are fully described by one-dimensional solution.

It was first theoretically predicted by Rubinstein and Zaltzman [1], [2] that the transition from limiting to overlimiting currents is connected with a novel type of electro-hydrodynamic instability, which is known as electrokinetic instability. This instability triggers a hydrodynamic flow and, in turn, intensifies the ion flux which is responsible for the overlimiting currents. The first direct experimental proof of the electroconvective instability that arises with an increasing potential drop between ion-selective membranes was reported by Rubinstein *et al.* [3], who managed to show the existence of small vortices near the membrane surface. A unified theoretical description of the linear electrokinetic instability, valid for all three regimes (underlimiting, limiting and overlimiting currents), was presented by Zaltzman and Rubinstein [4], based on asymptotic analysis of the problem The DNS for two-dimensional (2D) Nernst–Planck–Poisson–Stokes (NPPS) equations were considered in [5, 6] and others. A full scale direct numerical simulation (DNS) for the three-dimensional (3D) formulation is presented in Demekhin *et al.* [7].

In all the aforementioned theoretical and numerical analyses, thermal effects are neglected. Although, Zabolotsky and Nikonenko [8] have found experimentally that a typical temperature difference between the electrolyte inside the membrane system and the environment can be up to several degrees. Such a temperature difference can not only have an influence on the electrokinetic instability near a charge-selective surface, but can also be a driving force for a

[1]Supported, in part, by the Russian Foundation for Basic Research (Project Nos. 12-08-00924-a, 13-08-96536-r_yug_a, 14-08-31260 mol-a, and 14-08-00789-a

new kind of instability based on the spatial nonuniformity of the electrical conductivity. It can also be shown that Joule heating has a significant effect on the voltage–current (VC) characteristic. These phenomena are investigated in the present paper.

Statement

A symmetric, binary electrolyte with a diffusivity of cations and anions $\tilde{D}$, dynamic viscosity $\tilde{\mu}$, and electric permittivity $\tilde{\varepsilon}$, and bounded by ideal, semiselective ion-exchange membrane surfaces at $\tilde{y} = 0$ and $\tilde{y} = \tilde{h}$ with a potential difference $\Delta\tilde{V}$ between these surfaces, is considered. The Joule heating generated by the passage of a current through the electrolyte is taken into account. Notations with tilde are used for the dimensional variables, as opposed to their dimensionless counterparts without a tilde. $\{\tilde{x}, \tilde{y}\}$ are the coordinates, where $\tilde{x}$ is directed along the membrane surface and $\tilde{y}$ is normal to it.

What differs the present mathematical model of the phenomena from the mathematical model in [9] is adding the energy equation

$$\frac{\partial\tilde{T}}{\partial\tilde{t}} + \tilde{\mathbf{u}} \cdot \nabla\tilde{T} = \tilde{a}\nabla^2\tilde{T} - \frac{\tilde{\mathbf{I}} \cdot \nabla\tilde{\Phi}}{\tilde{c}_p\tilde{r}_0} \tag{1}$$

and appearance of the additional term, corresponding to the buoyancy force in Boussinesq approximation, in the Stockes equation:

$$\begin{aligned} \nabla\tilde{\Pi} = \tilde{\mu}\nabla^2\tilde{\mathbf{u}} + \tilde{F}\nabla\tilde{\Phi}\left(\tilde{c}^- - \tilde{c}^+\right) &+ \tilde{g}\tilde{r}_0\tilde{\beta}(\tilde{T} - \tilde{T}_0)\mathbf{e_y}, \\ \nabla \cdot \tilde{\mathbf{u}} &= 0, \end{aligned} \tag{2}$$

where $\tilde{F}$ is Faraday's constant, $\tilde{R}$ is the universal gas constant, $\tilde{T}_0$ is the temperature of the environment, $\tilde{\varepsilon}$ is the electric permittivity, $\tilde{g}$ is the acceleration due to gravity, $\tilde{r}_0$ is the density, $\tilde{\beta}$ is the thermal expansion coefficient, $\tilde{c}_p$ is the specific heat capacity, and $\tilde{a}$ is the thermal diffusivity.

In the above equations, the two-dimensional case is treated; $\tilde{\mathbf{u}} = \left(\tilde{U}, \tilde{V}\right)$ is the fluid velocity vector; $\tilde{\Pi}$ is the pressure. the unit vector $\mathbf{e_y}$ is directed along the y-axis. The energy equation contains the source term associated with the Joule heating of the electrolyte. Electric current

$$\tilde{\mathbf{I}} = -\frac{\tilde{F}^2\tilde{D}}{\tilde{R}\tilde{T}}(\tilde{c}^+ + \tilde{c}^-)\nabla\tilde{\Phi} - \tilde{F}\tilde{D}\nabla(\tilde{c}^+ - \tilde{c}^-), \tag{3}$$

is made up by two mechanisms: ion transport and diffusion. Note, that relation for the full electric current contains also convective term, but this term isn't significant for analyze of Joule heatig' influence.

The boundary conditions are the same as in [9], excepting the boundary conditions for temperature

$$\tilde{y} = 0: \quad -\frac{\partial \tilde{T}}{\partial \tilde{y}} + \frac{\tilde{\alpha}}{\tilde{\lambda}_T}(\tilde{T} - \tilde{T}_0) = 0, \tag{4}$$

$$\tilde{y} = \tilde{h}: \quad \frac{\partial \tilde{T}}{\partial \tilde{y}} + \frac{\tilde{\alpha}}{\tilde{\lambda}_T}(\tilde{T} - \tilde{T}_0) = 0, \tag{5}$$

where α is heat transfer coefficient, $\tilde{\lambda}_D = \sqrt{\dfrac{\tilde{\varepsilon}\,\tilde{\Phi}_0}{\tilde{F}\,\tilde{c}_\infty}}$ is the Debye length.

In order to make the system dimensionless, let us use some characteristic values, mentioned in [9], and the additional one $\tilde{T}_{ch} = \frac{\tilde{\Phi}_0 \tilde{D} \tilde{F} \tilde{c}_\infty \tilde{\lambda}_T}{\tilde{a}\tilde{c}_p \tilde{r}_0 alpha}$ (here $\tilde{c}_\infty$ – typical electrolyte concentration, $\tilde{\Phi}_0$ – characteristic thermal potential)

In dimensionless formulation the system of equations is as follows,

$$\frac{\partial c^\pm}{\partial t} + \mathbf{u} \cdot \nabla c^\pm = \pm \nabla \cdot (c^\pm \nabla \Phi) + \nabla^2 c^\pm, \tag{6}$$

$$\nu^2 \nabla^2 \Phi = -\rho, \tag{7}$$

$$\nabla \Pi = \nabla^2 \mathbf{u} - \frac{\varkappa}{\nu^2} \nabla \Phi \cdot \rho + Ra \cdot T\, \mathbf{e_y}, \quad \nabla \cdot \mathbf{u} = 0, \tag{8}$$

$$Le \left(\frac{\partial T}{\partial t} + \mathbf{u} \cdot \nabla T \right) = \nabla^2 T - \mathbf{I} \cdot \nabla \Phi, \tag{9}$$

here,

$$\mathbf{I} = -K \cdot \nabla \Phi - \nabla \rho + \mathbf{u} \cdot \rho, \quad K = c^+ + c^-, \quad \rho = c^+ - c^-, \tag{10}$$

with the boundary conditions,

$$y = 0: \quad c^+ = p, \quad -c^- \frac{\partial \Phi}{\partial y} + \frac{\partial c^-}{\partial y} = 0 \quad \Phi = 0, \quad \mathbf{u} = 0, \quad \frac{\partial T}{\partial y} - BiT = 0; \tag{11}$$

$$y = 1: \quad c^+ = p, \quad -c^- \frac{\partial \Phi}{\partial y} + \frac{\partial c^-}{\partial y} = 0 \quad \Phi = \Delta V, \quad \mathbf{u} = 0, \quad \frac{\partial T}{\partial y} + BiT = 0, \tag{12}$$

where, $T = (\tilde{T} - \tilde{T}_0)/\tilde{T}_{ch}$.

Using the standard stream function and making some conversions, one can reduce equations (8) to one biharmonic equation, which is convenient for numerical solving. Characteristic electric current in case of cation-exchacge membrane is determined only by cation's flow: $j = c^+ \frac{\partial Phi}{\partial y} + \frac{\partial c^+}{\partial y} \Phi$ for $y = 0$.

From the analysis of the above mentioned dimensional values, it follows that the dimensionless parameters vary within the range: $\nu = 10^{-6}-10^{-2}$, $\varkappa = 0.05-0.5$, $Ra = 10^{-6} - 100$. It is assumed that the other dimensionless parameters can be fixed as $p = 5$ (see [2, 4, 5]) and $Le = 0.013$ (for water). We assume that $Bi = 10^{-2}$ is taken. The problem has three parameters: ν, Ra, and $\varkappa$. This fact greatly complicates the numerical investigation of the problem. The first small parameter, the Debye number, makes the problem singular and forms a thin EDL near the boundaries of the investigated domain, $y = 0$ and $y = 1$.

I Numerical solution

The numerical calculations of the linear stability of the 1D quiescent solution with respect to sinusoidal perturbations with wave number k, $f = f_0 + \hat{f}\,\exp(\lambda t + i\,k\,x)$ for $f = \{c^{\pm}, \Phi, V, T\}$ were perfomed. The Galerkin pseudo-spectral τ-method with Chebyshev polynomials taken as the basic functions [10] is employed to discretize the eigenvalue problem. The generalized matrix eigenvalue problem is solved by the QR algorithm [10]. The number of Chebyshev functions in the expansion is up to 512.

The two competing mechanisms of instability are determined by the parameters $\varkappa$ and Ra. The relation between these parameters determines which of the instability mechanisms will be decisive for the destabilization of the system. Fig. 1 presents the numerically obtained marginal stability curves for different values of $\varkappa$ and Ra. For the case without thermo-effects, $Ra = 0$, the numerics are compared with the analytics of Zaltzman and Rubinstein [4]: our numerical approach is in good correspondence with the asymptotical results. The case $Ra = 0$ separates the destabilizing and stabilizing effects of the Joule heating.

For $Ra < 0$, with decreasing $\varkappa$ or increasing $|Ra|$, the heat effects prevail over the electrokinetic effects and a drastic change of instability modes occurs: the critical voltage ΔV_* decreases dramatically. Moreover, the short-wave instability changes to a long-wave instability. Universal character of the behavior of the long-wave marginal stability curves near ΔV_* can be seen from Figs. 1(a)–1(b). For the case without thermo-effects, $Ra = 0$, the numerics are compared with

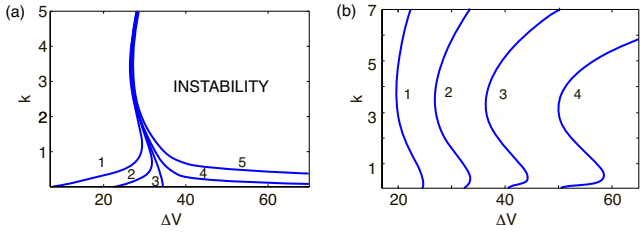

Figure 1. Marginal stability curves of the numerical solution, the wave number k vs. the voltage ΔV for $\nu = 0.01$, (a) $\varkappa = 0.2$, Ra: 1: -50, 2: -10, 3: 0, 4: 10, 5: 50 and (b) $Ra = -10$, $\varkappa$: 1: 0.5, 2: 0.2, 3: 0.1, 4: 0.05.

the analytics of Zaltzman and Rubinstein [4]: our numerical approach is in good

correspondence with the asymptotical results. The case $Ra = 0$ separates the destabilizing and stabilizing effects of the Joule heating.

Conclusion

A new long-wave kind of instability caused by Joule heating near charge selective surfaces and its influence on the electrokinetic instability are investigated numerically. The physical mechanism of the thermal instability is found to be very different from that of Rayleigh–Bénard convection, and the instability is caused by an induced nonuniformity of the electrical conductivity in the electrolyte. In addition, the previous discrepancies between the experiments [3] and the theory [6] have shown, in the present study, a trend of better agreement by taking into account the Joule heating for the appropriate Rayleigh numbers.

Bibliography

1. *Rubinstein I., Zaltzman B.* Electro-osmotically induced convection at a permselective membrane // Phys. Rev. E. 2000. Vol. 62. pp. 2238–2251

2. *Rubinstein I. and Zaltzman B.* Wave number selection in a nonequilibrium electro-osmotic instability // Phys. Rev. E. 2013. Vol. 68, Paper number 032501.

3. *Rubinstein S.M., Manukyan G, Staicu A., Rubinstein I., Zaltzman B., Lammertink R.G.H., Mugele F., and Wessling M.* Direct observation of a nonequilibrium electro-osmotic instability // Phys. Rev. Lett. 2008. Vol. 101, Paper number 236101

4. *Zaltzman B., Rubinstein I.* Electro-osmotic slip and electroconvective instability // J. Fluid Mech. 2007. Vol. 579. P. 173–226

5. *Chang H.-C., Demekhin E. A., and Shelistov V. S.* Competition between Dukhin's and Rubinstein's electrokinetic modes // Phys. Rev. E. 2012. Vol. 86. Paper number 046319.

6. *E. A. Demekhin, N. V. Nikitin, and V. S. Shelistov.* Direct Numerical Simulation of Electrokinetic Instability and Transition to Chaotic Motion // Phys. Fluids. 2013. Vol. 25. p. 122001.

7. *E. A. Demekhin, N. V. Nikitin, and V. S. Shelistov.* Three-dimensional coherent structures of electrokinetic instability // Phys. Rev. E. 2014. Vol. 90. Paper number 013031.

8. *Zabolocky V. I. and Nikonenko V. V.*, Ion transport in membranes [Perenos ionov v membranah], Nauka, Moscow (1996) [in Russian].

9. *Kiriy V. A., Khasmatulina N. Yu, Demekhin E. A.* Numerical finding of border separating limited and overlimiting currents in a semiconducting electric membrane // Ecological bulletin of research centres of the BSEC. 2014, No 3, P. 31-37 [in Russian]

10. *Orszag S. A.* Accurate solution of the Orr-Sommerfeld stability equation // J. Fluid Mech. 1971. Vol. 50. pp. 689–703.

THE DISPERSION PROPERTIES OF HETEROGENEOUS TRANSVERSELY ISOTROPIC CYLINDRICAL WAVEGUIDE

Morgunova A.V.*, Vatulyan A.O.**

* *Don State Technical University, Rostov-on-Don, Russia*

** *Southern Federal University, Rostov-on-Don, Russia*

The problem of propagation of waves in an infinite transversely isotropic cylinder with a circular cross-section is considered $a \leq r \leq b$. The problem is solved in cylindrical coordinates, the deformation is considered to be axially symmetric. It is also considered that the physical characteristics are arbitrary positive function of the r coordinate. The following notation for the components of the displacement vector are introduced by $U_r(r,z,t)$ – radial and $U_z(r,z,t)$ axial. We assume that the components of the stress tensor and the strain tensor components are related by Hooke's law for transversely isotropic inhomogeneous body with radial inhomogeneity:

$$\sigma_r = C_{11}\frac{\partial U_r}{\partial r} + C_{12}\frac{\partial U_r}{r} + C_{13}\frac{\partial U_z}{\partial z}$$
$$\sigma_\theta = C_{12}\frac{\partial U_r}{\partial r} + C_{11}\frac{\partial U_r}{r} + C_{13}\frac{\partial U_z}{\partial z}$$
$$\sigma_{rz} = C_{11}\left(\frac{\partial U_r}{\partial z} + \frac{\partial U_z}{\partial r}\right)$$
$$\sigma_z = C_{13}\left(\frac{\partial U_r}{\partial r} + \frac{\partial U_r}{r}\right) + C_{33}\frac{\partial U_z}{\partial z}$$

where C_{ij} – functions of the radial coordinate.

The equations of motion in cylindrical coordinates are

$$\frac{\partial \sigma_r}{\partial r} + \frac{\sigma_r - \sigma_\phi}{r} + \frac{\partial \sigma_{rz}}{\partial z} = \rho\frac{\partial^2 U_r}{\partial t^2}$$
$$\frac{\partial \sigma_{rz}}{\partial r} + \frac{1}{r}\sigma_{rz} + \frac{\partial \sigma_z}{\partial z} = \rho\frac{\partial^2 U_z}{\partial t^2}$$

We assume that the cylindrical surfaces of the cylinder subjected to the normal load, respectively. The boundary conditions are

$$\sigma_{rr}\mid_{r=a} = pe^{i(kz-\omega t)}, \sigma_{rr}\mid_{r=a} = 0$$

A boundary value problem of wave propagation in inhomogeneous cylinder formulated. The solution of the boundary value problem is formulated as a guided waves along the cylinder axis.

We have obtained first order canonical system of differential equations

$$\frac{d\tilde{Y}}{dr} = A(r, k, \omega, \tilde{Y})$$

with the following boundary conditions

$$X(a) = p_0, X(b) = 0, Z\mid_{r=a,b} = 0.$$

the following notation options are: $\gamma = kb$ – dimensionless wave number, $\kappa^2 = \rho\omega^2 b^2/C_{44}^0$ – the dimensionless frequency, $\varepsilon = r/b, \varepsilon \in [\varepsilon_0, 1], \varepsilon_0 = a/b$.

We have formulated the following homogeneous boundary value problem for the operator with two spectral parameters γ, κ

$$\frac{C_{11}}{C_{44}^0} = g_1, \frac{C_{13}}{C_{44}^0} = g_2, \frac{C_{12}}{C_{44}^0} = g_3, \frac{C_{44}}{C_{44}^0} = g_4, \frac{C_{33}}{C_{44}^0} = g_5$$

$$\begin{aligned} Y_1' &= -a_1\frac{Y_1}{\xi} - \gamma a_2 Y_2 + a_3 Y_3 \\ Y_2' &= \gamma Y_1 + a_4 Y_4 \\ Y_3' &= (a_6\frac{1}{\xi^2} - \kappa^2)Y_1 + a_7\frac{\gamma}{\xi}Y_2 - a_5\frac{Y_3}{\xi} - \gamma Y_4 \\ Y_4' &= a_7\frac{\gamma}{\xi}Y_1 + (\gamma^2 a_8 - \kappa^2)Y_2 + \gamma a_2 Y_3 - \frac{Y_4}{\xi} \end{aligned} \tag{1}$$

where:

$$a_1 = \frac{g_3(\xi)}{g_1(\xi)}, a_2 = \frac{g_2(\xi)}{g_1(\xi)}, a_3 = \frac{1}{g_1(\xi)}, a_4 = \frac{1}{g_4(\xi)}, a_5 = \frac{g_1(\xi) - g_3(\xi)}{g_1(\xi)},$$
$$a_6 = \frac{g_1^2(\xi) - g_3^2(\xi)}{g_1(\xi)}, a_7 = \frac{g_2(\xi)(g_1(\xi) - g_3(\xi))}{g_1(\xi)}, a_8 = \frac{g_5(\xi)g_1(\xi) - g_2^2(\xi)}{g_1(\xi)}$$

So we have built a system of dimensionless differential equations with boundary conditions. Only numerical investigation of the problem is possible. In some combinations between the parameters, which forms the set of dispersion points, the problem is insoluble. The problem of constructing the set of dispersion points is very important in general theory of waveguides, however, for arbitrary heterogeneity functions requires the use of numerical methods. Solving boundary value problem we have used the shooting method.

For each value of κ and γ, set up in the cycle with some step, solves two Cauchy problems for the system (1) with the following boundary conditions for the first one:
$Y_1^{(1)}(\xi_0) = 1, Y_2^{(1)}(\xi_0) = 0, Y_3^{(1)}(\xi_0) = 0, Y_4^{(1)}(\xi_0) = 0$, solutions vector $Y^{(1)} = (Y_1^{(1)}, Y_2^{(1)}, Y_3^{(1)}, Y_4^{(1)})$.

for the second Cauchy problem:
$Y_1^{(2)}(\xi_0) = 1, Y_2^{(2)}(\xi_0) = 0, Y_3^{(2)}(\xi_0) = 0, Y_4^{(2)}(\xi_0) = 0$, solutions vector $Y^{(2)} = (Y_1^{(2)}, Y_2^{(2)}, Y_3^{(2)}, Y_4^{(2)})$.

linear combination of these vectors

$$\alpha_1 Y^{(1)} + \alpha_2 Y^{(2)}$$

This combination should meet the remaining boundary conditions $Y_3(1) = Y_4(1) = 0$. Obtained the linear system to determine the parameters α_1, α_2

$$\alpha_1 Y_3^{(1)} + \alpha_2 Y_3^{(2)} = 0$$
$$\alpha_1 Y_4^{(1)} + \alpha_2 Y_4^{(2)} = 0$$

To determine the set of dispersion points it is necessary to find the relation between γ and κ, for which system would have a nontrivial solution; then the determinant of the system is zero.

Numerical experiments to determine the structure of the dispersion sets for various heterogeneity functions displayed in the following figures. Figure 1. identify the components of the dispersion sets for the non-monotonic heterogeneity functions $f(\xi), g(\xi)$, in Figure 2 for a layered cylinder.

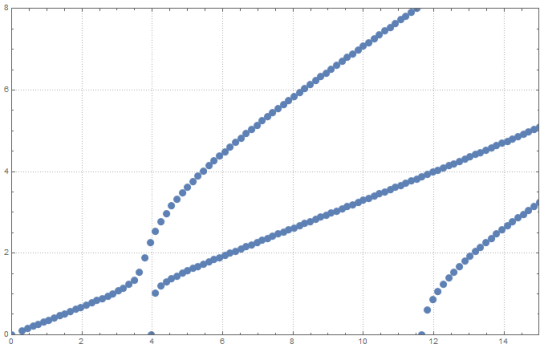

Figure 1. Non-monotonic heterogeneity

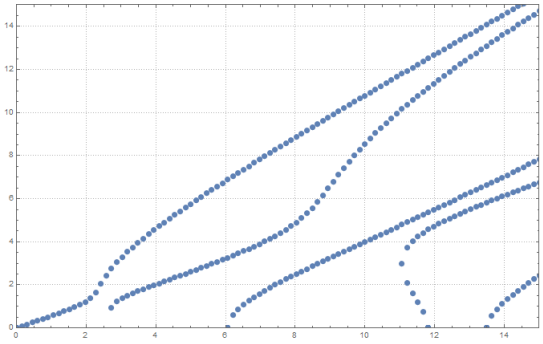

Figure 2. Layered cylinder

Bibliography

1. *Chree C.* Longitudinal vibrations of a circular bar //J. Quart. Pure Appl. Math. 1886. V. 21. P. 287-298.

2. *T. Miker, A. Meitzler* "Waveguide Propagations in Extended Cylinders and Plates," in Physical Acoustics, Collection of paper. Mir: Moscow, 1966, Vol. 1, pp. 140-203 (Russian translation)

3. *V. T. Grinchenko, V. V. Meleshko* Harmonic Vibrations and Waves in Elastic Bodies. Naukova Dumka, Kiev, 1981. 282pp. (in Russian)

ON THE OCCURRENCE OF SELF-OSCILLATIONS IN A VERTICAL LAYER OF A BINARY MIXTURE IN THE PRESENCE OF A THERMAL DIFFUSION EFFECT

Petrova E.I., Morshneva I.V.

Southern Federal University, Rostov-on-Don, Russia

The problem of convection in a binary mixture consisting of two non-reacting components is considered. The binary mixture is placed between two vertical infinite isothermal plates. In the model under consideration thermal diffusion effect is taken into account, diffusive thermal conductivity is neglected. The convective flow of the binary mixture is governed by the Navier-Stokes equations under Oberbeck-Boussinesq approximation ([1]):

$$\begin{aligned} &\frac{\partial \mathbf{v}}{\partial t} + Gr(\mathbf{v}, \nabla)\mathbf{v} = -\nabla p + \triangle \mathbf{v} + (T + C)\mathbf{k}, \\ &\frac{\partial T}{\partial t} + Gr\mathbf{v}\nabla T = \frac{1}{Pr}\triangle T, \\ &\frac{\partial C}{\partial t} + Gr\mathbf{v}\nabla C = \frac{1}{Pr_d}(\triangle C - \varepsilon \triangle T), \\ &\operatorname{div} \mathbf{v} = 0. \end{aligned} \tag{1}$$

The corresponding boundary conditions are:

$$y = \pm 1 : \mathbf{v} = 0, \;\; T = \mp 1, \;\; \frac{\partial C}{\partial y} = \varepsilon \frac{\partial T}{\partial y}, \tag{2}$$

where $\mathbf{v} = (v_x, v_y, v_z)$ is the flow velocity, T is the temperature, C is the light component concentration, p is the pressure, $\mathbf{k}$ is the up-directed vertical vector.

The problem (1), (2) contains four dimensionless parameters: $Gr = \dfrac{g\beta_1\theta d^3}{\nu^2}$ — the Grashof number; $Pr = \dfrac{\nu}{\chi}$ — the Prandtl number; $Pr_d = \dfrac{\nu}{D}$ — the diffusion Prandtl number (the Schmidt number); $\varepsilon = -\dfrac{\alpha\beta_2}{\beta_1}$ — the thermodiffusion coefficient; where ν is the kinematic viscosity coefficient, χ is the thermal diffusivity, D is the diffusivity, β_1 is the coefficient of thermal expansion, β_2 is the density concentration coefficient, α is the thermodiffusion parameter.

The motion equations (1), (2) have a steady-state (basic) solution with a cubic velocity profile, constant pressure, linear distribution of temperature and concentration. Linear stability of the basic solution was studied by G. Gershuni, E. Zhukhovitsky and L. Sorokin ([1]). They found that both monotonic and oscillatory stability loss of the basic regime are possible.

This research is devoted to the study of branching and stability of time-periodic flow regimes arising from oscillatory stability loss of the basic regime relatively plane perturbations $2\pi/\beta$–periodic on a vertical variable z, where β is wave number. The perturbation equations are invariant under the group O(2) (invariant under inversion and vertical translation), and the Andronov-Hopf bifurcation theory in the systems with such symmetry is suitable. This theory has been developed by V. Yudovich and I. Morshneva ([2], [3]). In our research we employ the Lyapunov-Schmidt method. We propose that solution is time periodic with $2\pi/\omega$ period, where ω is unknown cyclic frequency. Thus the solution is sought as follows:

$$v(\tau) = (\alpha_0\varphi_0 + \alpha_1\varphi_1)e^{i\tau} + (\alpha_0^*\varphi_0^* + \alpha_1^*\varphi_1^*)e^{-i\tau} + u(\tau), \tag{3}$$

where φ_0, φ_1 is eigenvectors of the linear problem, which are connected by inversion symmetry and correspond to the eigenvalue $-i\omega_0$; α_0, α_1 — complex amplitudes; $\tau = \omega t$, $\omega = \omega_0 + \mu$.

The branching equations inherit the symmetry of the original problem and are given as

$$\begin{aligned} g(\alpha_0, \alpha_1) &\equiv \alpha_0(-i\mu + a\delta + b|\alpha_0|^2 + c|\alpha_1|^2 + \dots) = 0, \\ g(\alpha_1, \alpha_0) &\equiv \alpha_1(-i\mu + a\delta + b|\alpha_1|^2 + c|\alpha_0|^2 + \dots) = 0. \end{aligned} \tag{4}$$

The expressions for a, b, c coefficients are provided in [2]. These coefficients represent functionals, which are expressed through eigenfunctions of the linear and conjugate stability problem, and through the solutions of inhomogeneous boundary-value problems with right sides that emplicity dependent on the same eigenfunctions.

Investigation of the system (4) has reveal ([2]) that when the parameter Gr pass through the critical value of the oscillatory stability loss Gr_* three types of self-oscillating modes are arising: the nonlinear mixture of couple simple waves, two traveling simple waves moving in the opposite direction to each other. The type of branching and stability of these regimes depends on the relations between the coefficients a, b, c of the branching equations.

The coefficients of the branching equations were found numerically for the problem of binary mixture convection in the vertical layer in consideration of thermal diffusion effect. Computations for a wide range of parameters Pr, Pr_d, ε, β showed that the following five branching types of periodic modes are realized:

I. the traveling waves are stable and branched in supercritical region, the nonlinear mixture of waves is unstable and branched in supercritical region;

II. the traveling waves are unstable and branched in supercritical region, the nonlinear mixture of waves is stable and branched in supercritical region;

III. the traveling waves are branched in supercritical region, the nonlinear mixture of waves is branched in subcritical region, all regimes are unstable;

IV. the traveling waves are branched in subcritical region, the nonlinear mixture of waves is branched in supercritical region, all regimes are unstable;

V. all regimes are unstable and branched in subcritical region.

A variety of neutral stability curves of the oscillatory stability loss have been plotted for different values of Pr, Pr_d, ε. Each of the five branching types of periodic modes is denoted in different styles. For example, Fig. 1 represents the neutral stability curves, corresponding to the oscillatory stability loss, for the values of the Prandtl number $Pr = 12,\ 14,\ 15.6$, the Schmidt number $Pr_d = 4$ and the thermodiffusion coefficient $\varepsilon = 1.214$ in the parameter space $(\beta,\ \omega,\ Gr)$. The nonlinear mixture of waves is stable at the cyclic frequency below the average value, and the traveling waves are stable at the cyclic frequency near and above the average value. On the remaining curve parts all the modes are unstable and differ only by the branching type.

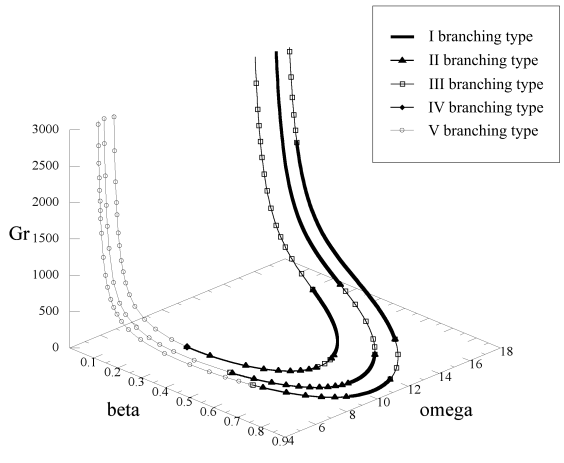

Figure 1. Branching types of self-oscillating modes on the neutral stability curves for $Pr = 12,\ 14,\ 15.6$, $Pr_d = 4$, $\varepsilon = 1.214$.

Bibliography

1. *Gershuni G. Z., Zhukhovitsky E. M., Nepomnjaschy A. A.* Stability of convective flows. M.: Nauka, 1989. 320 p.

2. *Morshneva I. V., Yudovich V.I.* Bifurcation of cycles from equilibria of inversion- and rotation- symmetric dynamical systems // Sibirsky Matematichesky Zhurnal. 1985. Vol. 26. N 1. P. 124–133.

3. *Morshneva I. V., Yudovich V.I.* On the phase portrait of inversion-rotation symmetric dynamical systems in the neighborhood of the losing stability focus // Izv. SKNC VSH. Estv. nauky. 1984. N 3. P. 30–32.

MATHEMATICAL MODELS AND METHODS TO DESCRIBE SELF-ASSEMBLY OF SPHERICAL CRYSTALS AND TO STUDY THEIR DEFECTS[1]

Roshal D.S., Myasnikova A.E.

Faculty of Physics, Southern Federal University, Rostov-on-Don, Russia

Rapid development of experimental methods to obtain spherical crystals and to study them causes high scientists' interest in theoretical modeling of colloidal crystal self-assembly and defects in them. It is known, that this material is among the first that were obtained by means of self-assembly. The most interesting material from the practical point of view is colloidosome, which is a system of densely packed particles at an interface between two liquids. Hexagonal order dominates on its surface, but it also contains few topological defects. According to Euler theorem a sum of defects' topological charges is 12. Usually triangulation method (drawing lines connecting each particle with its closest neighbors) is useful to find defects areas. In this case particles related to hexagonal order have zero topological charge, particles with five neighbors have charge +1, particles with seven ones have charge -1, etc. Recently, we proposed a method [4] of rapid determination of the extended defects' topological charge using the contours surrounding them. In this case the value of the topological charge is 6 minus the number of the contour sides. So the pentagonal defect topological charge is +1, and an area of square order [1] has the charge +2. Similar topological defects may be called extended topological defects (ETDs) [2].

To explain the arrangement of particles on the colloidosome surface it is reasonable to use Lennard-Jones potential. To simulate the colloidosome self-assembly it is enough to place randomly the particles on the sphere surface and then to minimize the system energy by the gradient descent method.

As simulation shows [1] at the number of particles on the sphere surface slightly less than the maximum possible, the area with the square order may be formed (Fig.1b), which was experimentally observed (Fig.1a). The area of square order can be understood as the result of interaction of two pentagonal defects, and its topological charge (+2) is the sum of topological charges of two disclinations (+1) [1]. Packing density is much lower in such areas, which is important for applications.

To study the ETD properties and interaction between different defects we suggest a new method of surrounding the ETD with a contour. The most common defects in the spherical crystals are dislocations and disclinations. However, in colloidosomes and colloidal crystals with large maximum number of particles and high-density packing they are combined into ETD with the topological charge +1. The number of them on the sphere surface is 12, and they are located near the

[1]This work was supported by Russian Foundation for Basic Research (Grant N13-02-12085 ofi_m)

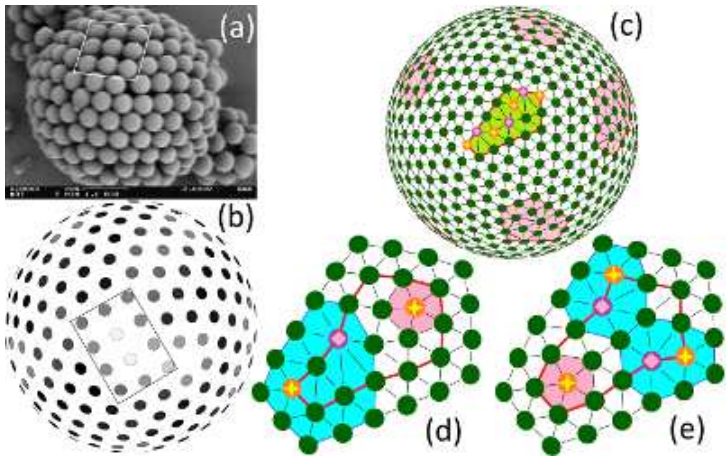

Figure 1. Experimental (a) and simulated colloidosomes with the number of particles (b): slightly less than maximum and (c): larger and maximum. Panels (d, e) show two possible ways to decompose green extended topological defect (ETD) from (c) by the application of external forces.

vertices of icosahedron (Fig. 1c). Let's surround such defect by scalene pentagon. It seems that the dislocations enter the longer sides of the pentagonal defect area, but it is not so. As it is shown in [2], increasing the area occupied by the ETD, we can make the surrounding contour equilateral. Thus, the order outside the defect doesn't display existence of dislocations in any way.

Also, the interaction between the topological defects can be studied with mathematical modeling methods. Over the last decade experimental methods for studying 2D colloidal crystals were substantially advanced. Using new experimental methods like the optical tweezers technique it is possible to move individual colloidal particles or to shift coherently whole groups of such particles. After these enforced changes colloidal structures relax. This experimental technique can be modeled by a virtual optical tweezers method [2]. It consists in that after the change of particles coordinates on the sphere surface the system relaxation is modeled by applying a gradient descent method. Thus, we apply the system energy minimization with the specific initial conditions in the form of modified coordinates of particles.

Let us use this method to consider the ETD in the center of the figure 1c. It is highlighted in the green pentagon. Only after triangulation it looks like a scar - a chain of 5- and 7-fold disclinations. Panels (d, e) present two possible ways to decompose this ETD by the application of external forces (virtual optical tweezers). In both enforced reactions the elementary 5-fold disclination is detached and it carries out all the topological charge of the ETD. The disclination region is colored in red. Hexagons containing the dislocations are colored in blue. The length of the Burgers vector of the dislocation (d) is 2, while the length of the total Burgers vector of two dislocations shown in panel (e) is 2sin(?/3). Considering the reactions between ETDs and dislocations, we have found that the ETDs emit and absorb the dislocations without preservation of their dislocational charge.

With the specific choice of initial conditions it is possible not only to model

the virtual optical tweezers, but also to find new solutions of Thomson problem. Self-organization of repelling particles retained on a spherical surface is under discussion for more than a century and is called Thomson problem after J.J. Thomson suggested his model of atom 110 years ago. Thomson problem is included in various lists of the most important unsolved mathematical problems of the 21st century. Now we know that Thomson problem arises on different levels of the matter self-organization. Arrangements in multi-electron bubbles in superfluid helium almost perfectly correspond to structures formed by charged particles in the frame of the problem. Also the pores in the pollen grains (the Tammes problem) and the various two-dimensional colloidal crystals including colloidosomes [1, 2] are similar to Thomson problem solutions.

However, the classical spherical Thomson structures (TSs) corresponding to the global energy minima are also very interesting. Search of them is a challenging work since the energies of structures corresponding to global and local minima are very close. Moreover, the difference between the equilibrium energies is strongly reduced and number of equilibrium structures grows exponentially with the number N of particles in the structure. Usually the lowest minima corresponding to the TS structure are searched with numerical methods. The list of spherical TSs with the lowest ever seen energy is constantly updated [3] by Bowick group of physicists.

Some of the TSs are similar to spherical viral capsids, which were for the first time described in terms of simple geometric model proposed by Caspar and Klug (CK) half a century ago. Unfortunately, viral capsids are not Thomson problem solution, and besides, such symmetric arrangements of particles are possible only at the particular N values. However, it allows us to adapt and develop the initial CK geometrical model to search for the lowest-energy TSs.

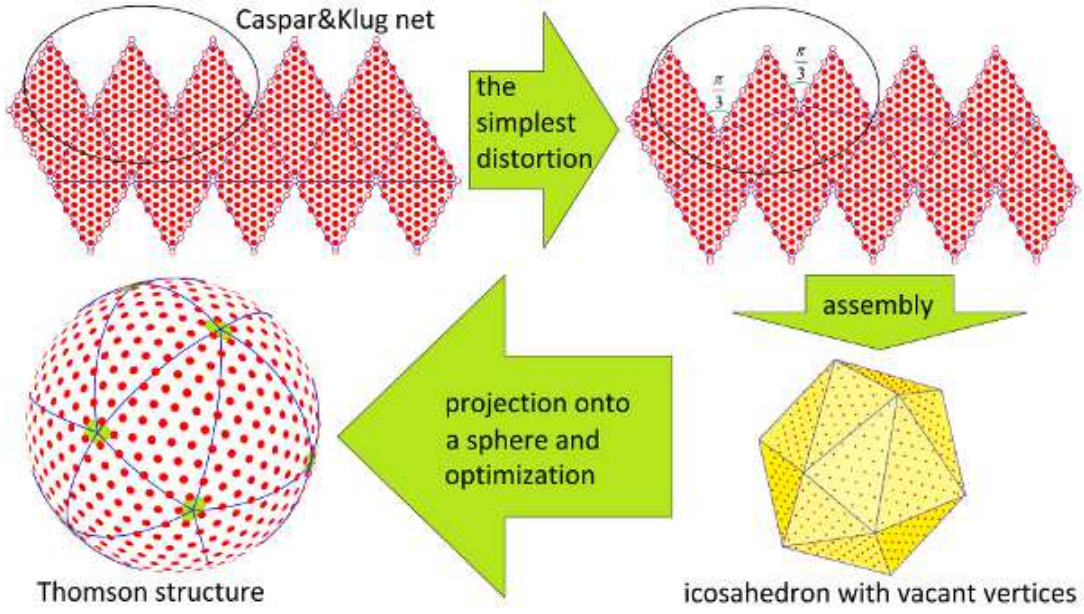

Figure 2. The method to obtain new Thomson structures

In my work [4], a new method of obtaining trial structures for further opti-

mization is suggested. It is based on a deformation of regular or slightly distorted icosahedron smoothly covered with hexagonal lattice. The particles are located in the nodes of this lattice. The trial structure is obtained by projecting the particles from the icosahedron surface onto the sphere.

In this work [4] the spherical structures with the number of particles in the interval of $600<N<1000$ were analyzed. Thus 40 spherical crystals having energies lower than the previously known structures with the same number of particles N were obtained. It is possible that the obtained structures are Thomson problem solutions. Our results may be interesting for physicists working on theoretical and experimental problems of self-assembly in various types of spherical nano- and micro-structures. For example, the structures with the above considered simplest distortions can be discovered in course of further experimental investigations of misassembled viral capsids or fullerenes.

Thus, by means of developing new models and mathematical methods [1, 2, 4] we managed to explain the mechanism of unusual defects formation on the colloidosome surface and to study the interaction between various defects. It was proved that ETD can absorb or emit dislocations without preserving their dislocation charge (the Burgers vector). Moreover, using initial conditions with slightly broken symmetry in the frames of the gradient descent method we find 40 new Thomson problem solutions.

Bibliography

1. *D. S. Roshal* Physics of the Solid State. 55, 2128 (2013).
2. *D.S. Roshal, K.Yu. Petrov, A.E. Myasnikova, S.B. Rochal* Phys. Lett. A. 378, 1548 (2014)
3. *M.J. Bowick, C. Cecka, L.Giomi, A.Middleton, K.Zielnicki* http:thomson.phy.syr.edushellsshelltable.php
4. *D.S. Roshal, A.E. Myasnikova, S.B. Rochal* Phys. Lett. A. 379, 372 (2015)

ONE APPROACH TO CALCULATING THE MOVEMENT AND INTERACTION OF INDIVIDUAL ICE FLOES[1]

Tarelkin A.A.*, Chikina L.G.*, Shabas I.N.*, Chikin A.L.**

* *Southern Federal University, Rostov-on-Don, Russia*

** *Institute of Arid Zones, Southern Scientific Center, Russian Academy of Sciences, Rostov-on-Don, Russia*

I Introduction

Ice cover is important component of the hydrological mode of the seas. Drifting ice significantly complicates shipping, coastal zone development, creates a heavy load on the bridge supports. Simulation of ice floes movement is an important area of research in development in areas of ice formation.

In different models the ice is considered as the porous structure, in the case of consideration of floes as individual objects, they're described as a material point [1, 5]. In this paper movement of floe takes into account its configuration, as well as the effects of streams and wind loads.

II Statement of the Problem

As the object of study is considered the process of ice floes movement with arbitrary shape of the floes in the pond filled with homogeneous ideal incompressible fluid. The border of the pond is vertical, and depth of water bigger than ice floes thickness.

The rectangular grid with information about flow velocity is obtained.

The object in question is a resilient plate of arbitrary shape, in some approximation are ice floes. As initial conditions must be seted the density and shape of the ice floe. With these parameters square, mass and center of mass could be calculated. The initial time it is assumed that the floe is at rest, $u^{t=0} = v^{t=0} = 0$.

Upon contact with the boundary of the reservoir, the movement of ice floes will be considered as an elastic collision with a solid surface.

III Movement modeling

The model of ice floes moving is based on two-dimensional model of the drift of the iceberg [6]. This model doesn't take into account the interaction with the soil, wind waves and tilt of pond. The equation can be described by :

[1]Supported by The Ministry of Education and Science of Russia (grant 1420)

$$M\frac{du}{dt} = F_{nx}^{W} + F_{nx}^{A}, M\frac{dv}{dt} = F_{ny}^{W} + F_{ny}^{A} \quad (1)$$

where $F_{nx}^{W}, F_{nx}^{A}, F_{ny}^{W}, F_{ny}^{A}$ – projection of radial force components on the axis x and y.

By replacing the time derivatives of the finite-difference analogues, we get:

$$\frac{\Delta u}{\Delta t} = \frac{F_{nx}^{W} + F_{nx}^{A}}{M}, \frac{\Delta v}{\Delta t} = \frac{F_{ny}^{W} + F_{ny}^{A}}{M}$$

where Δt – time step, Δu and Δv – components of the velocity gradients in time ($\Delta u = u^{t+1} - u^{t}, \Delta v = v^{t+1} - v^{t}$)

For the angular velocity we take tangential components of the forces:

$$\frac{\Delta \omega}{\Delta t} = \frac{F_{\tau}^{W} + F_{\tau}^{A}}{I}$$

where I – moment of inertia of the ice floe, $F_{\tau}^{W}, F_{\tau}^{A}$ – the tangential components of the forces acting on an ice floe.

After determining the speed of a drifting ice floe, we find the coordinates of its provisions (x, y) at the next time step:

$$x^{t+1} = x^{t} + u^{t+1}\Delta t, y^{t+1} = y^{t} + v^{t+1}\Delta t, \varphi^{t+1} = \varphi^{t} + \omega^{t+1}\Delta t$$

At first we shall partition the entire area floe with triangulation [4, 7] . We assume that all of the mass of each member is concentrated in the center of mass of the element, and the speed of the entire area of the element is equal to the velocity of its center of mass. Thus the resultant force acting on an ice floe, is the sum of the forces acting on each element of the partition:

$$F_{res} = \sum_{i=0}^{n} \left(F_{i}^{W} + F_{i}^{A}\right)$$

$$F_{i}^{W} = c_{w}\rho_{w}S_{i}\left(V^{W} - V_{i}^{ice}\right)$$

$$F_{i}^{A} = c_{a}\rho_{a}S_{i}\left(V^{A} - V_{i}^{ice}\right)$$

where V^{W} – water flow velocity, V^{A} – wind flow velocity, V_{i}^{ice} – rate of i floes element, ρ_{w}, ρ_{a} – the density of water, air, c_{w}, c_{w} – the friction coefficient of water, air, S_{i} –Square of i floes element in contact with the water.

The interaction between objects is reduced to the problem of collision detection and its solving [2, 9]. Stage collision detection is divided into two steps:

1. Determination of the candidates for the collision. For each ice floe determines the minimum radius of the circle centered at the center of mass and

fully containing this ice floe. By comparing the distance between the centers of mass of the two floes and the amount received by the radius of the circles we make a conclusion about the possibility of a collision. If the distance is greater than the sum of the radiuses, that means that floes don't collided, else a couple of ice floes are candidates for collision and go to step 2.

2. Search for common points ice floes. In the simplest case can be checked that vertexs of the second floe are belong to the first ice floe.

If couple of objects has common points, than the value of the impulse should be calculated. With this impulse objects interact with each other.

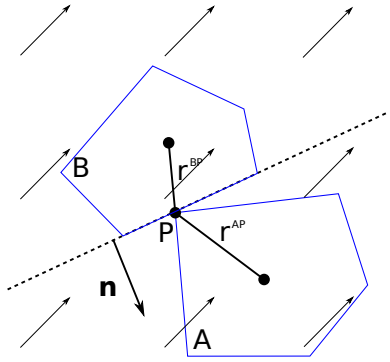

Figure 1. The moment of two ice floes collision.

$$j = \frac{-(1+\varepsilon)\, v_1^{AB} \cdot n}{n \cdot n \left(\frac{1}{M^A} + \frac{1}{M^B}\right) + \frac{\left(r_\perp^{AP} \cdot n\right)^2}{I^A} + \frac{\left(r_\perp^{BP} \cdot n\right)^2}{I^B}}$$

where j – impulse, ε – coefficient of elasticity, v_1^{AB} – the difference between the velocities of the bodies before collision, $\overline{n}$ – the normal vector of the point of collision, M^A, M^B – mass of colliding objects, I^A, I^B – the moment of momentum of the colliding objects.

IV Results

This model allows the calculation of:

1. Values of forces acting on an arbitrary area floes.
2. Values of the resultant force.
3. Collision forces.
4. Values of linear and angular speed and acceleration.

As the pond to test model was chosen square shaped pond, filled with a uniform ideal incompressible fluid with a steady flow. Presented in the form of a grid of the velocity field, with known values at the nodes of the grid.

There was a numerical simulation of the interaction of different type objects – two ice floes with a predetermined density in the range from 0.85 to 0.94 g / cm 2 and static body.

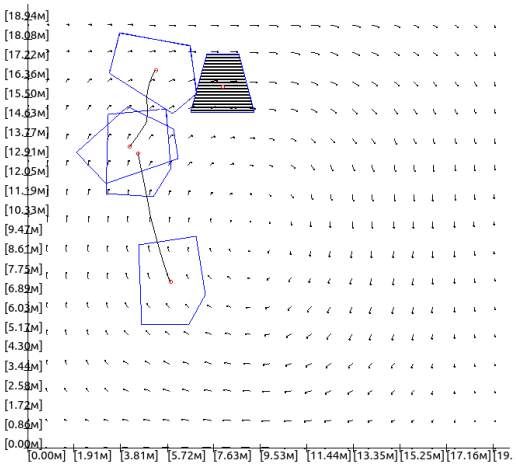

Figure 2. The results of calculations movement of ice floes

Fig. 1 shows the path of the ice floes, calculated using this model.

Bibliography

1. *D. Holland M. M.* Modelling the impact of icebergs on the Southern Ocean freshwater budget and circulation // National Science Foundation. – 2004.

2. *Ericson C.* Real-Time Collision Detection / под ред. T. Cox. – Elsevier, 2005.

3. *K. Weiler P. A.* Hidden surface removal using polygon area sorting // Program of Computer Graphics. Cornell University. – 1977. – C. 214–222.

4. *Owen S.* A Survey of Unstructured Mesh Generation Technology // Proceedings of 7th International Meshing Roundtable. – 1998. – C. 239–269.

5. *Schäfer-Neth C., Stattegge K.* Computerized modeling of sedimentary systems // / под ред. H. J. – Springer, 1999. – Ch. Icebergs in the North-Atlantic: Modelling circulation changes and glacio-marine deposition. C. 63–78.

6. *Klyachkin S.* Prognosticheskaya model dreyfa aysberga // Problemy arktiki i antarktiki. – 2012. – P. 78–88.

7. *Skvortsov A.* Obzor algiritmov postroeniya triangulyacii Delone // Vychislitelnye metody i programmirovanie. – 2002. – No 3. – P. 14–39.

8. *Joe B.* Construction Of Three-Dimensional Delaunay Triangulations Using Local Transformations // Computer Aided Geometric Design. – 1991. – T. 8. – C. 123–142.

9. *Coumans E.* Continuous Collision Detection and Physics // Sony Computer Entertainment. – 2005.

THE SPECIAL BROADCAST SECURITY SCHEME BASED ON RM-CODES AND THE PROTECTION FROM SOME LINEAR ALGEBRAIC ATTACKS

Yevpak S.A.

Southern Federal University, Rostov-on-Don, Russia

The special broadcast security scheme which is based on Reed-Muller codes is considered in [1]. The scheme allows distributors to protect digital products from unauthorized access. Each user gets from the distributor the id sequence and the keys which give access to duplicated data.

However, there are possibilities to get access to the data with help special linear algebraic attack [1, 2]. For this, legal users of the scheme unite in groups or coalitions and modify own key data for getting new pirate keys which give access to duplicated data. The coalition size is not more than c users for the concrete scheme. Besides, if the possible size of coalition members is more than c then there are another attacks [3].

In this paper, it is introduced the parameters of Reed-Muller codes, which help to protect the distributor data.

Let $\mathbb{F}_q[X_1, X_2, \ldots, X_m]$ be the ring of polynomials in m variables with coefficients in the finite field $\mathbb{F}_q$ with q elements. Let $P_1, P_2, \ldots, P_n$ be an enumeration of the points of $\mathbb{F}_q^m$, where $n{=}q^m$. The q-ary Reed-Muller code $RM_q(r, m)$ of order r in m variables is defined as

$$RM_q(r, m) = \{(f(P_1), f(P_2), \ldots, f(P_n)) | deg(f) \leq r\}.$$

Suppose c is the maximum size of coalition, N is the number of all users in the scheme. Then,

$$r, m(\in \mathbb{N}) : |RM_q(r, m)| = N$$

and

$$q \geq rc^2 + 1.$$

Bibliography

1. *Yevpak S.A., Mkrtichan V.V.* The Reed-Muller codes application in the special broadcast security schemes // Trudi nauchnoi shkoli I.B. Simonenko - Rostov-on-Don: Sfedu, 2010. P. 93-99. (in Russian)

2. *Yevpak S.A., Mkrtichan V.V.* About the link between the bounds of applying of the special information protection scheme based on the q-ary Reed-Muller codes // Izvestiya Sfedu. Engineering sciences. - 2013. - N 12. - P. 194-200. (in Russian)

3. *Yevpak S.A., Mkrtichan V.V.* Applicability conditions for q-ary Reed-Muller codes in traitor tracing // Vladikavkaz mathematical journal. V.16 (2), 2014. - P. 27-34. (in Russian)

MATHEMATICAL MODELING OF LASER PULSE INTERACTION WITH PLASMA[1]

Zaytseva A.A.*, Echkina E.Y.*

** Moscow State University Department of Computational Mathematics and Cybernetics, Moscow, Russia*

Recent years are marked with great progress of laser physics. Laser pulse power is constantly increasing and reached values of $10^{22}W/cm^2$. This fact has led to active theoretical and experimental researches of ion acceleration, and is expected to use the high power lasers.

Plasma can be considered cold and collisional for the examined laser pulse. Mechanisms of ion acceleration in the interaction of ultrashort and superstrong laser pulses with collisional plasma based on the generation of large-scale collective electric fields due to changes in the electron density under the action of electromagnetic radiation.

A detailed research of this problem requires a full-scale computer simulations based on the use of the so-called method of particles-in-cell or PIC – method.

This work is devoted to the description of computational experiment built on a multiprocessor platform. The experiment was conducted in the framework of 2D3V, when the desired ion distribution function depends on two spatial values and three components of the pulse. Plasma is examined in the Vlasov approximation, that is a medium consisting of electrons and ions in which there is a self-consistent field. Therefor it is represented with the finite number of electrons and ions (up to 10^7) disposed at discrete points of space. Particles move under the influence of external and self-consistent fields. The interaction of particles is divided into two stages: the calculation of fields, generated with particles, and determination of the motion of particles under the influence of forces, applied to them. Fields are calculated from Maxwell's equations, in which the currents and charges are searched out with the positions and velocities of all particles. Motion of the particles is determined by the numerical solution of the Newton-Lorentz equation with sufficient accuracy.

Computing cycle consists of alternate solutions to these two tasks. The variable and spatial grid are put in, it satisfyies the necessary requirements of accuracy and stability.Particles are noted with index i, for example v_i and x_i. Field values are computed only at the nodes of the spatial grid, marked with index j, for example E_j. Cycle of the program work is showed on the picture.1.

The work presents a method for calculating a large number of system parameters based on multi-platfoma, namely parallelization is based on the "parameter search". This parallelization gives a great time advantage, in the construction of a computational experiment.

[1]Finance supported by RFFI grant 14-01-00337

Figure 1. PIC Methods

Bibliography

1. *Bulanov S. V., Esirkepov T. Zh., Khoroshkov V. S. et al.* // Phys. Lett. A. 2002. V. 299. P. 240.
2. *Echkina E. Yu., Inovenkov I. N., Esirkepov T. Zh. et al.* // Laser Physics. 2009. V. 19. P. 228.
3. *Mourou G., Tajima T., Bulanov S. V.* // Rev. Mod. Phys. 2006. V. 78. P. 309.

SOME STEADY-STATE NUMERICAL SOLUTIONS OF EULER EQUATION[1]

Zhdanov I.A.*, Govorukhin V.N. *

* *Southern Federal University, Rostov-on-Don, Russia*

Consider a two-dimensional steady-state Euler's equation in terms of vorticity and stream-function, describing flow of incompressible inviscid fluid which was described in [1] :

$$\begin{cases} \frac{\partial \omega}{\partial x}\frac{\partial \psi}{\partial y} - \frac{\partial \omega}{\partial y}\frac{\partial \psi}{\partial x} = 0 \\ \Delta\psi = -\omega \end{cases} \tag{1}$$

With boundary conditions: $\psi|_{x=0} = g_1(y)$; $\psi|_{x=a} = g_2(y)$; $\psi|_{y=0} = const$; $\psi|_{y=b} = const$; $\omega|_{x=0} = f_1(y)$; $\omega|_{x=a} = f_2(y)$; $\omega|_{y=0} = const$; $\omega|_{y=b} = const$; where $\psi = \psi(x, y)$ — stream function, $\omega = \omega(x, y)$ — vorticity function.

Using finite-difference method we got system of non-linear algebraic equations:

$$\begin{cases} (\omega_{i+1,j} - \omega_{i-1,j})(\psi_{i,j+1} - \psi_{i,j-1}) - (\psi_{i+1,j} - \psi_{i-1,j})(\omega_{i,j+1} - \omega_{i,j-1}) = 0 \\ -\omega_{i,j} = \frac{\psi_{i+1,j} - \psi_{i,j} + \psi_{i-1,j}}{h_x^2} + \frac{\psi_{i,j+1} - \psi_{i,j} + \psi_{i,j-1}}{h_y^2} \end{cases} \tag{2}$$

where $i = 2..N_x - 1$; $j = 2..N_y - 1$; $h_x = \frac{a}{N_x - 1}$; $h_y = \frac{b}{N_y - 1}$

Unfortunately it is practically impossible to obtain analytical solution for such systems. However numerical methods provide acceptable results. The best of them were obtained using Newton's method. The key problem here is how to choose the correct initial data.

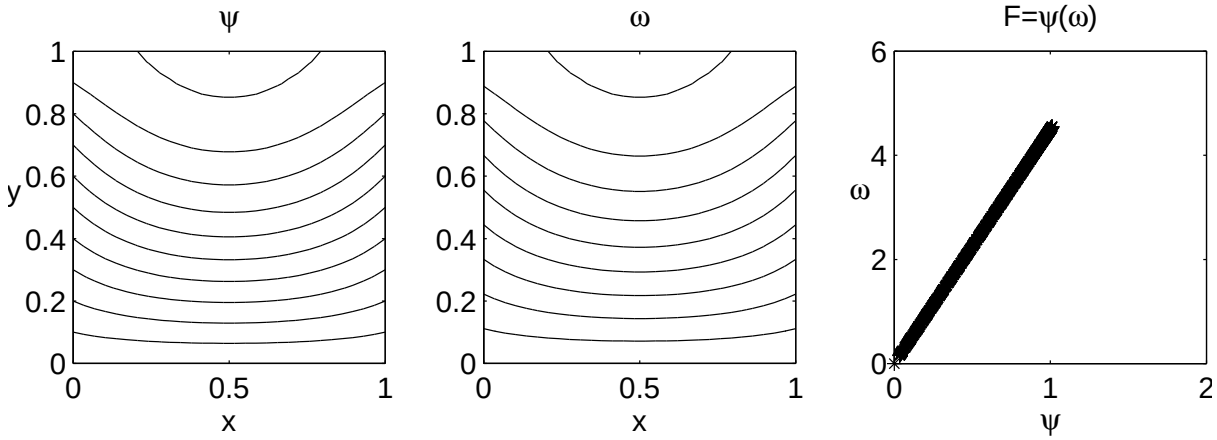

Figure 1. $K_1 = 4.5$; $K_2 = 0$; Regime with linear functional dependency that is identical to analytical solution from article [2]

We suggest the following algorithm:

[1]Supported by RFBR Grant N 14-01-00470

- To find solution for the smallest possible number of cells (6 by 6) using near-zero values as an initial data for Newton's method
- To "stretch" result using interpolation methods to increase number of cells and use the result of interpolation as an initial data for Newton's method.
- If boundary conditions are close to some boundary conditions for which solution has already been obtained, this solution is used as initial data for Newton's method.

The reliability of results was controlled by the verification of famous analytical facts and relations. Particularly, the fact that there should be a functional dependency $\psi = F(\omega)$ for the solution of (1).Besides, the algorithm was tested for cases where analytical solution is known [2] The described algorithm was successfully applied for analyzing problem (1).

We consider a square domain 1×1 with boundary conditions: $f_1(y) = f_2(y) = K_1 y + K_2 \sin(\frac{\pi y}{b})$; $g_1(y) = g_2(y) = y$, where K_1 and K_2 – some numerical parameters.

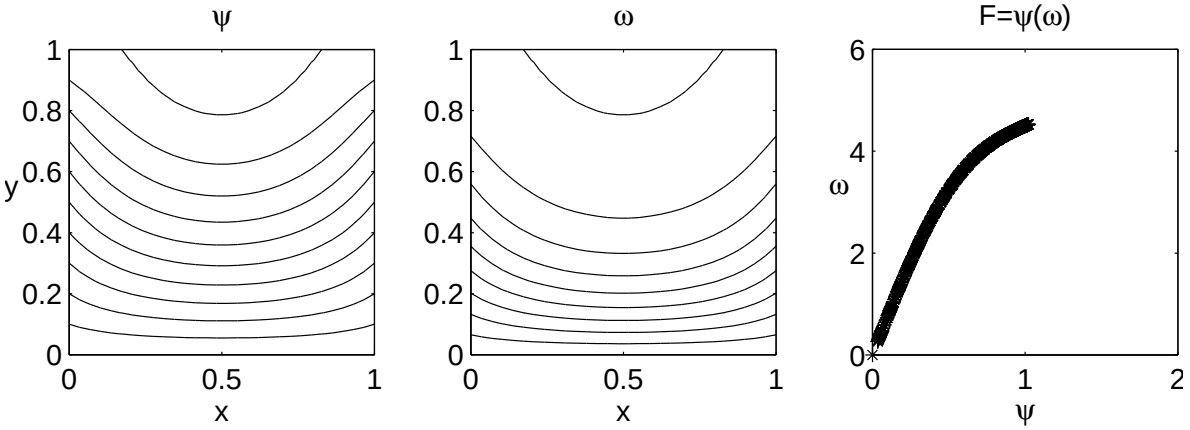

Figure 2. $K_1 = 4.5$; $K_2 = 1$; Increasing K_2 makes functional dependency non-linear but monotonic function

The main goal of the numerical experiments was to find a steady-state flows with different functional dependency $\omega = F(\psi)$. The linear dependency ($K_2 = 0$) was described in [2].

The results are presented graphically. The left picture illustrates stream-lines of fluid particles, the central picture illustrates isolines of vorticity field and the right graphics shows the dependency $\psi(\omega)$. Here, we used a solution with linear dependency $\omega = K\psi$ to perform reliability tests.

Bibliography

1. *Yudovich V.I.* The two-dimensional unsteady problem of flow of an ideal incompressible fluid through a given area // Math. Sat 1964. T. 64. Number 4. S. 562-588.

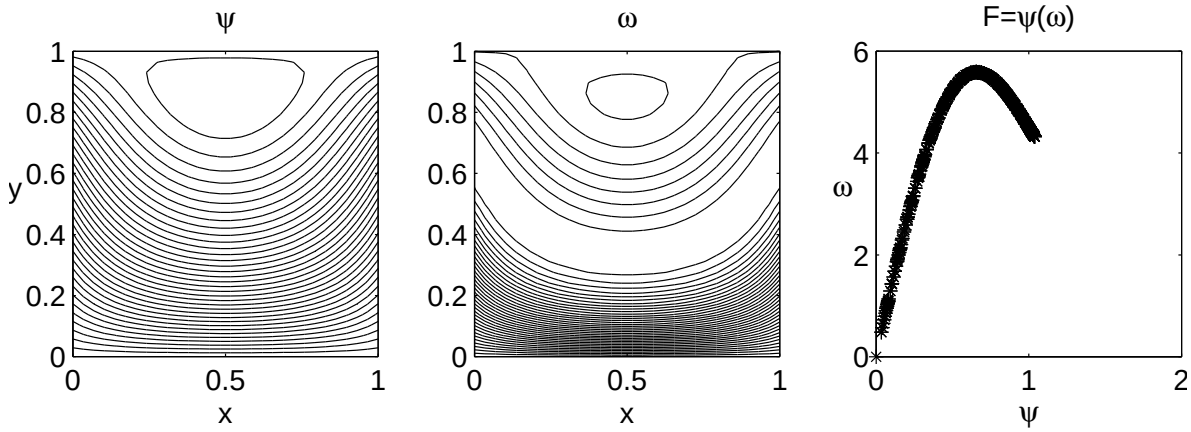

Figure 3. $K_1 = 4.5$; $K_2 = 3$; Further increasing K_2 makes functional dependency to become non-monotonic function

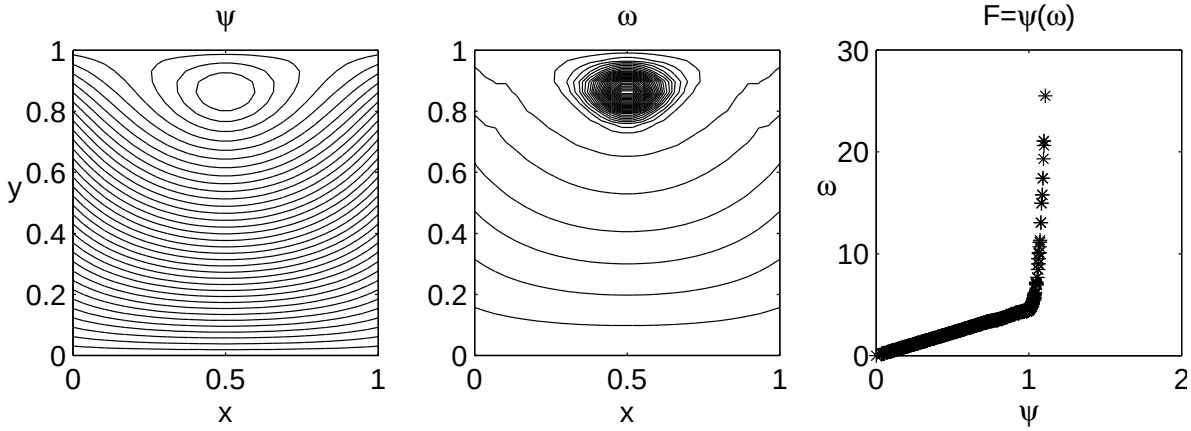

Figure 4. $K_1 = 4.5$; $K_2 = 0$; The solution with the same parameters as on Figure 1. This picture illustrates that there can be different solutions with the same border conditions.

2. *Govoruhin V.N.* Stationary vortex structures in the flow of an ideal fluid through the channel // Fluid Dynamics, 2012, Vol. 47, No. 2, pp. 147–156.

NUMERICAL ALGEBRA WITH APPLICATIONS

Proceedings of Fourth China-Russia Conference.

Executive editors: Zhong-Zhi Bai, Lev A. Krukier, Galina V. Muratova

Technical editors: Irina N. Shabas, Sergey A. Zharinov

Signed for printing 19.06.2015.
Offset paper. Offset printing.
Cond. sheet 7,7. Publ. sing. 5.
100 copies. Order № 2968.

Southern Federal University Publishing
Stachki Ave., 200/1, 344090 Rostov-on-Don, Russia